Special Technical Report 31

ORIENTATION MEASUREMENTS IN THAILAND WITH HF DIPOLE ANTENNAS FOR TACTICAL COMMUNICATION

By: LT. CDR. PAIBUL NACASKUL, R. T. N.

Prepared for:

U. S. ARMY ELECTRONICS COMMAND
FORT MONMOUTH, NEW JERSEY 07703

CONTRACT DA 36-039 AMC-00040(E)
ORDER NO. 5384-PM-63-91

STANFORD RESEARCH INSTITUTE

MENLO PARK, CALIFORNIA

Sponsored by
ADVANCED RESEARCH PROJECTS AGENCY
ARPA ORDER 371
FOR THE
THAI-U.S. MILITARY RESEARCH AND DEVELOPMENT CENTER
SUPREME COMMAND HEADQUARTERS
BANGKOK, THAILAND

STANFORD RESEARCH INSTITUTE
MENLO PARK, CALIFORNIA

June 1967

Special Technical Report 31

ORIENTATION MEASUREMENTS IN THAILAND WITH HF DIPOLE ANTENNAS FOR TACTICAL COMMUNICATION

By: LT. CDR. PAIBUL NACASKUL, R. T. N.

Prepared for:

U. S. ARMY ELECTRONICS COMMAND
FORT MONMOUTH, NEW JERSEY 07703

CONTRACT DA 36-039 AMC-00040(E)
ORDER NO. 5384-PM-63-91

SRI Project 4240

Approved: W. R. VINCENT, MANAGER
Communication Laboratory

D. R. SCHEUCH, EXECUTIVE DIRECTOR
Electronics and Radio Sciences

Sponsored by
ADVANCED RESEARCH PROJECTS AGENCY
ARPA ORDER 371
FOR THE
THAI-U.S. MILITARY RESEARCH AND DEVELOPMENT CENTER
SUPREME COMMAND HEADQUARTERS
BANGKOK, THAILAND

ABSTRACT

The magneto-ionic theory is described with a view to optimizing the orientation of a linearly polarized antenna such as a half-wave dipole for short-range communication via the ionosphere near the geomagnetic equator. The practical application, together with its limitations, is also considered. Continuous-wave measurements, performed with the goal of determining a suitable wave mode of propagation and hence the desired orientation of horizontal dipoles, demonstrate the superiority of the ordinary wave (north-south dipoles) for overall performance over a major part of the day when communication traffic is normally active. The coupling between the ordinary and the extraordinary modes is studied and the stability within a particular mode of propagation is discussed, together with its susceptibility to atmospheric noise. Pulse measurements confirm the results of the CW measurements and give additional information on the amplitude and phase stability of received waves, and on ionospheric layers supporting these waves. The overall results of the CW and pulse tests suggest that, although the optimum orientation of horizontal dipoles for both transmission and reception is parallel to the earth's magnetic field, communication performance may be further improved by orientation diversity reception. The use of an additional horizontal dipole aligned orthogonally to the north-south dipole permits utilization of the extraordinary mode whenever the ordinary wave fades or becomes inferior. Orientation diversity and its properties have been investigated by radioteletype measurements, which afford a ready means for assessing the performance of various antenna systems for transmission and reception. Initial investigations indicate that system performance of the diversity-combining teletype can be significantly improved by use of orientation diversity. The overall results of this study produce a simplified method of planning antenna configurations for tactical HF communication in Thailand.

CONTENTS

CONTENTS (Concluded)

ILLUSTRATIONS

ILLUSTRATIONS (Continued)

ILLUSTRATIONS (Continued)

ILLUSTRATIONS (Continued)

ILLUSTRATIONS (Continued)

ILLUSTRATIONS (Continued)

ILLUSTRATIONS (Concluded)

TABLES

SYMBOLS

$\bar{B}$ = magnetic flux density in weber/meter^2 ($\bar{B}_o$ for free space)

c = velocity of light in free space = 3×10^8 meters/second

$\bar{D}$ = electric displacement in Coulomb/meter^2

$\bar{E}$ = electric field intensity in volt/meter

e = charge on the electron = -1.602×10^{-19} Coulomb (also used for the exponential)

f = wave frequency in Hertz

$\bar{H}$ = magnetic field intensity in Ampere/meter

H_z = frequency in cycles/second

h = altitude above mean sea level in kilometer

h′ = virtual height of reflection in kilometer

k = free-space wave number in radian/meter

m = mass of electron = 9.107×10^{-31} kilogram

N = electron density, average number of electrons per cubic meter of magnetoionic medium

n = complex refractive index of the ionosphere

$\bar{P}$ = electric polarization of free electrons in Coulomb/meter^2

R = wave polarization = $-H_y/H_x = E_x/E_y = P_x/P_y$

$\bar{r}$ = average vector displacement, in meter, of an electron from the position it would have occupied if there were no electric field

t = time in second

$\bar{v}$ = electron velocity in meter/second = $\partial\bar{r}/\partial t$

X = normalized plasma frequency squared = ω_N^2/ω^2

x = Cartesian coordinate

Y = normalized gyrofrequency = ω_H/ω

Y_T = transverse component of Y

Y_L = longitudinal component of Y

y = Cartesian coordinate

Z = normalized collision frequency = ν/ω

z = Cartesian coordinate

SYMBOLS (Concluded)

α = attenuation constant, real part of Γ

β = phase constant, imaginary part of Γ

Γ = complex propagation constant

Δ = elevation angle of the wave propagation from a transmitter

ϵ = geomagnetic dip angle at the ionospheric height

ϵ_o = electric permittivity of free space = $1/(36\pi \times 10^9)$ Farad/meter

ϵ_r = relative electric permittivity of a medium

θ = angle between the static geomagnetic field and the wave normal

θ_L = the angle θ at which QL approximation becomes valid

θ_T = the angle θ at which QT approximation is valid

κ = absorption coefficient = $\omega\chi/c$

κ_o = absorption coefficient for the ordinary characteristic wave

κ_x = absorption coefficient for the extraordinary characteristic wave

λ = wavelength in free space (meter)

μ = refractive index, real part of n

μ_o = refractive index for the ordinary characteristic wave (also, magnetic permeability of free space = $4\pi \times 10^{-7}$ Henry/meter)

μ_x = refractive index for the extraordinary characteristic wave

ν = collision frequency in Hertz, average frequency of effective collisions between an electron and heavy particles

ρ = electric charge density in Coulomb/meter^3

σ = electric conductivity of a medium in mho/meter

ϕ = azimuth angle that the base line of wave propagation path makes with the magnetic north

χ = absorption index, minus imaginary part of n

ω = angular wave-frequency in radian/second

ω_H = angular gyrofrequency = $|e\bar{B}_o|/m$

ω_N^2 = angular plasma frequency squared = $Ne^2/\epsilon_o m$

ACKNOWLEDGMENTS

Appreciation is expressed to Captain Prapat Chandaket, R.T.N., Program Manager for Communications, Military Research and Development Center, Bangkok, and to Robert E. Leo, Technical Director, Military Research and Development Center, Electronics Laboratory, for their helpful support, and to George H. Hagn for the initiation of this project and for many valuable suggestions.

The author also wishes to acknowledge Robert D. Daniel of SRI, John W. Chapman of Vitro, and Kenneth L. Taylor of Vitro for their cooperative work on circuitry and data reduction.

I INTRODUCTION

Previous studies of high-frequency (HF) radio propagation in a dense forest[1,2*] indicate that military ground-wave communication operations, normally utilizing a vertical-whip antenna, have been hampered by such a serious path loss, even for as short a distance as 2 or 3 km. Sky-wave transmission has therefore been necessary when using man-pack sets (i.e., low-power sets). Horizontal half-wave dipoles and slant-wire antennas have been used for communication via the ionosphere under these conditions. Present military manuals recommend main-beam-to-main-beam coupling, which (in the case of half-wave dipoles) means the antennas should be oriented physically orthogonal to the line joining their phase centers.[3] While this recommendation has been widely used for most applications and in most parts of the world, it has been recognized that, in order to utilize the effects resulting from interaction of the earth's magnetic field and the electromagnetic wave traversing the ionosphere[4] at low latitudes, linearly polarized antennas (horizontal dipoles, etc.) should be aligned with axes as near as possible to the magnetic meridian.[5] Consideration of the magneto-ionic theory led Hagn to suggest that there exists an optimum orientation for linearly polarized antennas used on short ionospheric paths near the geomagnetic equator.[6] Hagn's revised work[7] includes an extensive bibliography on the investigation of effects of the earth's magnetic field on the propagation of radio waves in the ionosphere, including polarization of downcoming waves.

Thailand is situated in the geomagnetic equatorial region: Bangkok has a magnetic dip angle of 10° 27'N; dip angles elsewhere within the territorial borders range between approximately 24°N and 8°S (see Fig 1). Many parts of Thailand are covered with jungle or heavy forests, making ground-wave propagation difficult, particularly when man-pack sets are

---

* References are given at the end of the report.

FIG. 1 MAP OF THAILAND SHOWING MAGNETIC DIP ANGLE

employed. This country, therefore, provides a good environment for investigation of HF propagation via the ionosphere on short-range jungle communication paths, using dipoles and other linearly polarized antennas.

Since the magneto-ionic theory is important to the understanding of wave propagation in the ionosphere, a review of the theory leading to the optimization of alignment of linear antennas (e.g., horizontal dipoles) is presented in Sec. II. Sections III and IV deal with CW and pulse measurements employed for the evaluation of skywave propagation. The results of measurements with dipoles oriented north-south (N-S), east-west (E-W), and northeast-southwest (NE-SW) enable one to compare the performance using ordinary wave with that obtained by using the extra-ordinary wave. The radio-teletype equipment at the Military Research and Development Center (MRDC) Electronics Laboratory, Bangkok, provided a facility to test the orientation diversity system using the ordinary wave or the extraordinary wave. Radio-teletype measurements, described in Sec. V, also afford a practical and ready means of comparing performance under various conditions, and of assessing errors due to interference such as atmospheric noise or propagation from other stations or due to fading of duration as short as 1/35 second. Section VI discusses the application of the findings of the dipole orientation project, with a suggestion for further investigations on diversity systems of reception.

II MAGNETO-IONIC THEORY AND ITS APPLICATION TO DIPOLE ORIENTATION

A. GENERAL

Since 1902, when Kennelly and Heaviside independently suggested that radio waves might be propagated from England to America by reflection from an electrified layer in the upper atmosphere, investigators have presented theories supporting the phenomenon of radio-wave propagation via the ionosphere. It was not until 1932, however, when Appleton published his magneto-ionic theory in full,[8] that these workers began to pursue the same or similar lines of attack. This theory satisfactorily answered many of the questions that had remained unanswered up to that time, and Appleton's approach is still producing novel, useful insight into ionospheric problems.

B. MAGNETO-IONIC THEORY

1. Assumptions

The magneto-ionic medium considered is assumed to have the following properties:

(1) Free electrons and heavy positive ions are situated in a uniform (static) magnetic field.

(2) These charges are distributed with statistical uniformity, so that there is no resultant space charge (i.e., the medium is electrically neutral).

(3) Only electrons are effective in influencing the propagation of electromagnetic waves. (Effects due to heavy ions and other particles could be separately considered, but they are neglected in the present discussion, except as they affect losses from effective electron collisions.)

(4) Electronic collisions are independent of electron energy (i.e., "cold" plasma theory).

(5) The thermal motions of the electrons cancel out.

(6) The macroscopic magnetic properties of the medium are those of free space.

(7) The medium is locally homogeneous.

(8) The magnetic field of the radio wave propagating in the medium has a negligible effect upon the motion of an individual electron relative to the effect of the earth's static magnetic field.

2. Maxwell's Equations

An electromagnetic wave that enters the ionized region sets the free charges into motion by virtue of the electrostatic force, $e\overline{E}$, exerted on them. The resulting motion follows the incident field and therefore is harmonic. The oscillating electrons radiate secondary waves, which combine coherently with the incident field to form a new field that appears to traverse a medium characterized by macroscopic parameters: the dielectric constant ϵ_r and the conductivity σ.

The electromagnetic field in the ionosphere satisfies Maxwell's equations:

$$\begin{aligned} \text{curl } \overline{H} &= \frac{\partial \overline{D}}{\partial t} \\ \text{div } \overline{D} &= \rho \\ \text{curl } \overline{E} &= -\frac{\partial \overline{B}}{\partial t} = -\mu_o \frac{\partial \overline{H}}{\partial t} \\ \text{div } \overline{B} &= 0 \quad . \end{aligned} \tag{1}$$

Electric displacement $\overline{D}$, electric field intensity $\overline{E}$, and electric polarization $\overline{P}$ of free electrons are related by:

$$\overline{D} = \epsilon_o \overline{E} + \overline{P} \quad , \tag{2}$$

where

$$\overline{P} = Ne\overline{r} \tag{2-a}$$

N = average number of electrons per unit volume of magneto-ionic medium

e = charge on one electron = -1.602×10^{-19} coulomb

$\overline{r}$ = average vector displacement of an electron from the position it would have occupied if there were no electric field.

A plane wave traveling in the z direction can be represented by equations of the form:

$$\bar{E} = \bar{E}_o e^{i(\omega t - knz)} = \bar{E}_o e^{i(\omega t - \Gamma z)} \quad , \tag{3}$$

where

the free-space wave number, $k = 2\pi/\lambda_o = \omega/c$ radians/meter
the velocity of light in free space, $c = f\lambda_o$ m/sec
the wave frequency, $f = \omega/2\pi$ Hz
the complex refractive index of the medium, $n = \mu - i\chi$
the refractive index, $\mu = 1$ for free space
the absorption index, $\chi = 0$ for free space.

The wave thus travels along the z direction with the propagation constant,

$$\Gamma = \alpha + i\beta \tag{3a}$$

where the attenuation constant, $\alpha = k\chi = (\omega/c)\chi$, and the phase constant, $\beta = k\mu = (\omega/c)\mu$.

Since the electric and magnetic vectors of the wave do not vary with x and y directions,

$$\begin{aligned} \frac{\partial}{\partial z} &= -ikn \\ \frac{\partial}{\partial x} &= \frac{\partial}{\partial y} = 0 \\ \frac{\partial}{\partial t} &= i\omega \\ \frac{\partial^2}{\partial t^2} &= -\omega^2 \quad . \end{aligned} \tag{4}$$

From Eqs. (1), (2), and (4), one may obtain:

$$\text{curl } \bar{H} = \epsilon_o \frac{\partial \bar{E}}{\partial t} + \frac{\partial \bar{P}}{\partial t}$$

$$\frac{\partial H_z}{\partial y} - \frac{\partial H_y}{\partial z} = iknH_y = i\omega(\epsilon_o E_x + P_x) \tag{5a}$$

$$-\frac{\partial H_z}{\partial x} + \frac{\partial H_x}{\partial z} = -iknH_x = i\omega(\epsilon_o E_y + P_y) \tag{5b}$$

$$\frac{\partial H_y}{\partial x} - \frac{\partial H_x}{\partial y} = 0 = i\omega(\epsilon_o E_z + P_z) \tag{5c}$$

and

$$\text{curl } \bar{E} = -\mu_o \frac{\partial \bar{H}}{\partial t}$$

$$\frac{\partial E_z}{\partial y} - \frac{\partial E_y}{\partial z} = iknE_y = -i\omega\mu_o H_x \tag{6a}$$

$$\frac{\partial E_x}{\partial z} - \frac{\partial E_z}{\partial x} = -iknE_x = -i\omega\mu_o H_y \tag{6b}$$

$$\frac{\partial E_y}{\partial x} - \frac{\partial E_x}{\partial y} = 0 = -i\omega\mu_o H_z \quad . \tag{6c}$$

Combining Eq. (5a) with Eq. (6b) gives:

$$k^2 n^2 H_y E_x = \omega^2 \mu_o H_y \epsilon_o E_x + \omega^2 \mu_o H_y P_x \quad ,$$

or

$$\frac{k^2 n^2}{\omega^2 \mu_o \epsilon_o} = 1 + \frac{1}{\epsilon_o} \cdot \frac{P_x}{E_x} \quad . \tag{7a}$$

Similarly, from Eqs. (5b) and (6a):

$$\frac{k^2 n^2}{\omega^2 \mu_o \epsilon_o} = 1 + \frac{1}{\epsilon_o} \cdot \frac{P_y}{E_y} \quad . \tag{7b}$$

Hence, P_x and P_y must vary with z like E_x and E_y, and

$$\frac{P_x}{E_x} = \frac{P_y}{E_y} \equiv \text{polarizability} \quad , \tag{8}$$

which is the condition for characteristic waves capable of traveling along the z direction without changing their wave polarizations. The velocity of light in free space is also

$$c = \frac{1}{\sqrt{\mu_o \epsilon_o}} \tag{9}$$

where the absolute permeability of free space,

$$\mu_o = 4\pi \times 10^{-7} \text{ Henry/meter} \quad ,$$

and the absolute permittivity of free space,

$$\epsilon_o = \frac{1}{36\pi \times 10^9} \text{ Farad/meter} \quad .$$

By solving Eq. (7) with relations of Eqs. (9) and (3a), one may obtain:

$$n^2 = 1 + \frac{1}{\epsilon_o} \cdot \frac{P_x}{E_x} = 1 + \frac{1}{\epsilon_o} \cdot \frac{P_y}{E_y} \quad . \tag{10}$$

The wave polarization R may be defined in terms of $\bar{H}$ thus:

$$R \equiv -\frac{H_y}{H_x} \quad . \tag{11}$$

Equations (2), (6a), (6b), (8), and (11) may be combined to give

$$R = -\frac{H_y}{H_x} = \frac{E_x}{E_y} = \frac{P_x}{P_y} = \frac{D_x}{D_y} \quad . \tag{12}$$

3. Constitutive Relations

Consider the motion of an electron in an ionized medium under the influence of an electromagnetic wave and an imposed magnetic field B_o, having the longitudinal component B_L and the transverse component B_T, as shown in Fig. 2.

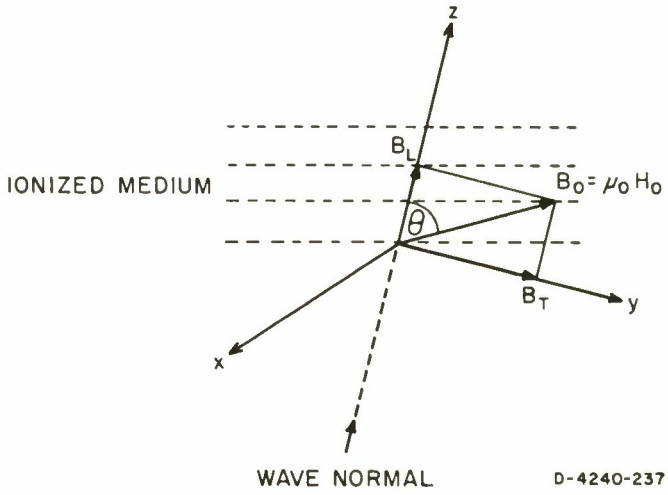

FIG. 2 COORDINATE SYSTEM OF WAVE PROPAGATION

In addition to the force $e\bar{E}$ on an electron as a result of the electric field $\bar{E}$ of the wave, there is the force $e(\bar{v} \times \bar{B}_o)$ resulting from the electron motion $\bar{v} = \partial\bar{r}/\partial t$ relative to the imposed magnetic field, B_o, and also the force $m\nu\bar{v}$ which represents the average rate of loss of momentum of the electron per collision, where ν is the average frequency of collisions between an electron and heavy particles. The equation of motion of an electron can thus be formed:

$$m\frac{\partial^2\bar{r}}{\partial t^2} = e\bar{E} + e\frac{\partial\bar{r}}{\partial t} \times \bar{B}_o - m\nu\frac{\partial\bar{r}}{\partial t} \quad . \tag{13}$$

Since, from Eqs. (2a) and (4), one has $\bar{r} = \bar{P}/Ne$, $\partial/\partial t = i\omega$, and $\partial^2/\partial t^2 = -\omega^2$, Eq. (13) is multiplied by $Ne/m\omega^2$ and becomes

$$-\bar{P} = \frac{Ne^2\bar{E}}{m\omega^2} + \frac{ie}{m\omega}\bar{P} \times \bar{B}_o - \frac{i\nu\bar{P}}{\omega} \quad .$$

Hence, we obtain:

$$-\epsilon_o X\bar{E} = \bar{P}(1 - iZ) + i\bar{P} \times \bar{Y} \quad , \tag{14}$$

where

$$\left.\begin{aligned} &\text{the normalized plasma frequency squared} = X = \left(\frac{\omega_N}{\omega}\right)^2 \equiv \frac{Ne^2}{\epsilon_o m\omega^2} \\ &\text{the normalized collision frequency} = Z \equiv \frac{\nu}{\omega} \\ &\text{and the normalized gyrofrequency} = Y = \frac{\omega_H}{\omega} \equiv \left|\frac{eB_o}{m\omega}\right| = \frac{|eB_o|}{m\omega} \quad . \end{aligned}\right\} \tag{15}$$

Equation (14) may be written out in Cartesian coordinates:

$$-\epsilon_o XE_x = (1 - iZ)P_x + iP_y Y_z - iP_z Y_y$$

$$-\epsilon_o XE_y = (1 - iZ)P_y - iP_x Y_z + iP_z Y_x$$

$$-\epsilon_o XE_z = (1 - iZ)P_z + iP_x Y_y - iP_y Y_x \quad .$$

Since it can be seen from Fig. 2 that

$$Y_x = 0$$

$$Y_y = \text{transverse component of } Y = Y_T$$

and

$$Y_z = \text{longitudinal component of } Y = Y_L \quad ,$$

one may finally arrive at the constitutive relations, in matrix form,

$$-\epsilon_o X \begin{bmatrix} E_x \\ E_y \\ E_z \end{bmatrix} = \begin{bmatrix} 1 - iZ & iY_L & -iY_T \\ -iY_L & 1 - iZ & 0 \\ iY_T & 0 & 1 - iZ \end{bmatrix} \begin{bmatrix} P_x \\ P_y \\ P_z \end{bmatrix} \quad . \tag{16}$$

4. Appleton Formula

From Eq. (5c), $\epsilon_o E_z + P_z = 0$, and from the third equation of Eq. (16), $E_z = -(1/\epsilon_o X)\{iY_T P_x + (1 - iZ)P_z\}$, one has: $(1 - X - iZ)P_z = -iY_T P_x$, which, when substituted in the first equation of Eq. (16), gives:

$$-\epsilon_o X E_x = (1 - iZ)P_x + iY_L P_y - \frac{iY_T(-iY_T)P_x}{1 - X - iZ}$$

or,

$$-\epsilon_o X \frac{E_x}{P_x} = \left[(1 - iZ) - \frac{Y_T^2}{1 - X - iZ}\right] + iY_L \cdot \frac{P_y}{P_x} \quad . \tag{17}$$

Equation (17) and the second equation of Eq. (16), together with the relation $P_x/E_x = P_y/E_y$ of Eq. (8), then give rise to:

$$(1 - iZ) - \frac{Y_T^2}{1 - X - iZ} + iY_L \cdot \frac{P_y}{P_x} = -iY_L \frac{P_x}{P_y} + (1 - iZ)$$

i.e.,

$$iY_L\left(\frac{P_x}{P_y}\right)^2 - \frac{Y_T^2}{1 - X - iZ}\left(\frac{P_x}{P_y}\right) + iY_L = 0 \quad , \tag{18}$$

which is a quadratic equation yielding two values for P_x/P_y, corresponding to two possible characteristic waves in the medium. (A characteristic wave is one that propagates with no change in wave polarization R in the locally homogeneous ionosphere.)

Because polarization of the wave R from Eq. (12) equals $P_x/P_y = E_x/E_y$, Eq. (18) may be solved to give:

$$R = \frac{E_x}{E_y} = -\frac{i}{Y_L}\left\{\frac{Y_T^2}{2(1 - X - iZ)} \mp \sqrt{\left[\frac{Y_T^2}{2(1 - X - iZ)}\right]^2 + Y_L^2}\right\} . \quad (19)$$

Equation (10) and the second equation of Eq. (16) may be combined to give the square of the complex refractive index:

$$n^2 = 1 + \frac{1}{\epsilon_o} \cdot \frac{P_y}{E_y} = 1 + \frac{P_y}{\epsilon_o} \cdot \frac{-\epsilon_o X}{-iY_L P_x + (1 - iZ)P_y}$$

i.e.,

$$n^2 = 1 - \frac{X}{(1 - iZ) - iY_L R} . \quad (20)$$

By combining Eqs. (19) and (20), one finally arrives at the Appleton formula:*

$$n^2 = (\mu - i\chi)^2 = 1 - \frac{X}{1 - iZ - \frac{Y_T^2}{2(1 - X - iZ)} \pm \sqrt{\left[\frac{Y_T^2}{2(1 - X - iZ)}\right]^2 + Y_L^2}} . \quad (21)$$

The Appleton formula suggests that an electromagnetic wave entering an ionized region under the influence of the earth's magnetic field will be split into two characteristic waves, the relative amplitudes of which are determined by the original polarization. Each wave will propagate with its polarization unchanged and with its own characteristic velocity and attenuation. As the combined wave progresses, the two components will add to give a resulting polarization that changes as the wave travels.

---

* Also known as the Appleton-Hartree formula. Hartree derived essentially the same equation from consideration of the interaction of a radio wave with a magneto-ionic plasma, but from the microscopic approach.

Only if the original wave is itself one of the characteristic waves will it travel with unchanging polarization. One characteristic wave, known as the ordinary wave [corresponding to the upper sign of Eqs. (19) and (21)] is little affected by the presence of the earth's magnetic field compared to the other wave, the extraordinary [corresponding to the lower sign of Eqs. (19) and (21)].

A full discussion of Eq. (21) is very involved, but useful properties of the Appleton formula may be derived when certain approximations are made, as follows:

$$\left.\begin{aligned} &\text{Quasi-transverse approximation (QT):} \quad \frac{Y_T^4}{4Y_L^2} \gg \left|(1 - X - iZ)^2\right| \\ &\text{Quasi-longitudinal approximation (QL):} \quad \frac{Y_T^4}{4Y_L^2} \ll \left|(1 - X - iZ)^2\right| \end{aligned}\right\} . \qquad (22)$$

This report considers the QT case, which is appropriate to short-range ionospheric propagation near the geomagnetic equator. The QL case is briefly studied with regard to ranges where it applies.

5. Quasi-Transverse Approximation

When the QT approximation is assumed, Eqs. (21) and (19) become:

$$n^2 = (\mu - i\chi)^2 \cong 1 - \frac{X}{\left[1 - iZ - \frac{Y_T^2}{2(1 - X - iZ)} \pm \frac{Y_T^2}{2(1 - X - iZ)}\right]}$$

and

$$R = -\frac{i}{2Y_L}\left(\frac{Y_T^2}{1 - X - iZ} \mp \frac{Y_T^2}{1 - X - iZ}\right) .$$

Hence, for the ordinary wave,

$$n^2_{QT(u)} = (\mu - i\chi)^2\big|_{QT(u)} \cong 1 - \frac{X}{1 - iZ} \qquad (23a)$$

$$R_{QT(u)} \cong 0 \quad , \tag{23b}$$

and for the extraordinary wave,

$$n^2_{QT(\ell)} = (\mu - i\chi)^2\big|_{QT(\ell)} \cong 1 - \frac{X}{1 - iZ - \dfrac{Y_T^2}{1 - X - iZ}} \tag{24a}$$

$$R_{QT(\ell)} \cong \infty \quad . \tag{24b}$$

The expressions for R_{QT} show that, when the QT approximation is valid, the two characteristic waves are linearly polarized along the principal directions.

Equations (23) and (24) are often referred to as the Booker expressions. Recent workers favor the approximation after taking the first two terms of a binomial expansion for the quadratic expression in Eq. (21).[9,10,11] Thus the upper-signed Eq. (21) may be rewritten:

$$n^2_{(u)} = 1 - \frac{X}{1 - iZ - \dfrac{Y_T^2}{2(1 - X - iZ)}\left\{1 - \left[1 + \dfrac{4Y_L^2(1 - X - iZ)^2}{Y_T^4}\right]^{1/2}\right\}} \quad ;$$

then the approximation

$$n^2_{QT(u)} \cong 1 - \frac{X}{1 - iZ - \dfrac{Y_T^2}{2(1 - X - iZ)}\left\{1 - \left[1 + (1/2) \cdot \dfrac{4Y_L^2(1 - X - iZ)^2}{Y_T^4}\right]\right\}}$$

or,

$$n^2_{QT(u)} \cong 1 - \frac{X}{1 - iZ + \dfrac{Y_L^2}{Y_T^2}(1 - X - iZ)} \quad .$$

Utilizing $Y_L/Y_T = \cot\theta$, as can be seen from Fig. 2, one may obtain for the ordinary wave:

$$n^2_{QT(u)} = (\mu_o - i\chi_o)^2 \cong 1 - \frac{X}{1 - iZ + (1 - X - iZ)\cot^2\theta} \quad . \tag{25}$$

Equation (25) may be rewritten:

$$\mu_o^2 - \chi_o^2 - 2i\mu_o\chi_o \cong 1 - \frac{X[1 + (1 - X)\cot^2\theta + iZ(1 + \cot^2\theta)]}{\left[1 + (1 - X)\cot^2\theta\right]^2 + Z^2\left(1 + \cot^2\theta\right)^2} \quad , \tag{25a}$$

the imaginary parts of which may be equated to give:

$$2\mu_o\chi_o\Big|_{QT(u)} \cong \frac{XZ\csc^2\theta}{\left[1 + (1 - X)\cot^2\theta\right]^2 + Z^2\csc^4\theta} \quad .$$

Hence, the absorption coefficient

$$\kappa \equiv \frac{\omega}{c}\chi \tag{26}$$

may be obtained for the QT-ordinary wave thus:

$$\kappa_o\Big|_{QT} \cong \frac{\nu}{2\mu_o c} \cdot \frac{X\sin^2\theta}{\left(1 - X\cos^2\theta\right)^2 + Z^2} \quad , \tag{27}$$

which will be identical with the Booker expression when the direction of the wave normal is at right angles to the earth's magnetic field:

$$\kappa_o\Big|_{\theta=90^o} \cong \frac{\nu}{2\mu_o c} \cdot \frac{X}{1 + Z^2} = \frac{\nu}{2\mu_o c} \cdot \frac{\omega_N^2}{\omega^2 + \nu^2} \quad . \tag{28}$$

Equation (24a) may be written:

$$[\mu^2 - \chi^2 - 2i\mu\chi]_{QT(\ell)} \cong 1 - \frac{X[(1-X)^2 + Z^2]}{(1 - iZ)[(1-X)^2 + Z^2] - Y_T^2[(1-X) + iZ]}$$

$$\cong 1 - \frac{X[(1-X)^2 + Z^2]\{[(1-X)^2 + Z^2 - Y_T^2(1-X)] + iZ[(1-X)^2 + Z^2 + Y_T^2]\}}{\left[(1-X)^2 + Z^2 - Y_T^2(1-X)\right]^2 + Z^2\left[(1-X)^2 + Z^2 + Y_T^2\right]^2} , \tag{29}$$

the imaginary parts of which may be equated to give the absorption coefficient for the QT-extraordinary wave:

$$\kappa_X\big|_{QT} \cong \frac{\nu}{2\mu_x c} \cdot \frac{X[(1-X)^2 + Z^2][(1-X)^2 + Z^2 + Y_T^2]}{\left[(1-X)^2 + Z^2 - Y_T^2(1-X)\right]^2 + Z^2\left[(1-X)^2 + Z^2 + Y_T^2\right]^2} . \tag{30}$$

One may return to Eqs. (25a) and (29) and equate their real parts in order to obtain the refractive indices for the ordinary wave and the extraordinary wave under the QL approximation. The results are not of primary importance to the present discussion. One may equate Eqs. (23a) and (24a) to zero to find that, for a frequency above the gyrofrequency ($Y < 1$), the ordinary wave will be reflected at or near the height corresponding to $X = 1$, and the extraordinary wave will be reflected at or near the height corresponding to $X = 1 - Y$, when the QT approximation is realized. The more the wave frequency exceeds the collision frequency, the more accurate are the ionospheric height conditions for reflections.

Differential absorption of the ordinary wave relative to the extraordinary in nondeviative regions may be studied in an approximate manner by taking a ratio of absorption coefficients and canceling μ's, since $\mu_o \cong \mu_x \cong 1$.

Equation (28) for $\omega^2 \gg \nu^2$ or $Z^2 \ll 1$ becomes:

$$\kappa_o \Big|_{\substack{QT,\theta\cong 90^o \\ Z^2 \ll 1 \\ X \ll 1}} \cong \frac{\nu X}{2\mu_o c} \tag{31}$$

Equation (30) for $Z^2 \ll 1$ becomes

$$\kappa_x \Big|_{\substack{QT,\theta\cong 90^o \\ Z^2 \ll 1 \\ X \ll 1}} \cong \frac{\nu}{2\mu_x c} \cdot \frac{X(1-X)^2\left[(1-X)^2 + Y_T^2\right]}{\left[(1-X)^2 - Y_T^2(1-X)\right]^2}$$

$$\cong \frac{\nu}{2\mu_x c} \cdot \frac{X\left[(1-X)^2 + Y_T^2\right]}{\left(1 - X - Y_T^2\right)^2} \quad . \tag{32}$$

Hence, the differential absorption in nondeviative regions may be indicated by the ratio:

$$\frac{\kappa_o}{\kappa_x} \Big|_{\substack{QT,\theta\cong 90^o \\ Z^2 \ll 1 \\ \mu_o \cong \mu_x \cong 1, \therefore X \ll 1}} \cong \frac{\left(1 - X - Y_T^2\right)^2}{(1-X)^2 + Y_T^2}$$

$$\cong \frac{\left(1 - Y_T^2\right)^2}{1 + Y_T^2} \quad , \tag{33}$$

which is always less than unity when the earth's magnetic field is taken into account. This, therefore, suggests that the ordinary wave is the better of the two modes of propagation at frequencies not too near the ionospheric layer critical frequency for the ordinary wave, where deviative absorption is becoming important. In support of the above discussion on the differential absorption under the QT and various other conditions, the curves in Figs. 3 and 4 show the variation of μ and χ with X for various values of Z.[12] These figures indicate the superiority of the ordinary wave, which is less affected by the earth's magnetic field.

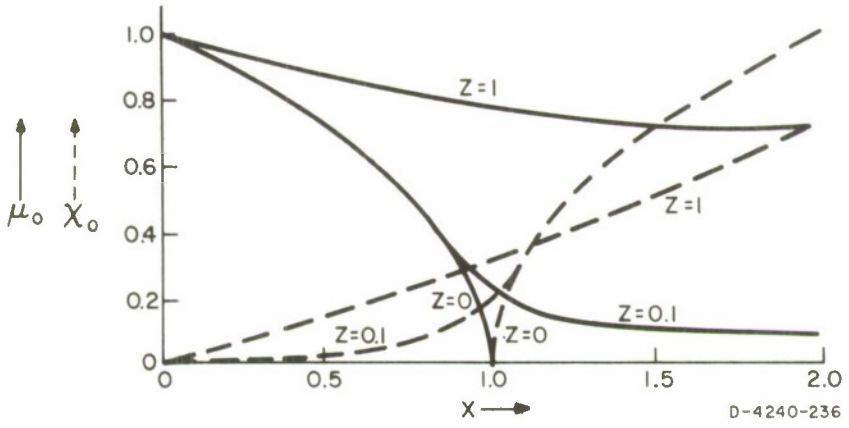

FIG. 3 μ_o AND χ_o AS A FUNCTION OF X FOR VARIOUS VALUES OF Z, Y < 1, TRANSVERSE PROPAGATION

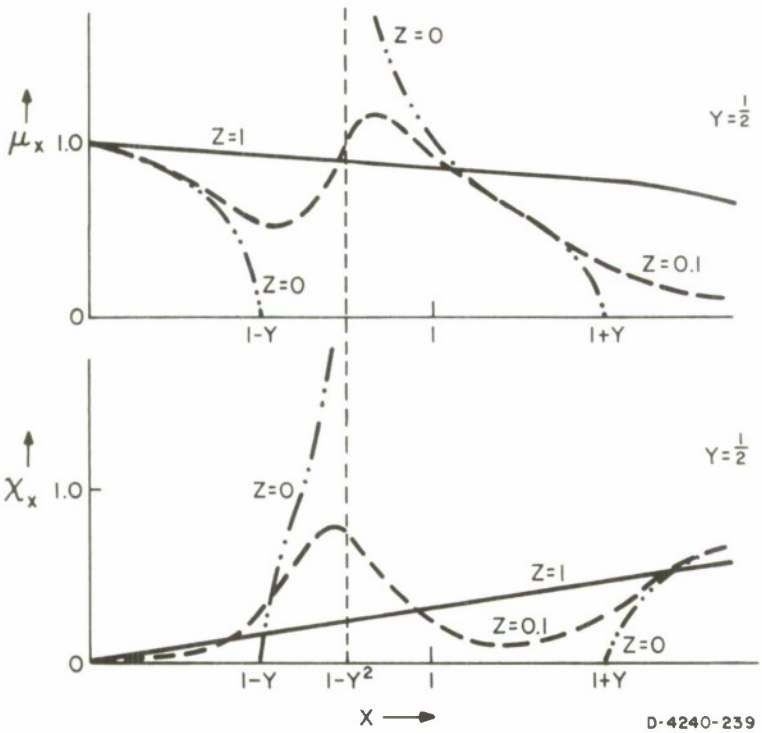

FIG. 4 μ_x AND χ_x AS A FUNCTION OF X FOR VARIOUS VALUES OF Z, Y < 1, TRANSVERSE PROPAGATION

It should be borne in mind, however, that the ordinary wave will travel a longer path in the ionosphere than the extraordinary; hence, the difference in attenuation over the whole path length may not be as great as Eq. (33) may suggest. The cumulative two-way absorption useful to the study of overall performance is expressed by:

$$\left.\begin{array}{l} 2\int_{0}^{\text{Height of reflection}} \kappa(h)\,dh \quad \text{in nepers,} \\ \text{or} \\ 17.37\int_{0}^{\text{Height of reflection}} \kappa(h)\,dh \quad \text{in dB} \end{array}\right\} \tag{34}$$

where $\kappa(h)$ is a function of height and hence a function of the electron density $N(h)$, the collision frequency $\nu(h)$, the earth's magnetic field $\overline{B}_o(h)$, and the propagation path.

Hagn, assuming the model ionosphere illustrated in Fig. 5 has computed various curves showing absorption coefficients (see Fig. 6), as well as cumulative two-way absorption (Fig. 7), for both daytime and nighttime transverse propagations at 1, 2, 5, and 10 MHz.[13] Although the assumed $N(h)$ profiles of Fig. 5 are not very typical (they give daytime absorption values much larger than those typically observed), they do illustrate several interesting points. From these curves, one can evaluate the differential absorption between O and X for the given frequencies. The curves show that the wave frequency should be as near the maximum usable frequency (MUF) as possible, and that the lower the wave frequency, the greater is the superiority of the ordinary wave over the extraordinary.

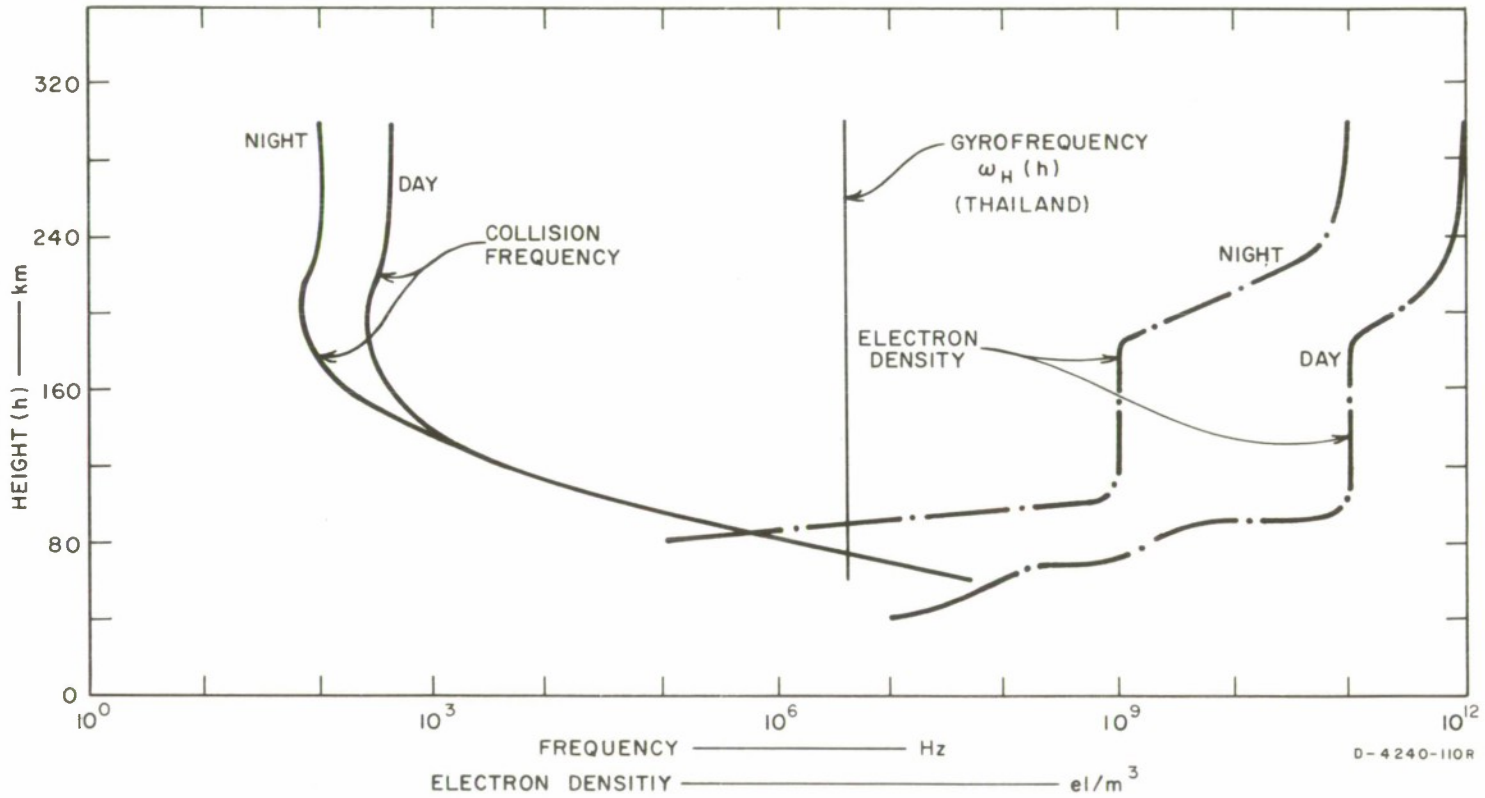

FIG. 5 MODEL IONOSPHERE

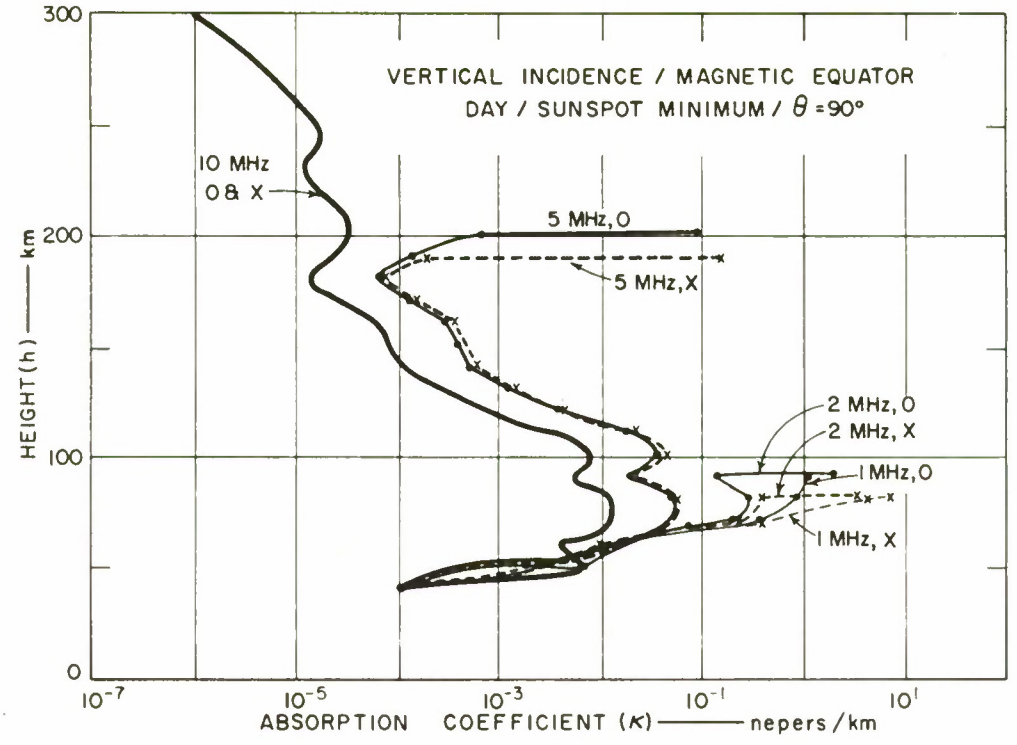

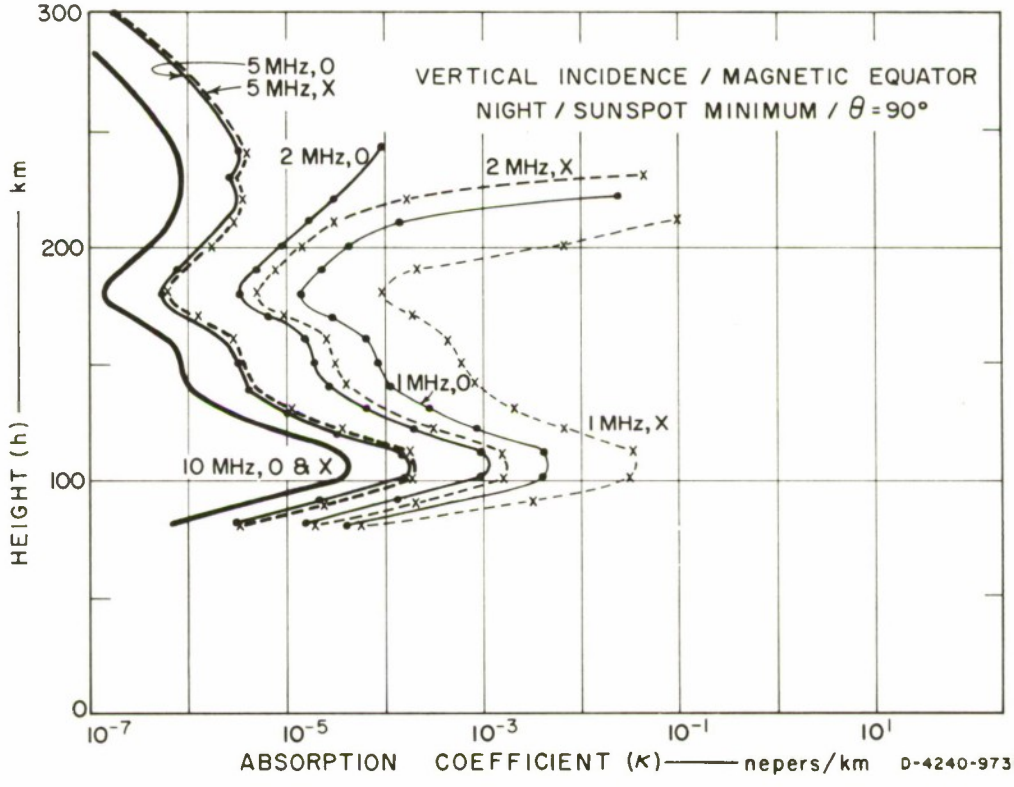

FIG. 6 ABSORPTION COEFFICIENT κ FOR DAY AND NIGHT

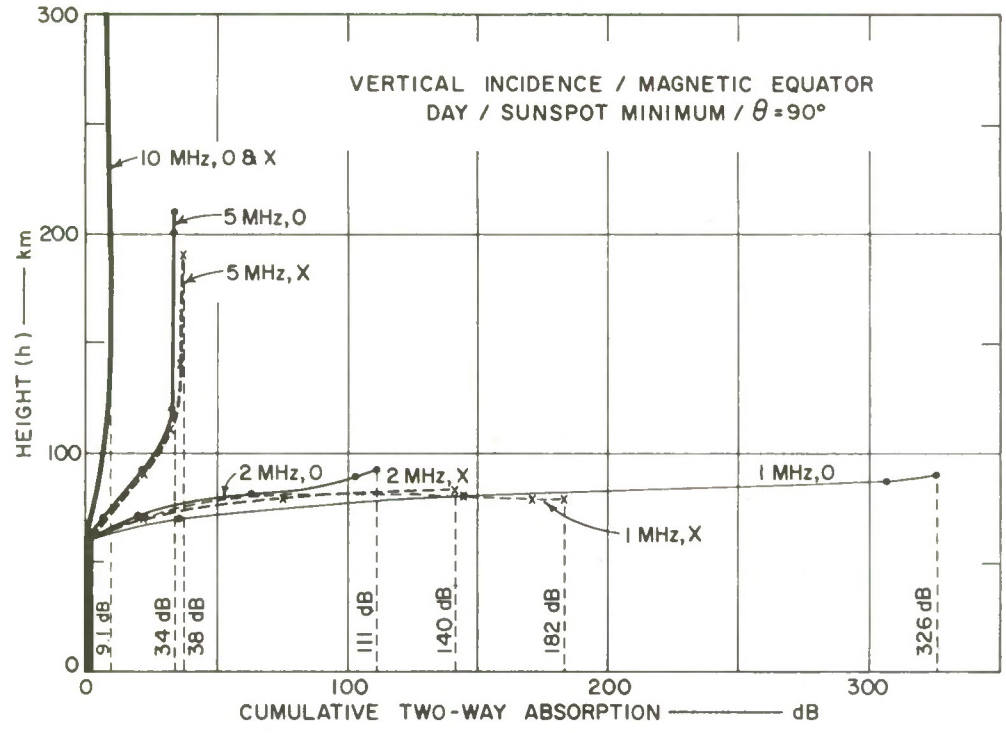

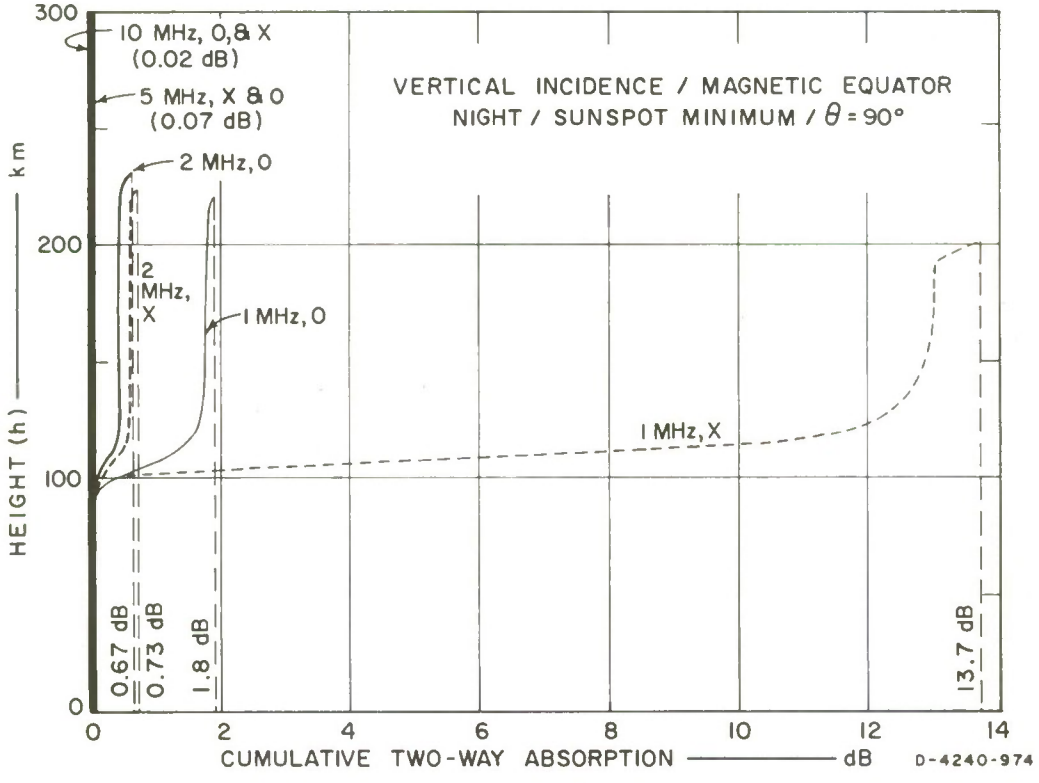

FIG. 7 CUMULATIVE TWO-WAY ABSORPTION FOR DAY AND NIGHT

6. Quasi-Longitudinal Approximation

Under the QL approximation

$$\frac{Y_T^4}{4Y_L^2} \ll \left|(1 - X - iZ)^2\right| \quad ,$$

Eqs. (21) and (19) become:

$$n_{QL}^2 \cong 1 - \frac{X}{1 - iZ \pm |Y_L|} \tag{35}$$

and

$$R_{QL} \cong \mp i \quad , \tag{36}$$

where the upper and lower signs correspond to the ordinary wave and the extraordinary, respectively. It can be seen that, when the QL approximation is valid, the two characteristic waves are circularly polarized.

The behavior of the waves under the QL conditions has been widely studied. Hagn presented various absorption curves under these conditions, which indicate that the differential absorption between the ordinary and the extraordinary waves is not as great for QT as for QL.[13] This further indicates that, as far as absorption is concerned, the ordinary wave is superior to the extraordinary under conditions varying from QT to QL.

C. APPLICATION AND SCOPE

1. Antenna and Wave Mode

The work on the magneto-ionic theory leading to the Appleton formula and the discussion of certain of its properties thereafter suggest that of the two characteristic waves, which when launched into the ionosphere will return to earth with their polarizations unchanged, the ordinary wave is the better mode, because it suffers less attenuation over the whole path length than the extraordinary wave.

A horizontal half-wave dipole is a convenient and suitable antenna for either transmission or reception of a radio wave over the QT-short-range ionospheric path near the geomagnetic equator. This mode of radio propagation is deemed necessary in jungle communication where the ground-wave (lateral wave) mode is too heavily attenuated to be effective over a communication circuit greater than a few kilometers. It can be seen from Eqs. (12), (23b), and (24b) and Fig. 2 that, for launching or receiving the characteristic ordinary wave, a dipole should be aligned with the magnetic meridian and, for the extraordinary wave, the dipole should be oriented perpendicular to the magnetic meridian. In general, when the communication circuit is in the northern hemisphere, the wave polarization is tilted some degrees east of magnetic north.[14] The dipole may have to be oriented accordingly to achieve a somewhat better result. One should return to the conditions of the QT approximation and consider the scope of variables within which the assumption of QT propagation is valid.

2. Frequency

The first variable to be discussed is the range of frequencies appropriate to short-range communication via the ionosphere. In general, when fading and radio noise are not considered, the orientation of an antenna is most significant for short paths near the geomagnetic equator, where one must carefully consider the polarization of the down-coming radio waves and where differential absorption between the ordinary wave and the extraordinary is significant. For ranges up to several hundred kilometers, this implies use of a frequency a little below the critical

frequency (a function of time of day) of an appropriate layer where the vertically incident wave is reflected.

3. Azimuthal Range

The critical parameter in determing the region of applicability of the QT approximation is the angle θ made by the wave normal with the earth's magnetic field. At certain angles of elevation, which vary smoothly with azimuth, either the up-going or the down-coming radio wave will cross the lower boundary of the ionosphere in a direction at right angles to the earth's magnetic field. Such a relation is given in Fig. 8,[15] where one can readily obtain an angle of elevation for the entirely transverse propagation in a given azimuthal bearing.

From the knowledge of Δ - ε - ϕ relations and for an appropriate height of reflection, the approximate ground range along various bearings may be obtained for different values of magnetic inclination. This is done by assuming the simple ray tracing illustrated in Fig. 9; the results are obtained in Figs. 10, 11, and 12 for the entirely transverse propagation via the E region and the F1 and F2 layers, respectively. The actual path traced by the wave propagating in an ionosphere under the influence of the earth's magnetic field is, in fact, governed by a much more complicated mechanism which can be described by ray tracing.[16]

For the case of QT propagation, the value of an angle θ may be slightly modified; the ground range, instead of a definite distance along the ground, is obtained for a particular set of conditions of propagation. By substituting the relations $Y_T = Y \sin \theta_T$ and $Y_L = Y \cos \theta_T$ into the conditions for the QT approximation, we obtain:

$$\frac{Y_T^4}{4Y_L^2} = \frac{Y^2 \sin^4 \theta_T}{4(1 - \sin^2 \theta_T)} \gg |(1 - X - iZ)^2|$$

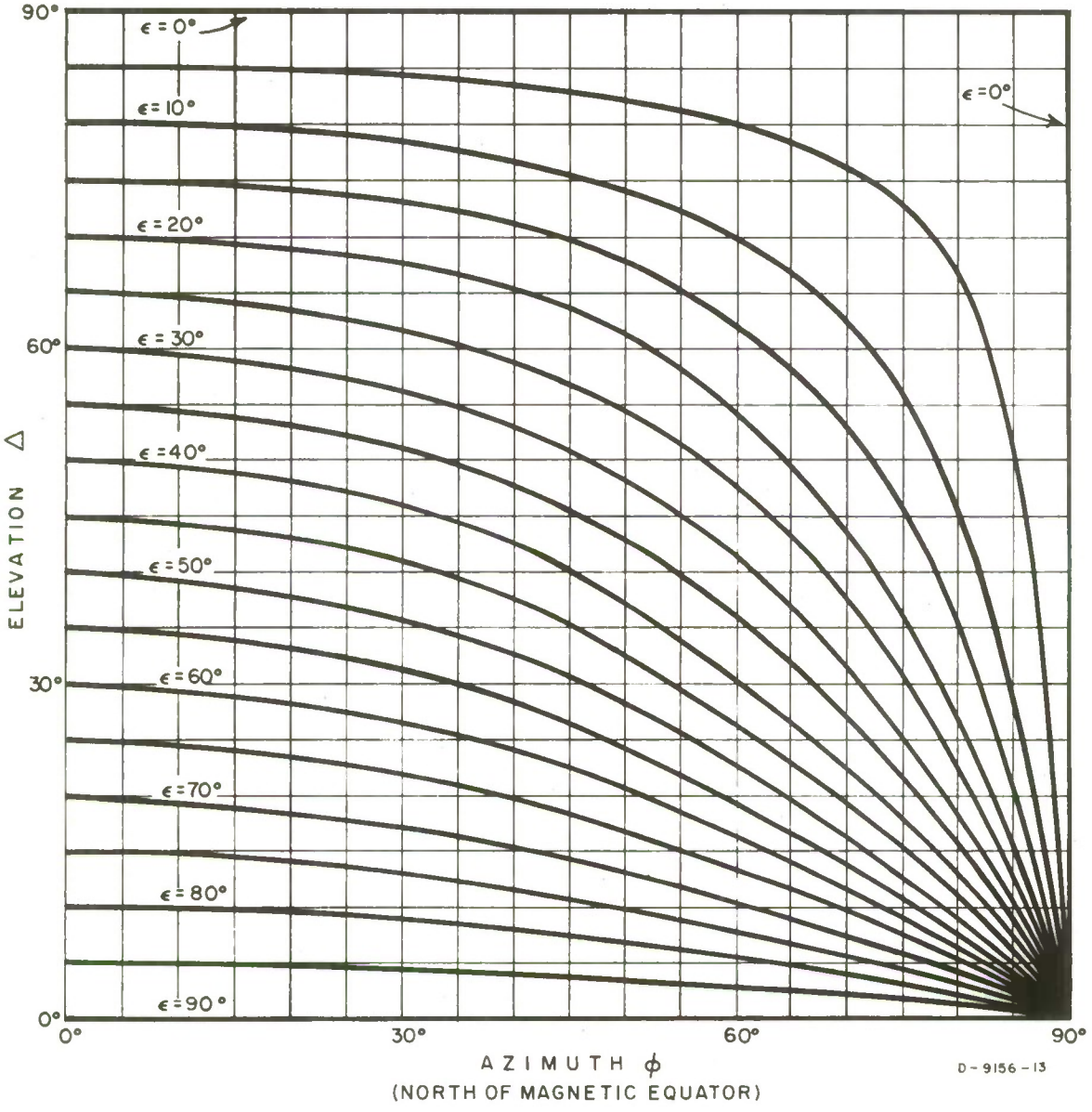

FIG. 8 DIRECTIONS FOR PROPAGATION TRANSVERSE TO EARTH'S MAGNETIC FIELD OF DIP ANGLE ϵ

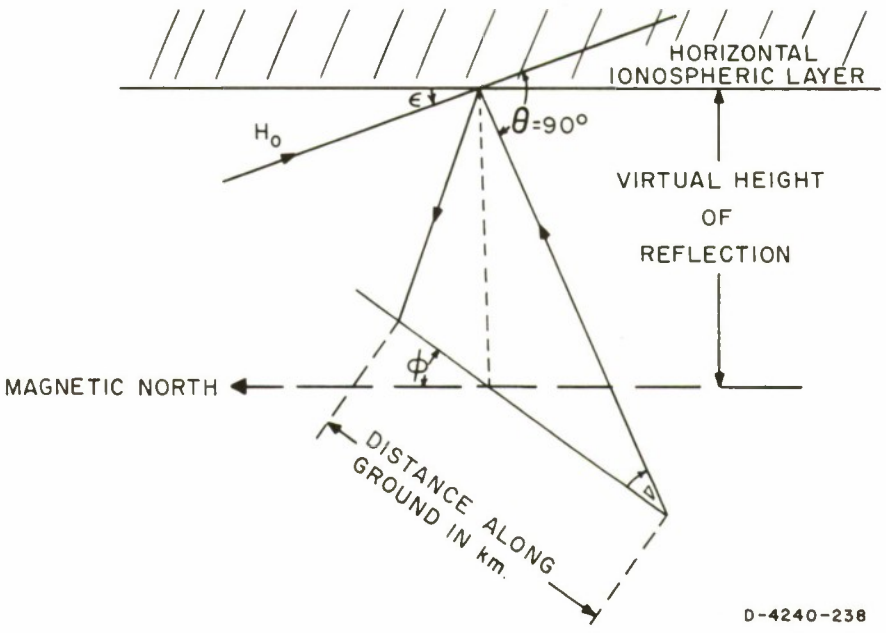

FIG. 9 SIMPLE RAY TRACING FOR ENTIRELY TRANSVERSE PROPAGATION

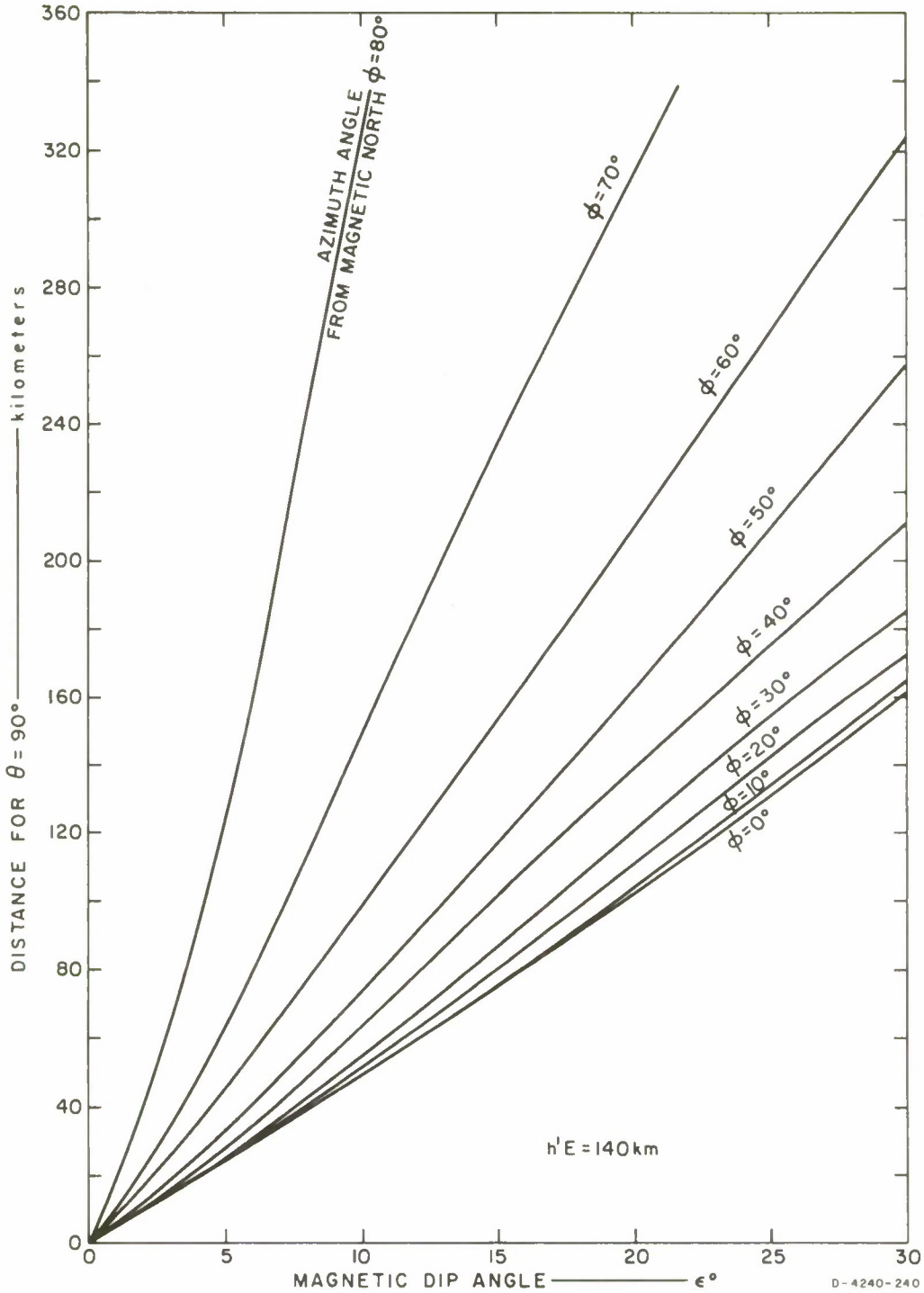

FIG. 10 DISTANCE FOR $\theta = 90°$ AS A FUNCTION OF MAGNETIC DIP ANGLE, E REGION

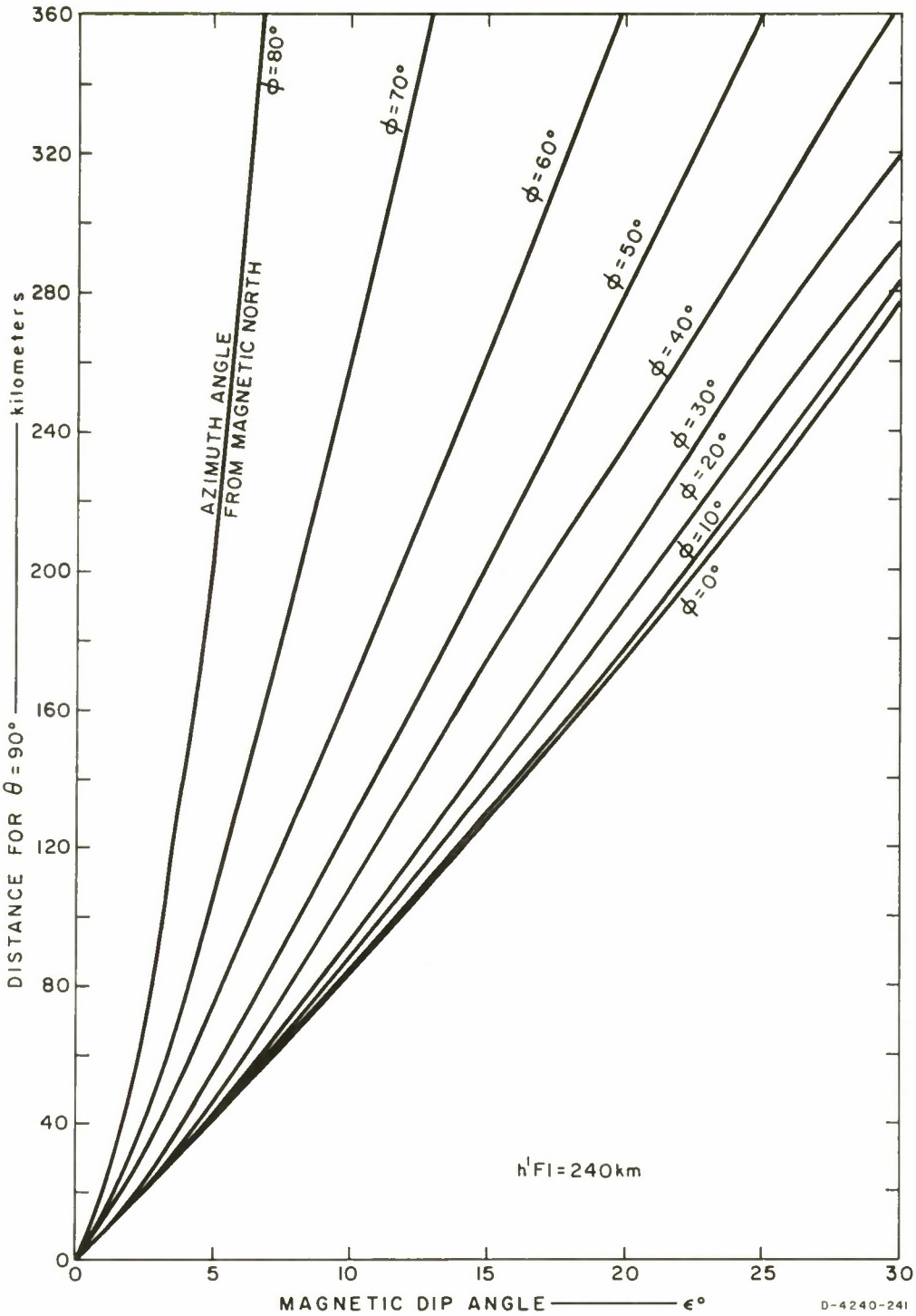

FIG. 11 DISTANCE FOR $\theta = 90°$ AS A FUNCTION OF MAGNETIC DIP ANGLE, F1 LAYER

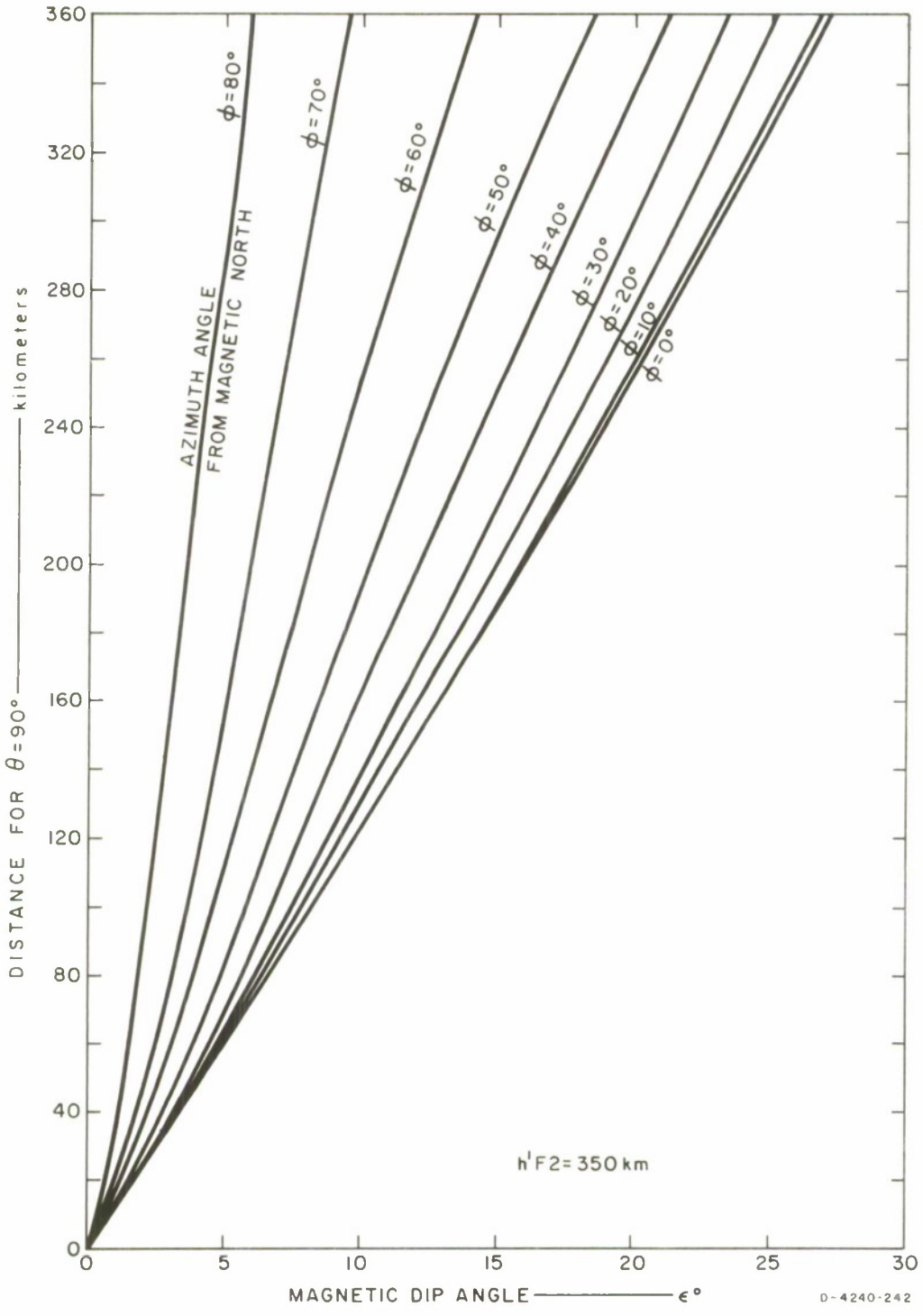

FIG. 12 DISTANCE FOR $\theta = 90°$ AS A FUNCTION OF MAGNETIC DIP ANGLE, F2 LAYER

or

$$\frac{\sin^4 \theta_T}{1 - \sin^2 \theta_T} >> \left(\frac{2}{Y}\right)^2 \left|(1 - X - iZ)^2\right| \quad .$$

It is sufficient[7,17] to take

$$\frac{\sin^4 \theta_T}{1 - \sin^2 \theta_T} = 10A \quad , \tag{37}$$

where

$$A = \left(\frac{2}{Y}\right)^2 \left|(1 - X - iZ)^2\right| \quad ,$$

as the conditions for the QT approximation.

The quadratic equation $\sin^4 \theta_T + 10A \sin^2 \theta_T - 10A = 0$ may be solved to give:

$$\sin^2 \theta_T = -5A \pm \sqrt{25A^2 + 10A}$$

$$= -5A \pm 5A\left[1 + \frac{1}{2} \times \frac{10}{25A} - \frac{1}{8}\left(\frac{10}{25A}\right)^2 + \frac{1}{16}\left(\frac{10}{25A}\right)^3 - \ldots\right]$$

$$\simeq -5A \pm 5A\left(1 + \frac{1}{5A} - \frac{1}{50A^2}\right)$$

$$\simeq 1 - \frac{1}{10A}$$

$$\sin \theta_T \simeq \left[1 - \frac{1}{10A}\right]^{1/2}$$

Hence,

$$\theta_T \simeq \sin^{-1}\left(1 - \frac{1}{20A}\right) \quad , \tag{38}$$

where

$$A = \left(\frac{2}{Y}\right)^2 \left|(1 - X - iZ)^2\right| \quad .$$

A modification of θ from 90° generally means an increase in the range of communication. The lower the wave frequency, the greater is the QT zone on either side of the distance for entirely transverse transmission and reception.

For the QL approximation, one takes:

$$\frac{\sin^4 \theta_L}{1 - \sin^2 \theta_L} = \frac{A}{10} \quad , \tag{39}$$

which may be solved to give:

$$\sin^2 \theta_L = -\frac{A}{20} \pm \frac{A}{20}\sqrt{1 + \frac{40}{A}} \quad , \tag{40}$$

where θ_L is the angle at which the QL approximation becomes valid.

For $\theta_L < \theta < \theta_T$, neither approximation holds, and both characteristic waves are elliptically polarized, with the ordinary mode being the stronger component. Thus, within this range of θ, the ordinary wave is to be preferred to the extraordinary.

The problem can now be considered more specifically. The QT approximation should be applied at the approximate height of 80 km where the wave enters the ionosphere. At this height over Bangkok, Thailand, we have

(1) Magnetic field of 0.4 Gauss with approximately zero declination and 10.5° of dip angle:

$$f_H = 2.8 \times 0.4 = 1.12 \text{ MHz}$$

and

$$Y = \frac{1.12}{f} \text{ , f in MHz} \quad .$$

(2) Electron density (daytime) of 3×10^9 m^{-3}:

$$X = \frac{80.61\ N}{(f \times 10^6)^2} = \frac{0.2418}{f^2} \quad .$$

(3) Collision frequency of 2×10^6 Hz^{-1}:

$$Z = \frac{\nu}{2\pi f \times 10^6} = \frac{0.318}{f} \quad .$$

By using the above values and Eqs. (38) and (40), one finally arrives at the results shown in Table I.

Table I

VARIATION IN θ_T WITHIN QT CONDITION

f (MHz)	X	Y	Z	A	θ_T (Deg.)	$\delta\theta_T$ off 90° (Deg.)	$\epsilon \pm \delta\theta_T$ (Deg.)	θ_L (Deg.)	$\epsilon + \delta\theta_L$ (Deg.)
1.7	0.0836	0.66	0.1870	8.03	83.6	6.4	4.1-16.9	49.8	50.7
3	0.0209	0.33	0.0935	35.50	87.0	3.0	7.5-13.5	64.4	36.1
5	0.0093	0.22	0.0623	81.50	88.0	2.0	8.5-12.5	71.6	28.9

The angle $\delta\theta_T$ by which θ_T is allowed to differ from 90° is, in effect, similar to allowing the dip angle to vary by the same amount in order to keep the same elevation angle, Δ, for $\theta = 90°$. The azimuthal range can thus be obtained for a particular reflecting layer of the ionosphere from the appropriate curve in Figs. 10, 11, or 12, by reading off ground distances in kilometers at $\epsilon \pm \delta\theta_T$ for various azimuth angles. Azimuthal ranges covering the Bangkok area are obtained in Table II and Figs. 13 through 18 for various frequencies and ionospheric layers. As mentioned previously, it is reasonable to expect the ordinary wave to predominate

Table II

AZIMUTHAL QT RANGE OVER BANGKOK AREA

ϕ	1.7 MHz		3 MHz		5 MHz	
	E region	F1 Layer	E Region	F1 Layer	F1 Layer	F2 Layer
0^0	20-86, 342*	33-143, 588	37-67, 204	63-116, 350	72-107, 267	104-156, 385
10^0	20-88, 351	33-144, 601	37-68, 206	64-117, 355	72-108, 272	104-156, 392
20^0	21-92, 379	34-152, 650	38-72, 215	65-123, 370	75-113, 284	109-166, 409
30^0	22-100, 404	34-164, 692	40-78, 235	68-131, 404	78-120, 310	116-176, 446
40^0	23-116, 454	36-194, 778	45-90, 261	76-156, 450	89-142, 350	133-207, 504
50^0	26-135, 539	42-224, 922	53-104, 311	91-178, 535	106-164, 410	160-247, 599
60^0	36-176, 682	56-292, >1000	72-136, 406	120-233, 700	139-214, 522	211-318, 762
70^0	49-266, 1000	80-420, >1000	105-208, 575	180-380, 985	212-344, 753	312-510, >1000
80^0	94-465, >1000	145-798, >1000	220-358, 1000	390-606, >1000	380-570, >1000	553-832, >1000

* 20-86, 342 signifies: The range under QT condition is between 20 and 80 km,
The range under QL condition is from 342 km and up.

Values assumed: $h'E = 140$ km; $h'F1 = 240$ km; $h'F2 = 350$ km.
ϵ over Bangkok area = 10.5^0.

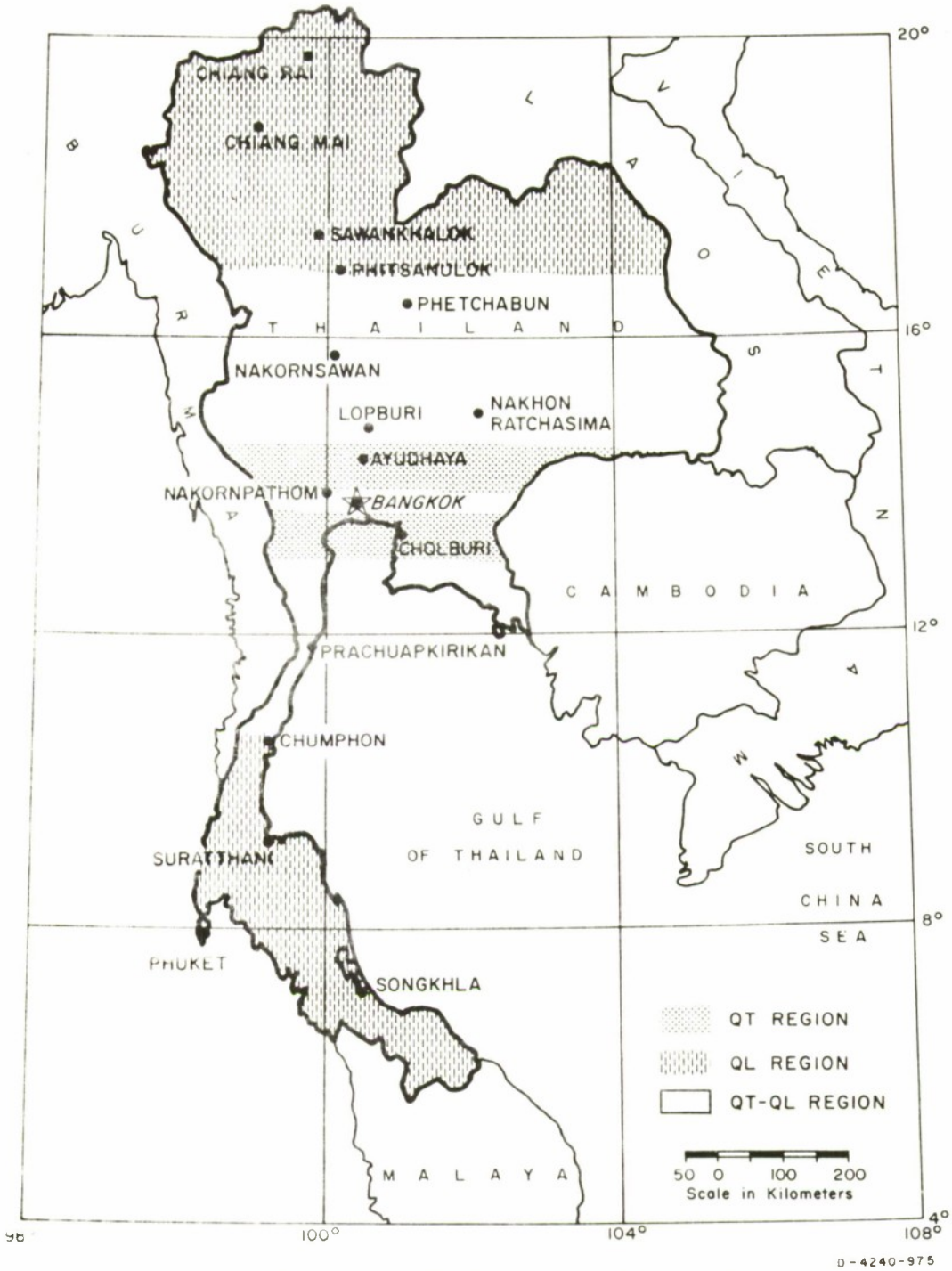

FIG. 13 AZIMUTHAL RANGE OVER BANGKOK AREA, 1.7 MHz, E REGION

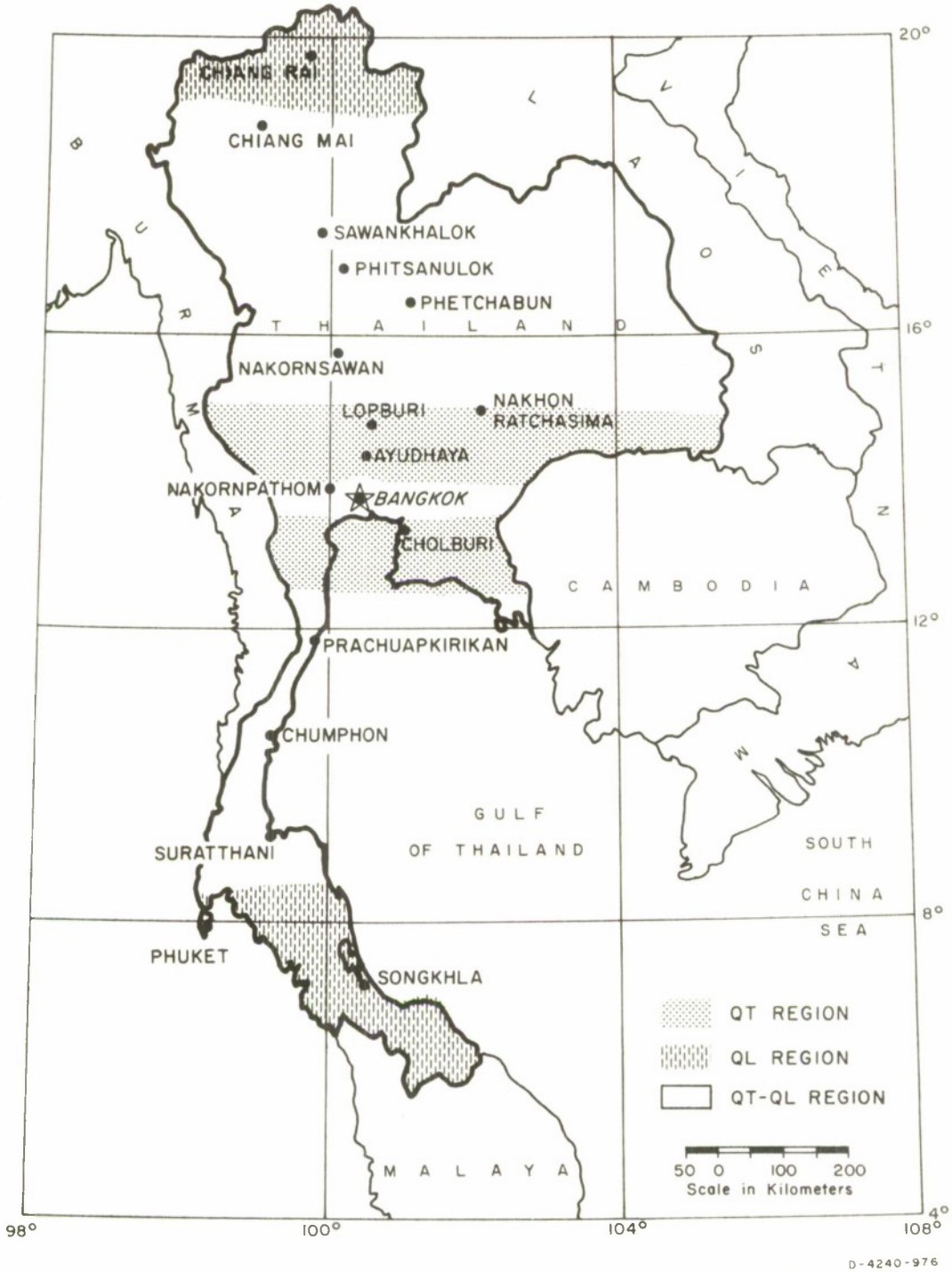

FIG. 14 AZIMUTHAL RANGE OVER BANGKOK AREA, 1.7 MHz, F1 LAYER

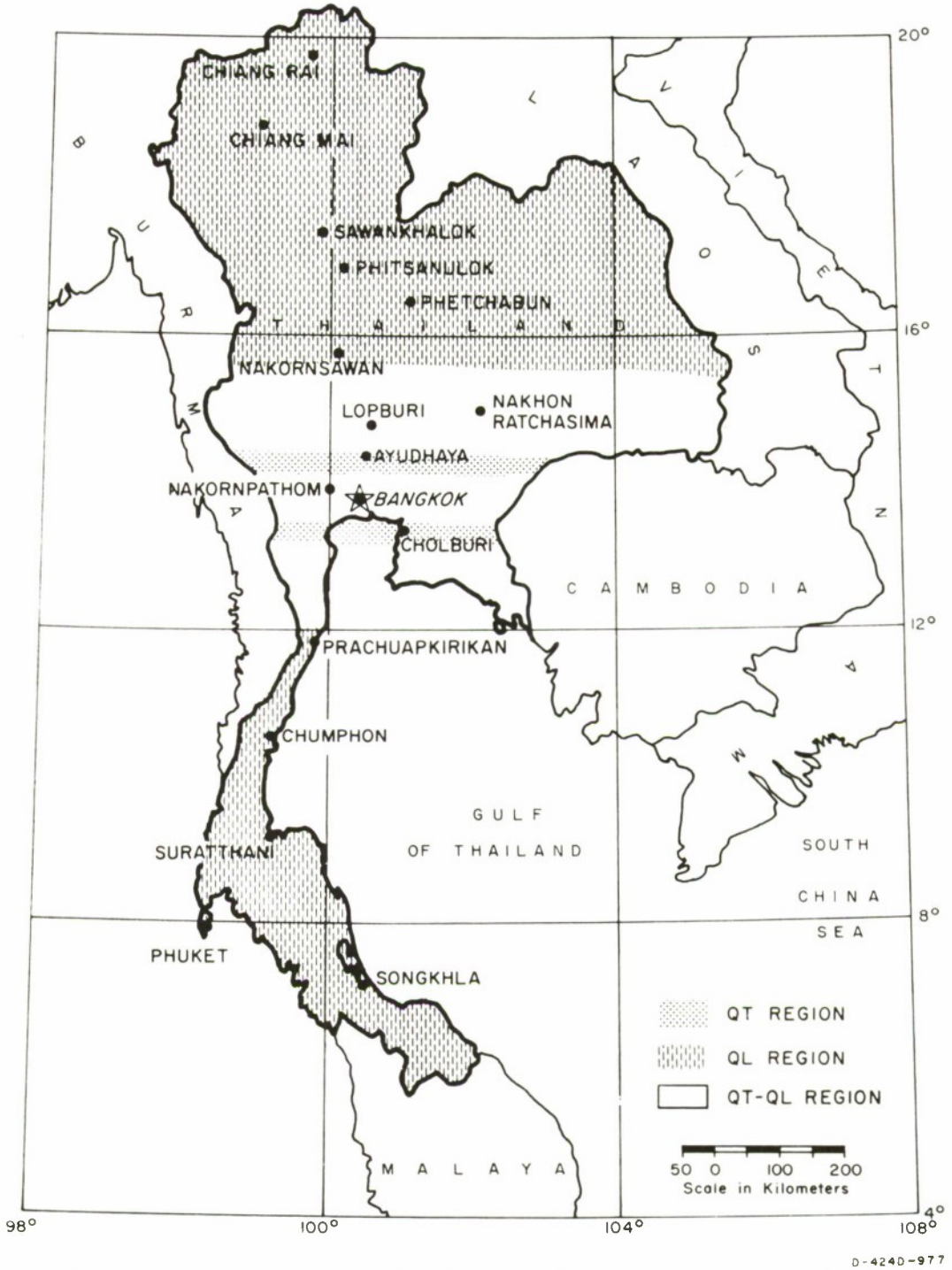

FIG. 15 AZIMUTHAL RANGE OVER BANGKOK AREA, 3 MHz, E REGION

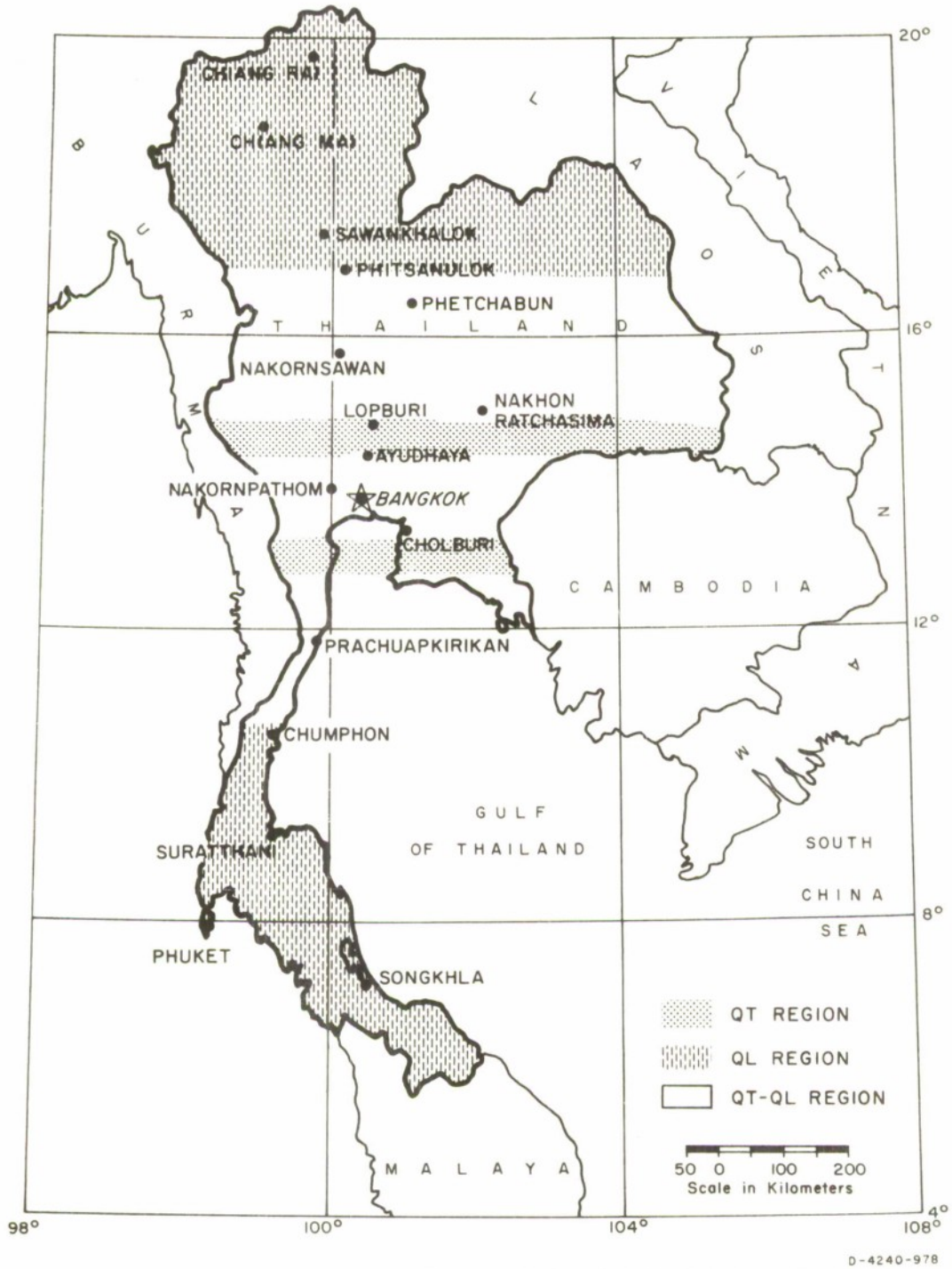

FIG. 16 AZIMUTHAL RANGE OVER BANGKOK AREA, 3 MHz, F1 LAYER

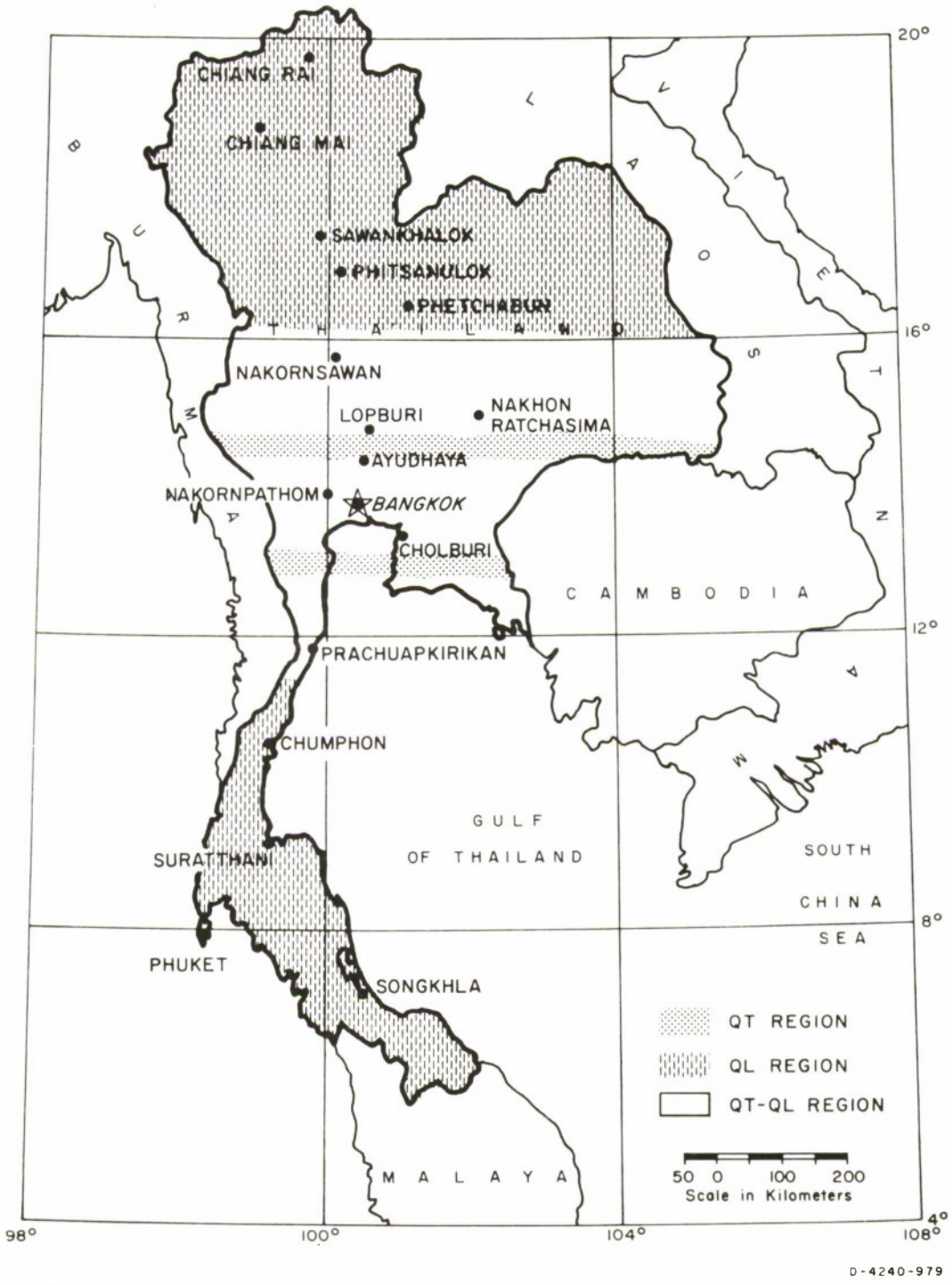

D-4240-979

FIG. 17 AZIMUTHAL RANGE OVER BANGKOK AREA, 5 MHz, F1 LAYER

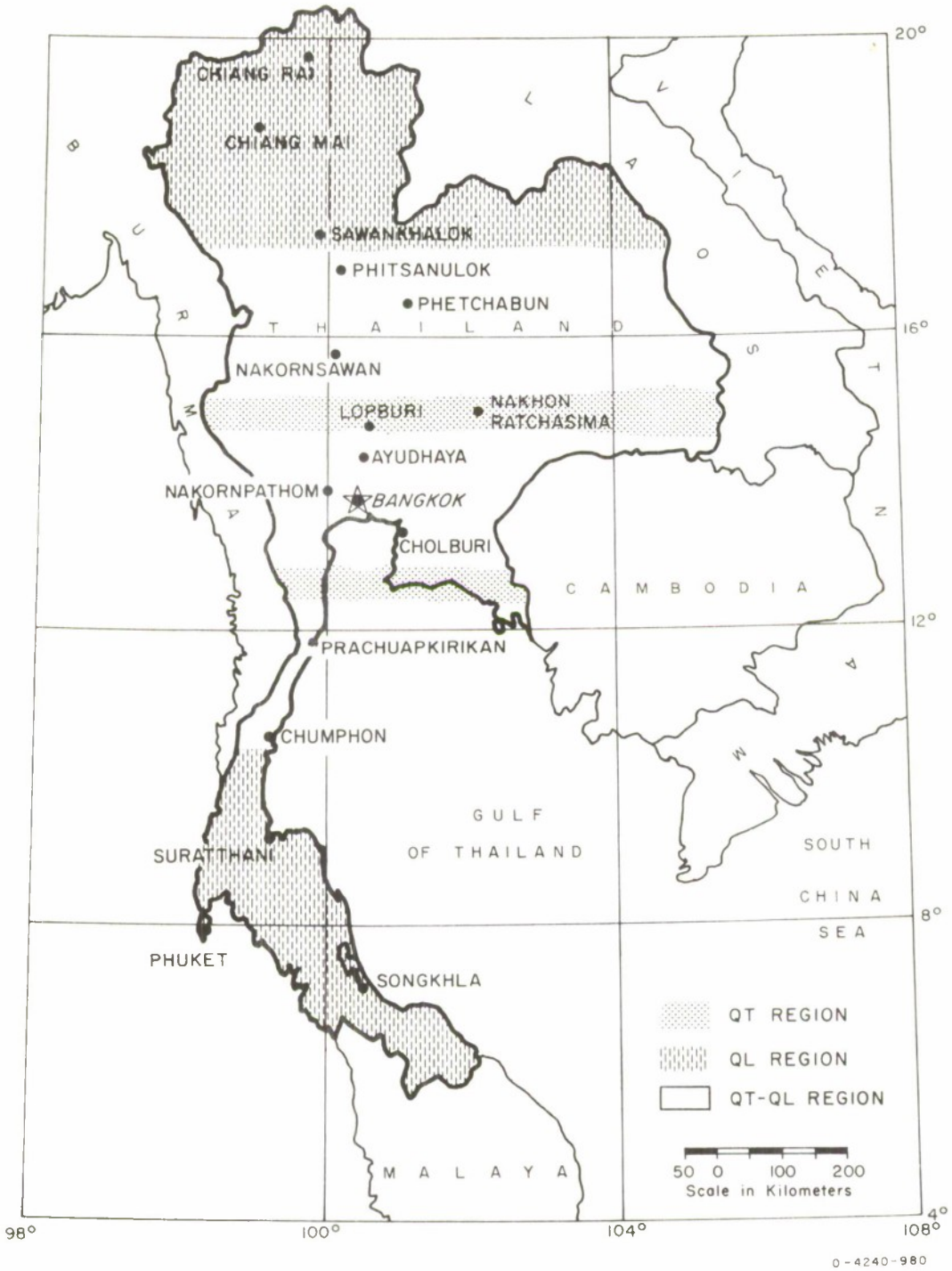

FIG. 18 AZIMUTHAL RANGE OVER BANGKOK AREA, 5 MHz, F2 LAYER

even outside the QT regions and up to the QL boundary. It can be seen then that, from magnetoionic considerations, one may use the ordinary wave for both transmission and reception via the ionosphere for ranges far exceeding those (say 100 km) expected for short-range communication purposes.

4. Dipole Orientation

The foregoing discussions, based on wave absorption and polarization considerations, indicate that many short-range sky-wave communication paths near the magnetic equator satisfy the QT conditions where the wave propagation may be optimized by the proper orientation of a horizontally and linearly polarized antenna to transmit or to receive a characteristic wave. Normally, the ordinary wave would be desirable, and an antenna such as a horizontal half-wave dipole should be placed in line with the magnetic meridian. During certain periods of the day, however, the extraordinary wave of a particular frequency may be more stable or less absorbed and hence more efficient than the ordinary wave (e.g., when the wave frequency is very near the ordinary-wave critical frequency); in such a case, a horizontal half-wave dipole should be aligned orthogonal to the magnetic meridian. When the magnetic dip is appreciable, the characteristic waves emerging from the ionosphere in the northern magnetic hemisphere will generally have their major axes in the NE-SW pair of quadrants;[14] horizontal dipoles should then be aligned with the polarization ellipse major axis. This may prove to be unnecessary and even undesirable, because dipoles of such orientation would be subject to polarization fading caused by the ordinary and the extraordinary modes beating together. The dipole placed in the NE-SW direction, however, may be suitable as a transmitting antenna when a type of polarization diversity is employed with two orthogonal receiving dipoles in the N-S and E-W directions, since the NE-SW dipole in the geomagnetic regions north of the geomagnetic equator will launch both the ordinary wave and the extraordinary.

D. PROPOSED INVESTIGATIONS

Optimum orientation of both the transmitting and the receiving antennas for sky-wave communication would be very beneficial to the tactical planning of a radio communication system. Investigations should therefore be carried out to prove the existence of such a preferred orientation. Any wave propagating through the ionosphere may be considered as being composed of two characteristic waves, the ordinary and the extraordinary. For geomagnetic regions such as Thailand, two orthogonally crossed dipoles, one aligned N-S and the other aligned E-W, could be used at a test location for either transmitting or receiving. The tests should be made with either of the two dipoles in the following transmitting/receiving antenna combinations: N-S/N-S, N-S/E-W, E-W/N-S, and E-W/E-W. These four combinations would give information on the performance of the ordinary mode in comparison with that of the extraordinary and on the mode conversion of one characteristic wave to the other.

To check the expected superiority of the ordinary wave in an efficient manner, the tests should be conducted over the N-S path. With no differential absorption of one characteristic mode relative to the other, i.e., with no optimum orientation, one would expect the E-W/E-W transmitting/receiving antenna combination to be better than the N-S/N-S for the N-S communication path because of antenna pattern effects as shown in Fig. 19. These pattern effects show the "worse-case" loss in dB when using the transmitting and receiving dipoles oriented end-on to each other instead of the usual arrangement of having them oriented broadside to each other. Circuits of other azimuth bearings would provide additional information on performance and ranges. Thus, we seek to determine at what range the antenna pattern effects begin to predominate over the differential ionospheric absorption effects. In other words, at what range, for a given frequency, path, time of day, etc., should one abandon orienting dipoles to take advantage of the lesser absorption of the ordinary wave and go back to the classical broadside-to-broadside dipole alignment.

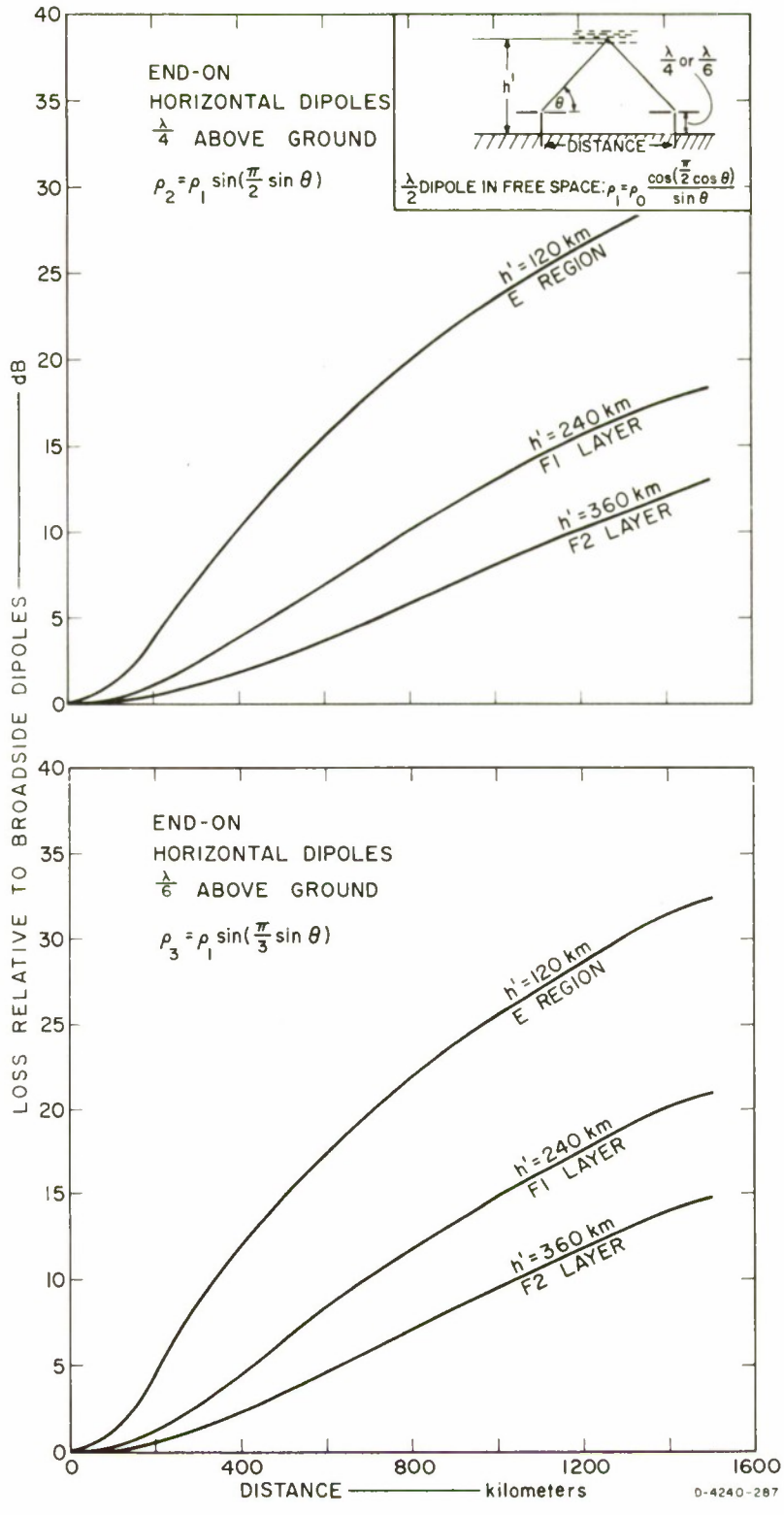

FIG. 19 RADIATION PATTERN EFFECTS

III CW MEASUREMENTS

A. PURPOSE

Two methods in general use for ionospheric investigations are CW recording and the pulse technique.[18] In addition to simplicity, the CW method has the advantage of giving a continuous record of fading characteristics. Some information on mode coupling also may be obtained from the CW data. The method has the disadvantage, however, of not providing a means for distinguishing various paths and modes of propagation, because it gives only the resultant effects.

Measurement and analysis were carried out by both methods with the purpose of discovering whether there is an optimum orientation of horizontal half-wave dipoles for short-range HF communication via the ionosphere in the region of the geomagnetic equator. This section discusses the CW measurements that were made in Thailand between 29 December 1963 and 31 January 1964.

B. TEST PROCEDURE AND DATA REDUCTION

1. Instrumentation

The requirements of the CW measurements were: the recording equipment must be able to respond to most of the rapid fadings expected; it must be simple to operate and to calibrate; and antenna switching and CW keying must be automatic. A block diagram of the CW receiver and transmitter setup is shown in Fig. 20. Photographs of the sites and apparatus appear in Figs. 21 through 24. A list of the equipment and its specifications follows.

a. Receiver

Type	R-390A/URR
Frequency range	Continuous tuning 0.5-32 MHz
Bandwidth	2 kHz

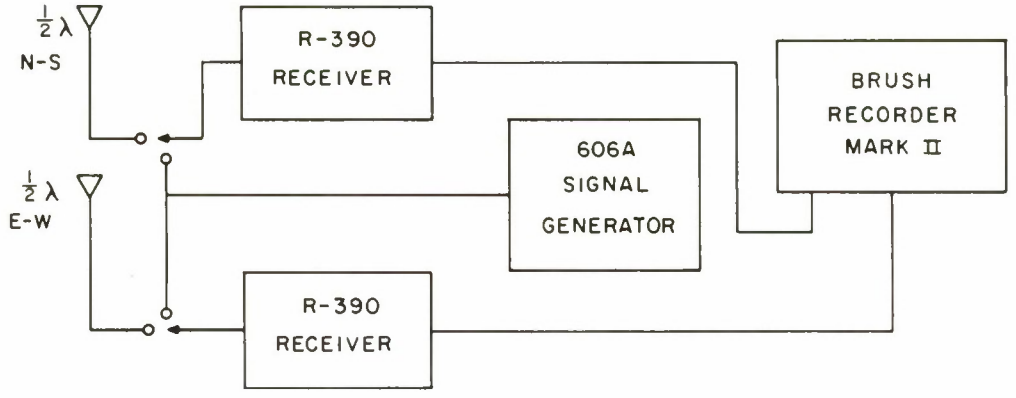

RECEIVER

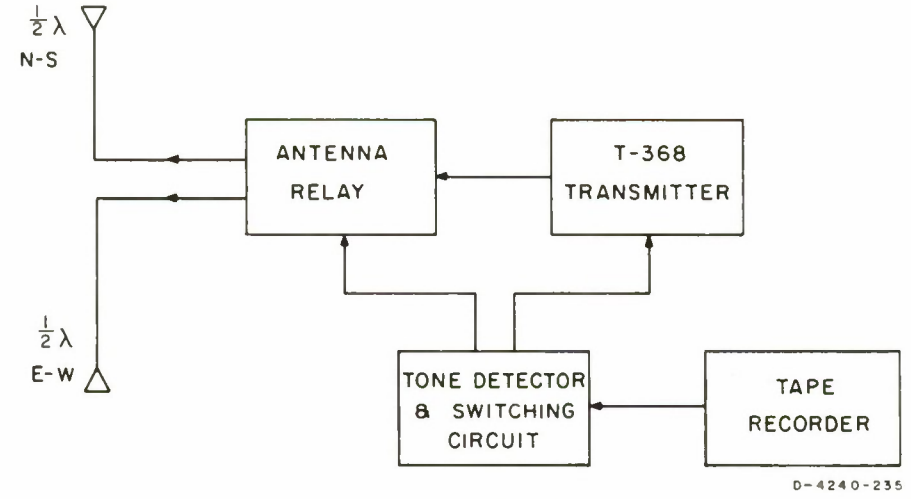

TRANSMITTER

FIG. 20 BLOCK DIAGRAM OF CW TEST SETUP

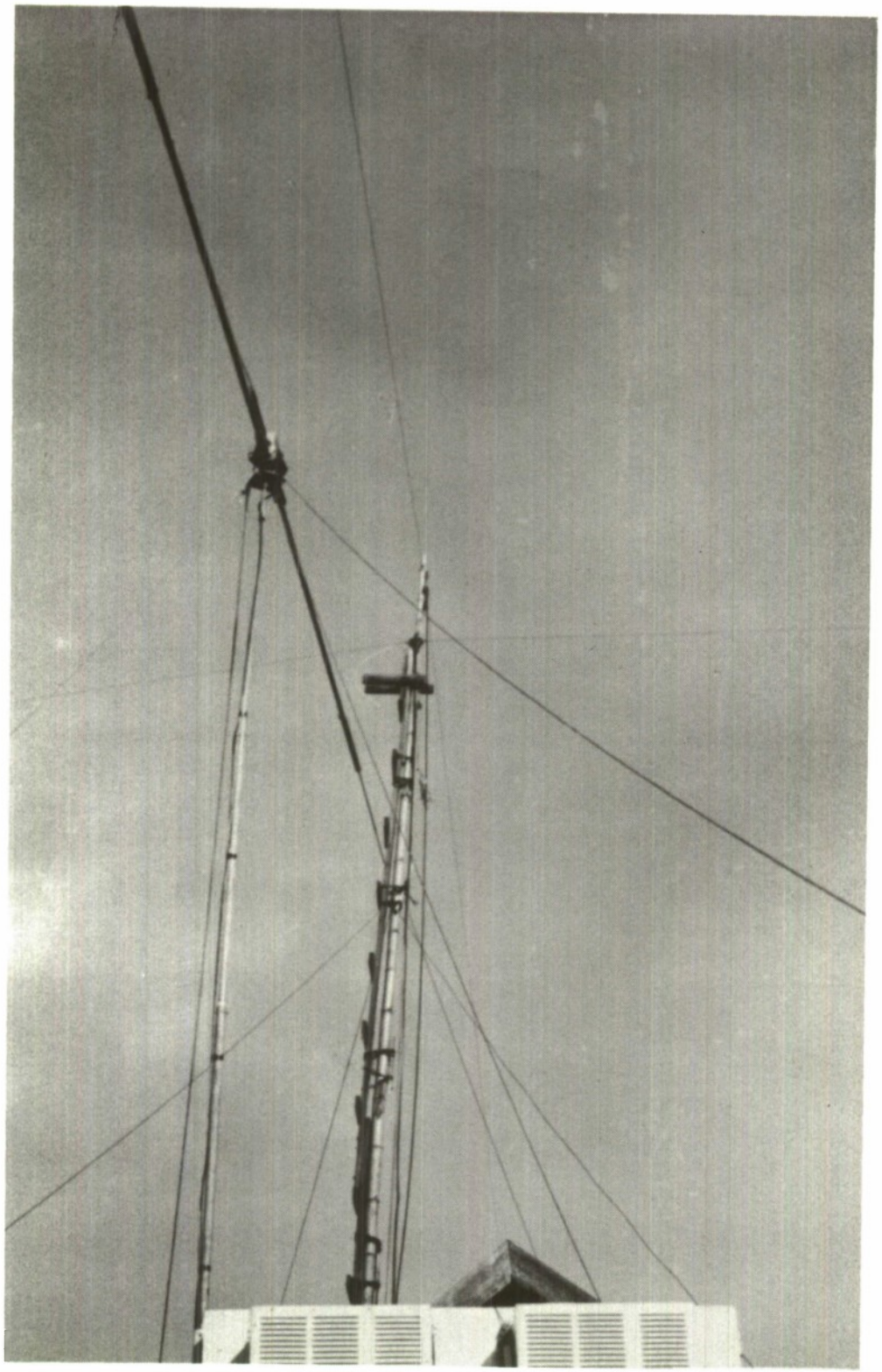

D-4240-982

FIG. 21 CLOSEUP PHOTOGRAPH OF ORTHOGONALLY CROSSED DIPOLES

FIG. 22 PHOTOGRAPH OF RECEIVING SITE AT AYUDHAYA

FIG. 23 PHOTOGRAPH OF RECEIVING SITE AT NAKORNPATHOM

D-4240-984

FIG. 24 PHOTOGRAPH OF CW RECORDING OPERATION

Control	Wide audio response; fast AGC; limiter off Manual gain control used Maximum RF gain setting and optimum antenna trim always used.

b. Signal Generator

Type	Hewlett-Packard (H-P) Model 606A
Frequency	50 kHz through 65 MHz

c. Recorder

Type	Brush Recorder Mark II
Sensitivity	1 Volt/chart line
Speed	1 mm/s

d. Transmitter

Type	T-368 C/URT
Frequency range	Continuous tuning, 1.5-10 MHz
Output	400 Watts, CW into dummy load

e. Antenna

Equipment	At each location, transmitting or receiving: two horizontal half-wave crossed dipoles
Elevation above ground	1/6 wavelength
Alignment	One dipole with magnetic N-S, the other with magnetic E-W
Radiation pattern	Vertical main beam.

f. Tape Recorder

Type	Sony Model 101
Taped message	Two tones, 700 and 4000 Hz, superimposed for operation of the two-tone detector.

g. Filter

Type	Spencer-Kennedy Laboratory, Model 302 variable electronic filter
Usage	One filter interconnected to give a band-pass to 700-Hz tone, the second filter to give a band-pass to 4000-Hz tone.

h. Two-Tone Detector and Relay Driver

Equipment	See Fig. 25 for setup of two-tone detectors and relay drivers with tape recorder and appropriate filters.
Usage	Automatic keying of antenna and transmitter relays. When the 700-Hz tone recorded on the tape is detected, the RF output is switched to the E-W antenna; in the absence of the 700-Hz tone, the RF output is switched to the N-S antenna. When the 4000-Hz tone is detected, the CW transmitter is keyed on; in the absence of the 4000-Hz signal, the CW transmitter is off.

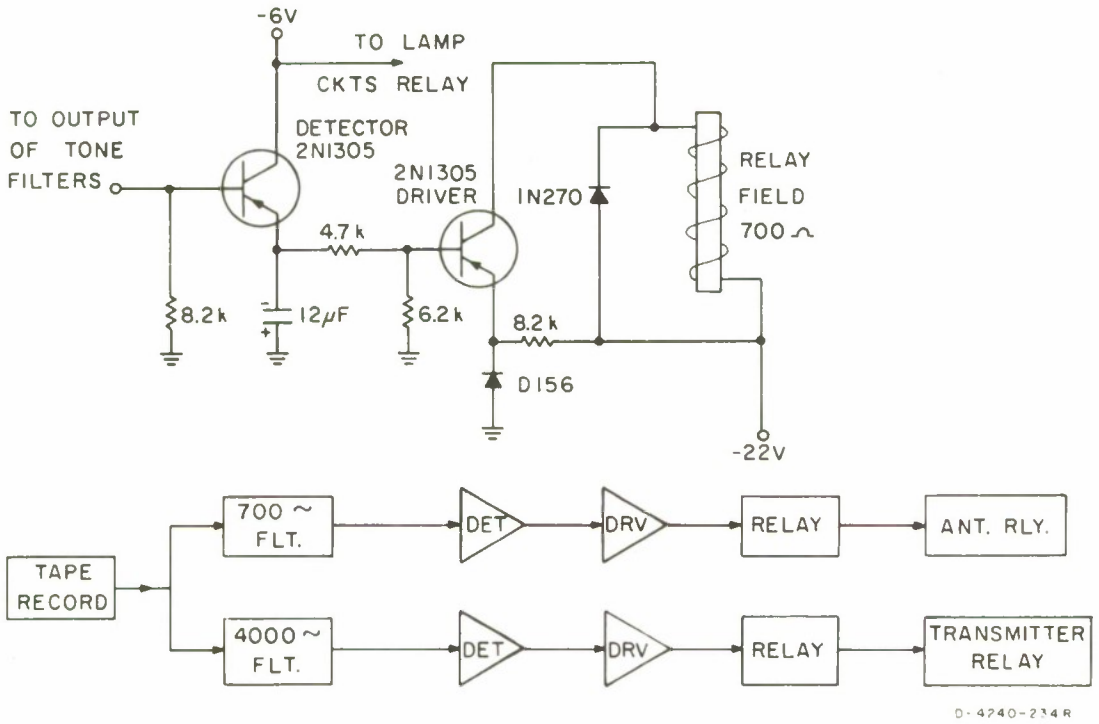

FIG. 25 CIRCUIT DIAGRAM OF TWO-TONE DETECTOR AND RELAY DRIVER

i. Communication Between Test Sites

Equipment	Collins Model KWM-2A HF single-sideband transceiver
Antenna	Hy-Gain Hustler, horizontal dipole, tunable and rotatable
Frequency	Approximately 3.4 MHz at all hours.

2. Test Procedure

The test involved CW transmission from Bangkok and simultaneous recordings of the reception at Ayudhaya and at Nakornpathom (at Srakatiam village), which are approximately 65 km due north and due west of Bangkok, respectively. The two test circuits were chosen to give N-S and E-W paths that were the extremities of transmitting-receiving azimuth bearings. Figure 26 is a map of the test sites. The test was carried on for five days on each of the following frequencies: 1.7, 3, 5, and 10 MHz. Each run consisted of a test for 4 min 20 sec, followed by a break for 10 min 10 sec, repeated four times in an hour in the following manner:

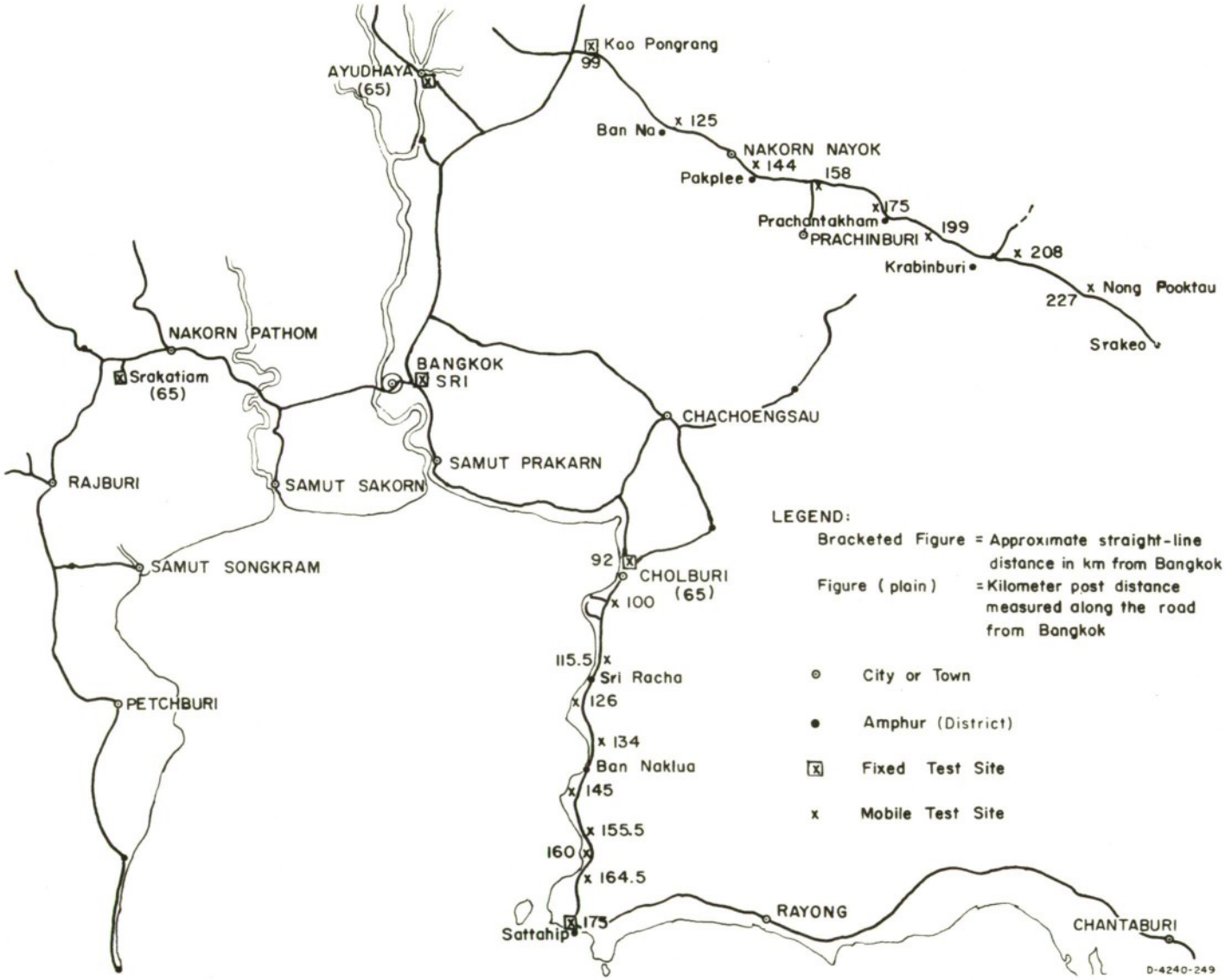

FIG. 26 MAP OF TEST SITES

(x - 1) h 53 min 00 sec	N-S antenna on	E-W antenna off
(x) h 05 min 00 sec	Transmission on	
07 min 00 sec	Transmission off	
07 min 10 sec	N-S antenna off	E-W antenna on
07 min 20 sec		Transmission on
09 min 20 sec		Transmission off
09 min 30 sec	N-S antenna on	E-W antenna off
19 min 30 sec	Transmission on	
21 min 30 sec	Transmission off	
21 min 40 sec	N-S antenna off	E-W antenna on
.		
etc.		
.		
53 min 00 sec	N-S antenna on	E-W antenna off

A standard 1-hour/1200-ft tape of the two-tone message was used for the above programming. It was rewound and the hourly cycle was resumed at (x + 1) h 05 min 00 sec.

Warning lights, which were lit when antenna and transmitter relays were actuated, together with the KWM-2A transceivers, were provided for data synchronization between the three test sites.

The transmitted signal was simultaneously received by the crossed N-S and E-W dipoles, which fed into separate receivers, the diode load outputs of which were then recorded on the two-channel Brush recorder.

3. Data Reduction

Because of the considerable amount of CW data obtained in an inconvenient form for informative displays (see Fig. 27), the following method was devised for the reduction of such data into readily meaningful forms. Let a random variable ξ have a continuous range (0, A) of possible values x with the probability density $P\xi(x)$, and let the range be divided into k divisions each of length $\Delta x = A/k$. Suppose that a sufficiently large number of trials $M = N_1 + N_2 + \ldots N_i + \ldots N_k$ is made and that of this number one finds N_i successes for ξ falling in

BANGKOK TO AYUDHAYA – 1.7 MHz
30 DEC. 1963 0834-0839 LOCAL TIME

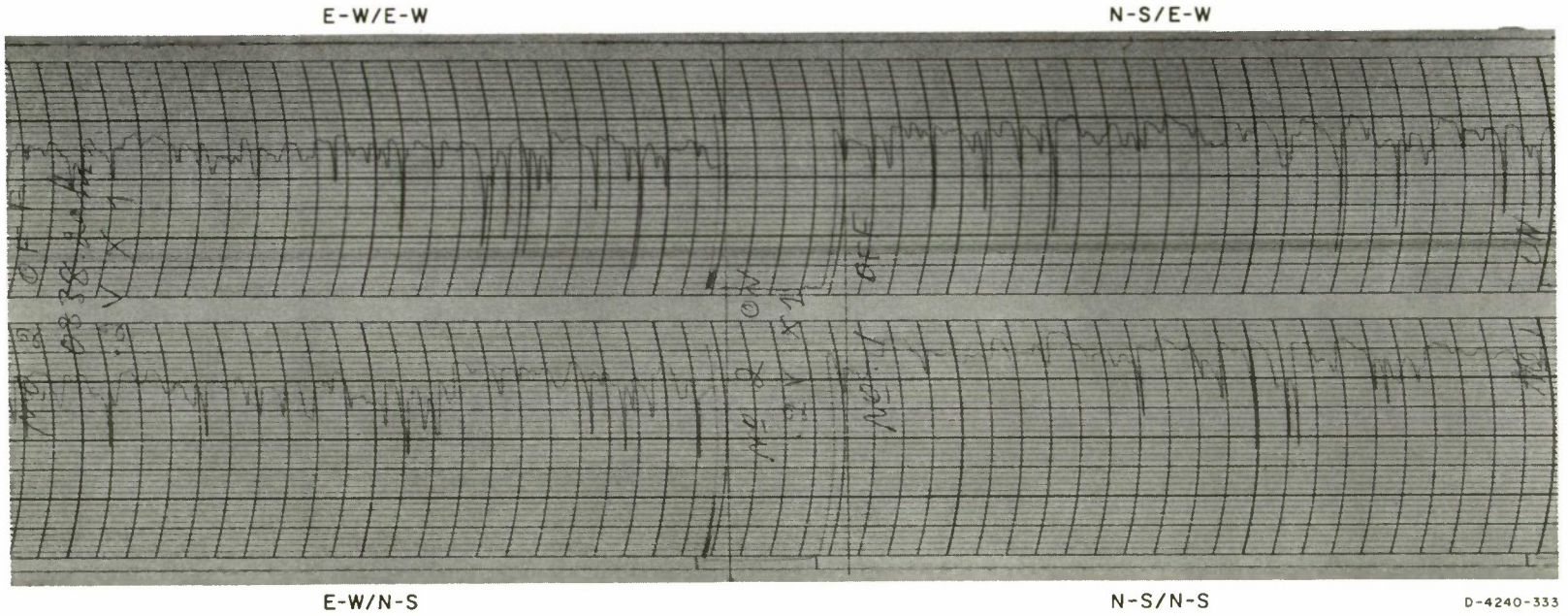

FIG. 27 SAMPLE OF CW RECORDING

$[(i - 1), i\Delta x]$, where $N_i\big|_{i=1,2 \ldots k}$ is nonzero. If Δx is small enough, one may assume that N_i observations are each of the same value $i\Delta x$ and that the experimental mean value of ξ per trial is given by

$$\xi(\text{mean}) = \frac{1}{M} \text{ (sum of observed values of } \xi \text{ in M trials)}$$

$$= \sum_{i=1}^{k} \frac{i\Delta x \cdot N_i}{M} \tag{41}$$

or

$$\xi(\text{mean}) = \sum_{i=1}^{k} i\Delta x \left(\frac{N_i}{M} \cdot \frac{1}{\Delta x}\right) \Delta x \quad . \tag{42}$$

Since $(N_i/M)/\Delta x$ is an estimate of the probability density $P\xi(x)$, Eq. (42) is an empirical value of the mean of ξ,

$$\overline{\xi} = \int_{o}^{A} xP\xi(x)dx \quad . \tag{43}$$

In the case of measured CW data, the ability to read off signal inputs to the receiver in decibels above 1 μV is essentially limited to the smallest increment of 5 dB. This $\Delta x = 5$ dB is not sufficiently small for the assumption that the N_i observations are each of value $i\Delta x$. The N_i observations are more likely to cluster about the value $[i\Delta x - (\Delta x/2)]$; hence $\xi_{(\text{mean})}$ as given by Eq. (41) would be too high by $\Delta x/2$ dB; i.e., the expression should be modified to

$$\xi'_{(\text{mean})} = \left\{ \sum_{i=1}^{k} \frac{i\Delta x \cdot N_i}{M} \right\} - \frac{\Delta x}{2}$$

$$= \frac{\Delta x}{M} (N_1 + 2N_2 + \ldots + iN_i + \ldots + kN_k) - \frac{\Delta x}{2} \quad . \tag{44}$$

Since $N_1 + N_2 + \ldots N_i + \ldots + N_k = M$, Eq. (46) may be rewritten thus:

$$\xi'_{(mean)} = \frac{\Delta x}{M}(N_1 + 2N_2 + \ldots + kN_k) - \frac{\Delta x}{2}\frac{(N_1 + N_2 + \ldots + N_k)}{M}$$

$$= \frac{\Delta x}{2}\frac{N_1}{M} + \frac{3\Delta x}{2}\frac{N_2}{M} + \ldots + \frac{(2k - 1)\Delta x}{2}\frac{N_k}{M} \quad , \qquad (45)$$

which will equal

$$\bar{\xi} = \frac{1}{M}(x_1 N_1 + x_2 N_2 + \ldots + x_i N_i + \ldots x_k N_k) \quad , \qquad (46)$$

where $\bar{\xi}$ is the mean of ξ for discrete variables

$$x_i = \frac{(2i - 1)\Delta x}{2} \quad , \; i = 1, 2 \ldots k \quad .$$

A random variable ξ having a continuous range (0, A) that is not capable of being subdivided into sufficiently small Δx increments, should be treated in the manner of a discrete random variable, and the mean value should be computed by Eq. (44). The CW recordings belong to this class of random variables. The calibration of data in microvolts per centimeter of deflection was converted into dB above 1 μV/cm. The ordinate was then scaled every 5 dB and noted by the K index, which equals 1, 2, 3, ... , k for decibel ranges 0-5, 5-10, 10-15, ···, 5(k - 1) - 5k, respectively. The signal was read by the K index every 5 seconds of 2-min data and was statistically recorded in the appropriate forms provided, so that the recordings could be analyzed to give hourly mean values of the signal input to receiver in dB above 1 μV for each receiving station, frequency, and transmitting/receiving antenna combination (i.e., N-S/N-S, N-S/E-W, E-W/N-S, or E-W/E-W). A sample data reduction is shown in Table III, where it may be seen that the hourly mean value of the signal input to receiver in dB above 1 μV is averaged from information of two 2-min periods before and two 2-min periods after the hour for a five-day test. The median value can also be obtained from this tabular form, if required. The mean value so computed is more reliable than the median value, however, when the data become less uniformly distributed.

Table III

SAMPLE DATA REDUCTION

FREQUENCY 1.7 Mc/s. TIME 1200 Hr.

ANTENNAS: Tx N-S Rx N-S

K		1	2	3	4	5	6	7	8	9	10	11	12	13	14	15	16	17	18	19	20	21	22	23	24
DB above 1μV		0/5	5/10	10/15	15/20	20/25	25/30	30/35	35/40	40/45	45/50	50/55	55/60	60/65	65/70	70/75	75/80	80/85	85/90	90/95	95/100	100/105	105/110	110/115	115/120
29 Dec. 1st Day	1									2	6	2	4	5											
1134-36 23	2									3	3	5	4	3	1										
1148-50 24	3									2	5	6	3	3											
1205-07 24	4									2	4	6	4	3											
1219-21 24	5							1		2	4	7	1	3											
30 Dec 2nd Day	6									3	5	4	4	2	1										
1134-36 23	7									3	2	5	6	2	1										
1148-50 —	8									4	1	6	3	4	1										
1205-07 25	9									2	4	4	3	5	1										
1219-21 24	10									2	3	5	7	1	1										
31 Dec 3rd Day	11							1	1	3	6	2	4	2											
1134-36 24	12								1	2	4	4	6	2											
1148-50 24	13									6	3	6	3	2											
1205-07 24	14									3	2	5	5	3											
1219-27 23	15									4	4	4	4	3											
1 Jan '64 4th Day	16								1	3	4	2	7	2											
1134-36 23	17									3	4	5	6	1											
1148-50 24	18									6	1	5	4	3											
1205-07 24	19									4	2	5	4	4											
1219-21 23	20							1	1	3	1	5	5	3											
2 Jan. 5th Day	21									4	4	2	6	2											
1134-36 24	22							1		4	4	4	3	3											
1148-50 24	23									2	5	6	2	3											
1205-07 24	24									3	5	2	3	1											
1219-21 24	25												1												
No. of successes Total M = 451								4	4	75	87	108	102	65	6										
$N_1+2N_2+\cdots+KN_K$ = 1446								28	32	675	870	1188	1224	845	84										

$\frac{\Delta x}{M}(N_1+2N_2+\cdots+KN_K) = 54.83$

.1M = 45.1

Mean Value = 52.33

10% Value = 42.48

90% Value = 61.99

C. ANALYSIS OF DATA AND DISCUSSION OF RESULTS

1. Diurnal Variation of Received Signals

a. General

The diurnal variation of CW signals received at Ayudhaya and Nakornpathom is shown in Figs. 28 through 43 in the form of the mean value of signal strength at the receiver input in dB above 1 μV as a function of hour of the day for the Bangkok CW transmitter output of 400 W. The upper and lower decile values have also been obtained; these are respectively the values that the signal level exceeded the mean value 10 percent and 90 percent of the time. The decile range indicates the amount of variation of signal level that might be expected during a particular hour. The range tended to be smaller during the day than during the night; the variation might be as small as 5 dB above and below the mean value at midday and as large as 34 dB above and 24 dB below the mean at 0200. Diurnal variations are best studied with the f plot as shown in Fig. 44, which summarizes the average ionospheric behavior over the test period.

In general, the 1.7-MHz signal received either at Ayudhaya or Nakornpathom by any combination of transmitting and receiving antennas was at a very high level of 70-85 dB (mean values in decibels above 1 μV) during the night, but at 0400 it began to fall gradually toward its lowest level of 35-50 dB at 1200. Then the signal received rose again gradually, reaching its nighttime level just after 1800. This variation was caused by the presence of the D region (which produced nondeviative absorption) during the day and its absence at night.

For the 3-MHz transmission, two peaks in the signal were received at both sites with all antenna combinations. The first peak of 70-77 dB occurred at 0700; the signal level then gradually fell to a low value of 50-58 dB around 1200-1400, followed by a gradual rise to the second peak of 73-81 dB around 1800-1900. The signal remained at this high level until 2200, then fell gradually to its minimum level of 36-45 dB around 0300. The signal remained at this minimum level until 0600, when it abruptly rose to the 0700 peak. The minimum signal level

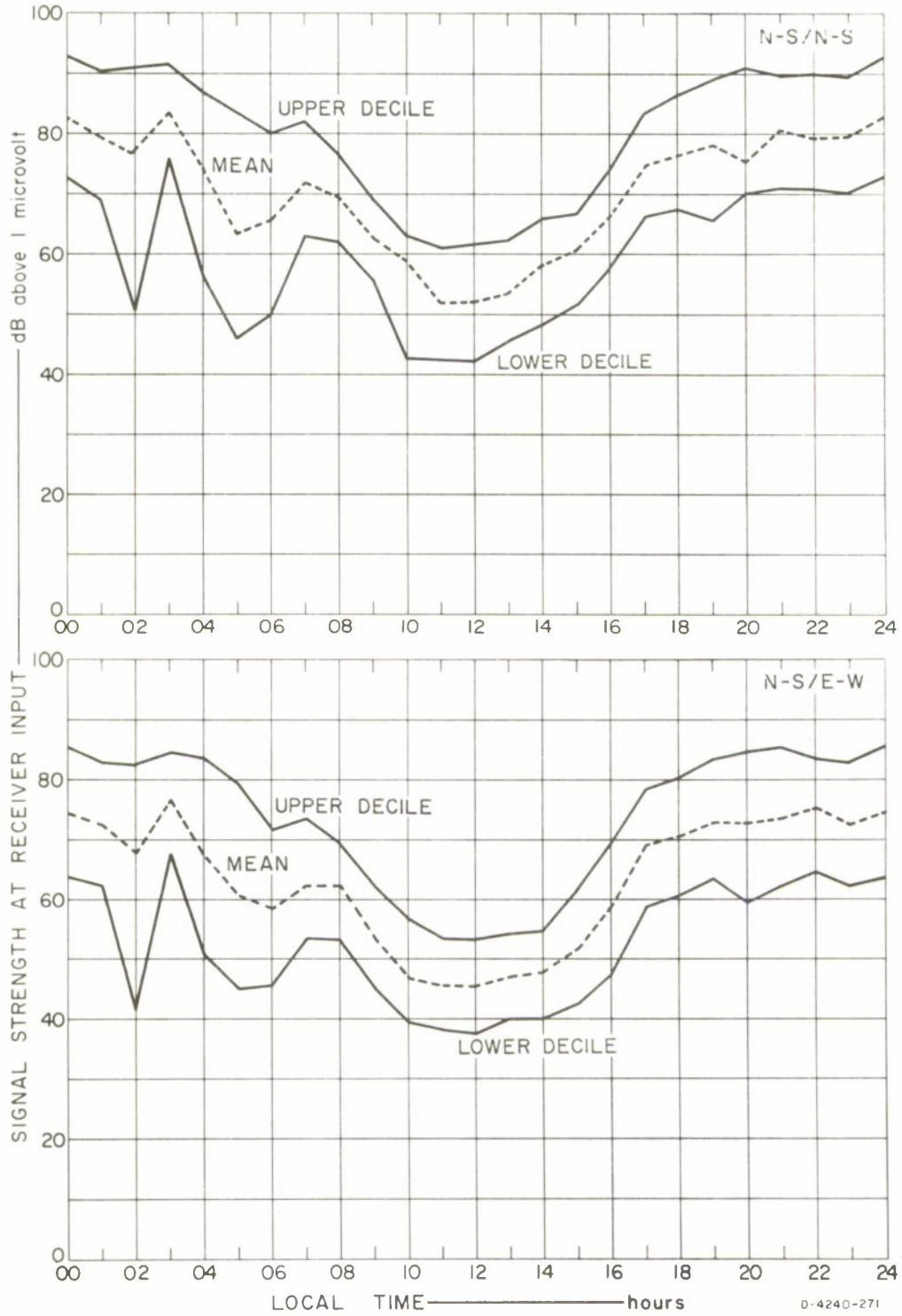

FIG. 28 AYUDHAYA: 1.7 MHz CW, N-S TRANSMITTING

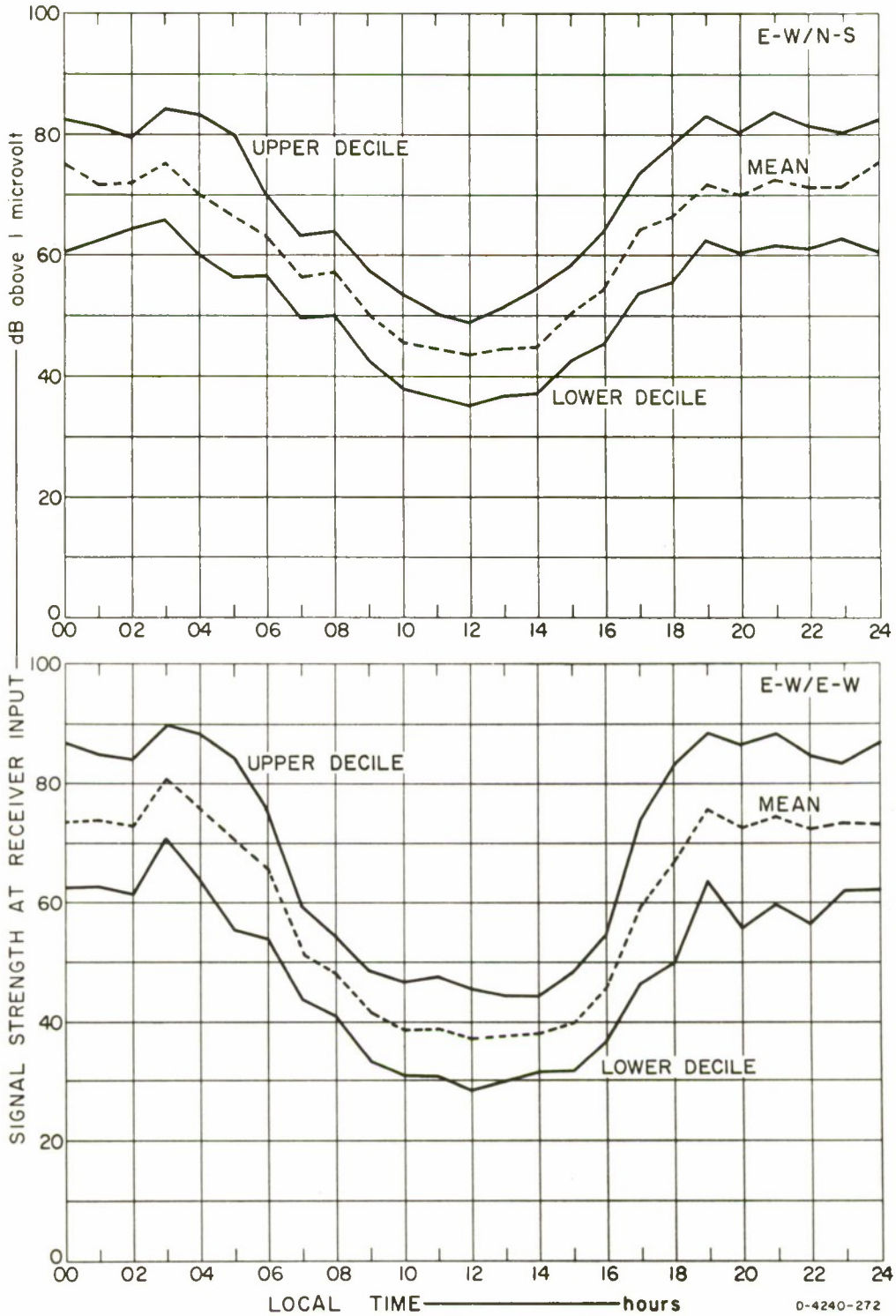

FIG. 29 AYUDHAYA: 1.7 MHz CW, E-W TRANSMITTING

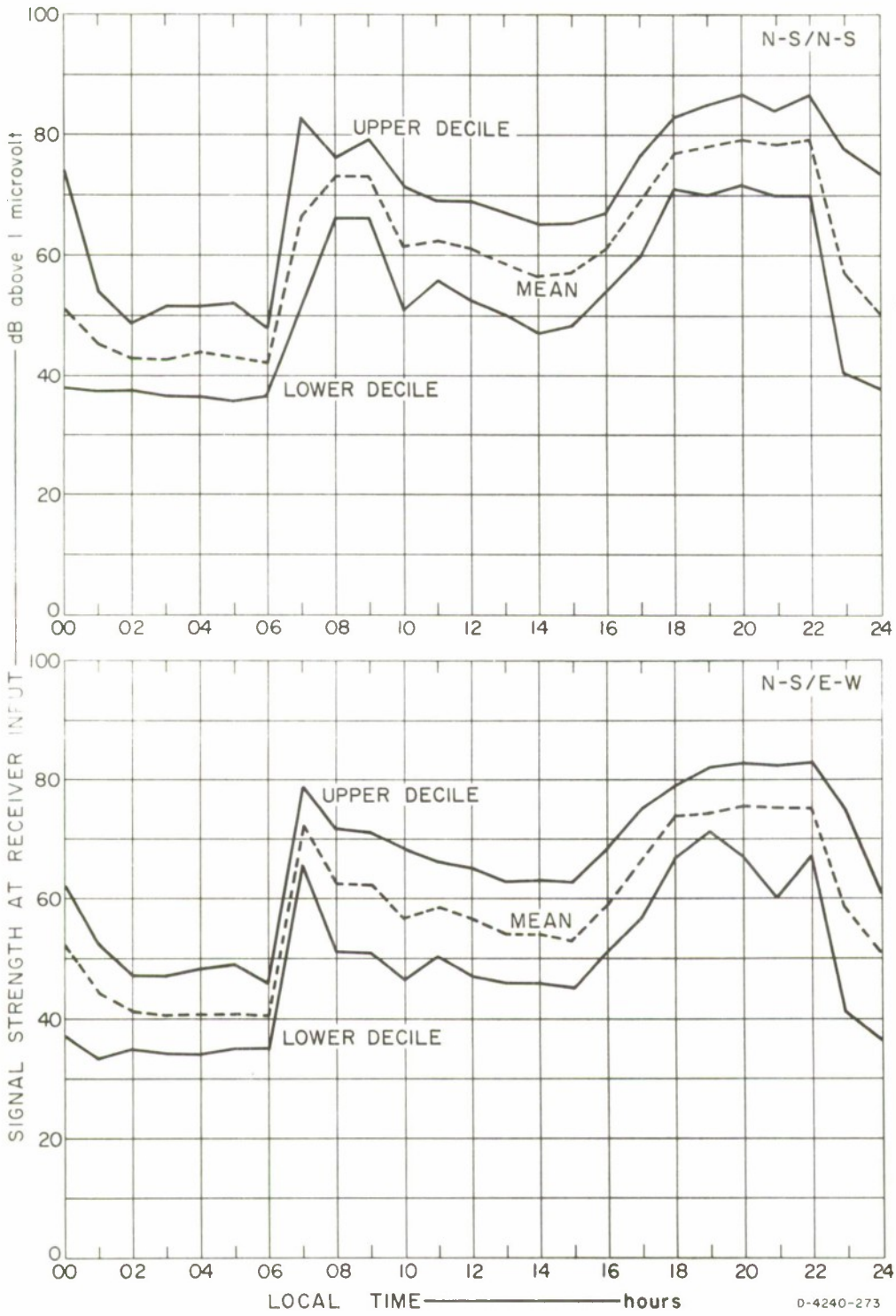

FIG. 30 AYUDHAYA: 3 MHz CW, N-S TRANSMITTING

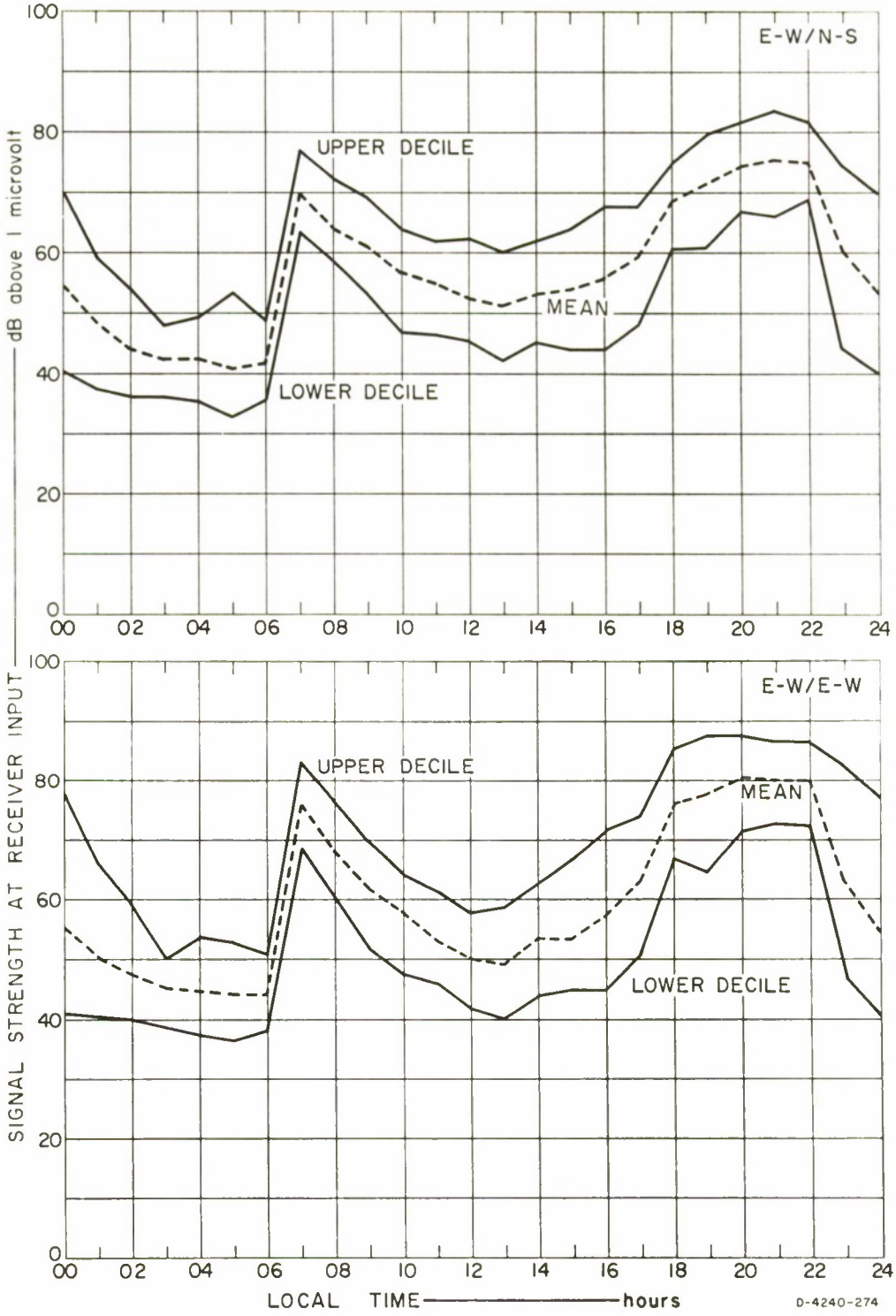

FIG. 31 AYUDHAYA: 3 MHz CW, E-W TRANSMITTING

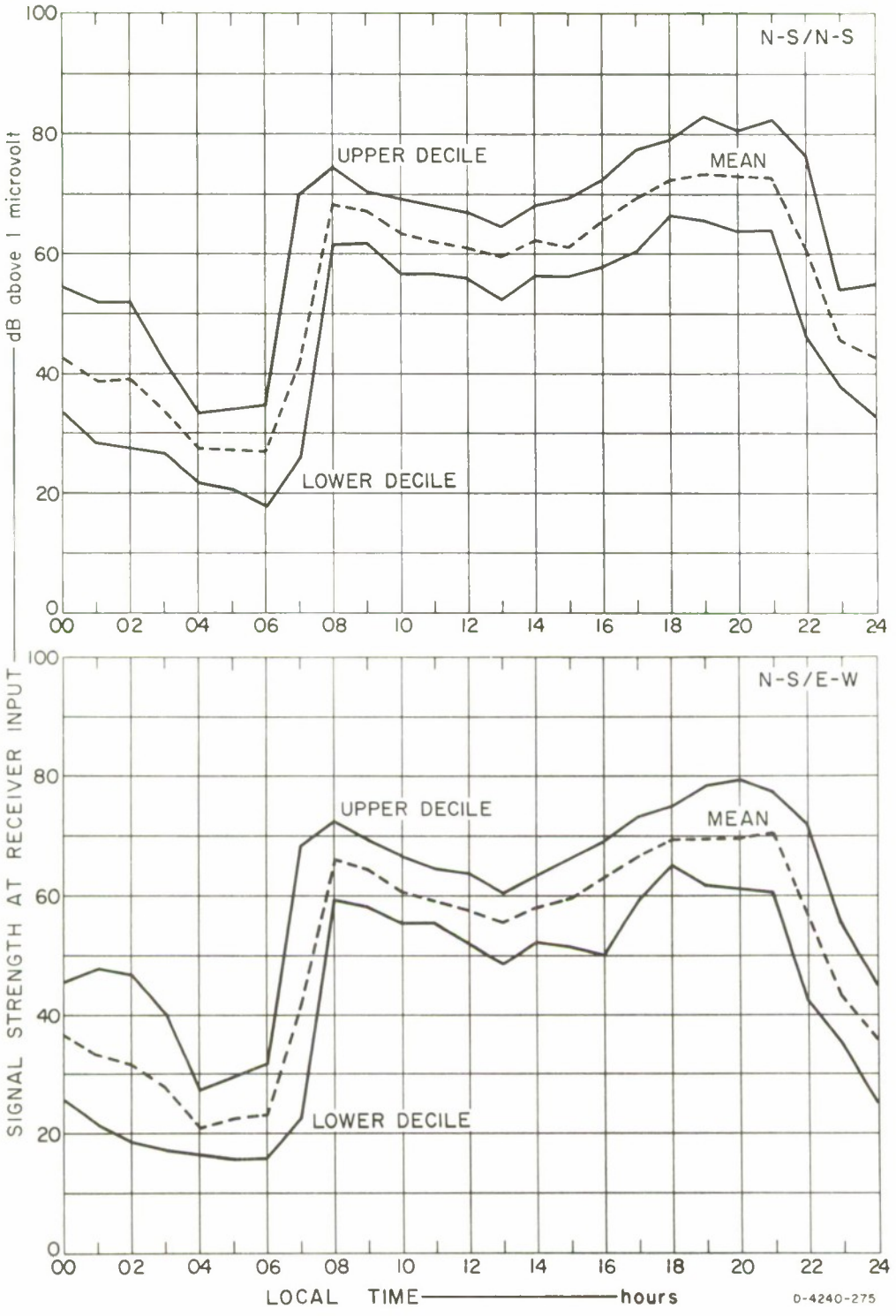

FIG. 32 AYUDHAYA: 5 MHz CW, N-S TRANSMITTING

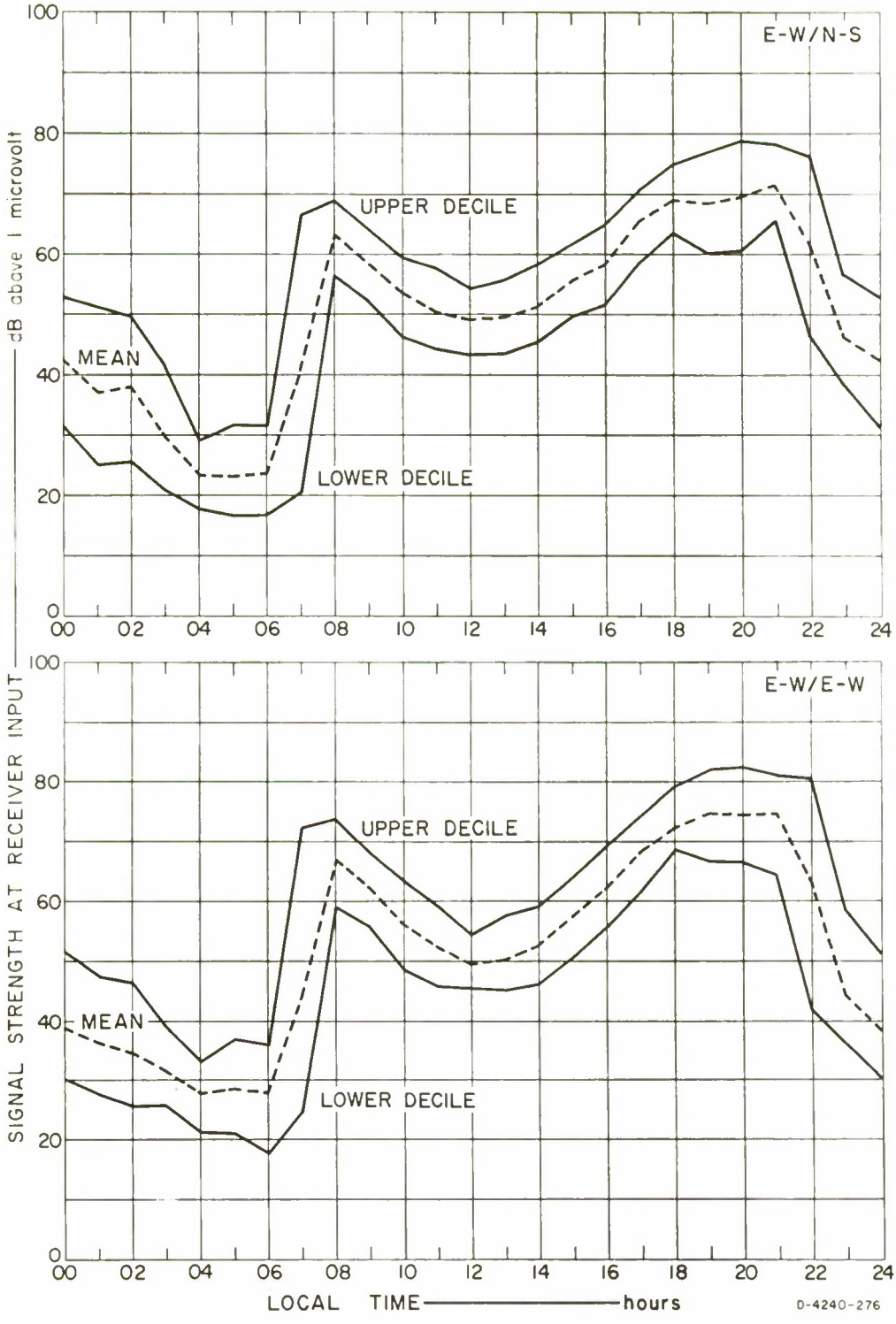

FIG. 33 AYUDHAYA: 5 MHz CW, E-W TRANSMITTING

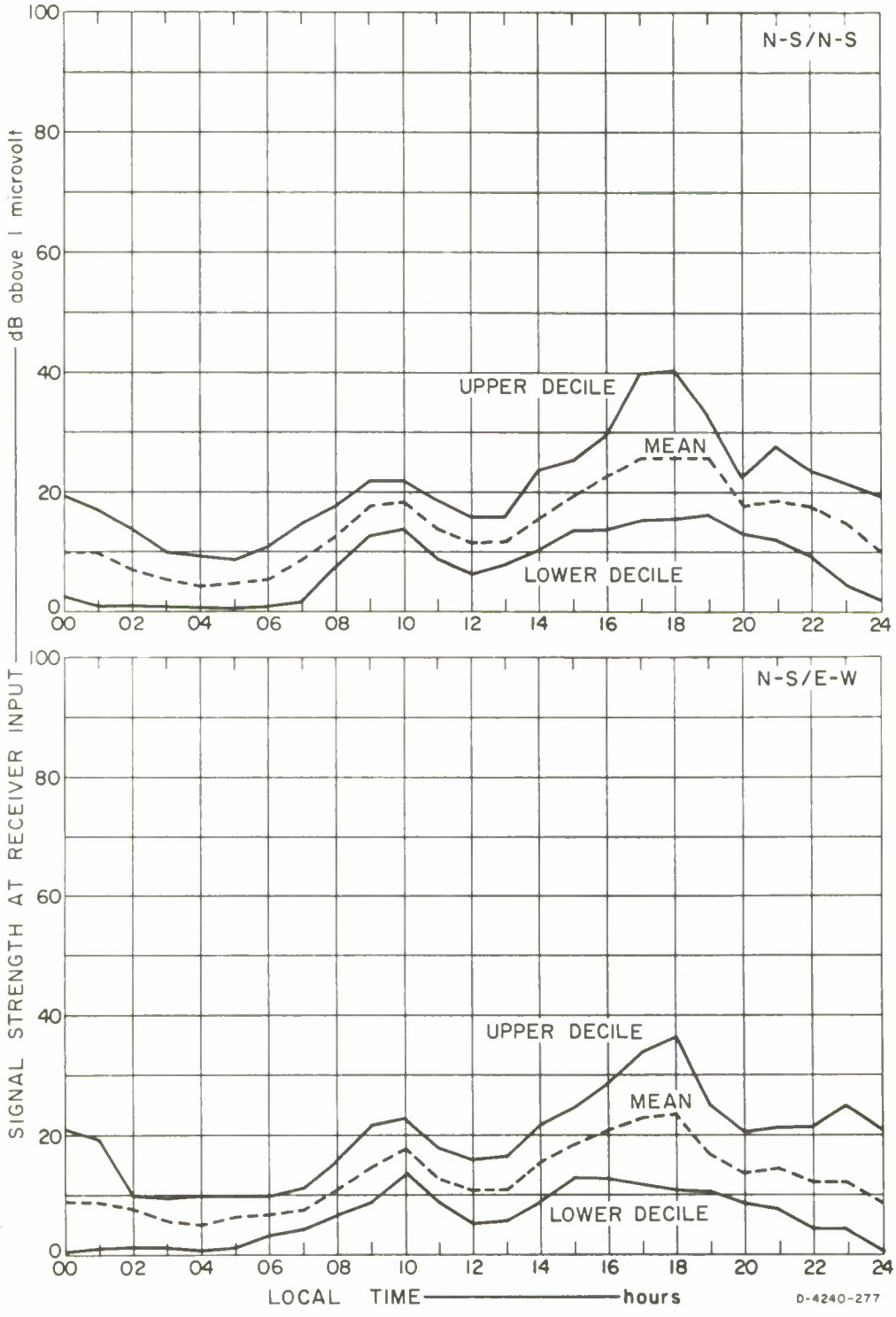

FIG. 34 AYUDHAYA: 10 MHz CW, N-S TRANSMITTING

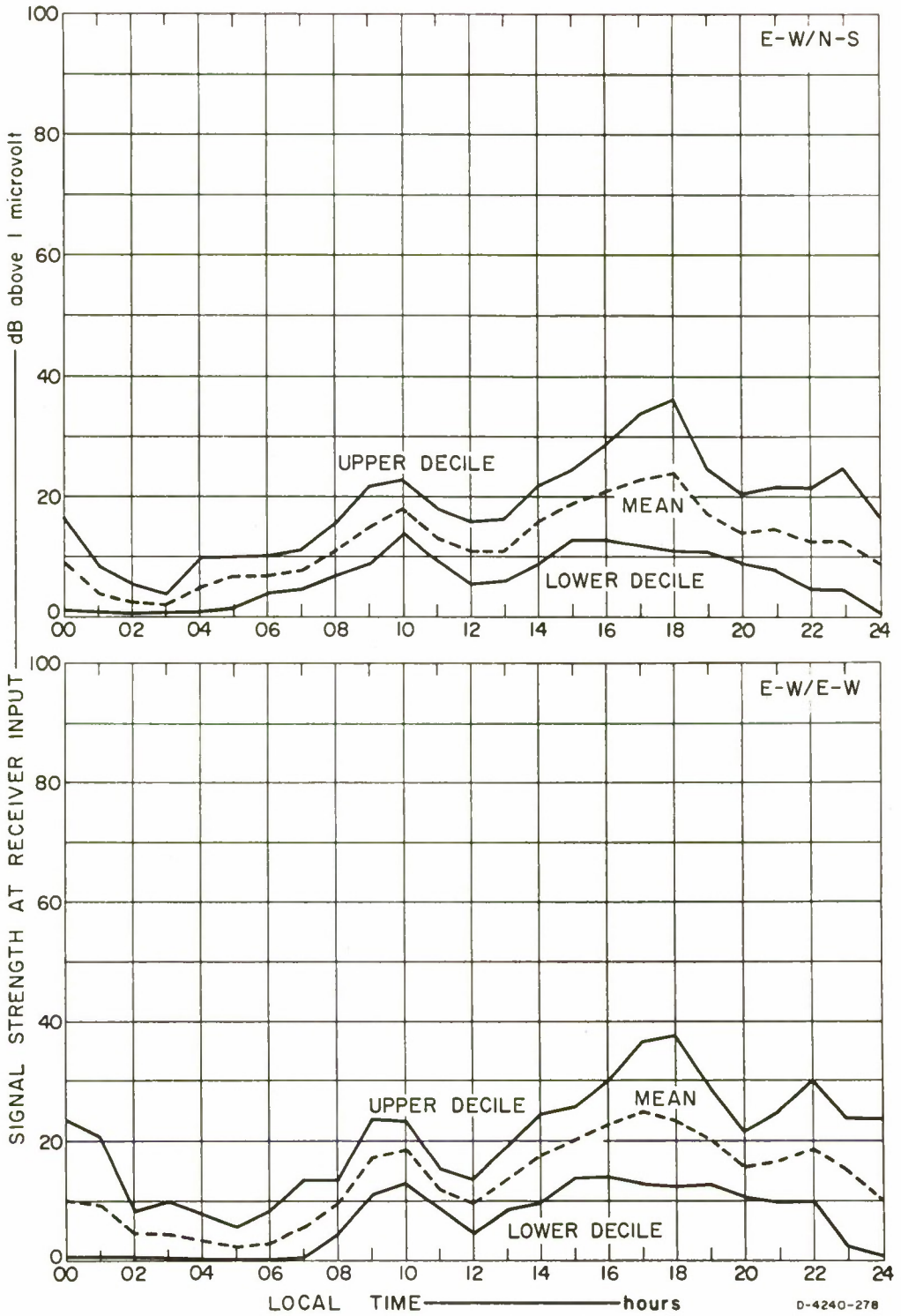

FIG. 35 AYUDHAYA: 10 MHz CW, E-W TRANSMITTING

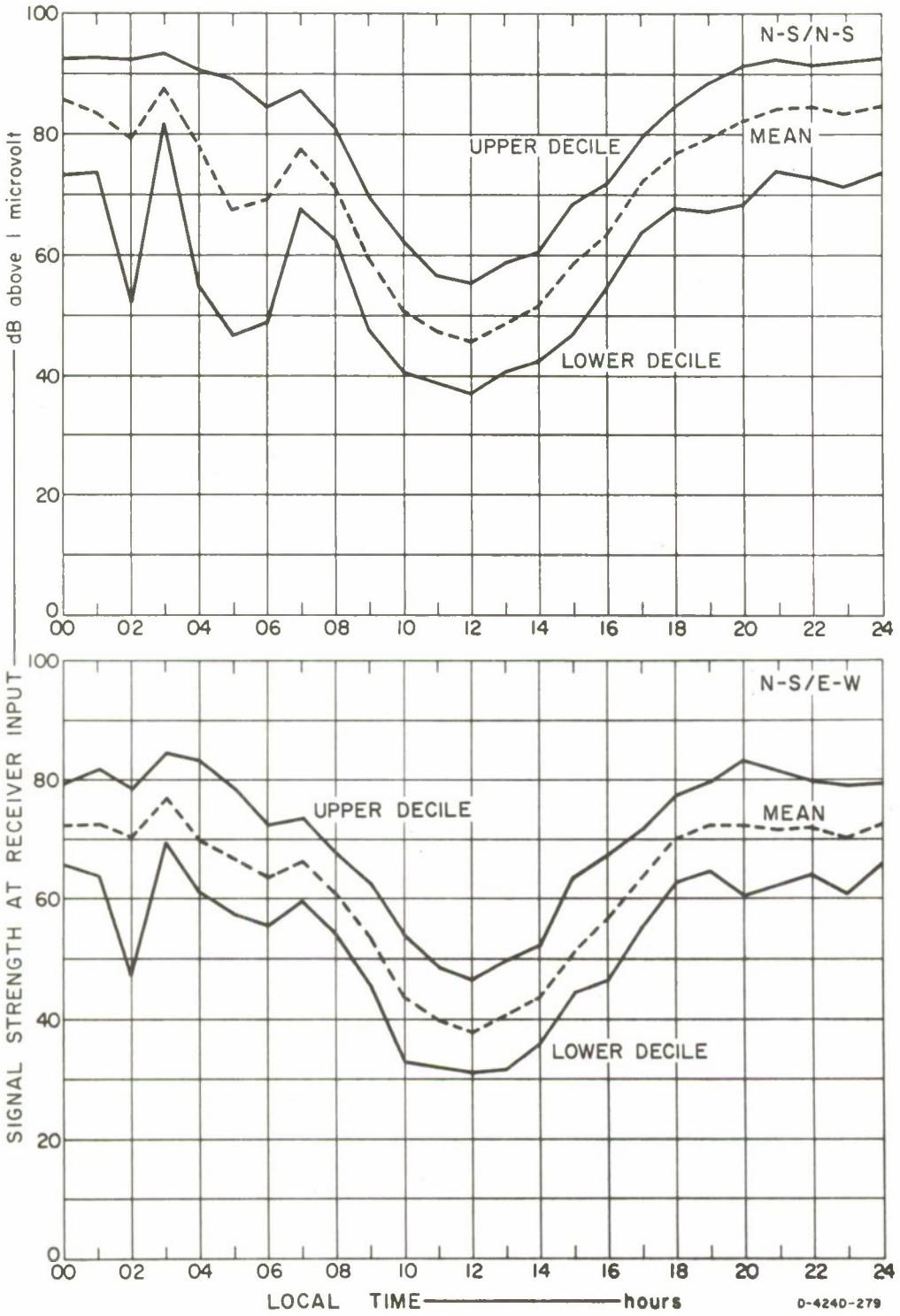

FIG. 36 NAKORNPATHOM: 1.7 MHz CW, N-S TRANSMITTING

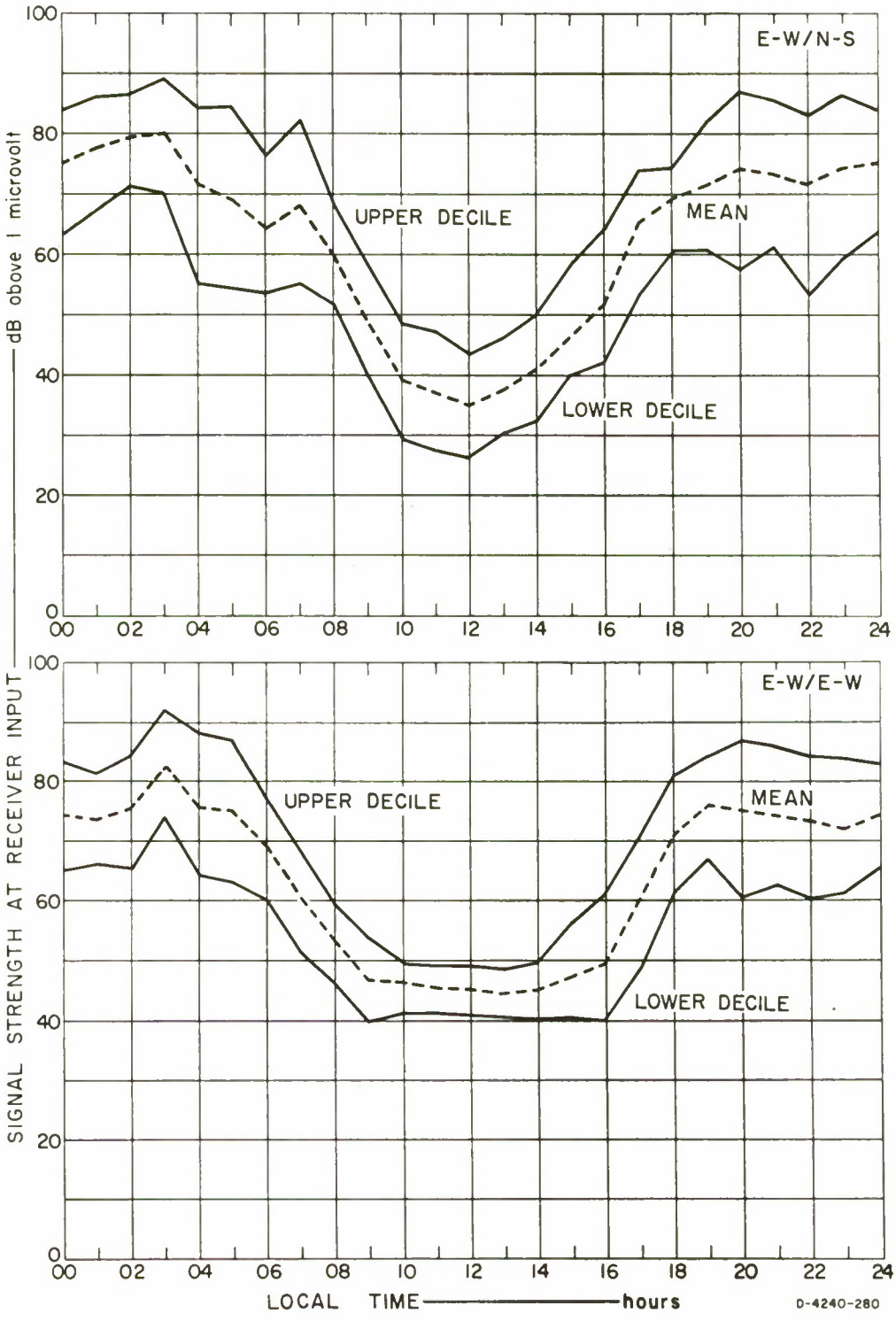

FIG. 37 NAKORNPATHOM: 1.7 MHz CW, E-W TRANSMITTING

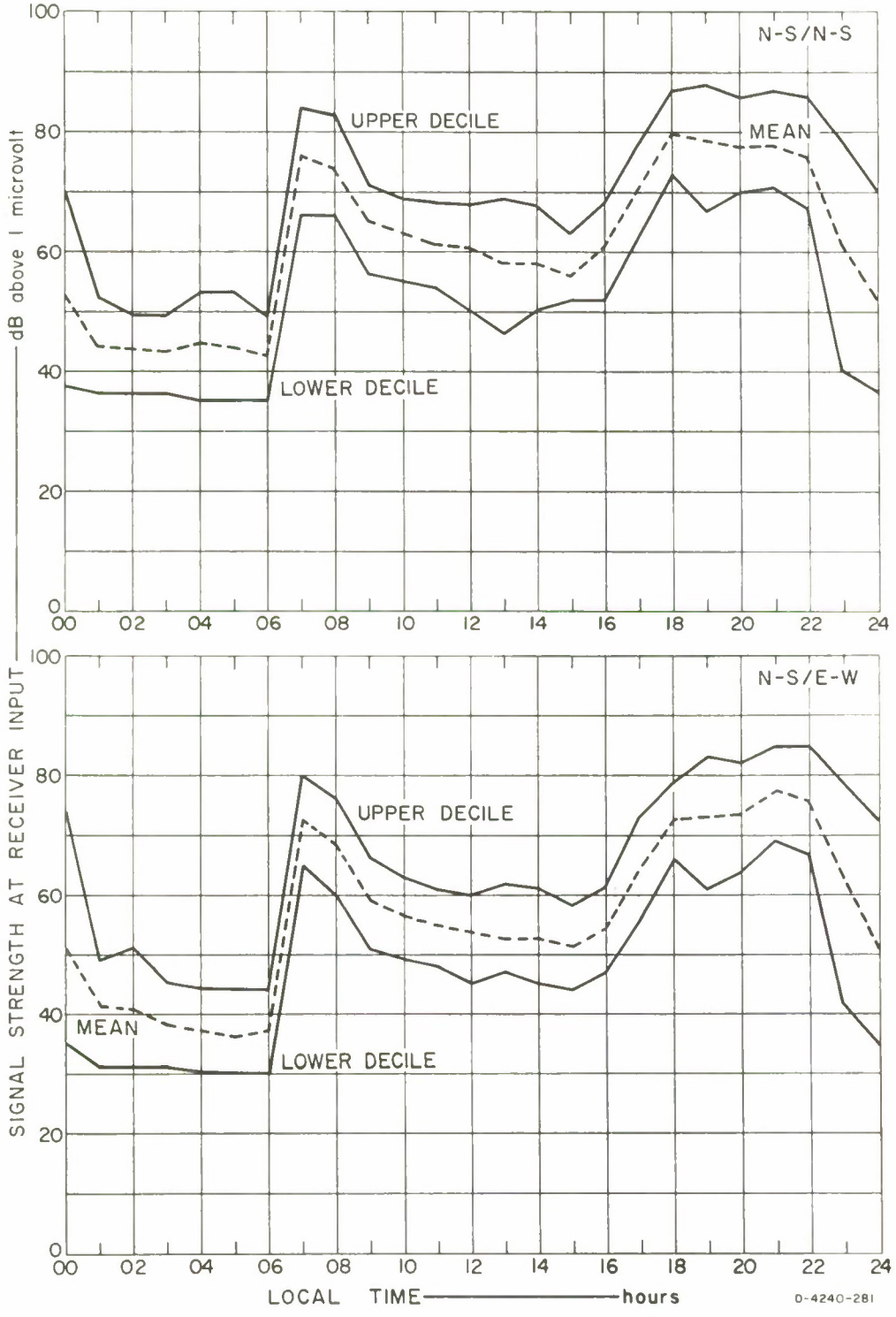

FIG. 38 NAKORNPATHOM: 3 MHz CW, N-S TRANSMITTING

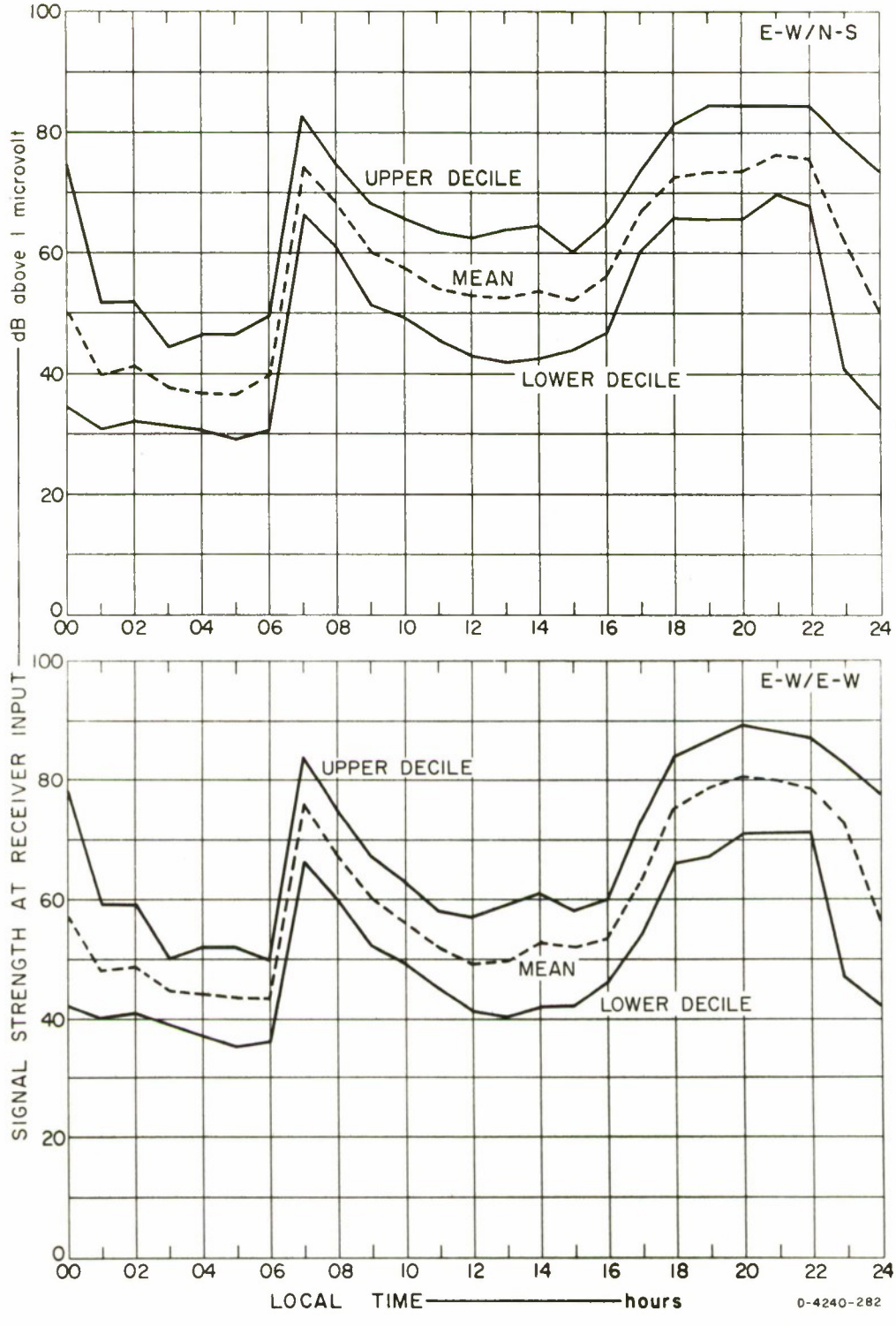

FIG. 39 NAKORNPATHOM: 3 MHz CW, E-W TRANSMITTING

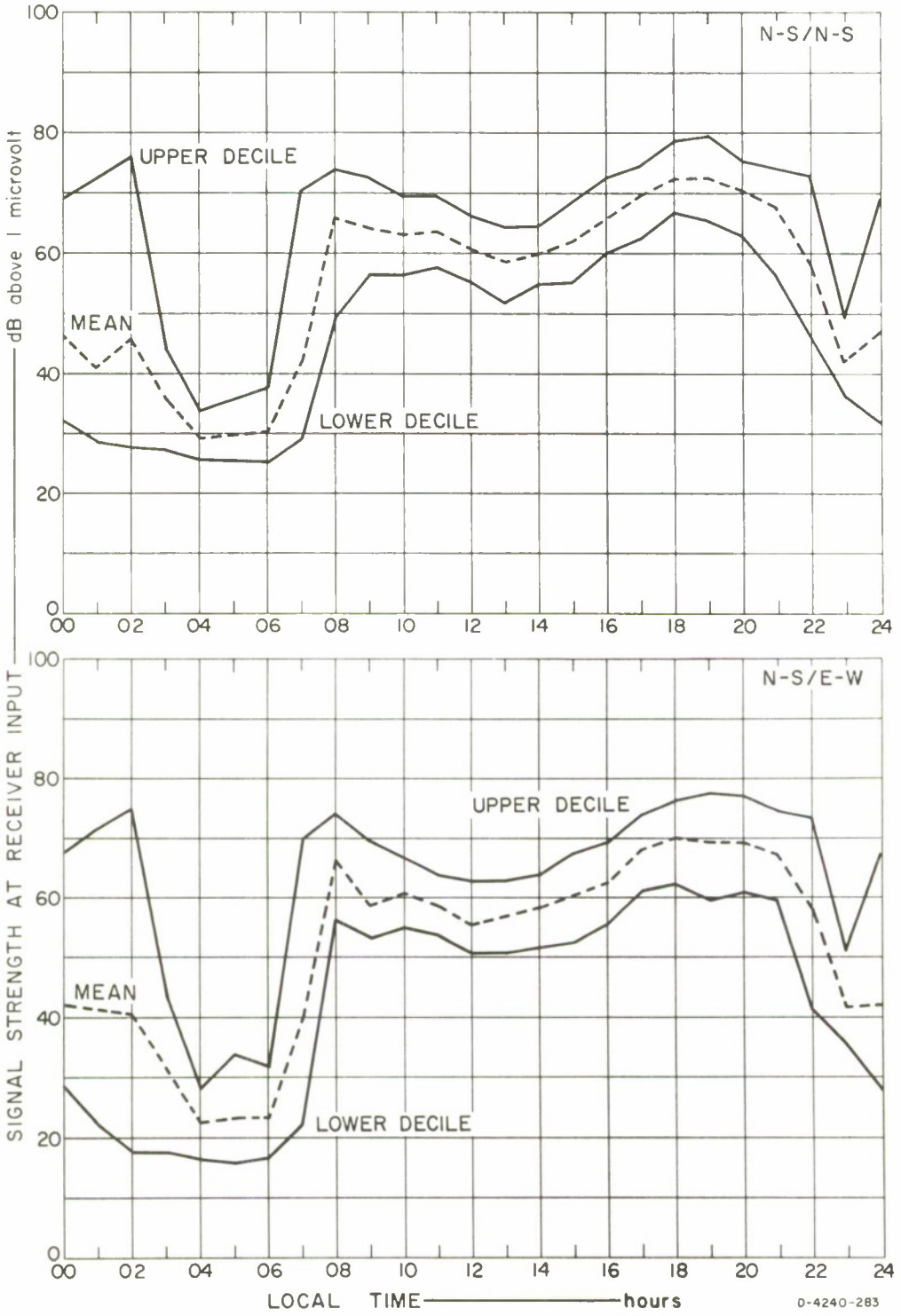

FIG. 40 NAKORNPATHOM: 5 MHz CW, N-S TRANSMITTING

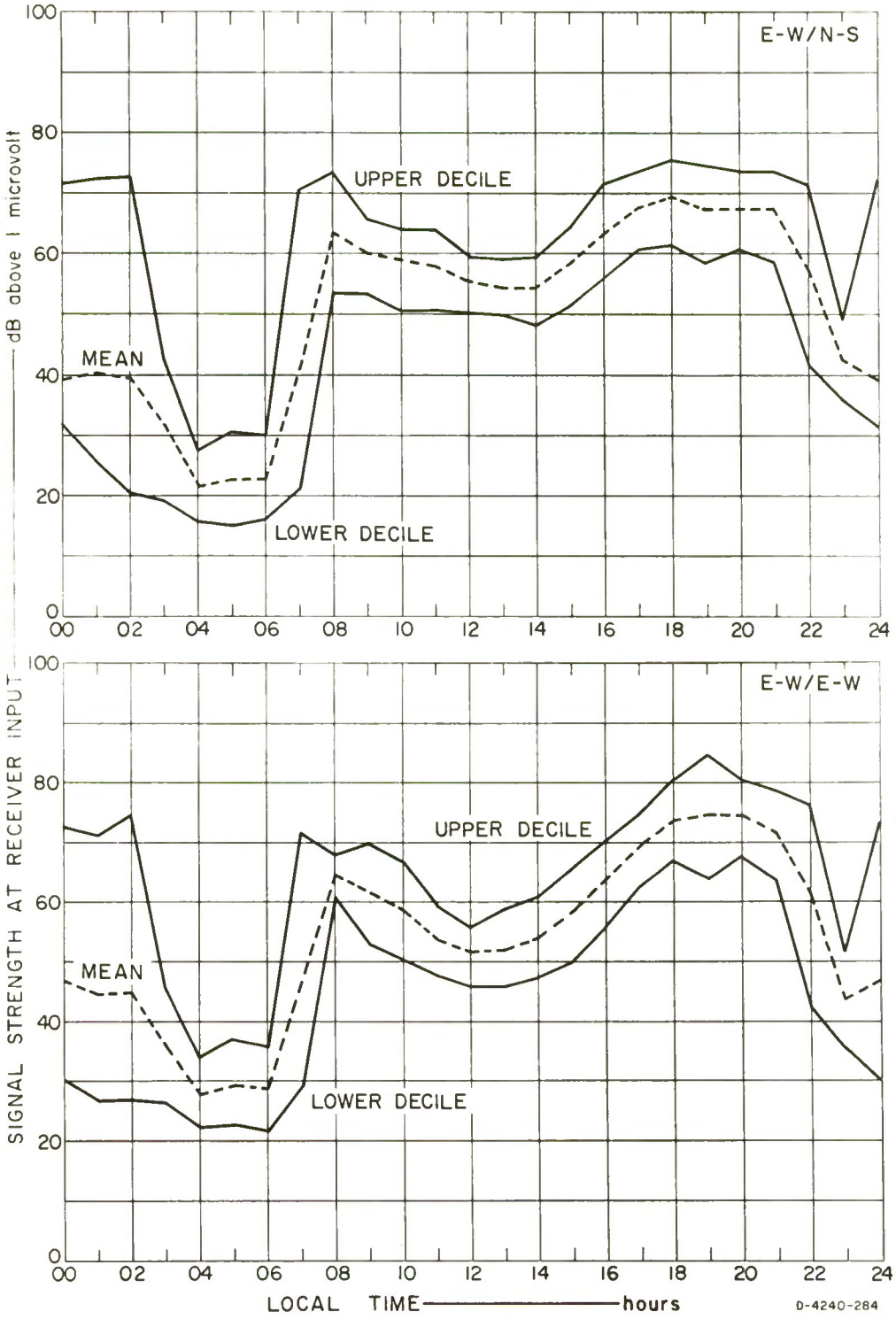

FIG. 41 NAKORNPATHOM: 5 MHz CW, E–W TRANSMITTING

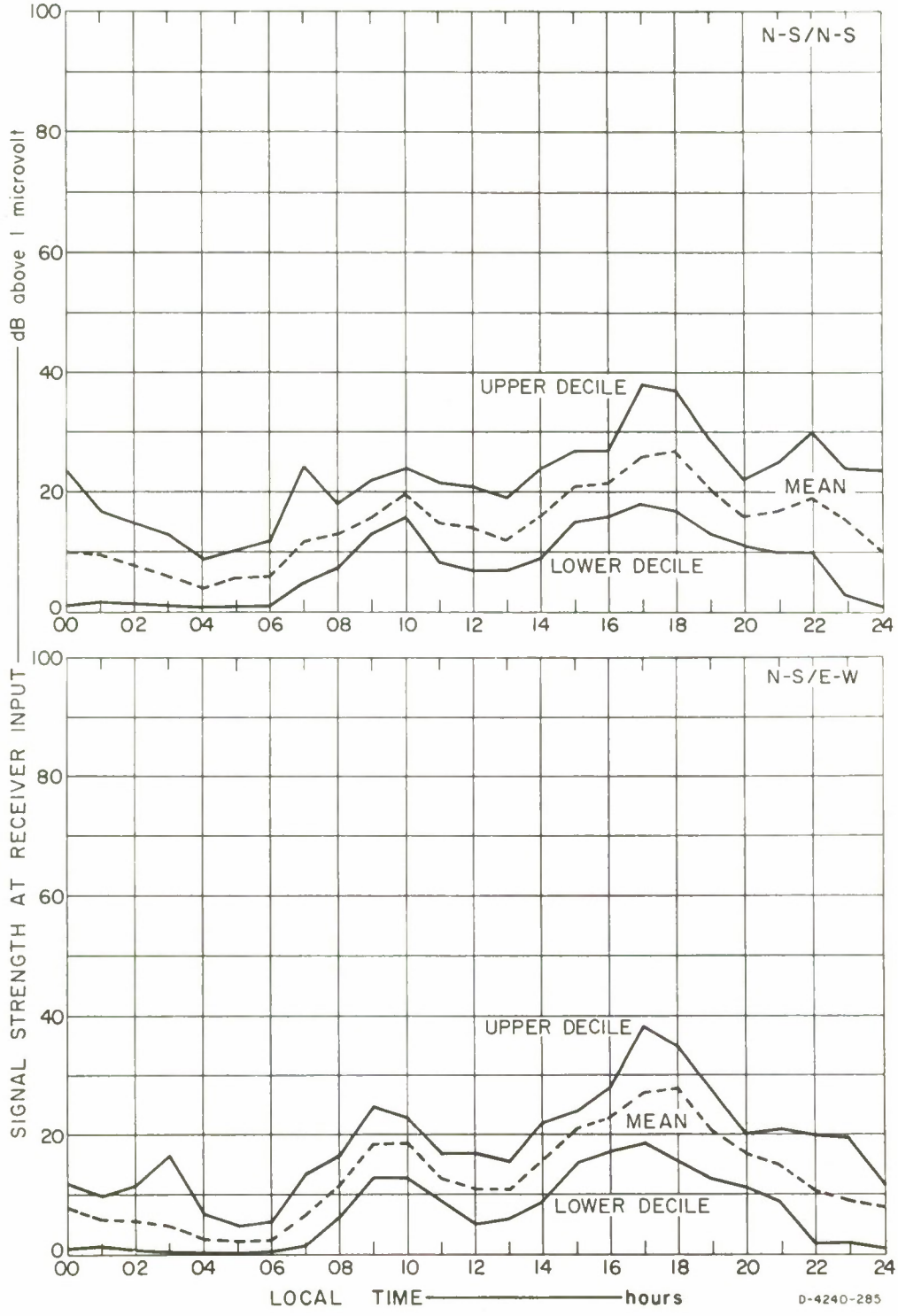

FIG. 42 NAKORNPATHOM: 10 MHz CW, N-S TRANSMITTING

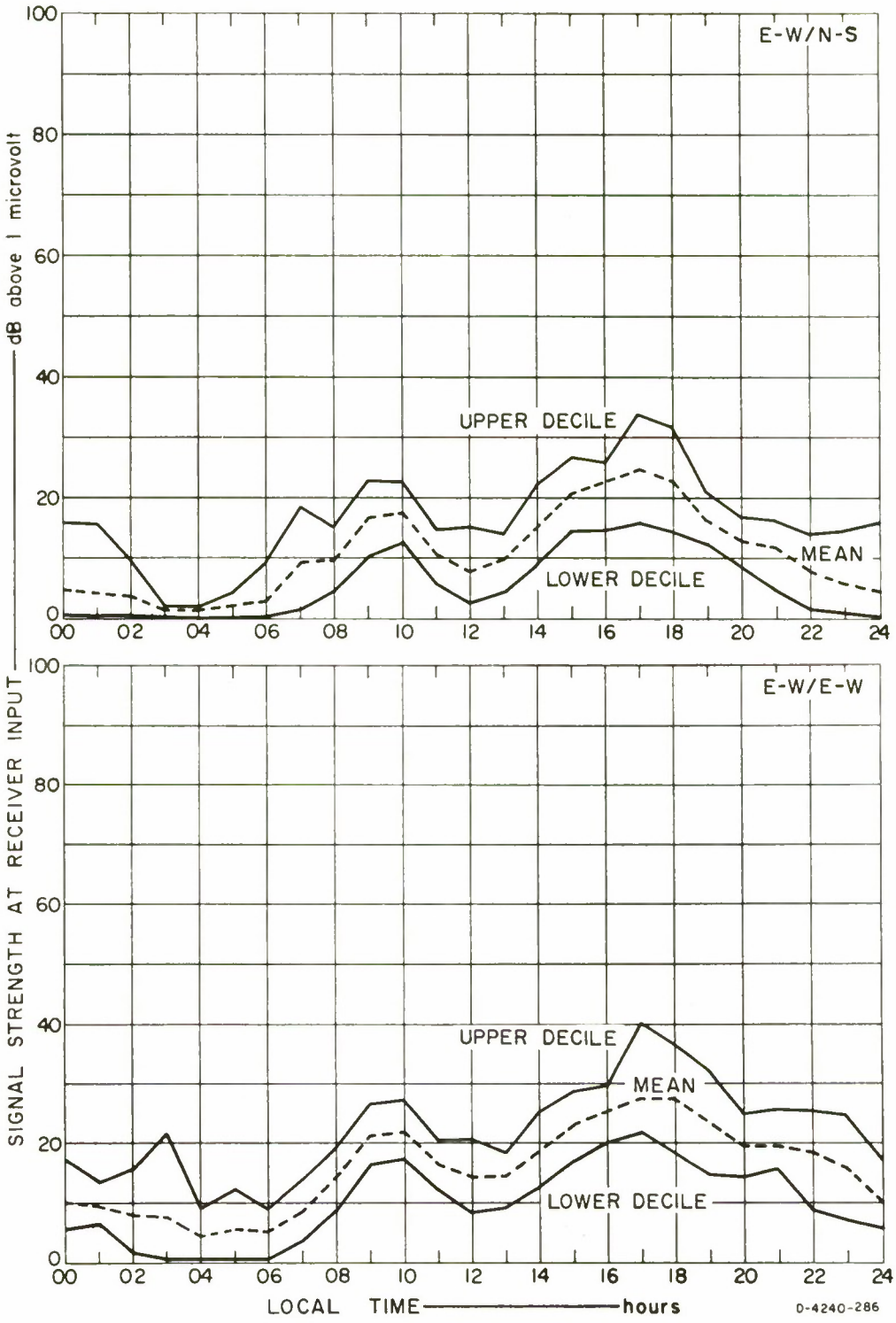

FIG. 43 NAKORNPATHOM: 10 MHz CW, E-W TRANSMITTING

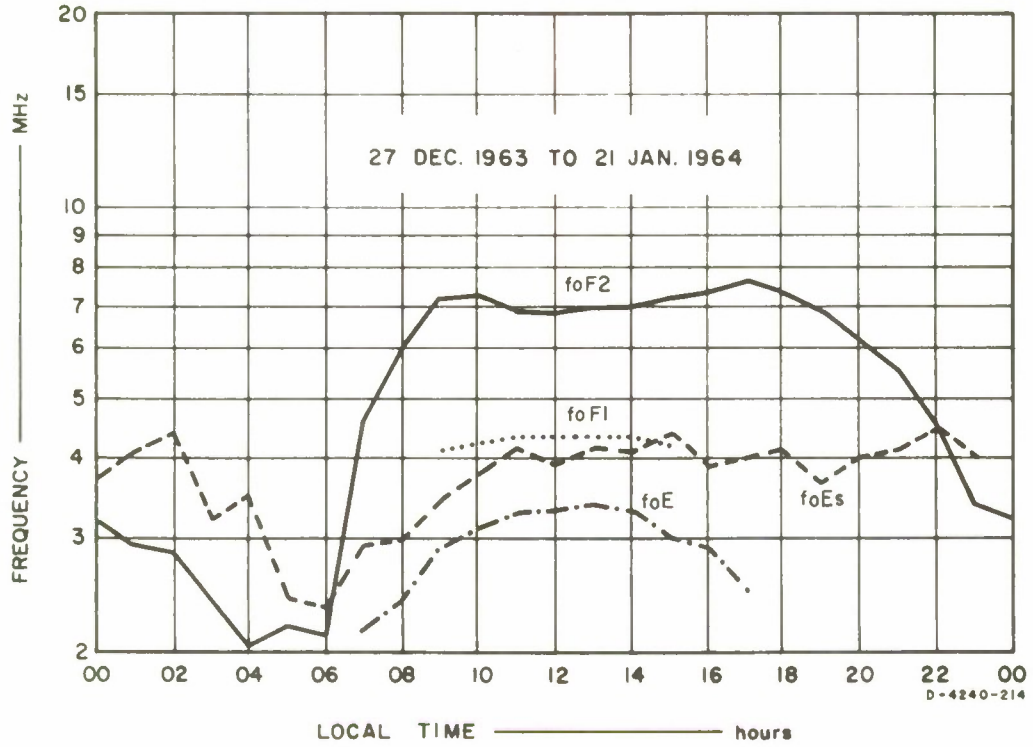

FIG. 44 f PLOT OF IONOSPHERIC VERTICAL SOUNDING OVER BANGKOK: CW TEST PERIOD

between 0300 and 0600 was probably owing to the fact that during this period the wave frequency of 3 MHz was above the critical frequency of the F layer, and hence only a minor portion of the signal might be partially reflected back to earth by a sporadic-E layer or other scatter mechanism (see Fig. 44). The abrupt rise in signal level corresponded to the increase in the F-layer critical frequency. The signal level reaches its morning maximum when the F layer becomes totally reflecting, and after the deviative absorption has dropped off to a reasonably low level but before the nondeviative absorption has become too great. It would be interesting to know whether the tests carried out under Project Yo-Yo included pre-dawn tests. A report of that test program states that the largest signal strengths were found to occur at night.[19]

The 5-MHz reception generally followed the trend of the 3-MHz reception, although the rise in signal strength after sunrise was not as abrupt as in the 3-MHz case. This is as expected since the critical

frequency cannot be raised quickly to a higher value than 3 MHz by the sunrise effect. The 5-MHz signal strength rose from a very low pre-dawn minimum of 23-30 dB at 0600 to the morning peak of 63-68 dB at 0800. The much lower value of pre-dawn minimum signal level in the 5-MHz case than in the 3-MHz case may be due to less efficient propagation when operating above the F-layer critical frequency, 5 MHz > 3 MHz > foF2 between 0300 and 0600. The daytime low level was 50-60 dB at 1200, and the second peak was 68-75 dB at 2000.

The 10-MHz diurnal variation followed the trend of the 3-MHz and 5-MHz fluctuations, although with a much narrower range and at much lower signal levels. Signal was very much flooded by noise during the night, especially the midnight-to-dawn period. It is believed that the signal that was still recognizable during this period might have arrived at the receiving antennas by scattering mechanism (ground backscatter or ionospheric scatter); the 10-MHz transmission was above the classical MUF for the paths for all hours of the day!

An overall picture of the test results, together with the effect of the ionosphere, can readily be derived by reference to Fig. 44 (the f plot), and to Fig. 45, where the mean values of the 1.7-, 3-, and 5-MHz diurnal variations at both Ayudhaya and Nakornpathom with all transmitting/receiving antenna combinations are superimposed and bounded. At night, the absorption would normally be small, and most of the nighttime absorption would be deviative. During the day, the nondeviative absorption would be significant, in addition to the deviative absorption. One would, therefore, expect all signals to be high at night and low during the day, provided the operating frequency remained below the F-layer critical frequency. This is found to be true in the case of the 1.7-MHz signal, which reflected in the highly absorbing region during the day, and is also supported by the cumulative two-way absorption curves for day and night in Fig. 7. The nighttime signal strength at 3 MHz, however, turned out to be lower than the daytime value. The 3-MHz signal strength jumped 30 to 40 dB in one hour around sunrise at 100-km height above earth (0600). Vertical-incidence sounder (C-2) data from Bangkok[20] are presented here in part as Table IV. The values of foF2

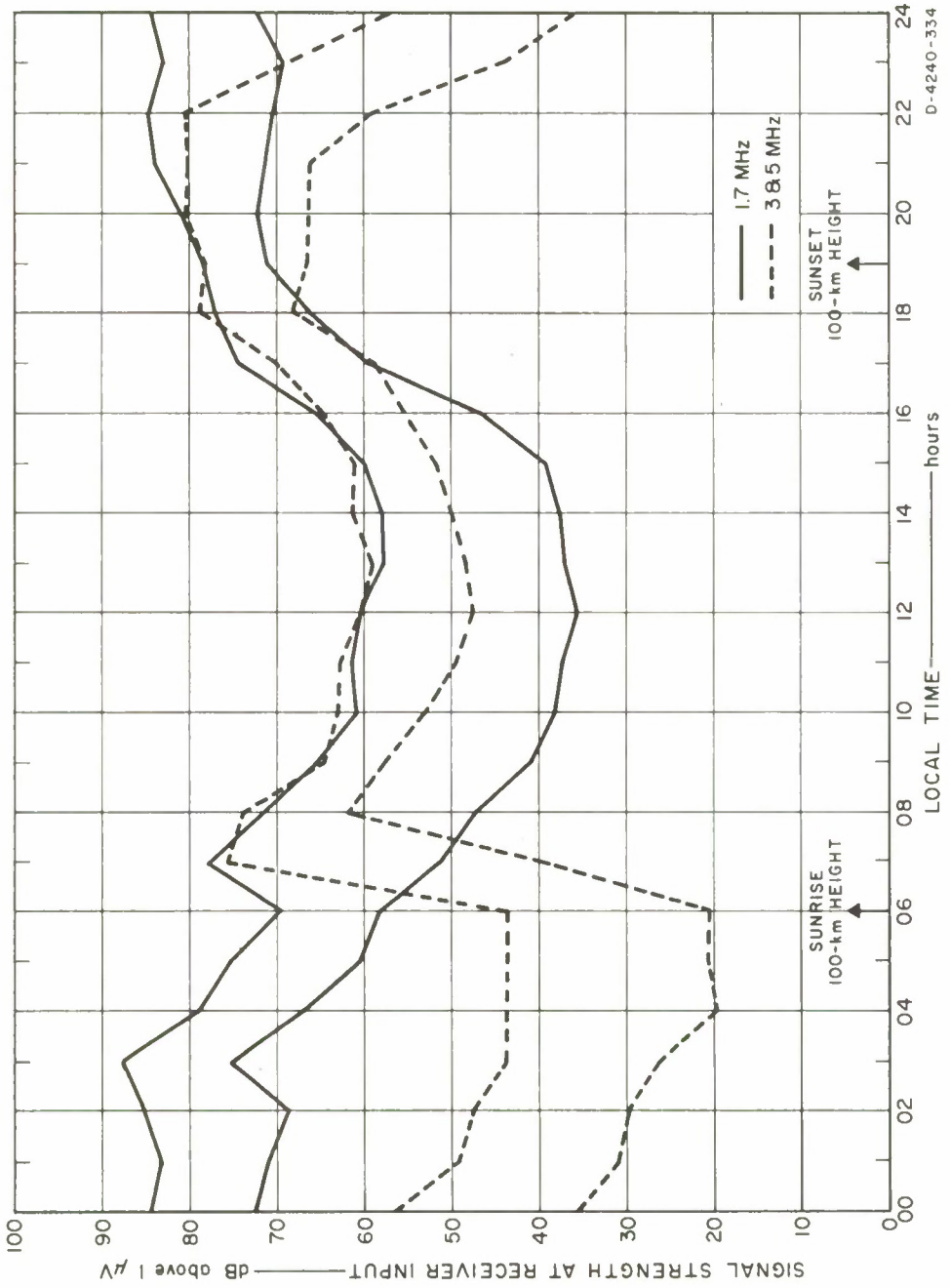

FIG. 45 AYUDHAYA AND NAKORNPATHOM MEAN VALUES

Table IV

CRITICAL FREQUENCIES: BANGKOK, JANUARY 1964

Local Time (hour)	foF2 Monthly Median (MHz)	foF2 Upper Quartile (MHz)	foF2 Lower Quartile (MHz)	foEs Monthly Median (MHz)	foEs Upper Quartile (MHz)	foEs Lower Quartile (MHz)	foE Monthly Median (MHz)
5	2.0	2.3	1.9	2.2	3.2	1.8	--
6	2.3	2.4	2.1	2.3	3.2	2.0	--
7	4.5	4.6	4.4	2.9	3.0	2.3	2.3*

* Only one recording for the entire month.

are very nearly the MUF values for the short (65-km) path used here. The secant-law correction is less than 1.05 for all heights of interest. The 3-MHz frequency is shown to be above foF2 during the sunrise period. Thus, the explanation that the large increase in signal strength was brought about by a change in layer height from F to E would not apply. As a further check, layer-height values as summarized in Table V have been obtained also from the Bangkok ionospheric data.[20] The table gives the monthly median h'Es = 110 km and h'F = 293 km at 0600. The greatest change that could be brought about by a change in layer height supporting the wave at sunrise would therefore be $10 \log_{10} (293/110)^2 \cong 8.5$ dB, which is four times lower than the observed values. A likely possibility for the nighttime reception of 3 MHz with comparatively low signal

Table V

VIRTUAL HEIGHTS: BANGKOK, JANUARY 1964

Local Time (hour)	h'F2 Monthly Median (km)	h'F2 Upper Quartile (km)	h'F2 Lower Quartile (km)	h'Es Monthly Median (km)	h'Es Upper Quartile (km)	h'Es Lower Quartile (km)
5	270	310	255	115	120	100
6	293	330	260	110	120	100
7	220	230	220	120	125	120

strength is the scatter-type reflections, either by the Es layer or other ionospheric mechanism or the ground backscatter from greater range than the 65-km path. Since scatter-type reflections are power sensitive, it is quite possible that the C-2 sounder would be less sensitive than the CW test equipment and would not show foEs appropriate for the CW test equipment on the ground backscatter echoes. It is also known that the secant law does not hold exactly for Es reflections,[21] thus suggesting Es scatter as a possible explanation for the observed propagation of 3-MHz signal at night. However, a study of pulse data shows less pulse stretching than would be expected for the ground backscatter mechanism (see Secs. IV-C-1-c and IV-C-1-d), which makes this possible explanation for propagation above F layer critical frequency less likely than explanations based on ionospheric scatter. The Es layer could also be responsible for the nighttime reception of the 5-MHz signal which should (according to the curves in Fig. 7 and the data in Table IV) penetrate the ionosphere. Ground backscatter and/or ionospheric scatter, however, would be more likely at this frequency, as observed in pulse measurements and described in Sec. IV-C-4.

The 1.7-, 3-, and 5-MHz signals show a decrease in daytime signal strength due to nondeviative absorption. The signal level is approximately symmetrical about noon when the electron density in the D layer of the ionosphere is expected to be greatest.

After sunset (1900 at 100-km height above earth), the D-layer electrons would recombine, decreasing the electron density-collision frequency product (see Sec. II-B-5) and the signal strength would be expected to increase. This is clearly seen in the 1.7-MHz post-sunset reception. The 3- and 5-MHz data show the same trend as the 1.7 MHz, and also show an apparent equilibrium between 1900 and 2100. This equilibrium indicates that ionospheric absorption is negligible during the period, after which the signals drop to the low nighttime level previously discussed.

As a basis for choice of an optimum transmitting/receiving antenna combination, the diurnal mean values are reproduced without decile values in Figs. 46 through 52 and are analyzed in detail in the following subsections with the notations:

N-S/N-S--(1) A transmitting dipole aligned with the magnetic N-S and hence launching (primarily) the ordinary wave, and

(2) A receiving dipole aligned with the magnetic N-S and hence receiving the ordinary wave returned from the ionosphere

N-S/E-W--(1) A transmitting dipole aligned with the magnetic N-S and hence launching the ordinary wave, and

(2) A receiving dipole aligned with the magnetic E-W and hence receiving the wave that has been converted in the ionosphere from the transmitted ordinary wave

E-W/E-W--(1) A transmitting dipole aligned with the magnetic E-W and hence launching the extraordinary wave, and

(2) A receiving dipole aligned with the magnetic E-W and hence receiving the extraordinary wave returned from the ionosphere

E-W/N-S--(1) A transmitting dipole aligned with the magnetic E-W and hence launching the extraordinary wave, and

(2) A receiving dipole aligned with the magnetic N-S and hence receiving the wave that has been converted in the ionosphere from the transmitted extraordinary wave.

b. 1.7 MHz: Bangkok/Ayudhaya (S-to-N) Path

On this path, the N-S/N-S was the best transmitting/receiving antenna combination. Its signal strength exceeded that of the E-W/E-W arrangement by about 13 dB (3-22 dB)* and exceeded any other combinations

* 13 dB is an arithmetic mean of decibel difference, not the mean of the lower and upper limits of the range in brackets.

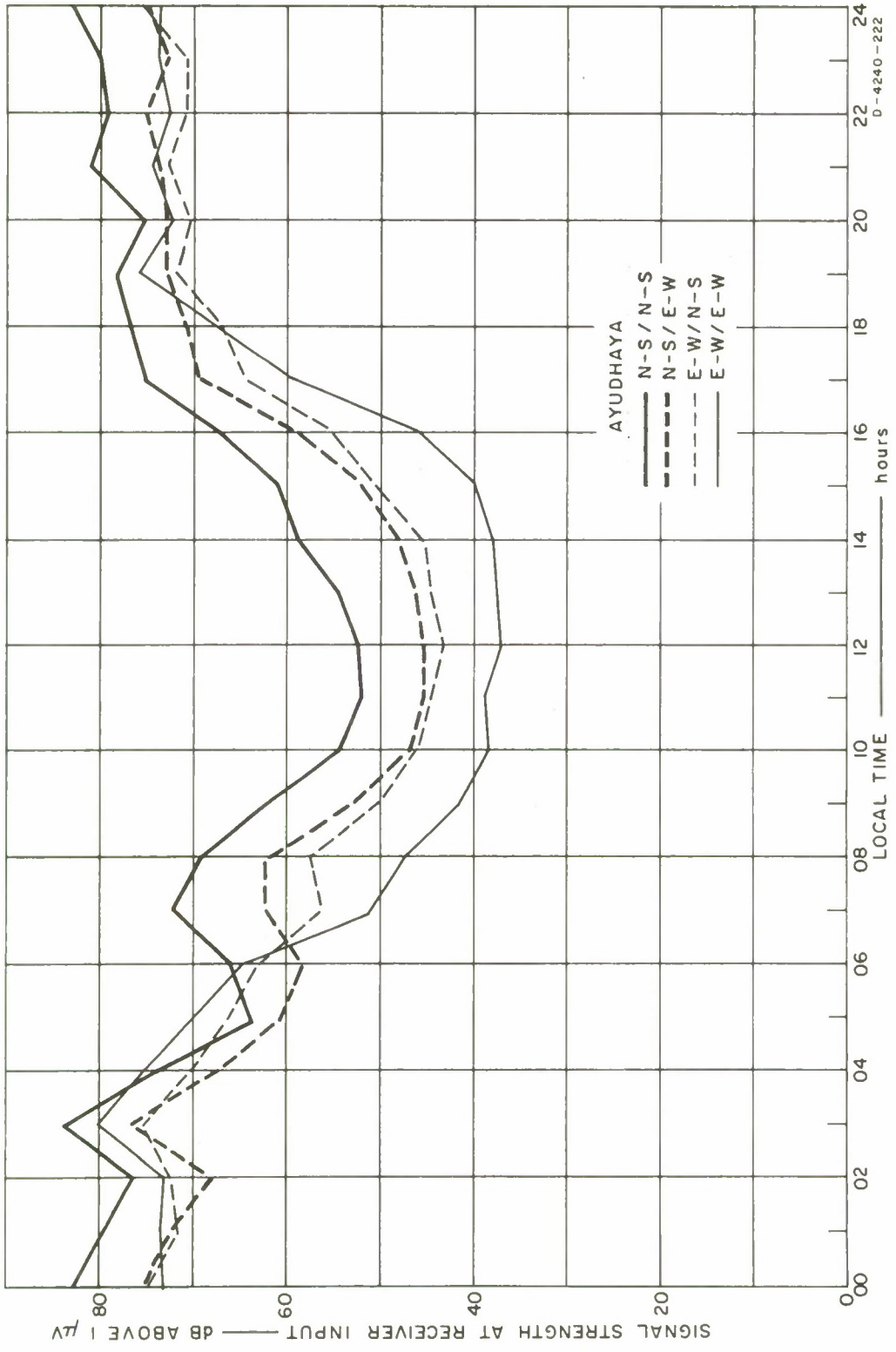

FIG. 46 AYUDHAYA: 1.7 MHz CW, ALL TRANSMITTING/RECEIVING ANTENNA COMBINATIONS

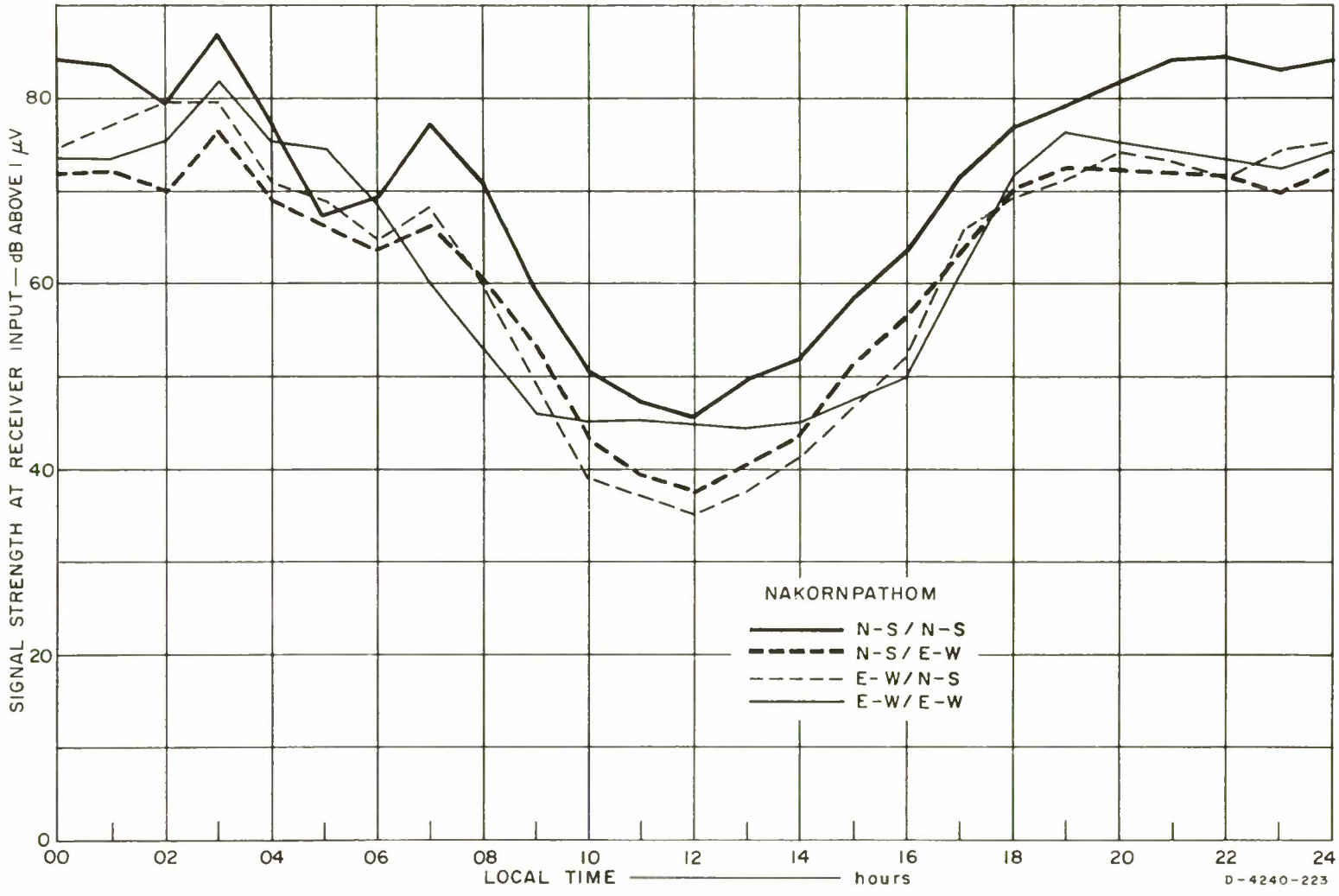

FIG. 47 NAKORNPATHOM: 1.7 MHz CW, ALL TRANSMITTING/RECEIVING ANTENNA COMBINATIONS

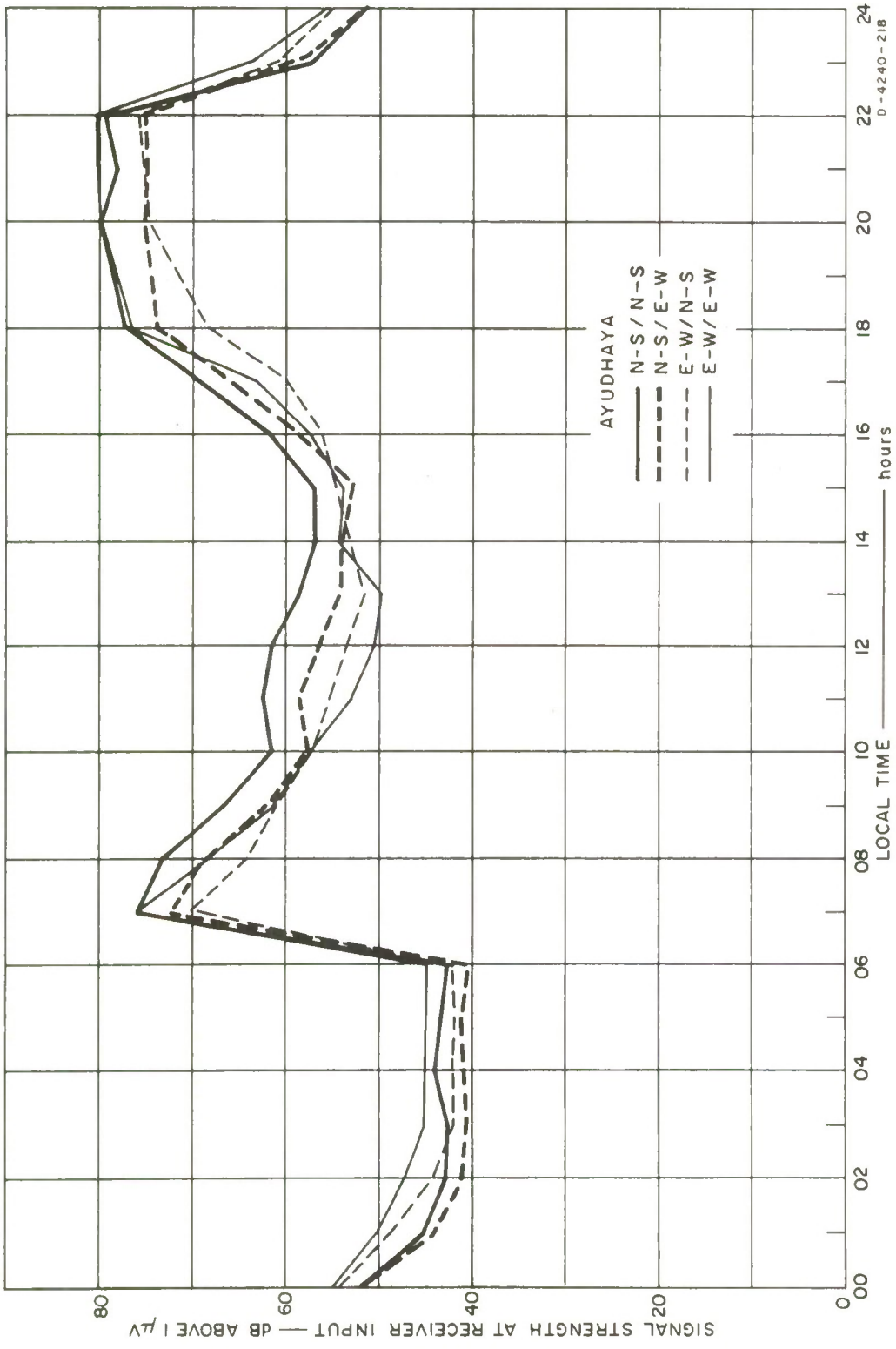

FIG. 48 AYUDHAYA: 3 MHz CW, ALL TRANSMITTING/RECEIVING ANTENNA COMBINATIONS

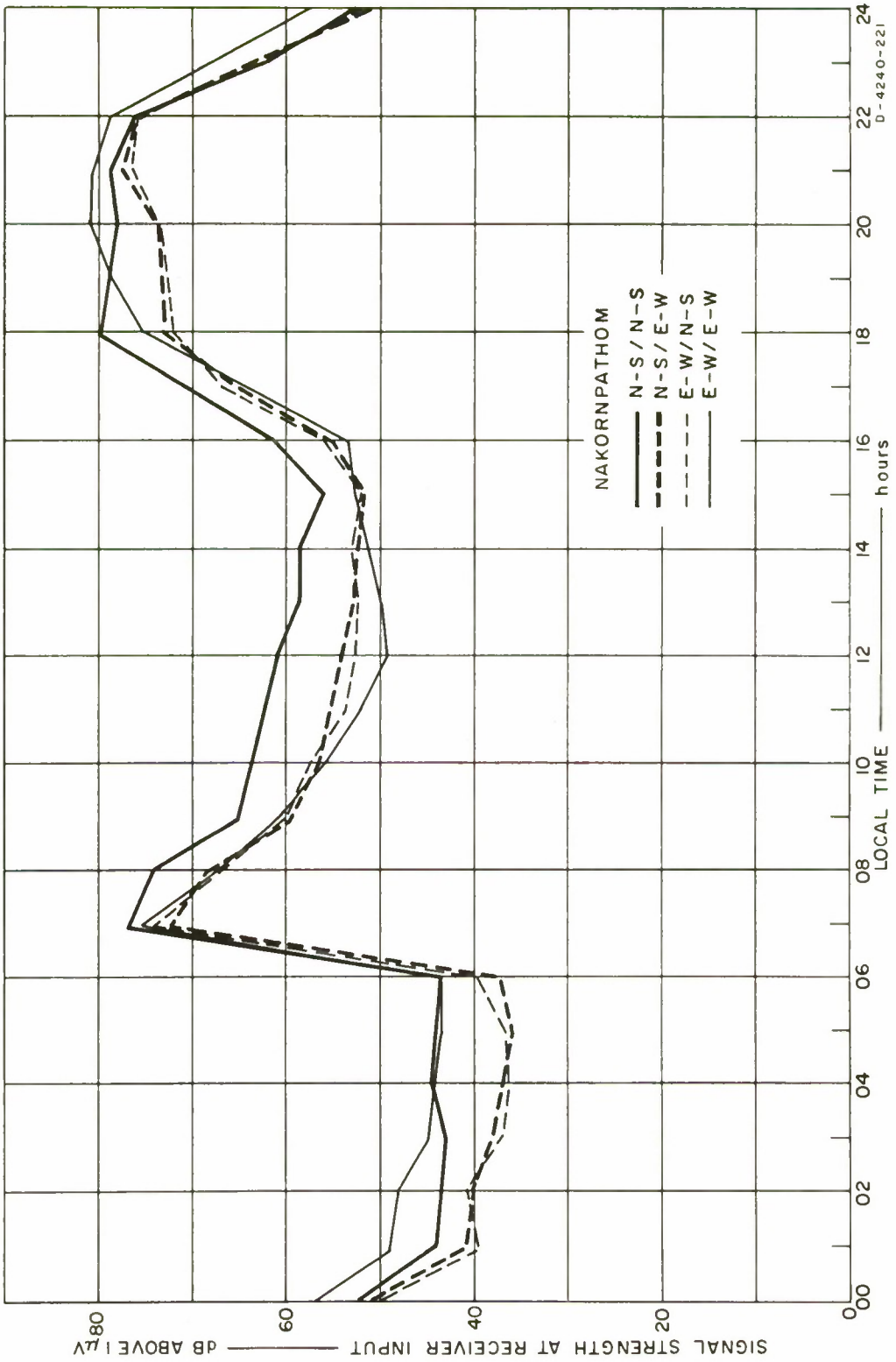

FIG. 49 NAKORNPATHOM: 3 MHz CW, ALL TRANSMITTING/RECEIVING ANTENNA COMBINATIONS

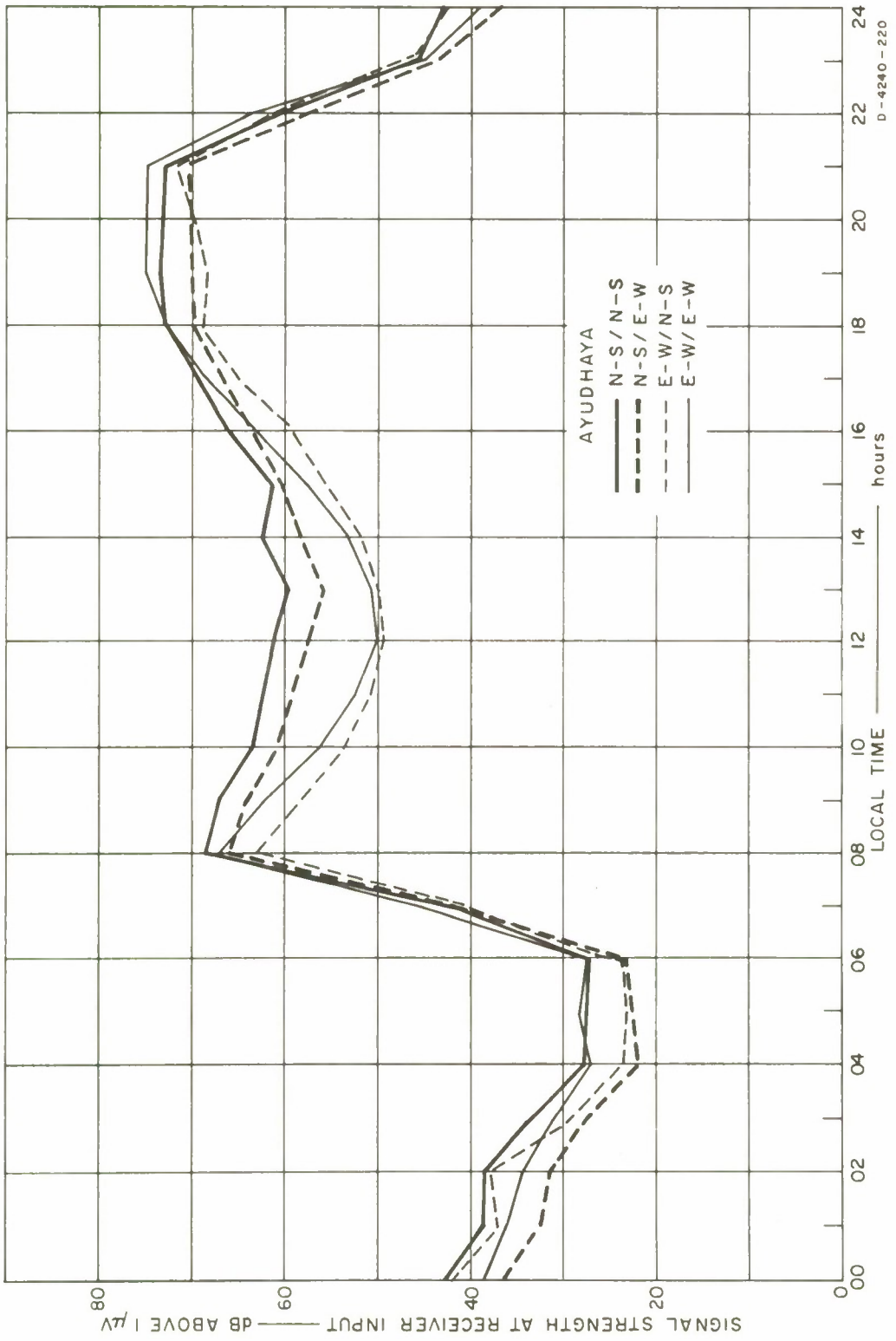

FIG. 50 AYUDHAYA: 5 MHz CW, ALL TRANSMITTING/RECEIVING ANTENNA COMBINATIONS

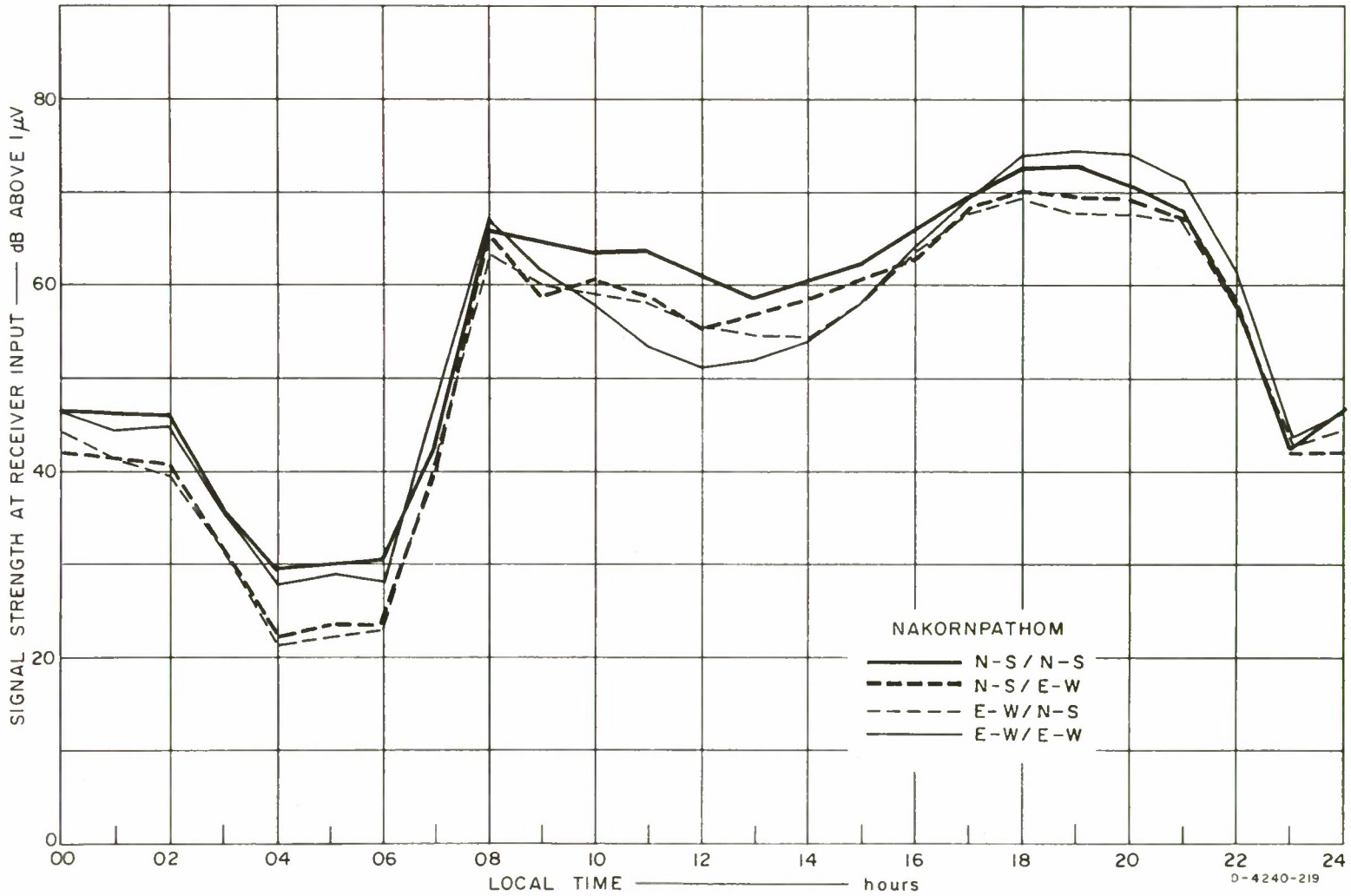

FIG. 51 NAKORNPATHOM: 5 MHz CW, ALL TRANSMITTING/RECEIVING ANTENNA COMBINATIONS

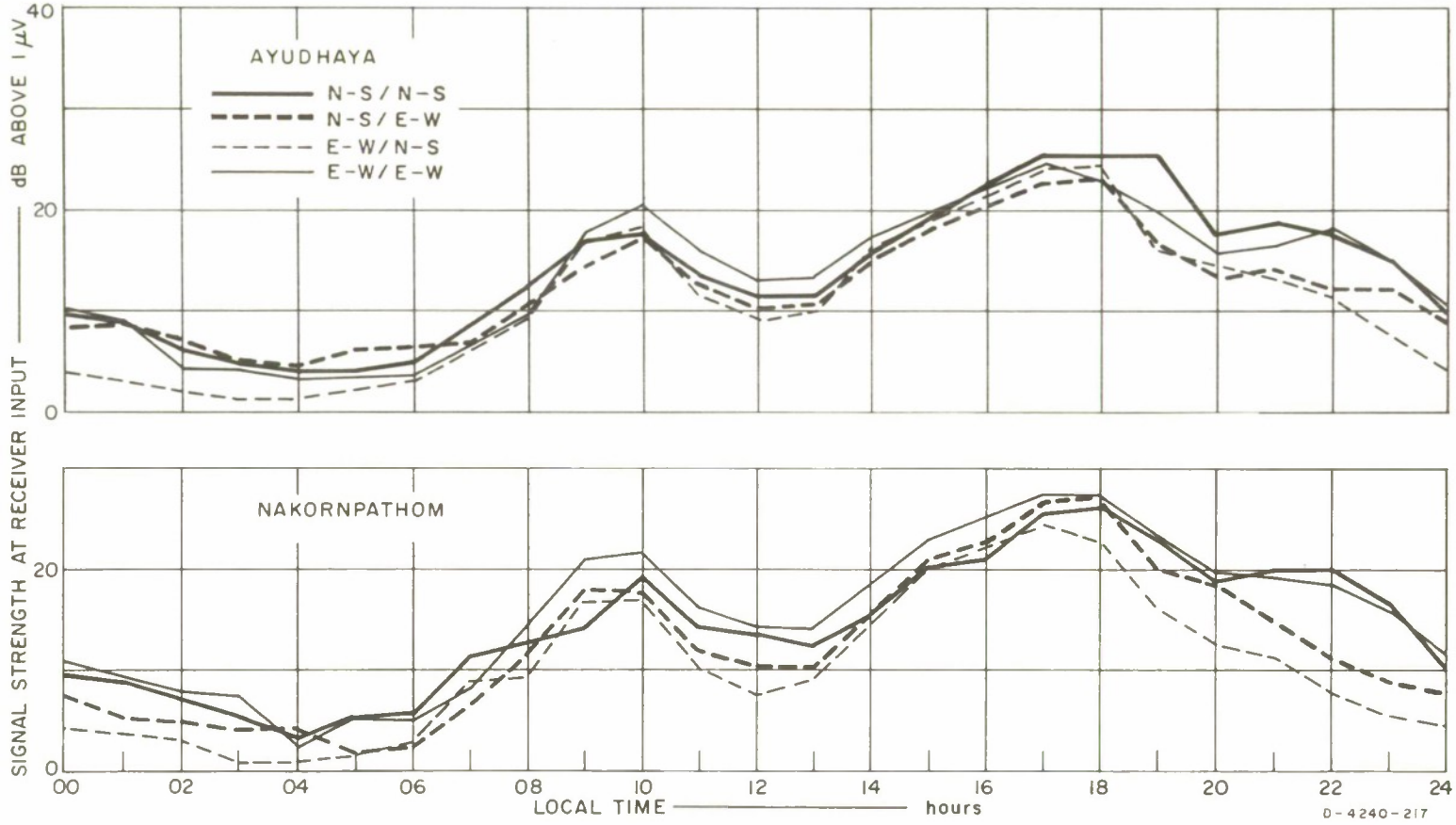

FIG. 52 10 MHz CW, ALL TRANSMITTING/RECEIVING ANTENNA COMBINATIONS

by about 7 dB (3-11 dB) throughout a 24-hour period, except during the pre-dawn period between 0330 and 0600, when the E-W/E-W mode was better by about 4 dB (1-6 dB) (see Fig. 46). These results generally supported the magneto-ionic theory, which predicts the superiority of the ordinary mode over the extraordinary during the day. The wave of a frequency nearer the critical value will traverse a longer path in the ionosphere before complete reflection, and the critical frequency of the ordinary mode is lower than that of the extraordinary. Consequently, although the nondeviative absorption of the ordinary wave is less than that of the extraordinary, the overall absorption of the ordinary wave (N-S/N-S mode) over the whole path could be greater than that of the extraordinary (E-W/E-W mode) during the period when the wave frequency is near the critical frequency of the F layer (i.e., when deviative absorption is becoming important for the ordinary wave but not yet important for the extraordinary wave).

The N-S/E-W combination followed closely the pattern of the fluctuation of the N-S/N-S mode and was lower by about 7 dB (3-11 dB). The amount of mode coupling is discussed in Sec. III-C-2.

The E-W/E-W was the poorest combination during the daytime, between 0700 and 1730, being lower than the N-S/N-S mode by about 18 dB (10-22 dB). This result is very important, for it firmly supports the magneto-ionic theory in that over the S-to-N (Bangkok/Ayudhaya) communication path, the normal practice[3] would require the dipole antennas to be of the E-W/E-W combination; however, the combination predicted as the worst when antenna pattern effects only are considered (viz., the N-S/N-S), proved to be the best method of orientation when both antenna pattern and ionospheric effect are considered, as predicted by theory.

The E-W/N-S mode followed the trend of the E-W/E-W mode, but the trends of these two modes did not correlate as well as did those of the N-S/N-S and N-S/E-W combination modes. This finding serves as an additional indication of the influence exerted by the earth's magnetic field over wave trajectories in the ionosphere, since the magnetic field over this S-to-N propagation path is tilted upward, and the waves at the entry to the ionosphere would satisfy the QT conditions better than the

waves leaving the ionosphere. Moreover, because conditions at entry are more important than those at exit, an optimum orientation of transmitting antennas is especially important. This statement is supported by the radio-teletype measurements described in Sec. V-C-2.

c. 1.7 MHz: Bangkok/Nakornpathom (E-to-W) Path

On this path also, the N-S/N-S was the best antenna combination (see Fig. 47). Its superiority over any other combination was very pronounced, as would be expected from the fact that the ordinary-wave performance should be further improved by the main-beam-to-main-beam coupling between N-S antennas for the E-to-W (Bangkok/Nakornpathom) path (see Fig. 19). The peak signal level was the same as that of Ayudhaya, but the trough was lower by about 6 dB. This latter observation would not be expected if the main-beam-to-main-beam coupling helped the propagation performance of the ordinary mode. It is therefore suggested that the ordinary wave over this E-W distance of 65 km at 1.7 MHz did not satisfy the QT conditions (see Figs. 13 and 14), and hence no strong preference for the ordinary mode would be expected.

The behavior of the N-S/E-W combination followed, as in the Ayudhaya case, that of the N-S/N-S and was lower by about 9 dB (1-13 dB). The other two antenna combinations--E-W/E-W and E-W/N-S--did not correlate well with each other.

d. 3 MHz: Bangkok/Ayudhaya and Bangkok/Nakornpathom Paths

Records obtained at both sites indicate the superiority of the N-S/N-S antenna combination during the daytime, between 0700 and 1900; this combination was better than the E-W/E-W mode by 6 dB (1-11 dB) at Ayudhaya and by 7 dB (3-11 dB) at Nakornpathom (see Figs. 48 and 49). At this frequency, QT conditions hold for the Bangkok/Ayudhaya propagation.

The E-W/E-W was the best combination between 2000 and 0600, being better than the N-S/N-S by 3 dB (1-7 dB) at Ayudhaya and by 3 dB (1-6 dB) at Nakornpathom. The superiority of the E-W/E-W mode over the N-S/N-S at 3 MHz was more pronounced than the corresponding superiority at 1.7 MHz. That the E-W/E-W mode at 3 MHz was so much stronger than the

N-S/N-S mode between 2000 and 0600, even for the E-W path, is because the ordinary wave would by this time be weaker than the extraordinary, which has a higher critical frequency.

One feature of interest is that 3 MHz is a better daytime frequency than 1.7 MHz, which is more suitable for nighttime propagation. For 24-hour communication, however, 1.7 MHz is the better overall frequency.

e. 5 MHz: Bangkok/Ayudhaya and Bangkok/Nakornpathom Paths

It should be recalled here that the QT conditions are just short of holding over the Bangkok/Ayudhaya path.

In general, except for some brief periods at night when the E-W/E-W became better, the N-S/N-S was the best combination throughout a 24-hour period. Between 0830 and 1630, the N-S/N-S was better than the E-W/E-W by 7 dB (3-11 dB) at Ayudhaya and by 6 dB (3-10 dB) at Nakornpathom (see Figs. 50 and 51). Between 1830 and 2230, the E-W/E-W was better than the N-S/N-S by 2 dB (1-3 dB) at Ayudhaya and by 3 dB (1-4 dB) at Nakornpathom. For the rest of the night, the ordinary wave (N-S/N-S) became stronger than the extraordinary, probably because both the ordinary wave and the extraordinary would be just above their critical frequencies and both would therefore traverse a long path in the ionosphere before being partially reflected, with the result that the signal strength of the less-absorbed ordinary mode could exceed that of the extraordinary.

During the day, diurnal fluctuations of the 5-MHz signal were not so great as those of the 3-MHz; their troughs were of the same level, but the 5-MHz peaks were lower than the corresponding 3-MHz peaks. In spite of the fact that 5 MHz would normally be advised for daytime communication, 3 MHz was shown by the results to be the better overall frequency. This might be accounted for by a sporadic-E layer strongly supporting the ionospheric propagation of an HF wave around 3 MHz, but is probably because 5 MHz is a greater amount above the layer critical frequency. These conclusions were supported quantitatively by the communication results with the Collins KWM-2A. (One must bear in mind that 1964 was the year of sunspot minimum.)

f. 10 MHz: Bangkok/Ayudhaya and Bangkok/Nakornpathom Paths

The results obtained on these paths were not easy to analyze. The frequency was above the MUF of the F2 layer most of the time, especially at night. No definite antenna combination showed superior performance (see Fig. 52). Only one mode, the E-W/E-W, deserves mention. It might be said to possess a certain degree of superiority, especially during the day, when the wave frequency was not too far from the F2 MUF. This might suggest the possibility of ionospherically propagated ground backscatter, but further study of this possibility is necessarily outside the scope of this investigation.

2. Mode Coupling

The amount of mode conversion or coupling from one mode (e.g., the ordinary) to the other mode may be extracted from the following relations:

$$(\text{N-S/N-S}) - C = (\text{N-S/E-W}) - (0 \rightarrow X)$$

$$(\text{E-W/E-W}) - C = (\text{E-W/N-S}) - (X \rightarrow 0) \quad ,$$

and hence the mode coupling,

$$0 \rightarrow X = \frac{(\text{N-S/E-W}) + 20 - (\text{N-S/N-S})}{(\text{N-S/N-S})}$$

and the mode coupling,

$$X \rightarrow 0 = \frac{(\text{E-W/N-S}) + 20 - (\text{E-W/E-W})}{(\text{E-W/E-W})} \quad , \qquad (47)$$

where $0 \rightarrow X$ indicates the conversion from the ordinary mode to the extraordinary; (N-S/E-W) means the signal input to the receiver in dB above 1 μV for the N-S/E-W antenna combination; and C = 20 dB is assumed to be the cross-polarization response between two orthogonally oriented dipoles. If C is some other value, then this gives a scale change and does not affect the relative diurnal variation of mode coupling observed; i.e., relative information on mode coupling is retained for different values of C. While this method of defining the mode coupling is not a standard usage, it does show the relative responses observed on the orthogonal dipole as a function of local time.

Extracted results, as shown in Figs. 53, 54, and 55, indicate that at 1.7 MHz there was an almost steady conversion in the ionosphere of the ordinary mode to the extraordinary, while the coupling of the extraordinary mode to the ordinary was very noticeably large during the day. This seeming nonreciprocity of mode conversion could probably be accounted for by the fact that during the daytime the absorption was large for either mode but larger for the extraordinary--so large that the ordinary-to-extraordinary-mode coupling failed to show as high a degree of conversion as the extraordinary-to-ordinary-mode coupling (i.e., mode purification of the ordinary mode occurred during the day because of the differential nondeviative absorption).

The 3-MHz data show that the amount of coupling was some 10 percent of the pure mode larger than the 1.7-MHz coupling. The ordinary-to-extraordinary-mode coupling increased to a high level just before midnight, when the extraordinary wave began to take over the superiority from the ordinary wave. Together with the mode coupling at 5 MHz, one can see that the effect of the conversion from one mode to the other was large when the ordinary mode showed better performance. The amount of mode coupling can be seen to be larger for a higher frequency; and for higher frequencies, the QT condition is more difficult to satisfy (smaller tolerance away from pure transverse propagation). It would be likely that the nearer the wave frequency approaches the critical frequency of a particular layer, the larger the amount of mode coupling becomes. It was observed (in pulse measurements, see Sec. IV-C-1-a) that the ordinary-to-extraordinary-mode coupling was greatest at the time of change from E to F layer.

3. Fading Characteristics

From a one-day data sample per test frequency of the signals received at Ayudhaya, a detailed analysis of fading characteristics was made. A survey of the total results obtained indicated that, as far as a qualitative analysis is concerned, the one-day data sample chosen is valid and typical of the total results obtained at both sites.

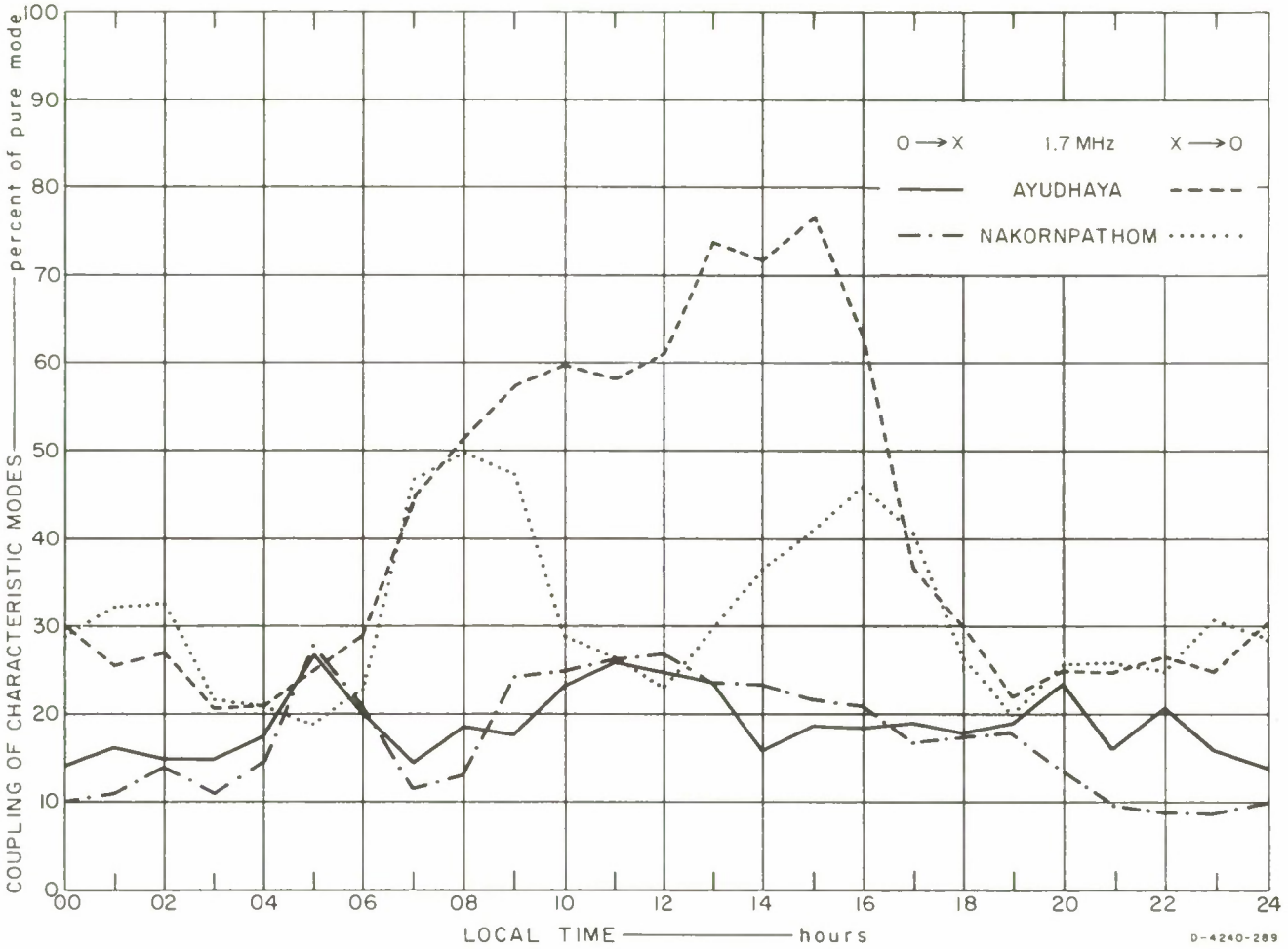

FIG. 53 MODE COUPLING BETWEEN ORDINARY AND EXTRAORDINARY WAVES, 1.7 MHz CW

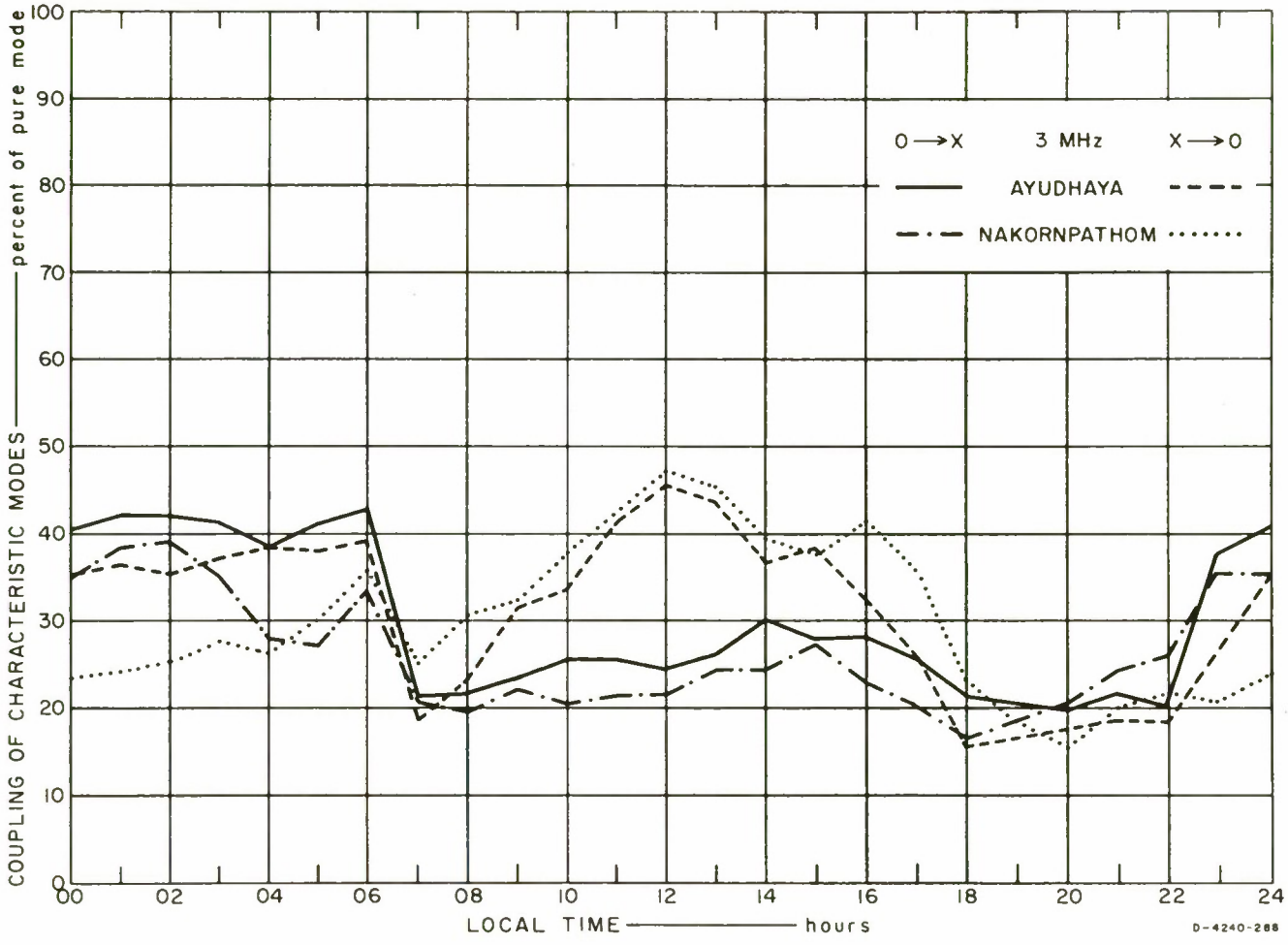

FIG. 54 MODE COUPLING BETWEEN ORDINARY AND EXTRAORDINARY WAVES, 3 MHz CW

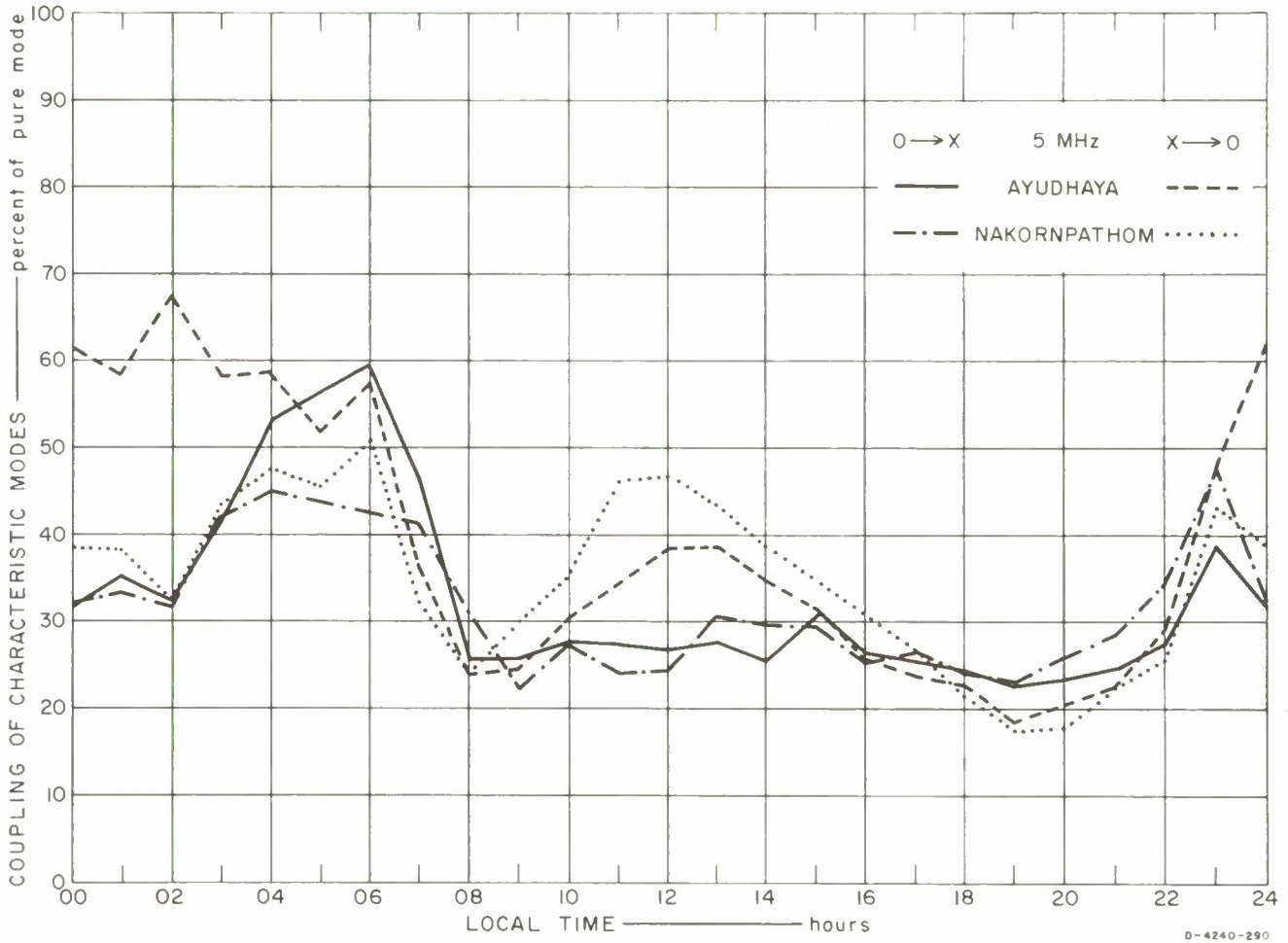

FIG. 55 MODE COUPLING BETWEEN ORDINARY AND EXTRAORDINARY WAVES, 5 MHz CW

a. Number of Fades per Minute

Figures 56 and 57 show the number of fades per minute for each hour of the day for all four transmitting/receiving antenna combinations and for 1.7, 3, and 5 MHz. Only fades of duration less than 5 seconds were counted. It can be seen that the N-S/N-S combination and hence the ordinary wave faded slightly more than the E-W/E-W or the extraordinary wave during the night, but during the day, when the signal strength of the ordinary wave was above that of the extraordinary, it faded less. Because the N-S/N-S also faded more than the N-S/E-W for most of the time, it appears possible to effect improvement by utilizing the polarization-diversity system of a special type to be referred to as orientation diversity, with N-S and E-W dipoles for reception.

Generally, the 1.7-MHz signal faded only a few times per minute: fading about five times per minute except during a few hours after sunset and before sunrise, when the fading occurred a little over ten times per minute. The 3-MHz signal faded less than six times per minute during the daytime; at night the fading was more frequent, reaching the peak value of about 40 times per minute around 0200. The 5-MHz fading generally followed the 3-MHz pattern, with a comparatively low rate during the day (about three times a minute) and with a high rate during the night, reaching a very high peak of about 80 times per minute around 0400. These observations strengthen the previous inference that 3 MHz is better frequency than 5 MHz and that, of the three frequencies considered, 1.7 MHz is the best all-round. (The reader is again reminded that the test was carried out during the period of the sunspot minimum.)

b. Duration of Fading

Beside the frequency of occurrence, another important factor governing the severity of fading is the duration, which is here defined as the time taken by the amplitude to change from a maximum to a minimum and back to a maximum. Figure 58 shows the duration of fading in seconds for each hour of the day for all four antenna combinations and for 1.7, 3, and 5 MHz over the Bangkok/Ayudhaya path. It is apparent that slow fades occurred during the day and rapid fades occurred during the night.

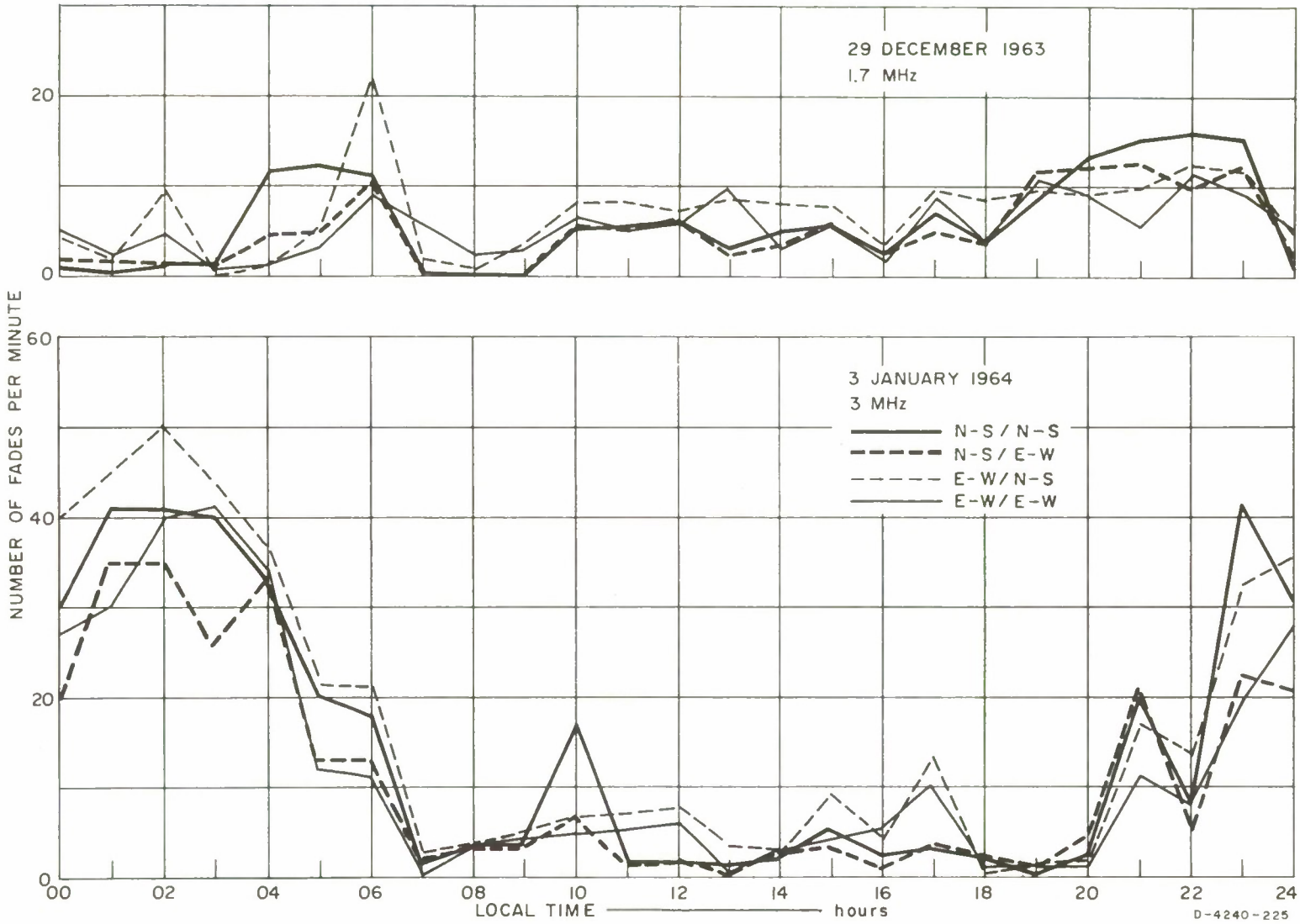

FIG. 56 NUMBER OF FADES PER MINUTE, 1.7 AND 3 MHz, AYUDHAYA ONLY

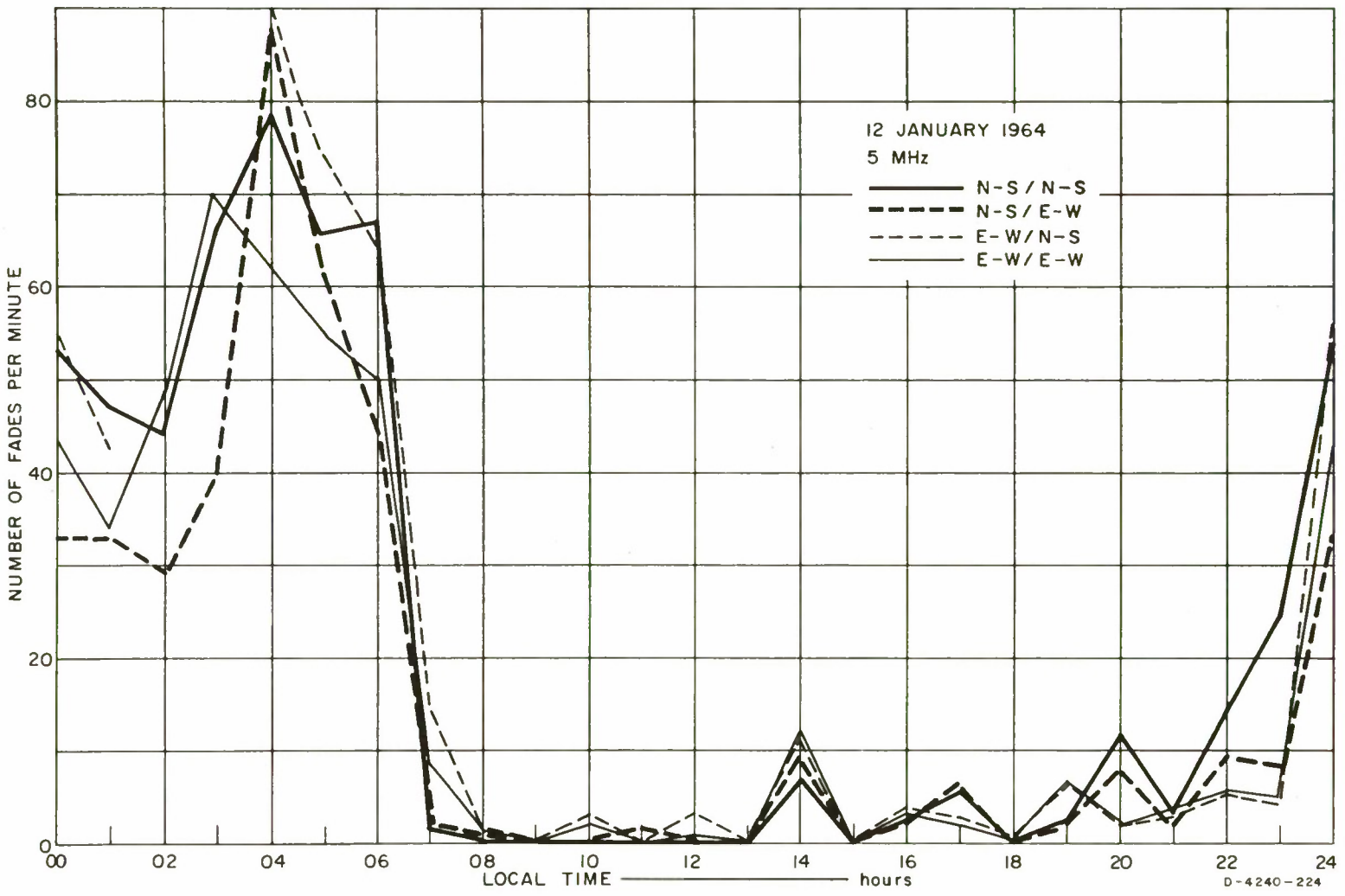

FIG. 57 NUMBER OF FADES PER MINUTE, 5 MHz, AYUDHAYA ONLY

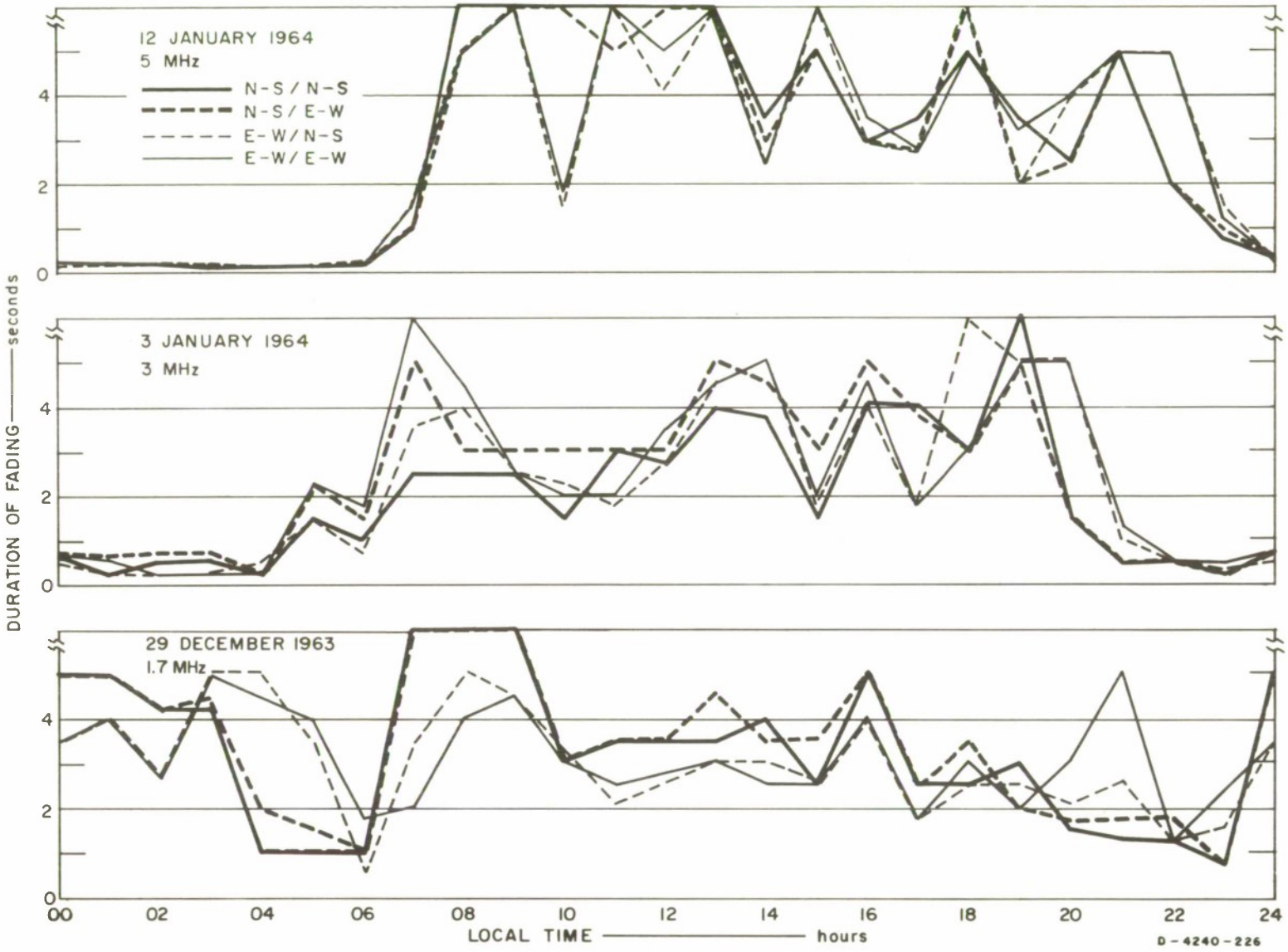

FIG. 58 DURATION OF FADING; 1.7, 3, 5 MHz; AYUDHAYA ONLY

Presumably, this rapid fading can be attributed to multipath caused by decreased absorption at night[13] as anticipated and observed on the pulse test (see Sec. IV-C-1-c), and when the signal was above the critical frequency of the F layer, the scattering mechanism would cause rapid fading (see Fig. 58 for 3 and 5 MHz relative to 1.7 MHz).

c. Severity of Fading

The severity of fading in relation to frequency is best seen from curves showing the number of fadings per minute against the duration of fading in seconds, as illustrated in Figs. 59, 60, and 61. The curves clearly show that the higher the frequency the more severe was the fading and that the ordinary wave in general faded more severely than the extraordinary. This is probably owing to the differential absorption (ordinary less absorbed) for the QT case.[13]

The most severe fading at 1.7 MHz, that of the ordinary wave, was likely to be of 1.5-s duration, occurring 2.5 times per minute; the fading of the extraordinary wave was likely to be of 1.8-s duration, occurring 2.1 times per minute. At 3 MHz, the most severe fading of the ordinary wave was likely to be of 0.4-s duration, occurring 4.8 times per minute, while that of the extraordinary was likely to be of the same duration but occurring about 4.4 times per minute. The fading of a 5-MHz signal could be very severe. Very rapid fadings of less than 0.1-s duration were observed 11.6 times per minute for the ordinary wave and about 10 times for the extraordinary.

On the basis of fading characteristics alone, the extraordinary wave is to be preferred over the ordinary, although not to a considerable degree. Since there was a difference in the fading characteristics, the possibility of improving system performance by using orientation diversity appears to be increased.

4. Noise at Receiver Input

The factor that has always been considered important to the performance of reception is noise; more precisely, a measure closely related to communication system performance is signal-plus-noise-to-noise ratio $[(S + N)/N]$. The measured noise level in dB above 1 μV at inputs to

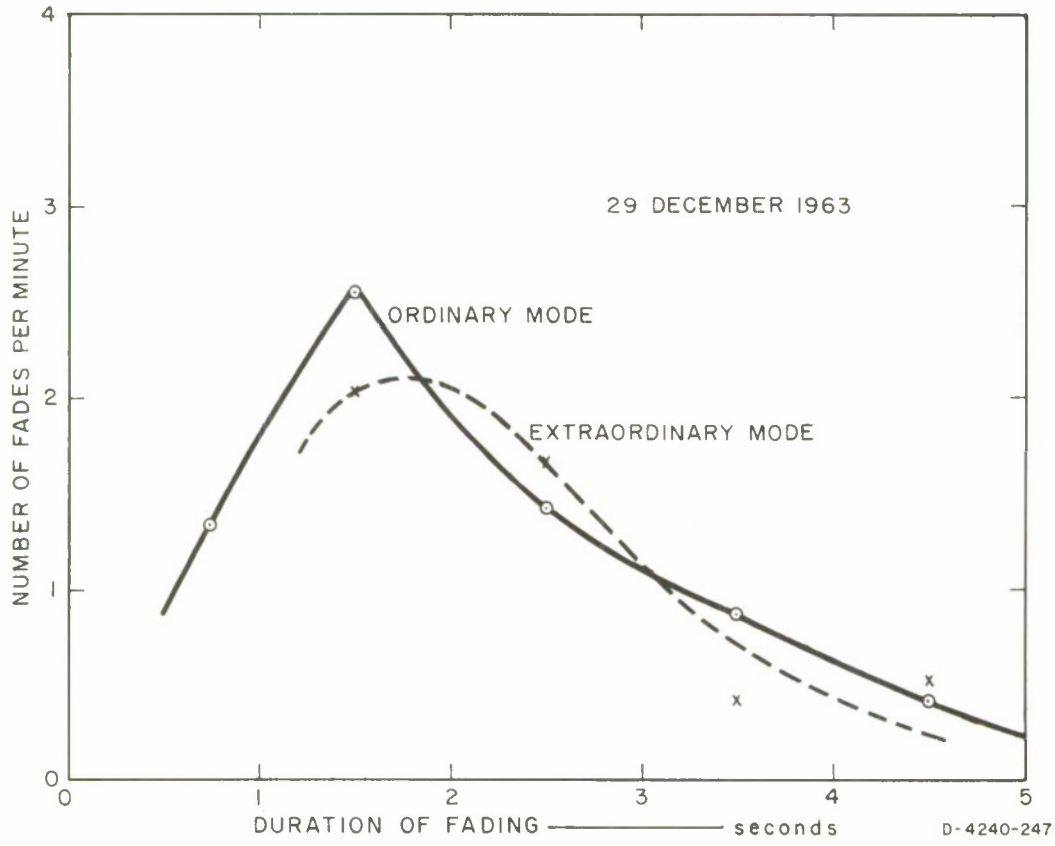

FIG. 59 SEVERITY OF FADING: NUMBER OF FADES PER MINUTE AS A FUNCTION OF DURATION OF FADING IN SECONDS, 1.7 MHz

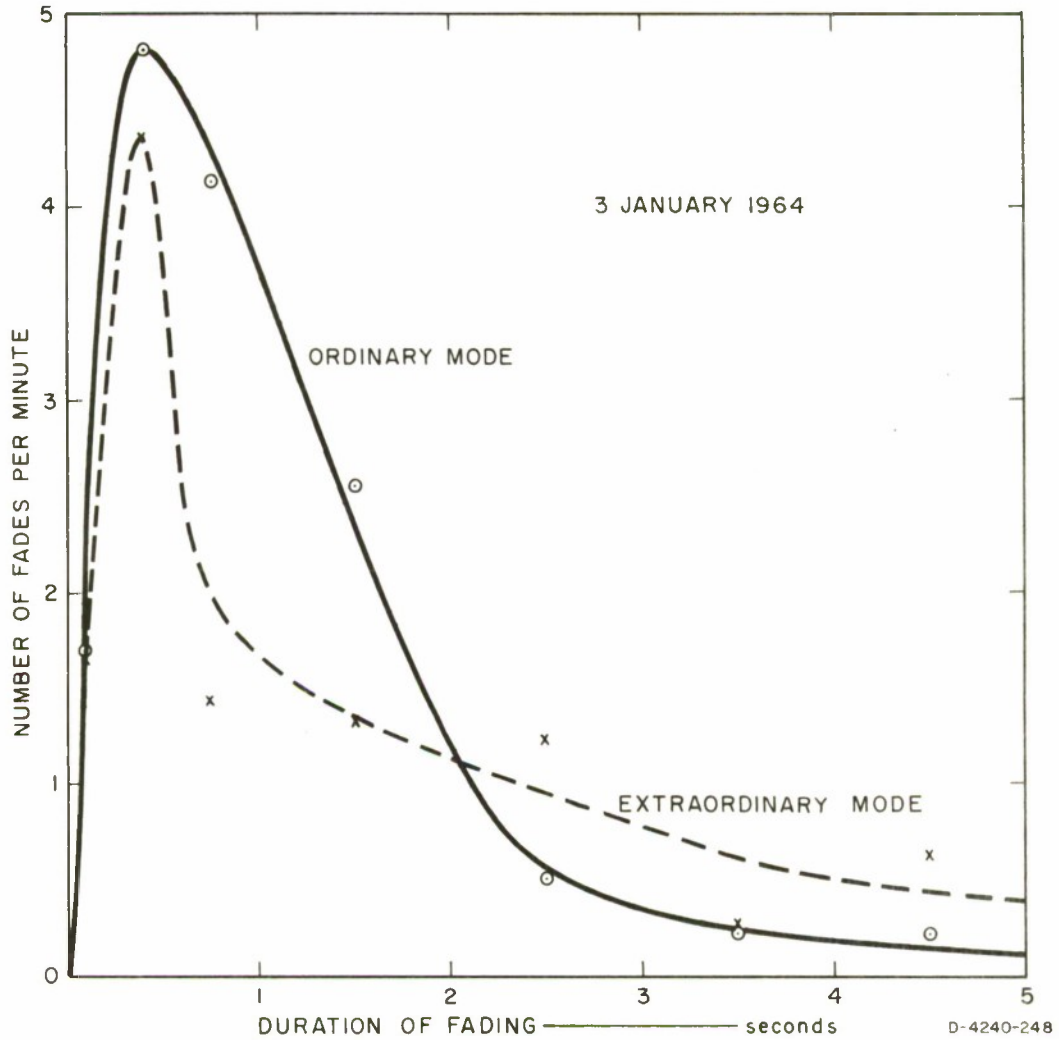

FIG. 60 SEVERITY OF FADING: NUMBER OF FADES PER MINUTE AS A FUNCTION OF DURATION OF FADING IN SECONDS, 3 MHz

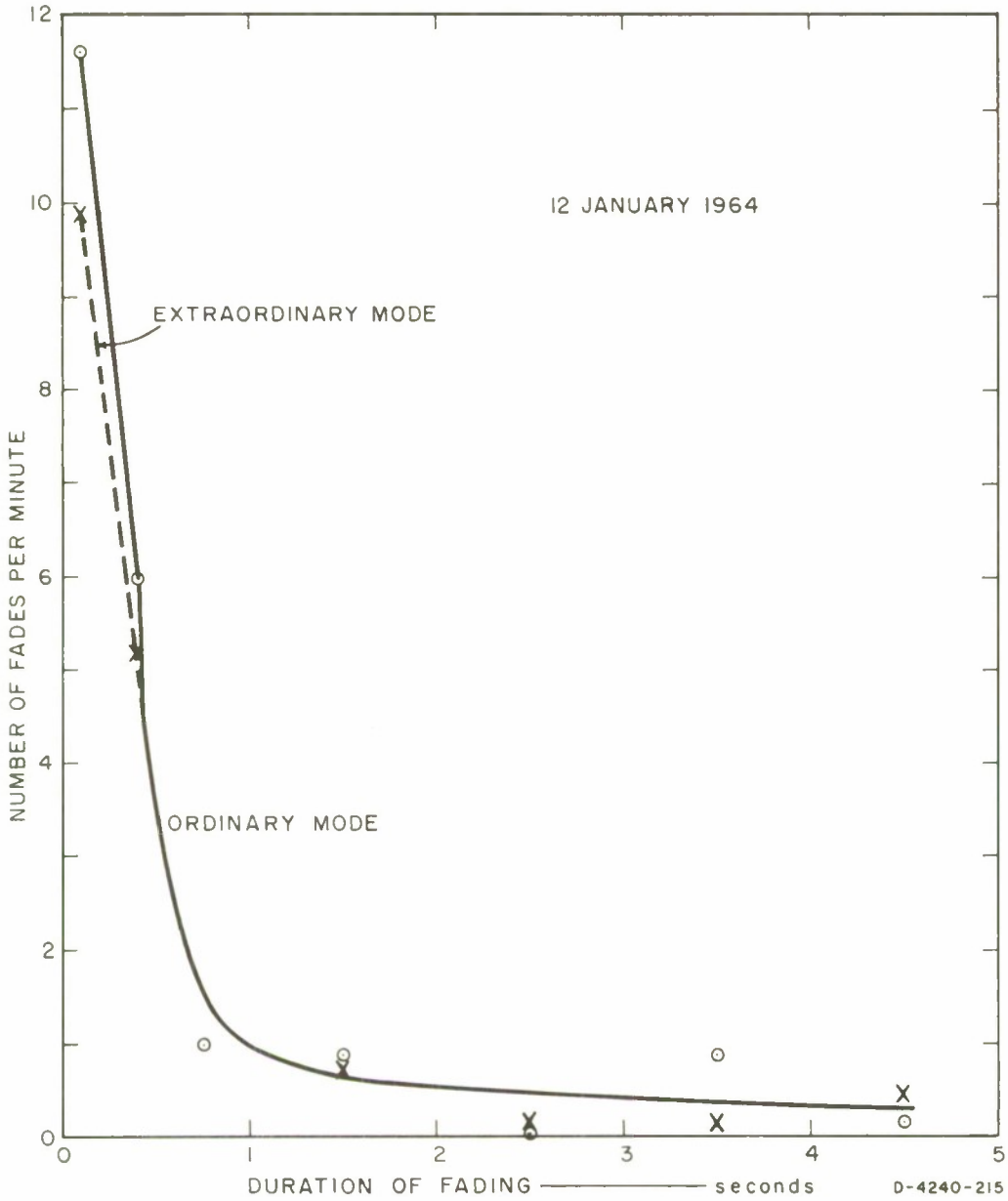

FIG. 61 SEVERITY OF FADING: NUMBER OF FADES PER MINUTE AS A FUNCTION OF DURATION OF FADING IN SECONDS, 5 MHz

receivers with 2-kHz bandwidth via a N-S and an E-W dipole was recorded each hour of the day for 1.7, 3, and 5 MHz, as shown in Fig. 62 for the Ayudhaya site. Noise level was only a few dB above 1 μV during the daytime, between 0800 and 1600. The noise became high for the rest of the day, with the general level of 20 dB above 1 μV for all three frequencies, with a single exception: between 1800 and 2300, the noise level at 5 MHz stayed high, approximately 42 dB above 1 μV.

Generally, the E-W antenna picked up about 3 dB more noise than the N-S antenna. Probably this can be explained by the fact that the storm belt near the equator produces atmospheric noises mainly in the E-W direction; because of their vertically polarized nature, these noises were probably induced end-on into the horizontal E-W dipole more than broadside into the horizontal N-S dipole.

That the E-W dipole picked up more noise than the N-S would tend to weigh against the desirable property of the extraordinary mode possessing less severe fading in the signal received. With all factors considered, including the previous discussion on signal strength, it can be said that better performance may be obtained by using the ordinary wave for both transmission and reception. The (S + N)/N curves, if constructed, would effectively remain identical with the signal-strength curves, since noises picked up by the N-S and E-W antennas did not noticeably differ. They, however, would yield low (S + N)/N ratios that could explain the large amount of rapid fading of the 3-MHz and the 5-MHz propagation at night.

5. Orientation Diversity

The possibility of still better performance with the help of orientation diversity cannot be neglected, however, since the extraordinary wave definitely has its merits, especially during the difficult nighttime periods. An attempt was made (see Fig. 63) to assess the degree of requirement for orientation diversity reception with the N-S and E-W crossed dipoles and with either the N-S or the E-W dipole for transmission. The degree of requirement for orientation diversity was assigned the values 0, 1, 2, and 3 with the following meanings:

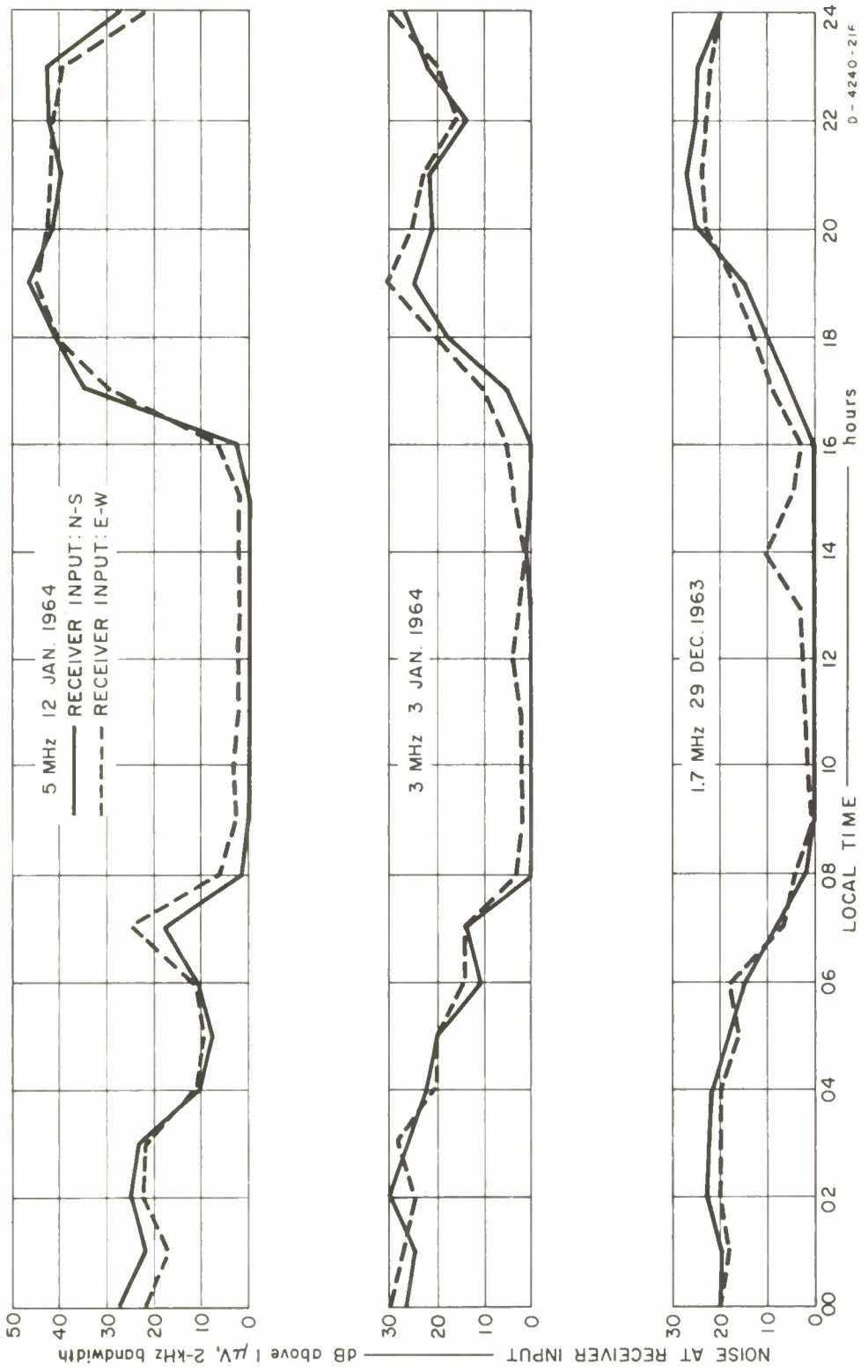

FIG. 62 NOISE AT RECEIVER INPUT, 1.7, 3, AND 5 MHz

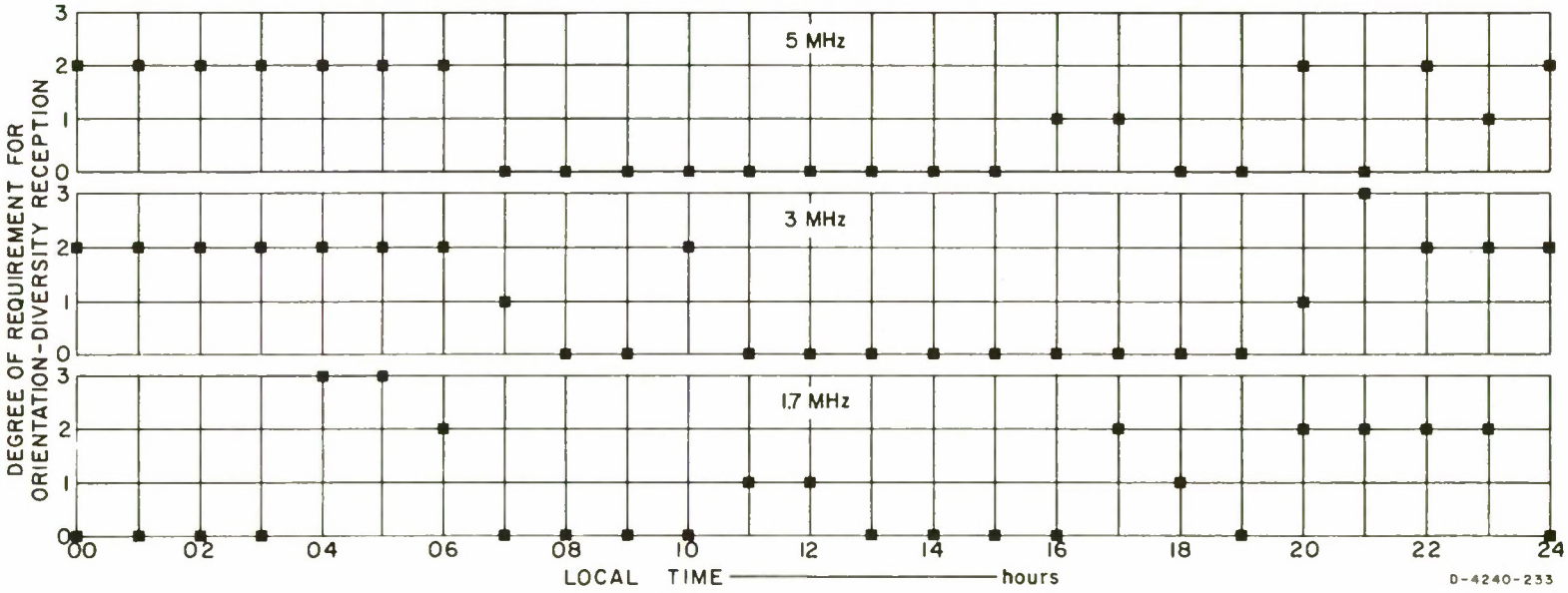

FIG. 63 DEGREE OF REQUIREMENT FOR ORIENTATION DIVERSITY RECEPTION

0--The ordinary wave is best suited to both the transmission and the reception, and hence the diversity is not at all needed.

1--The diversity, although not really necessary, is helpful, because the N-S/E-W combination has either shallower or less frequent fadings, while the ordinary wave, i.e., the N-S/N-S, is still sufficiently strong.

2--The diversity is necessary or desirable with the N-S dipole for transmission, because the N-S/N-S combination fades more rapidly or more frequently than the N-S/E-W, and consideration of the correlation between these two modes indicates that the diversity would improve the performance.

3--The diversity is desirable, with the E-W dipole for transmission, because the E-W/E-W combination has higher signal strength and fades less frequently than the N-S/N-S combination that the diversity with a transmitting E-W dipole considerably outperforms the diversity with a transmitting N-S dipole.

A sample of data with these values assigned, indicating the degree of diversity requirement, is given in Figs. 64 through 67.

It may be observed from Fig. 63 that 1.7 MHz generally did not need the diversity reception except between 2000 and 2300. The 3-MHz and 5-MHz reception was satisfactory during the day, without the need for orientation diversity, but the diversity was desirable during the night when signal strengths were low, the noise increased, and hence more pronounced fading effects.

When the communication contact is at stake, it is advisable to use sets with provision for a diversity reception with N-S and E-W crossed dipoles and with the N-S dipole for transmission. The system with the E-W dipole for transmission was not found to be as helpful as one might expect from the superiority of the extraordinary wave at 3 and 5 MHz during the night, since the E-W/N-S combination tended to fade too severely during this period.

BANGKOK TO AYUDHAYA - 1.7MHz
29 DEC. 1963 0705-0710 LOCAL TIME

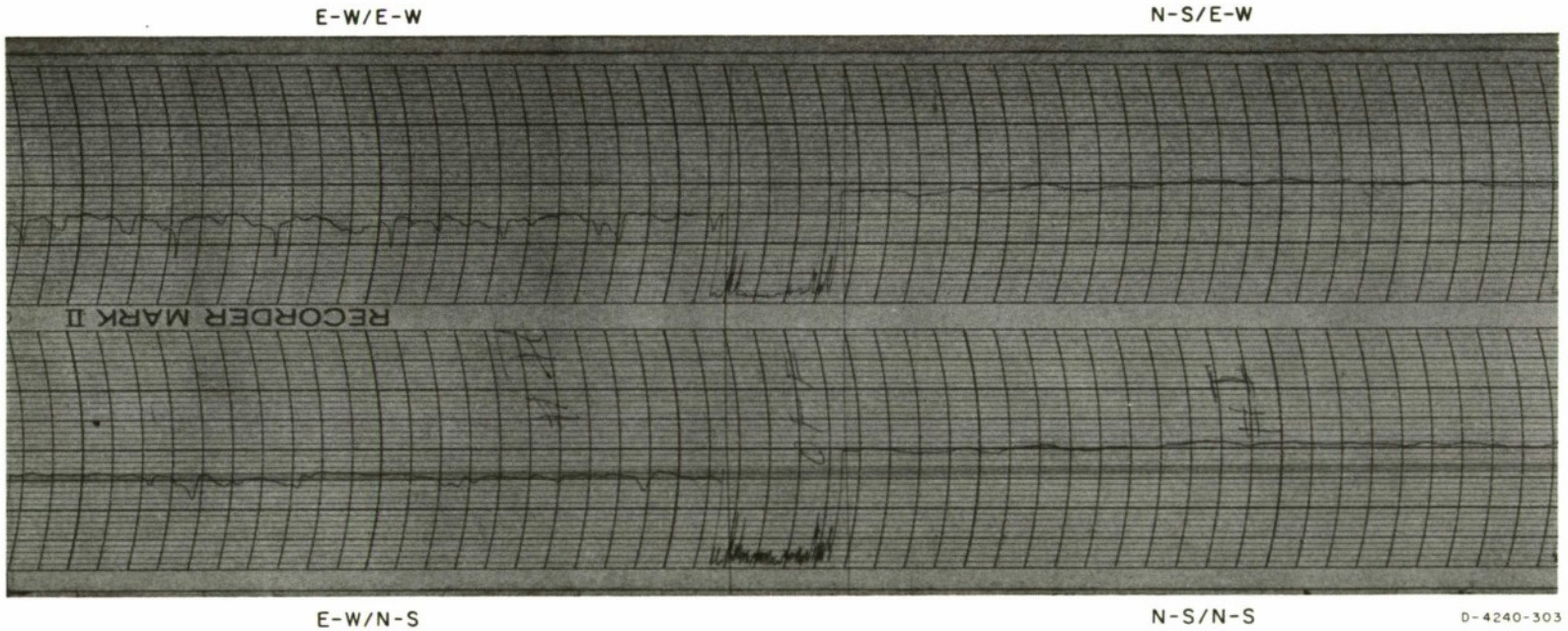

FIG. 64 SAMPLE SHOWING DEGREE OF REQUIREMENT FOR ORIENTATION DIVERSITY = 0

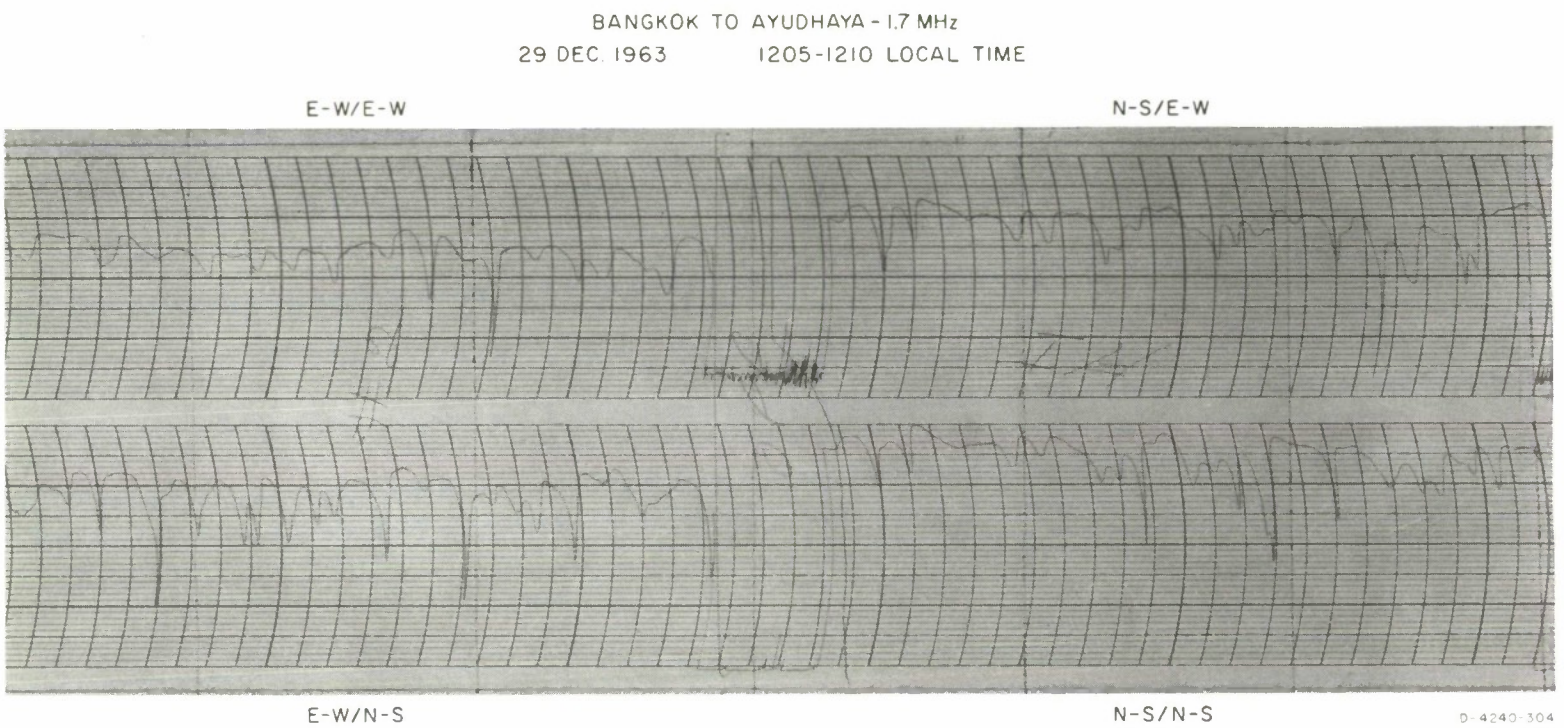

FIG. 65 SAMPLE SHOWING DEGREE OF REQUIREMENT FOR ORIENTATION DIVERSITY = 1

BANGKOK TO AYUDHAYA-1.7 MHz
29 DEC. 1963 0605-0610 LOCAL TIME

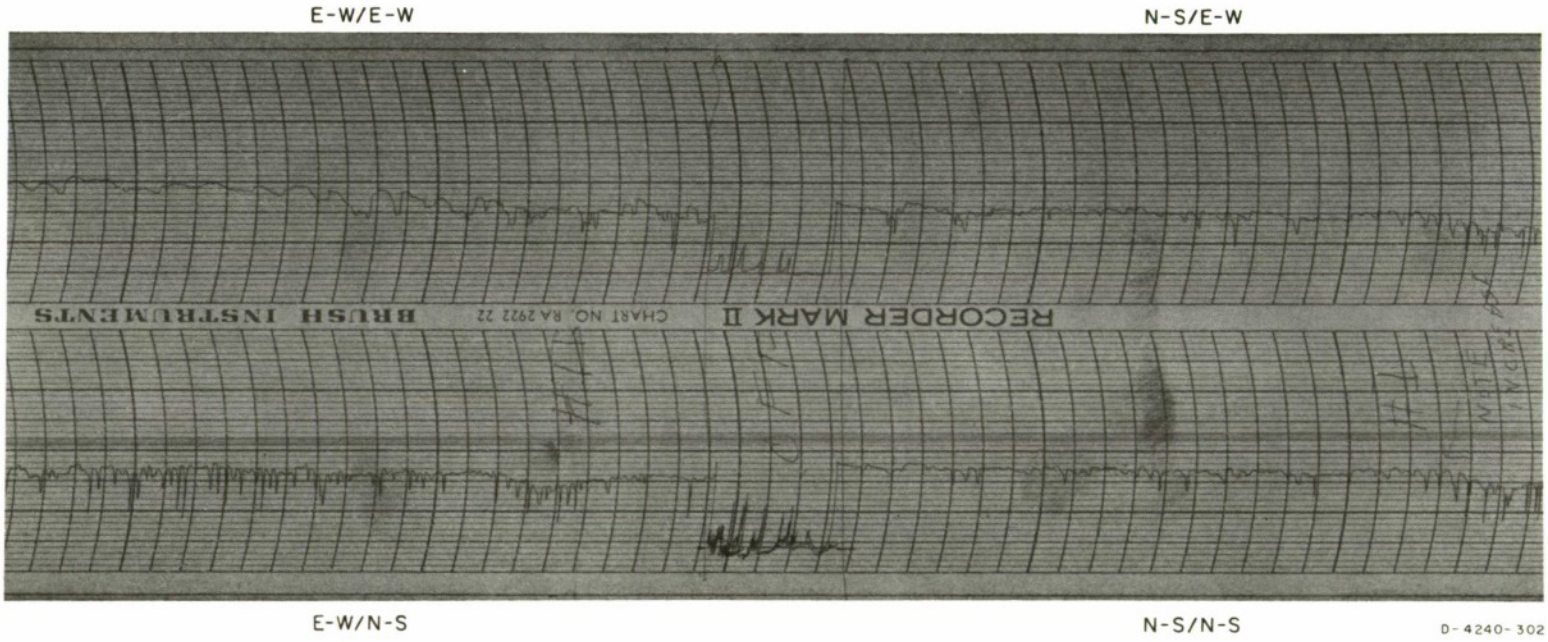

FIG. 66 SAMPLE SHOWING DEGREE OF REQUIREMENT FOR ORIENTATION DIVERSITY = 2

BANGKOK TO AYUDHAYA – 1.7 MHz
29 DEC. 1963 0505-0510 LOCAL TIME

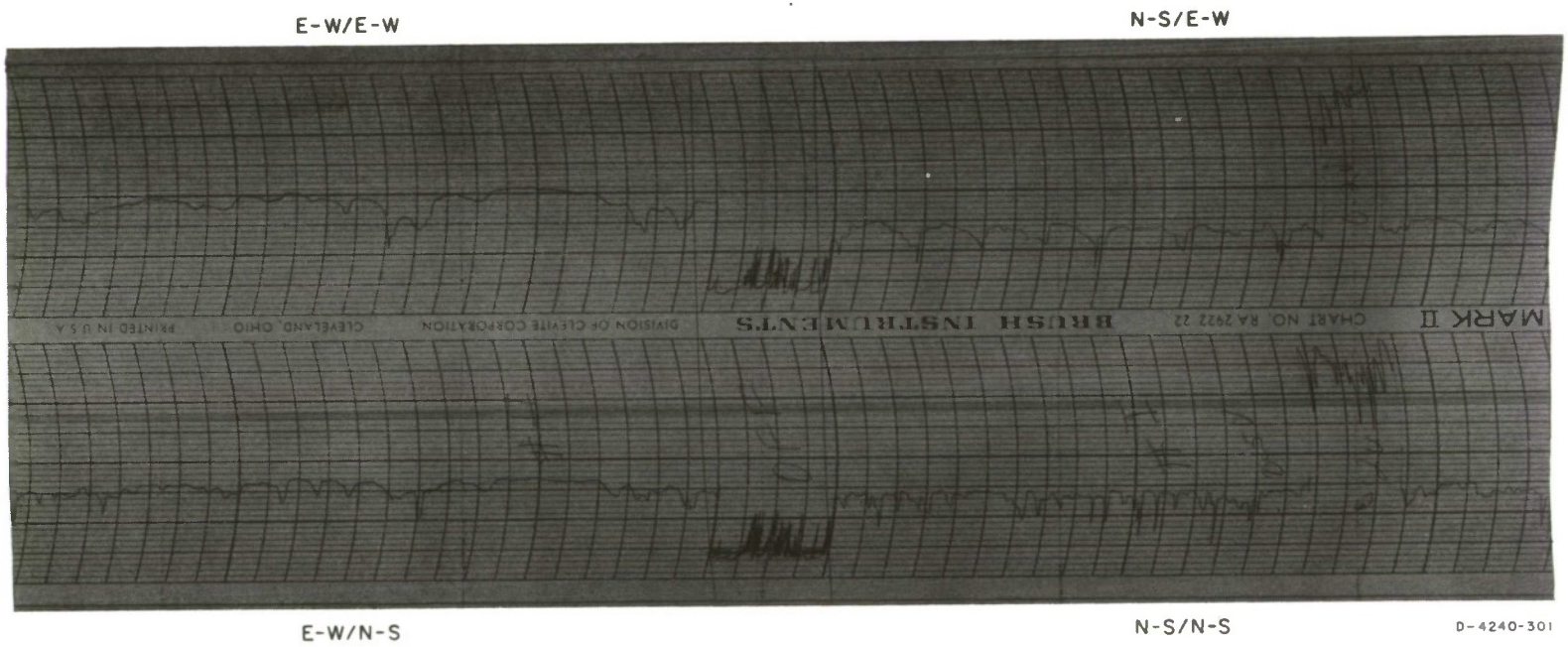

FIG. 67 SAMPLE SHOWING DEGREE OF REQUIREMENT FOR ORIENTATION DIVERSITY = 3

The results of tests with radio-teletype equipment as reported in Sec. V indicate that the orientation diversity reception may be further improved by aligning the transmitting antenna in the NE-SW direction, thus transmitting both the ordinary and the extraordinary waves (cf. Secs. V-C-3 and V-C-4).

IV PULSE MEASUREMENTS

A. GENERAL

The use of the pulse-recording method enables the trained analyst to distinguish various modes of propagation, including virtual heights of reflection; however, the technique is quite involved and requires trained personnel who have a special knowledge of ionospheric radio propagation. Amplitude stability and phase stability may be obtained from pulse data in a relatively simple manner. The ability to obtain information on the phase stability (pulse stretching) of a received signal is the decided advantage of the pulse method over the CW method.

The pulse test was designed with a view to

(1) Proving certain aspects of the magneto-ionic theory, leading to the optimization of antenna orientation, and

(2) Obtaining ranges within which the findings may be utilized.

B. TEST PROCEDURE AND DATA REDUCTION

1. Instrumentation

Some considerations in the design of pulse measurement instrumentation were: utilization of existing equipment, simplicity, flexibility, and synchronization of transmitter and receiver sites. The desired RF pulse was determined to be 50 μs wide, with fast rise or decay time (not exceeding 5 μs) and a PRF of 50 pps.

a. Pulse Transmission

The pulse transmission system is shown in block diagram form in Fig. 68. The synchronized PRF and sync generator, shown in Fig. 69, was designed to divide the 100-Hz output of the H-P Model 5243L electronic counter to 50 Hz. The PRF and sync circuit consists of a flip-flop, an emitter follower, and an amplifier. The output of the amplifier was used to trigger the Tektronix 161 pulse generator and the monitoring oscilloscope, at the transmitter site. The 50-μs pulse from the pulse

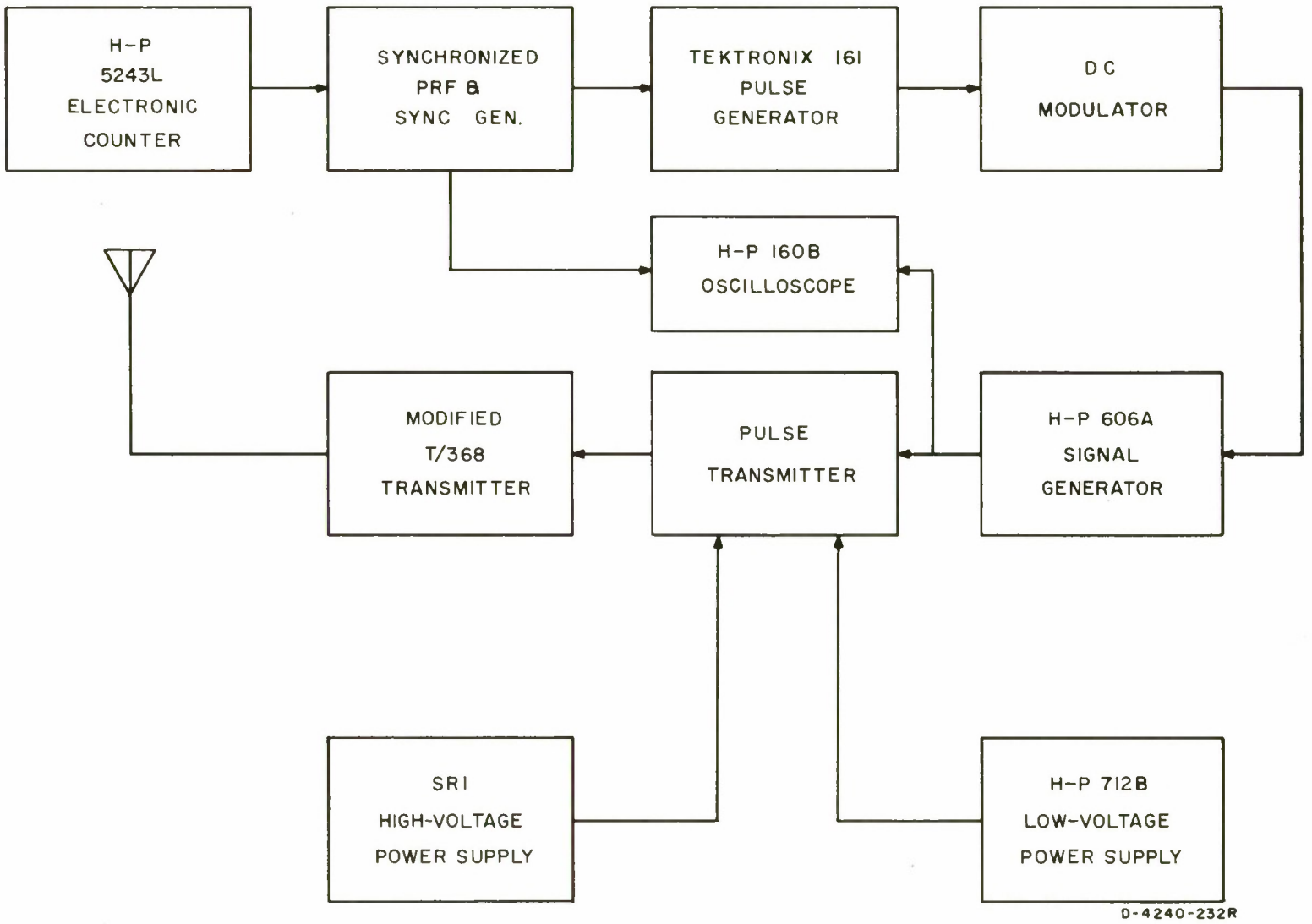

FIG. 68 INSTRUMENTATION BLOCK DIAGRAM FOR PULSE TRANSMISSION

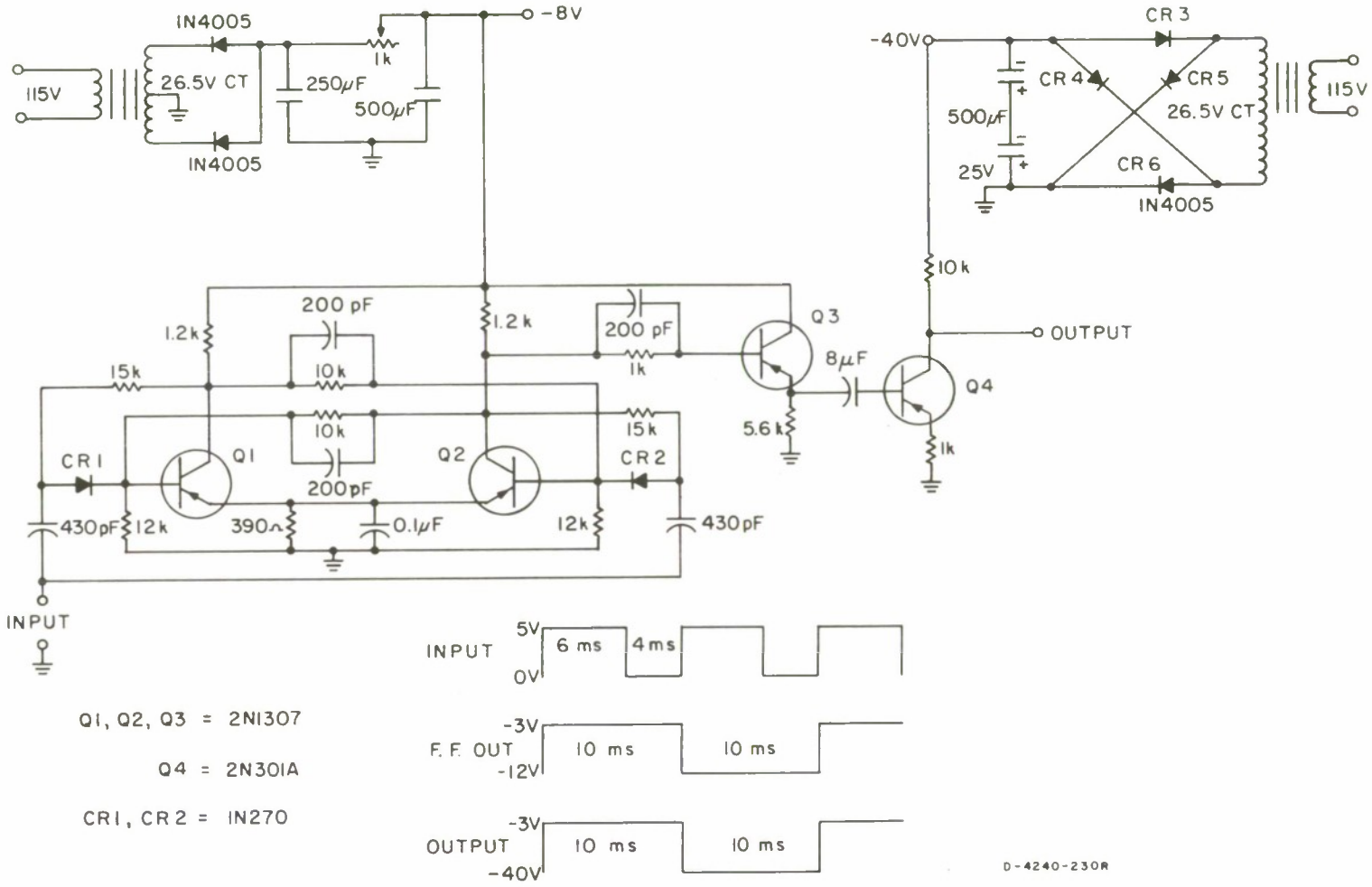

Q1, Q2, Q3 = 2N1307

Q4 = 2N301A

CR1, CR2 = IN270

FIG. 69 CIRCUIT DIAGRAM OF SYNCHRONIZED PRF AND SYNC GENERATOR

generator was converted by the dc modulator, as shown in Fig. 70, to drive the H-P Model 606A signal generator, which needs a negative voltage, (rather than a zero voltage), to maintain cut-off. When fed with the 50-μs pulse from the dc modulator, the H-P 606A produces a 50-μs RF pulse with a rise time of less than 2 μs and a decay time of 3 μs.

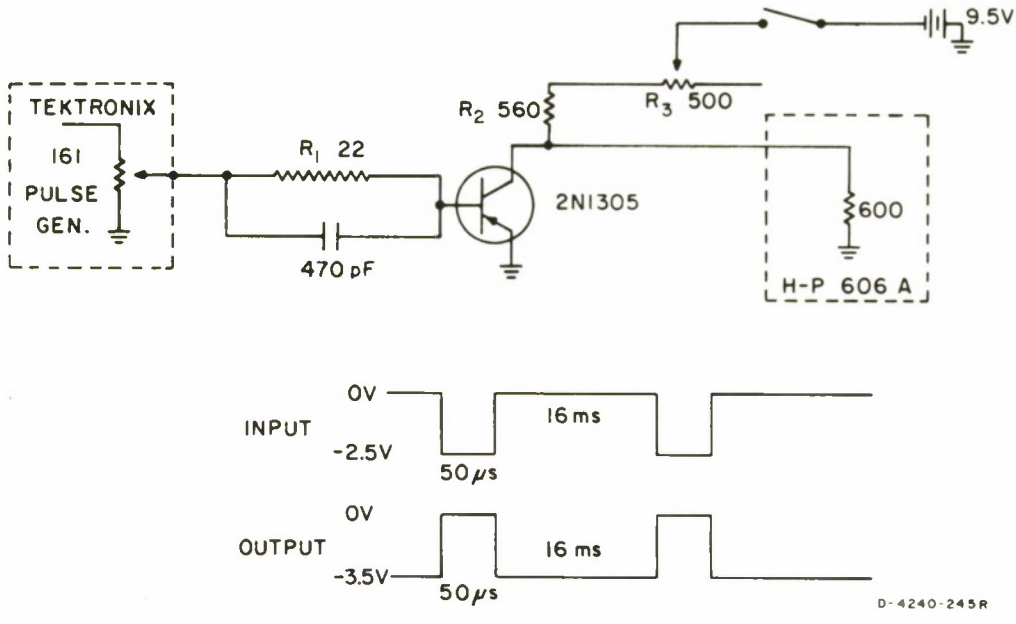

FIG. 70 CIRCUIT DIAGRAM OF DC MODULATOR

The pulse transmitter, designed to use the H-P 606A signal generator as the variable RF oscillator (see Figs. 71 and 72), was built to cover the frequency range of 1.5-10 MHz, with a peak pulse power of 150 W into a 50-Ω load. The first two stages use shunt peaking in the video amplifiers to provide a 9-MHz bandwidth (1-10 MHz). The final stage is run Class AB; Class C operation would require either a large grid swing to drive the 6146 or gating circuits to hold the 6146 at Class C bias, rising to a certain bias just prior to the start of the pulse. As can be seen in Fig. 68, this low-power transmitter serves as a driver for a T-368C/URT HF transmitter, which had previously been used in the CW measurements. For the pulse measurements, the T-368

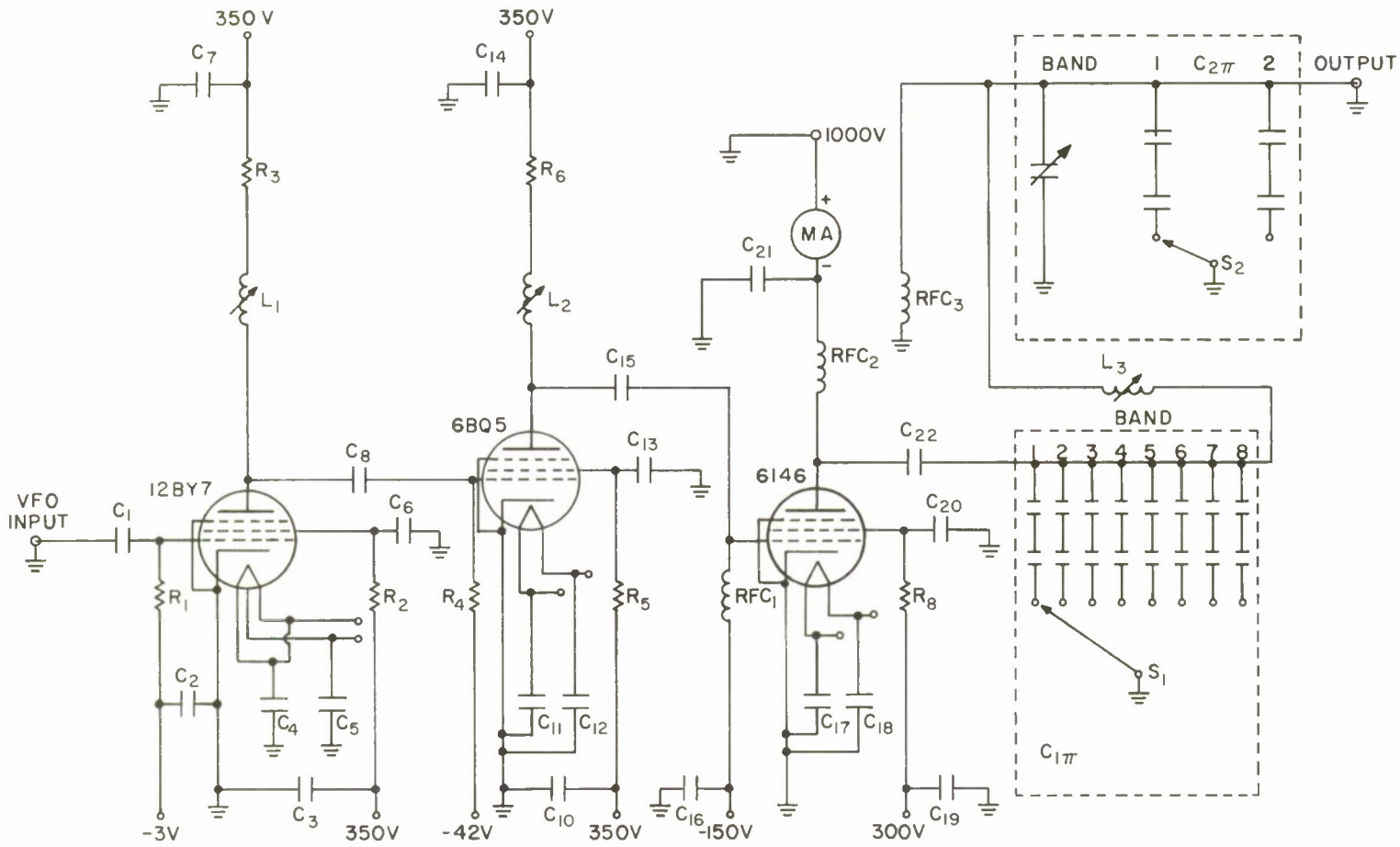

$C_1 - C_{14}$ = 1000 pF @ 500V C_{15} = 2300 pF @ 1 kV $C_{16} - C_{20}$ = 1000 pF @ 500V

C_{21}, C_{22} = 1000 pF @ 2.5 kV $R_1, R_2, R_4, R_5, R_7, R_8$ = 10 kΩ 2W R_3 = 660 Ω 2W

R_6 = 10 kΩ 10W L_1, L_2 = 16 – 28 μH RFC_1 = 1 mH RFC_2 = 2.5 mH RFC_3 = 5 mH

$C_{1\pi}$ SWITCHING ARRANGEMENT

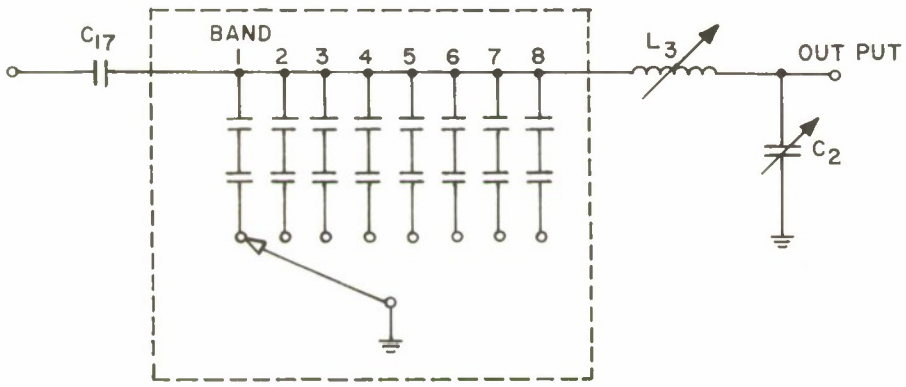

$C_{2\pi}$ SWITCHING CHARACTERISTICS

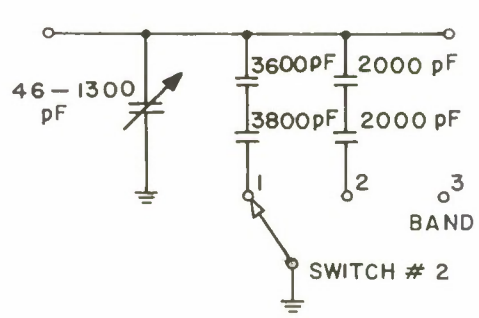

BAND	FREQ.	$C_{OPTIMUM}$	USE
1	1.5 – 2	460	1200 + 750
2	2 – 3	332	560 + 820
3	3 – 4	205	430 + 390
4	4 – 5	141	270 + 300
5	5 – 6	103	200 + 220
6	6 – 7	77	150 + 160
7	7 – 8	59	120 + 120
8	8 – 10	46	91 + 91

BAND 1 = 1.5 – 2 MHz

BAND 2 = 2 – 4 MHz

BAND 3 = 4 – 10 MHz

D-4240-231R

FIG. 71 CIRCUIT DIAGRAM OF PULSE TRANSMITTER

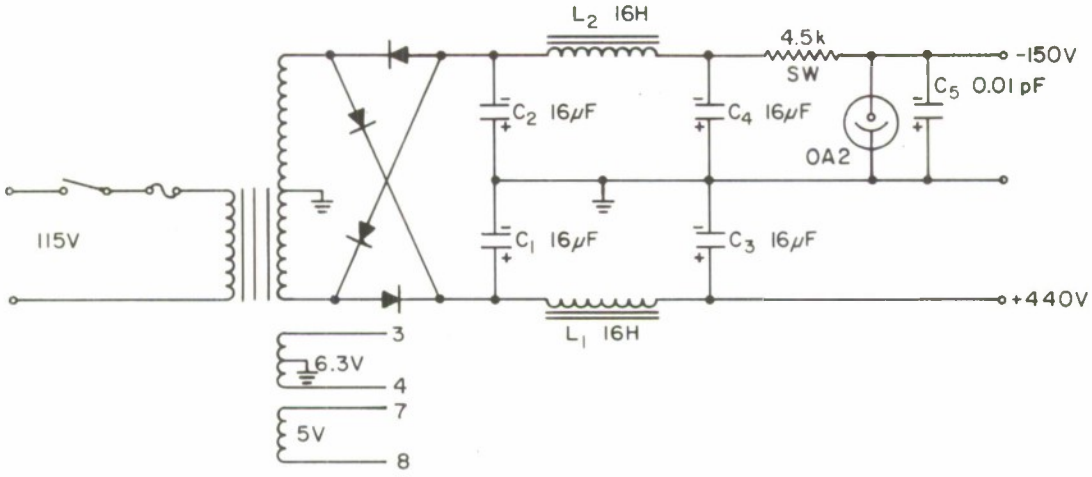

LOW-VOLTAGE POWER SUPPLY

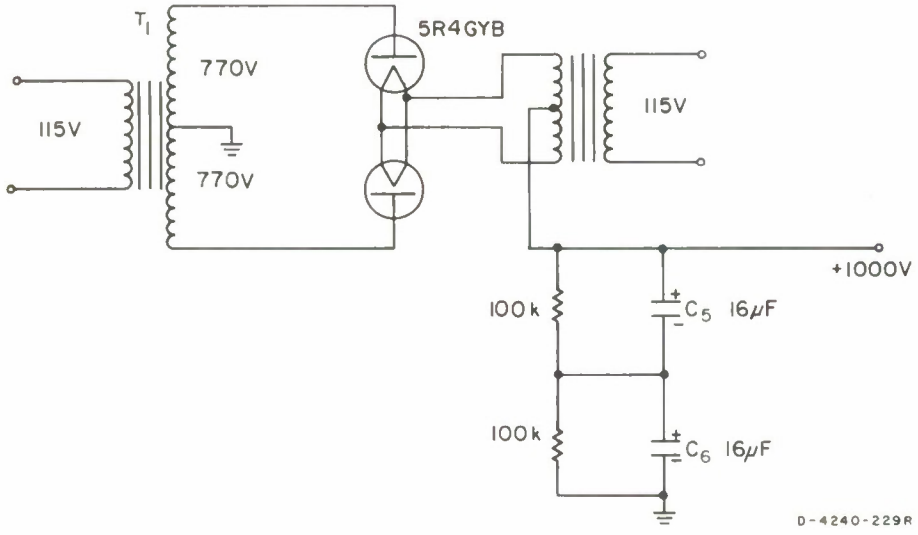

HIGH-VOLTAGE POWER SUPPLY

FIG. 72 CIRCUIT DIAGRAM OF 150-WATT TRANSMITTER POWER SUPPLY

transmitter was modified to include a variable-control grid bias for the clamper tube controlling the screen grid of the 4-400A. With proper biasing of the 4-400A, the transmitter was capable of 4-kW peak-pulse power output; however, for these experiments the transmitter was run at 1-kW peak pulse.

b. Pulse Reception

The R-390A/URR receiver served as a basic pulse receiver. To avoid ringing when the second IF output was used (see Fig. 73), the output from the third mixer was fed into a pulse receiver adapter via an emitter follower (see Fig. 74). The pulse receiver adapter, as shown in Fig. 75, consists of a broad double-tuned IF amplifier, an emitter follower, a detector, and a second emitter follower, which lowers the impedance so that a long length of coaxial cable can be run to the Tektronix 945 oscilloscope. As can be seen in Fig. 76, the scope was synchronized by the same method and circuit employed at the transmitter site.

The calibration of the pulse receiver was performed with a system similar to that used for pulse transmission (see Fig. 77). The signal output as read from the meter on the H-P 606A signal generator, is correctly calibrated, provided R_3 of the dc modulator (refer to Fig. 70) is adjusted to give zero carrier output from the H-P 606A during the absence of pulse.

c. Antenna System

At the transmitter site, a horizontal half-wave dipole approximately one-sixth wavelength above ground was employed, with means to orient it in one of three directions: along magnetic N-S, E-W, and NE-SW. The NE-SW antenna was used for the investigation of polarization tilt, as mentioned in Sec. II-C-4. The receiver site employed the same crossed-dipole system as for CW reception.

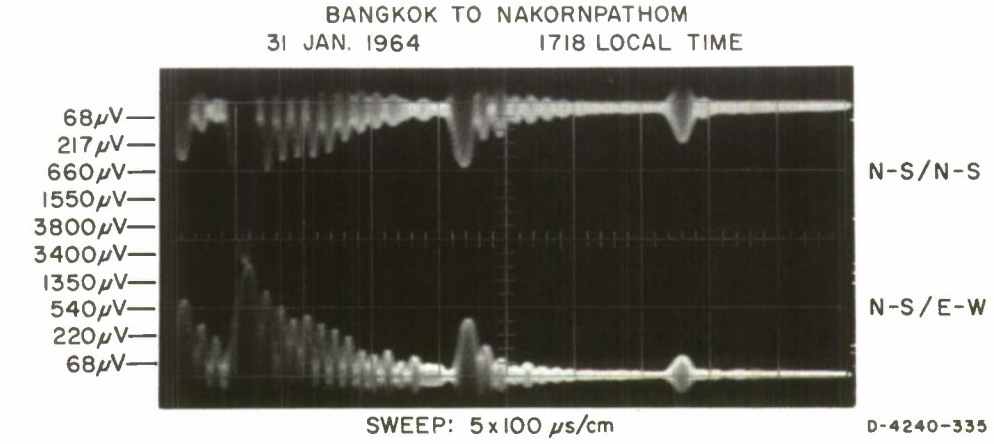

FIG. 73 PHOTOGRAPH OF RINGING OF SECOND IF 50-μs PULSE OUTPUT

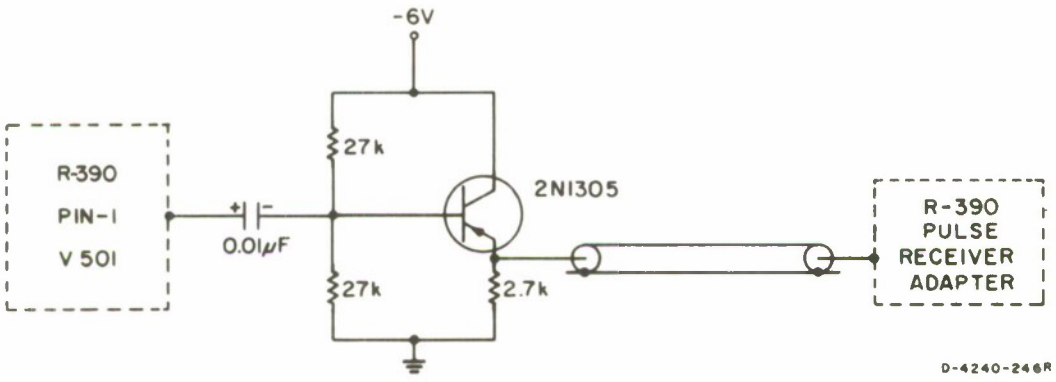

FIG. 74 CIRCUIT DIAGRAM OF EMITTER FOLLOWER FOR R-390 A/URR

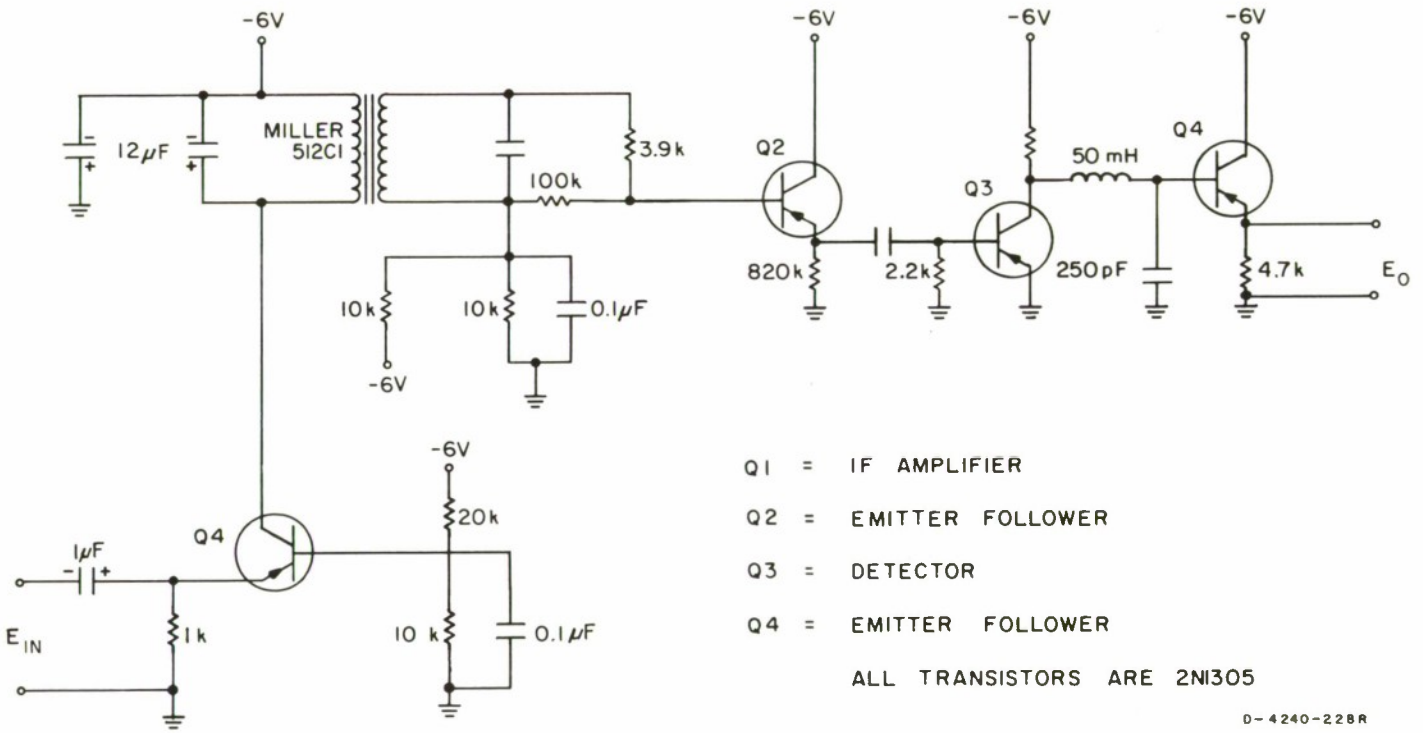

FIG. 75 CIRCUIT DIAGRAM OF PULSE RECEIVER ADAPTER FOR R-390 A/URR

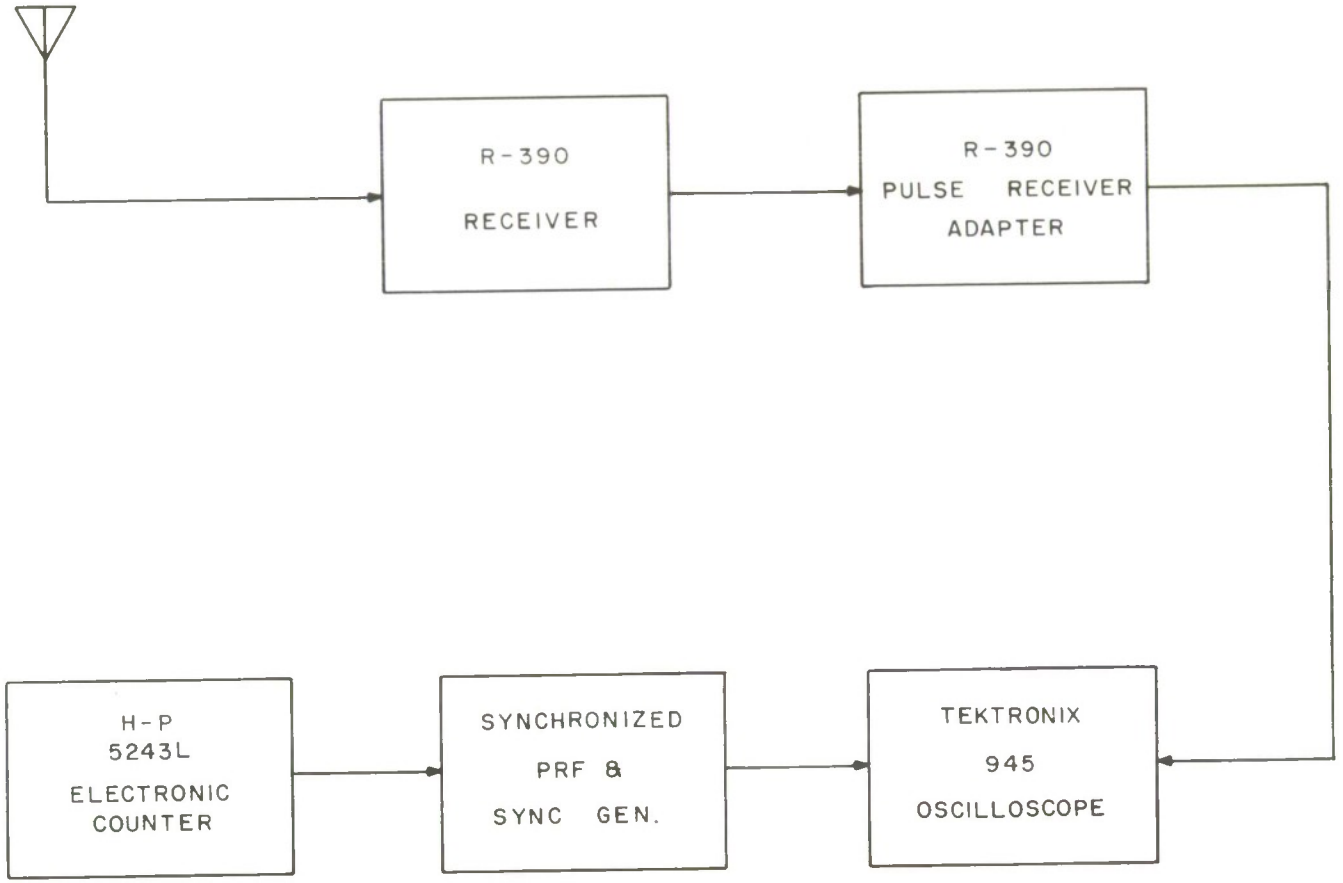

FIG. 76 INSTRUMENTATION BLOCK DIAGRAM FOR PULSE RECEPTION

D-4240-244R

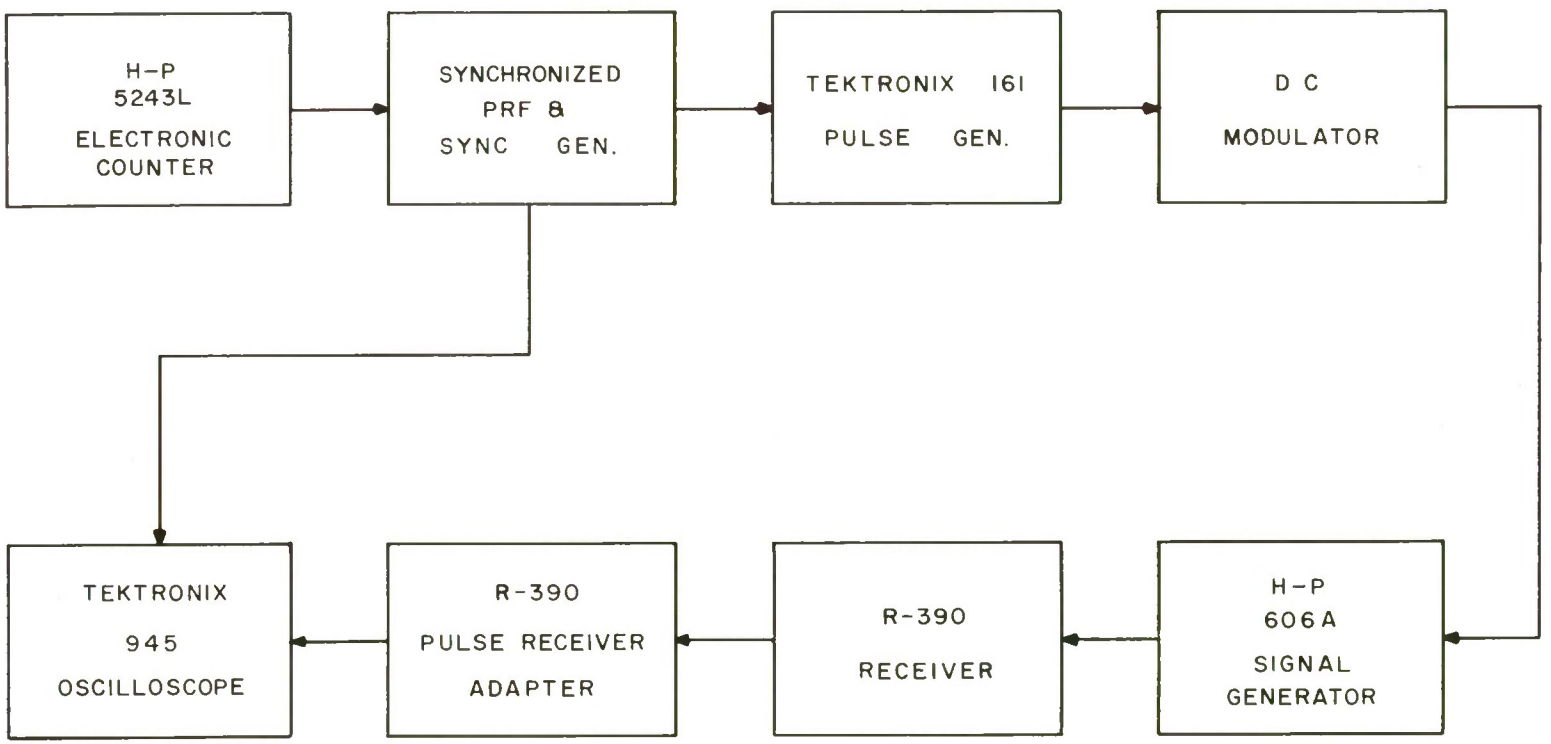

FIG. 77 INSTRUMENTATION BLOCK DIAGRAM FOR PULSE RECEIVER CALIBRATION D-4240-243R

A rotatable loaded dipole was tried with little or no success in differentiating the reception at different dipole orientations, varying from N-S to E-W and to S-N. This is because the cross coupling between the N-S and E-W modes of reception with the foreshortened dipole is much greater than in the normal case with a half-wave dipole.

2. Test Procedure

The test was conducted over two circuits. Over the circuit between Sattahip and Cholburi (see Fig. 26), the test was carried out in two directions, S-to-N and N-to-S, with the transmitter site at Sattahip and at Cholburi, respectively. The mobile receiver unit was located at distances of approximately 10, 15, 20, 30, 40, 50, 60, 75, and 83 km from the Sattahip site. The second circuit was approximately in the NW-to-SE direction, with the receiver unit at a distance of approximately 25, 45, 60, 75, 100, 110, and 130 km from the transmitter site at Kao Pongrang. Kilometer posts located every 0.5 km along the highway were helpful in logging the distance.

Tests were conducted over the Sattahip/Cholburi (S-to-N) circuit, at 1.7, 3.4, and 5.1 MHz, with both N-S and E-W antenna reception for each of the three transmitting antenna orientations. The goal was one set of 24-hour data per frequency per receiving site. Preliminary pulse tests indicated that 3.4 MHz was the test signal likely to give the most information over a distance up to about 100 km. Since intensive experimentation would require more time than could possibly be allowed, the test emphasized 3.4 MHz as an all-day (0200-2200) frequency, 1.7 MHz as a nighttime frequency, and 5.1 MHz as a daytime frequency. Generator failure and other problems, however, severely limited the amount of data taken. Incomplete information could (to some extent) be supplemented by data obtained at neighboring sites, although on different dates. Pulses received were photographed, 12 times per minute on a

single piece of Polaroid film using a Tektronix C-12 camera mounted on the Tektronix 945 oscilloscope with a shutter speed of 1/25 s. Information on pulses was interchanged between the receiving and the transmitting sites from time to time via a Collins KWM-2A transceiver. To aid in identification of the mode of the first pulse obtained at the receiving site when the ground pulse could not be received, the time delay between the ground pulse and the first pulse returned from the ionosphere was also recorded at the transmitting site.

The test in the reversed (N-to-S) direction, over the Cholburi/Sattahip circuit, was conducted at 3.4 MHz only, with the receiver unit at the same selected sites, up to and including the Sattahip location.

After a complete overhaul of the test equipment and the diesel generators, pulse measurements were taken over the NW-SE circuit, Kao Pongrang-to-Krabinburi (see Fig. 26). This test was conducted at 3.4 MHz, which had been found to be the frequency giving the greatest amount of information.

3. Data Reduction

The pulse data obtained in Polaroid photographs were complex, owing to various modes of propagation (which may or may not occur together). Each photograph is a "one-minute" record per antenna combination per hour. Since the camera is not of a continuously recording type, and often no recording could be made when absorption was too heavy or when noise was too great compared to the pulse signal received, pulse data do not lend themselves to the derivation of mean or median values so readily as do CW data. However, useful information may be gained from the pulse measurements: the ionospheric layer supporting a sky-wave propagation at a particular time of the day, the frequency of the wave that may be supported, and the best or most suitable polarization mode of propagation.

Calibration was so arranged that pulse amplitude could be recorded either in dB above 1 μV or directly in μV. In the case of a pulse of the form shown in Fig. 78(a), the pulse was very stable and its maximum value was recorded. Where the pulse was not as stable, but where the "average" value could be readily recognized, this average value was read, together with maximum and minimum values [see Fig. 78(b)]. When the pulse was not stable, as illustrated in Fig. 78(c), the maximum and minimum values were read. Together with pulse amplitude readings, the following information was recorded in tabular form: location, frequency, date, time, antenna combination, time delay, pulse amplitude, pulse width, ground pulse amplitude, and mean amplitude of noise.

The time delays between the ground pulse and the various pulses received enable one to attribute a particular pulse return to its appropriate reflecting layer. Knowledge of pulse amplitudes and the corresponding layers of reflection, together with information on times of occurrence and antenna combinations, enables one to recognize the performance of various modes of wave propagation, whether the E, Es, F1, or F2 modes or whether the ordinary-wave or the extraordinary-wave modes. Moreover, the stability of a particular mode may be assessed when an additional study is made of the form of pulses superimposed one upon another within the one minute time span.

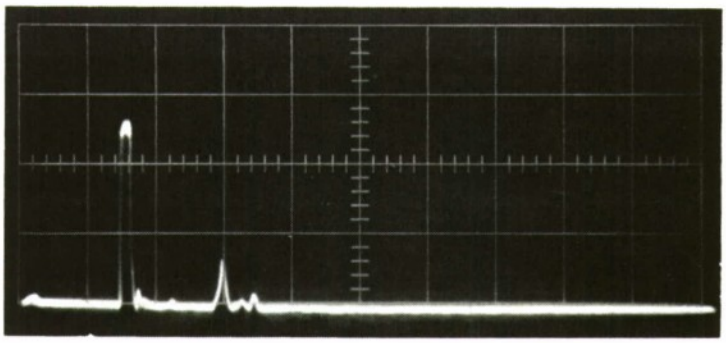

(a) STABLE PULSE, ONE-VALUE READING

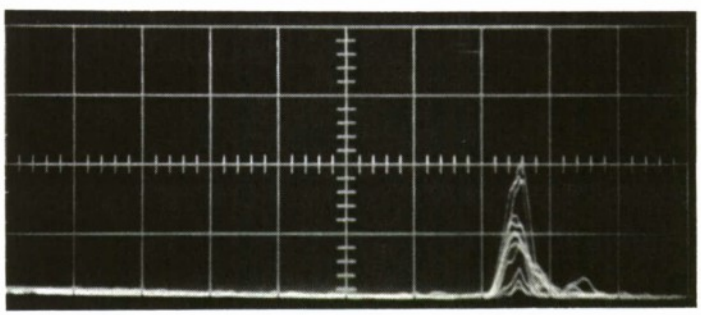

(b) NON-STABLE PULSE, THREE-VALUE READING

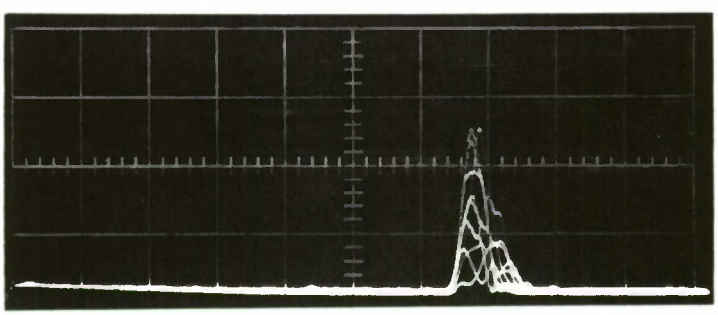

(c) NON-STABLE PULSE, TWO-VALUE READING

D-4240-433

FIG. 78 PHOTOGRAPH OF SAMPLES OF PULSE DATA

C. RESULTS AND DISCUSSION

1. Sattahip/Cholburi 3.4-MHz Pulse Test

The 3.4-MHz pulse test, being the most extensive, was analyzed in greater detail than the 1.7 MHz and 5.1 MHz pulse tests, as follows:

(1) Average pulse amplitudes, V_m, were plotted against time of day for each ground distance between the transmitting and the receiving sites and for each of the three transmitting antennas: the N-S, the E-W, and the NE-SW antennas. These are the top left plots of Figs. 79 through 102. Measurements were made between 0200 and 2200.

(2) Amplitude stability values, A_s, of the received pulses were plotted against time of the day for each ground distance and for each of the three transmitting antennas as shown in the middle left plots of Figs. 79 through 102.

A_s is defined by

$$A_s = \frac{V_{max} - V_{min}}{V_{max}} \quad , \tag{48}$$

where V_{max} = maximum amplitude of the pulses recorded within a one-minute period, and V_{min} = minimum amplitude of the pulses recorded within a one-minute period.

Samples of pulses associated with various values of A_s are illustrated in Fig. 103.

(3) Phase stability values, P_s, of the received pulses were plotted against time of the day for each ground distance and for each of the three transmitting antennas as shown in the bottom left plots of Figs. 79 through 102.

P_s is defined by

$$P_s = \frac{T_r - T_t}{T_r} \quad , \tag{49}$$

where

T_t = width of the transmitted pulse = 50 μs

T_r = overall width of the received pulses recorded within a one-minute period.

Samples of pulses associated with various values of P_s are illustrated in Fig. 104.

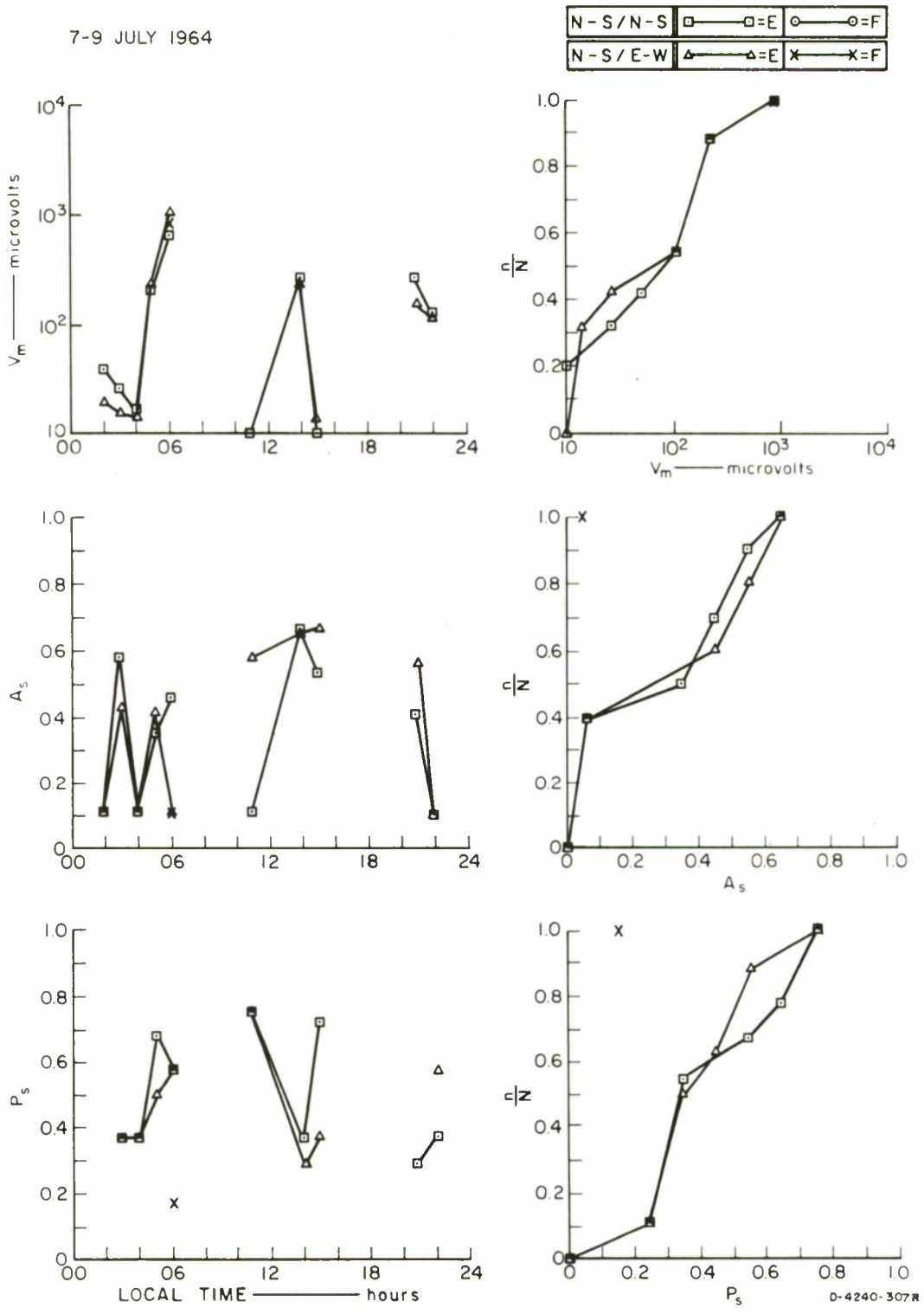

FIG. 79 3.4-MHz PULSE DATA, SATTAHIP/CHOLBURI CIRCUIT: N-S TRANSMITTING, 10 km

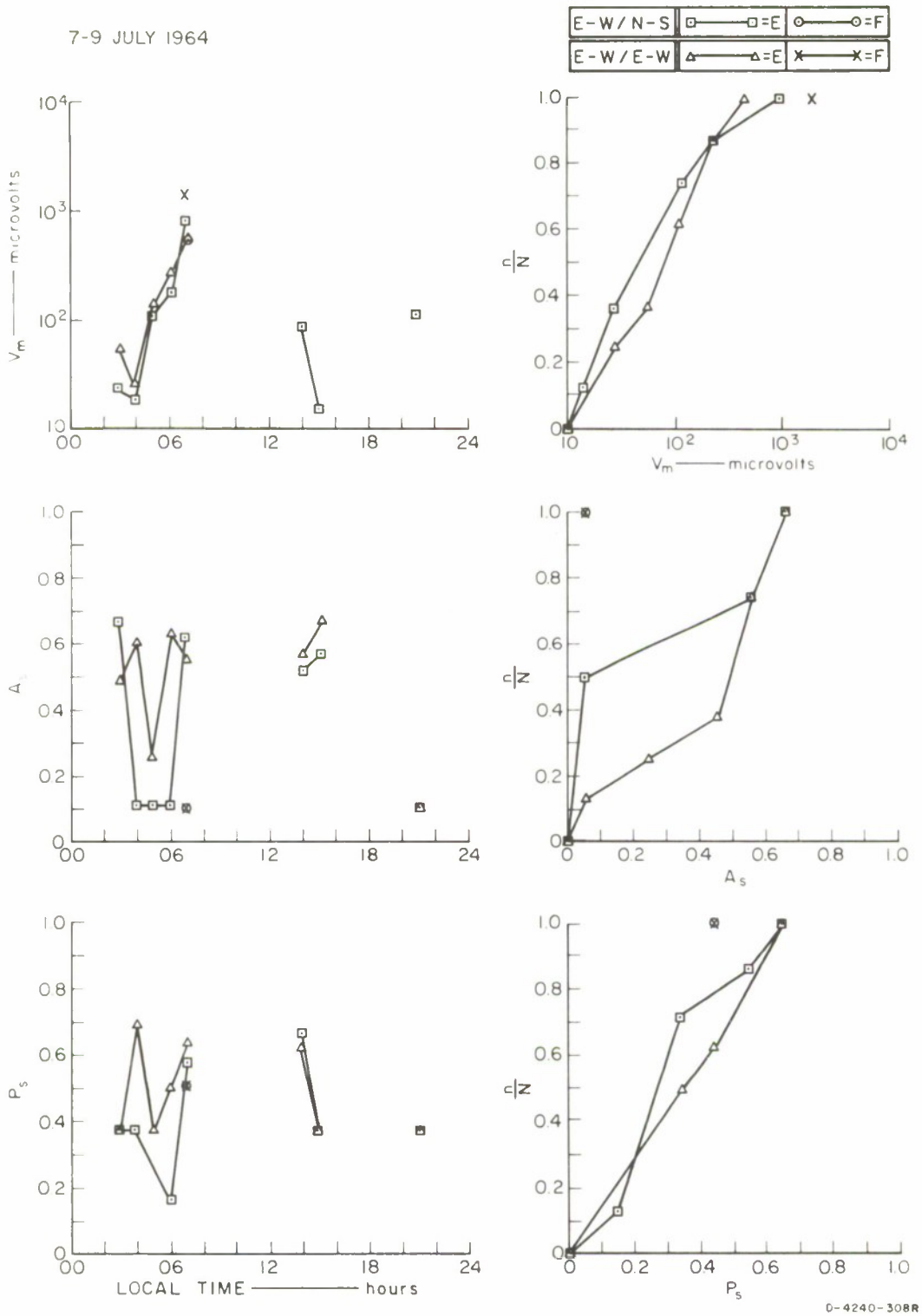

FIG. 80 3.4-MHz PULSE DATA, SATTAHIP/CHOLBURI CIRCUIT: E-W TRANSMITTING, 10 km

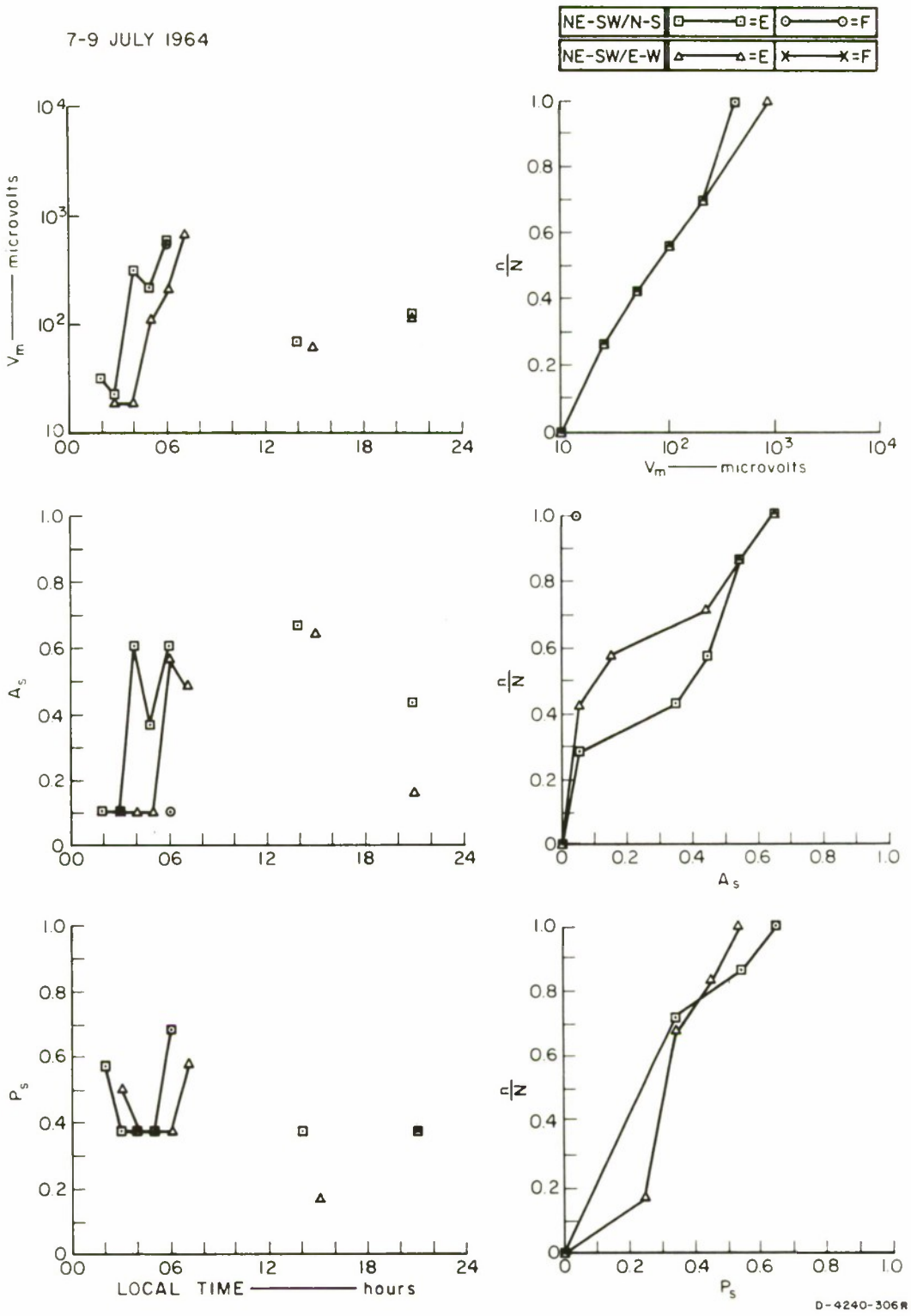

FIG. 81 3.4-MHz PULSE DATA, SATTAHIP/CHOLBURI CIRCUIT: NE-SW TRANSMITTING, 10 km

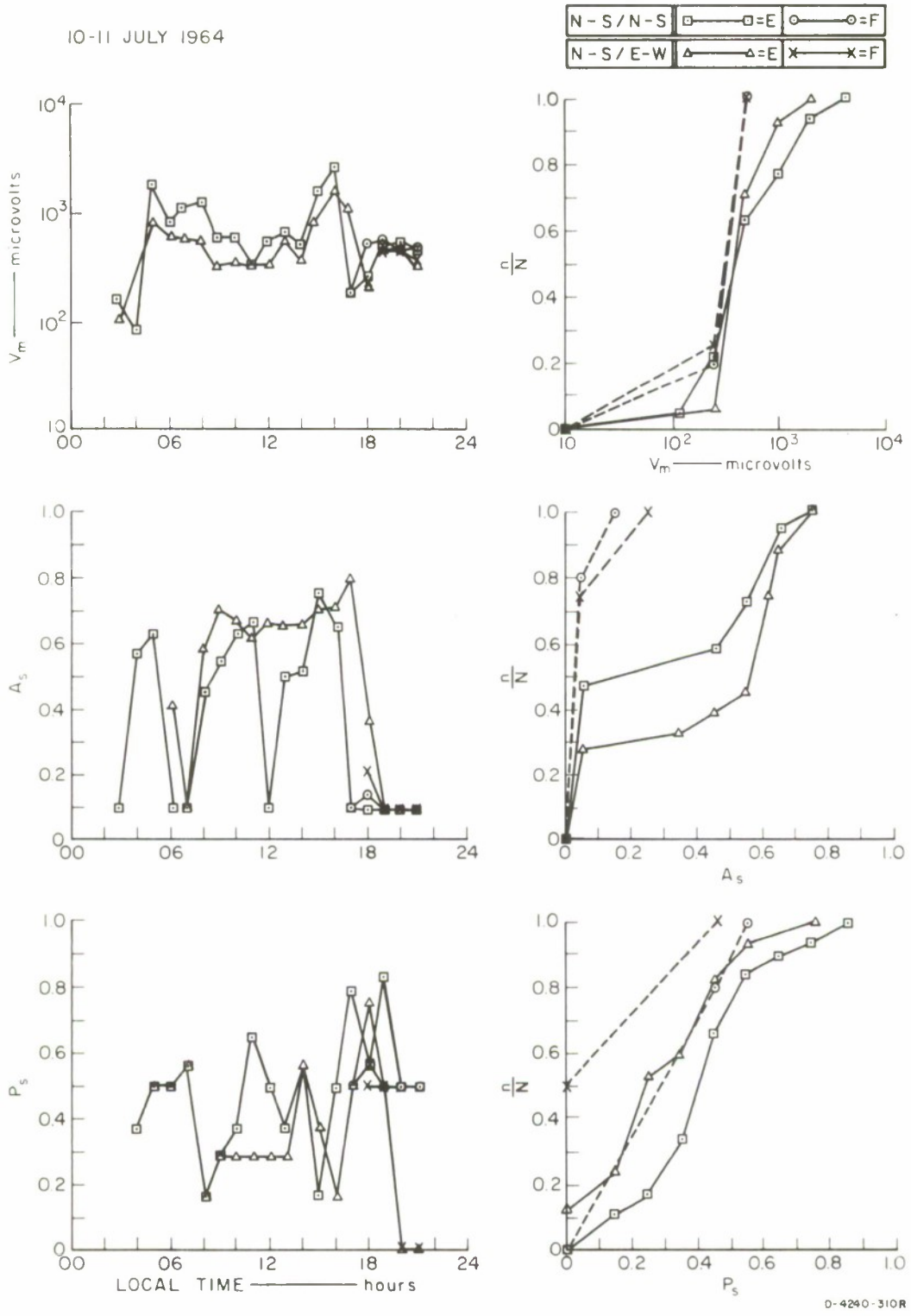

FIG. 82 3.4-MHz PULSE DATA, SATTAHIP/CHOLBURI CIRCUIT: N-S TRANSMITTING, 15 km

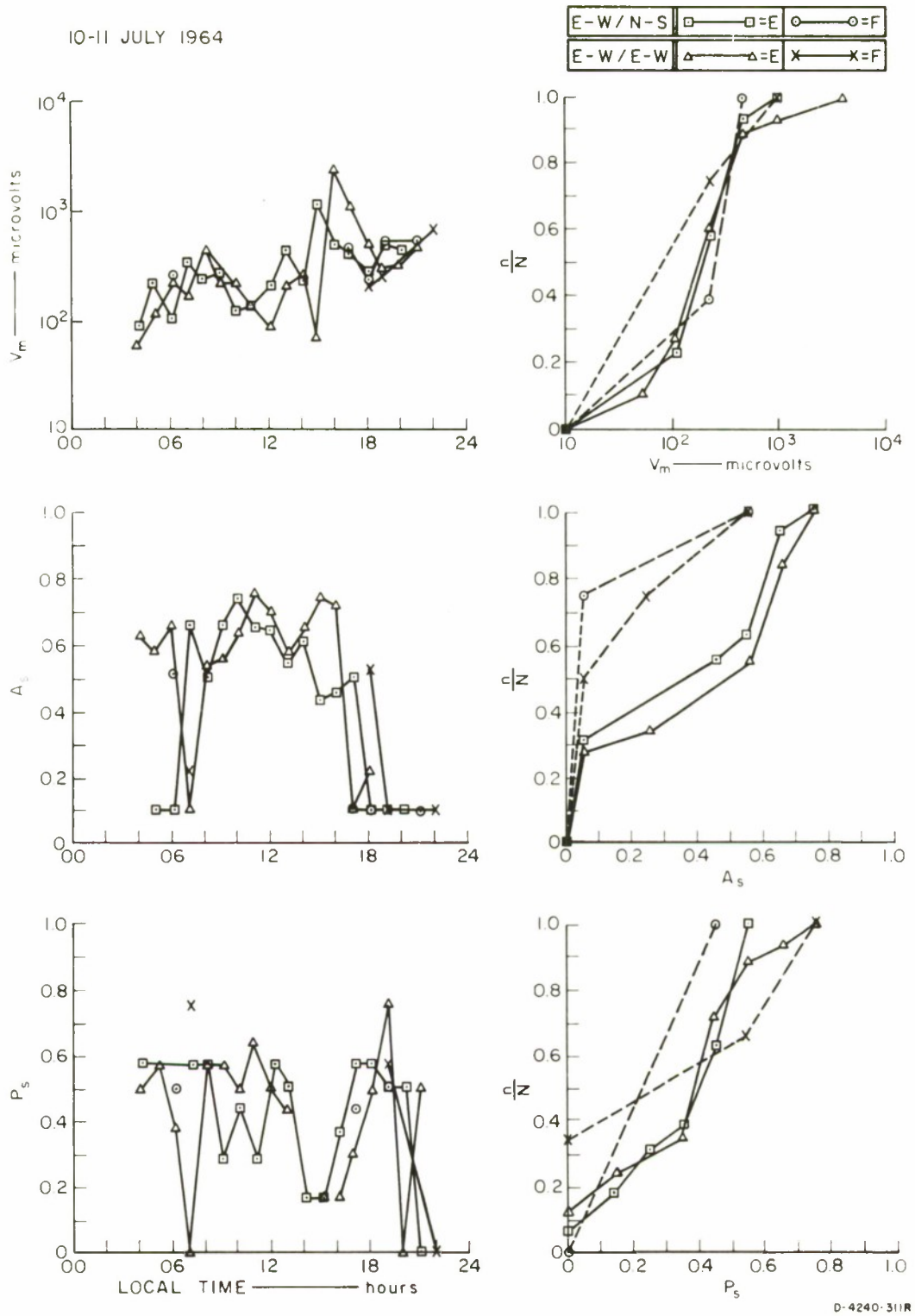

FIG. 83 3.4-MHz PULSE DATA, SATTAHIP/CHOLBURI CIRCUIT:
E-W TRANSMITTING, 15 km

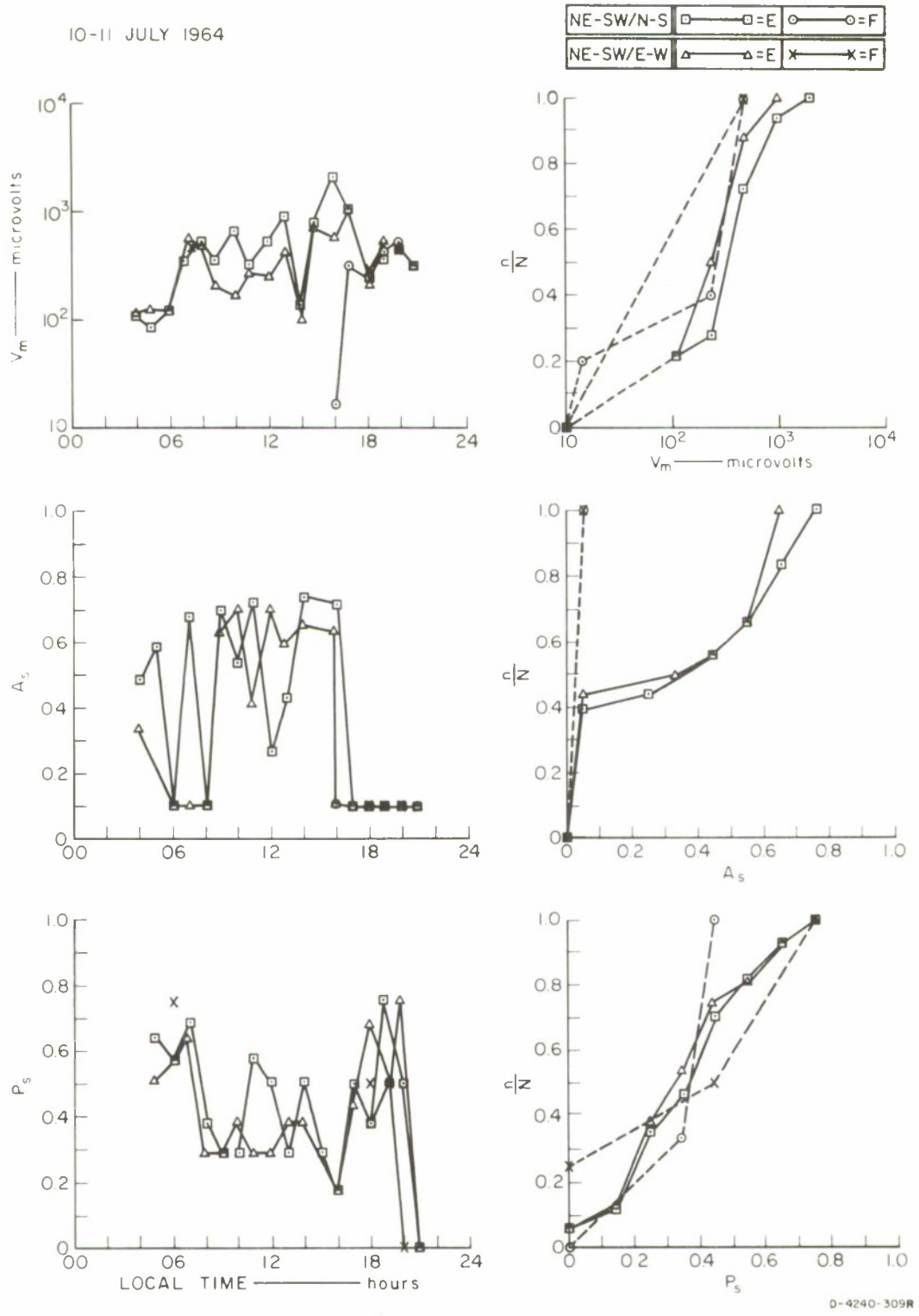

FIG. 84 3.4-MHz PULSE DATA, SATTAHIP/CHOLBURI CIRCUIT: NE-SW TRANSMITTING, 15 km

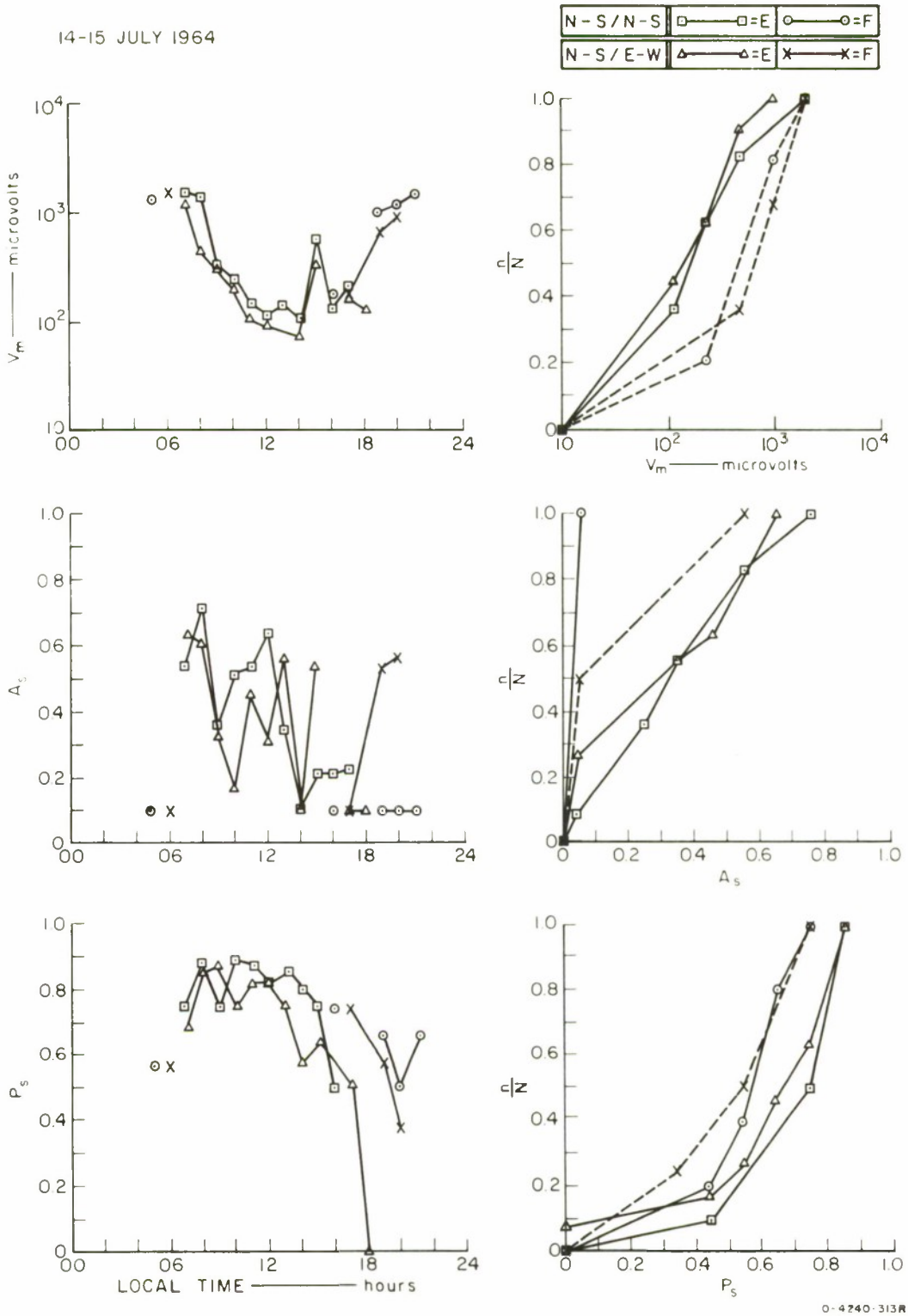

FIG. 85 3.4-MHz PULSE DATA, SATTAHIP/CHOLBURI CIRCUIT: N-S TRANSMITTING, 20 km

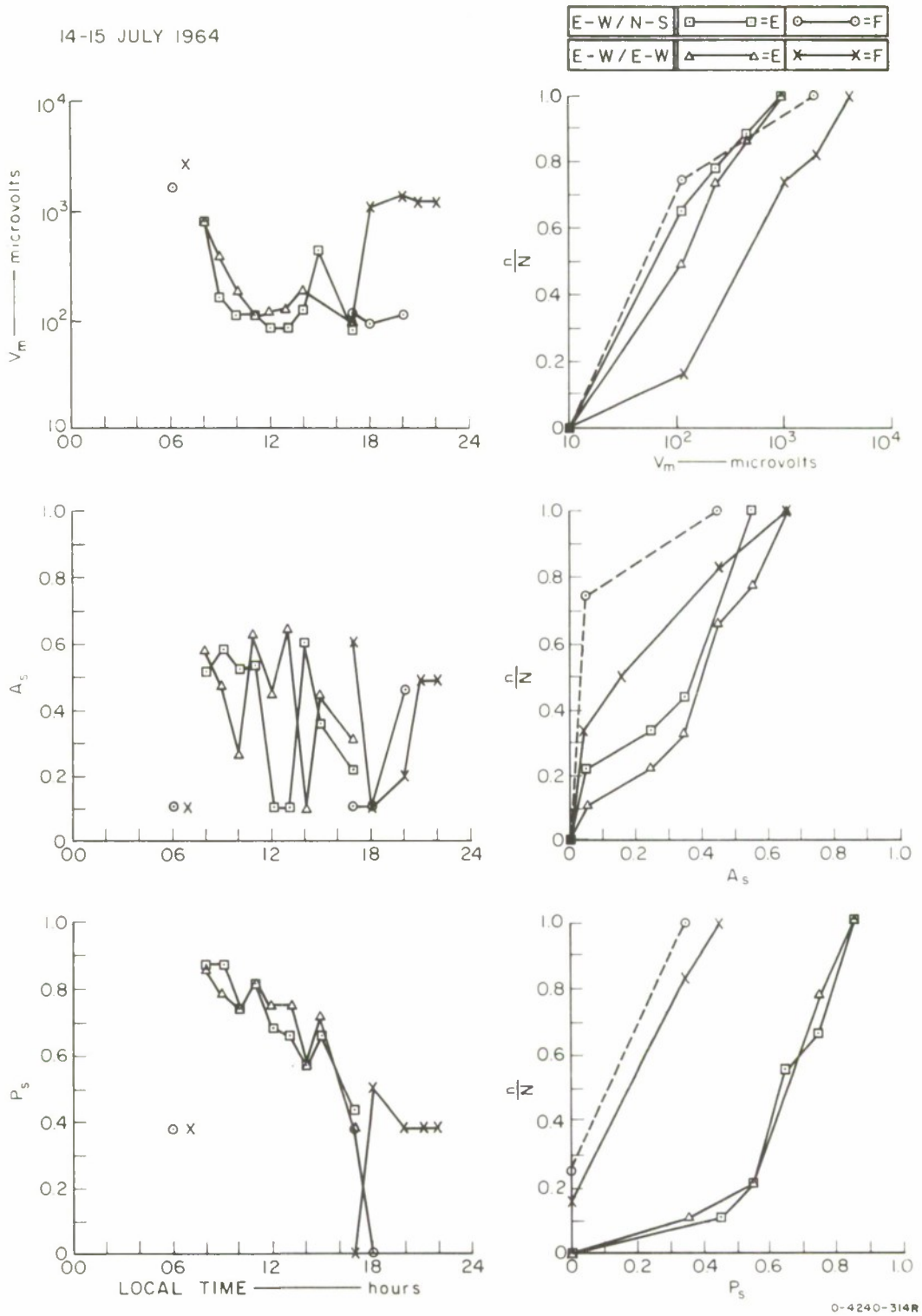

FIG. 86 3.4-MHz PULSE DATA, SATTAHIP/CHOLBURI CIRCUIT: E-W TRANSMITTING, 20 km

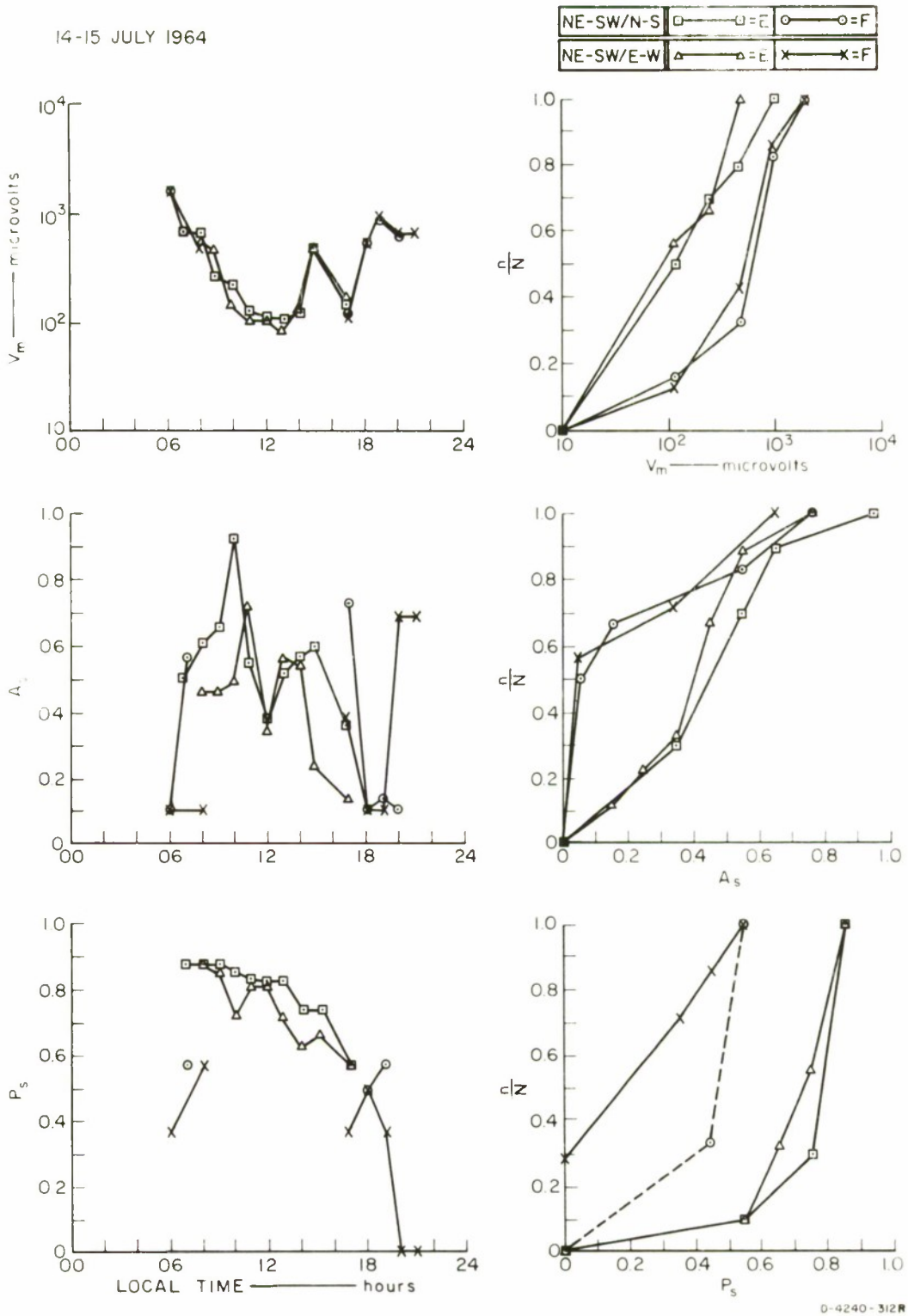

FIG. 87 3.4-MHz PULSE DATA, SATTAHIP/CHOLBURI CIRCUIT: NE-SW TRANSMITTING 20 km

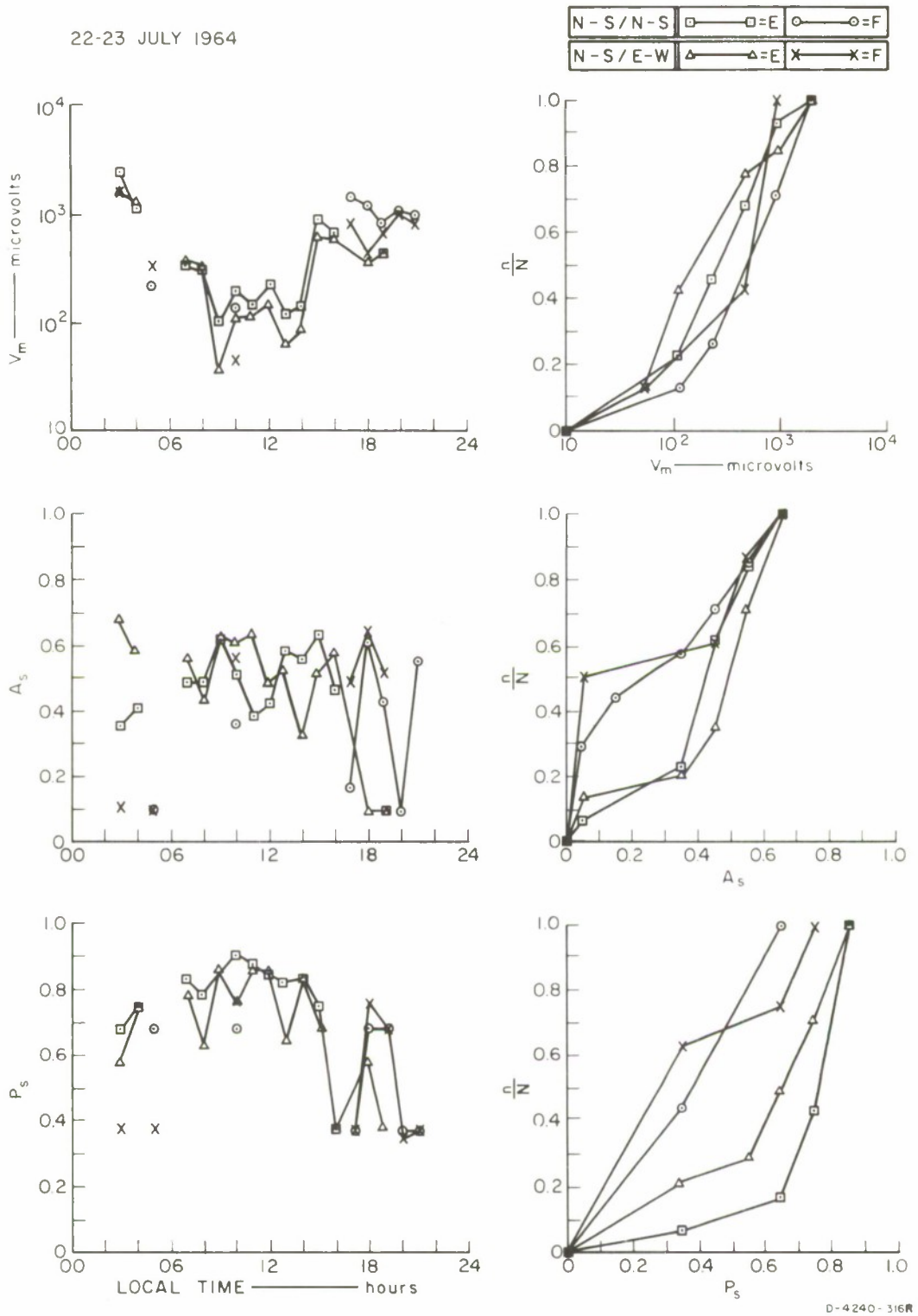

FIG. 88 3.4-MHz PULSE DATA, SATTAHIP/CHOLBURI CIRCUIT: N-S TRANSMITTING, 30 km

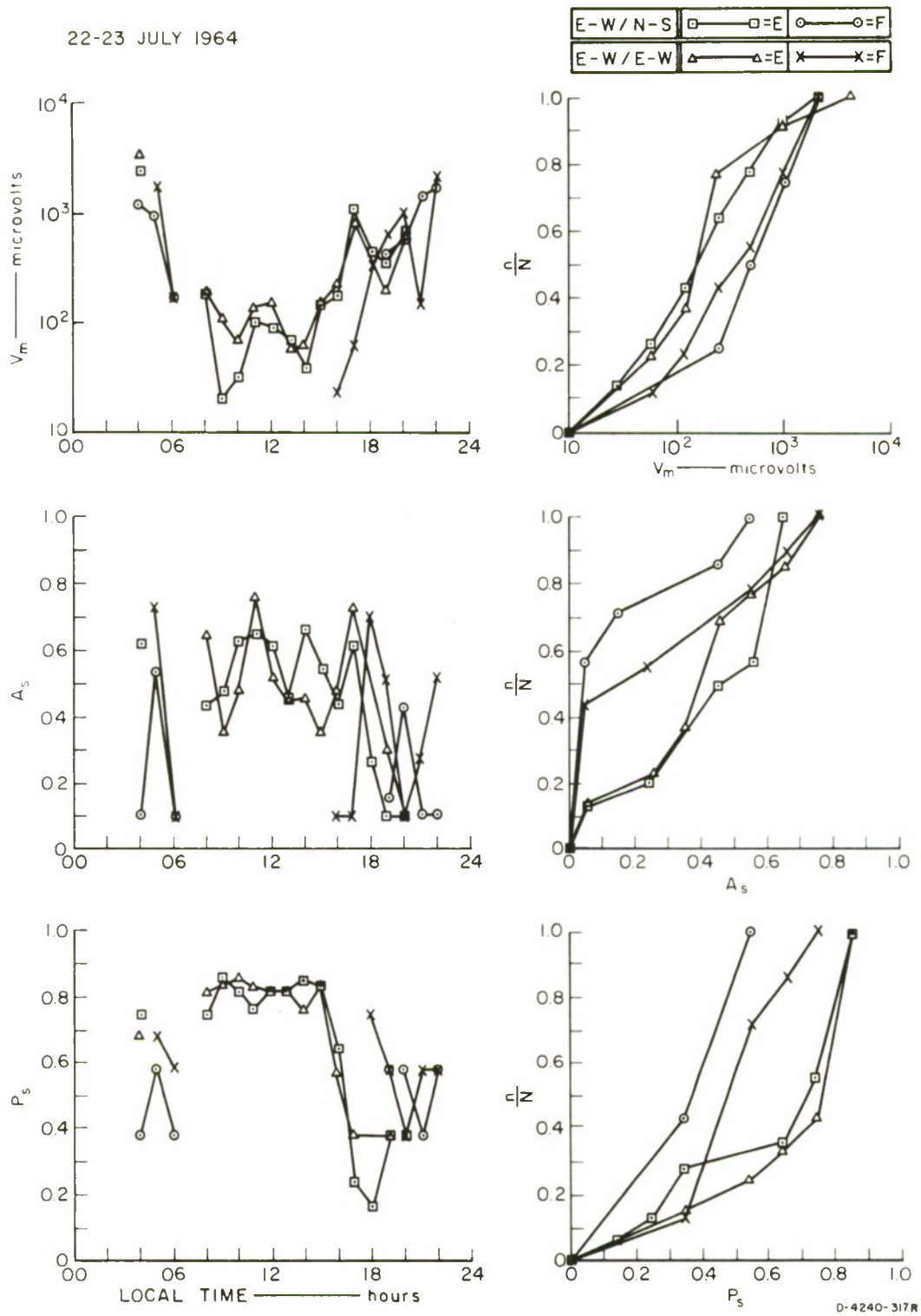

FIG. 89 3.4-MHz PULSE DATA, SATTAHIP/CHOLBURI CIRCUIT: E-W TRANSMITTING, 30 km

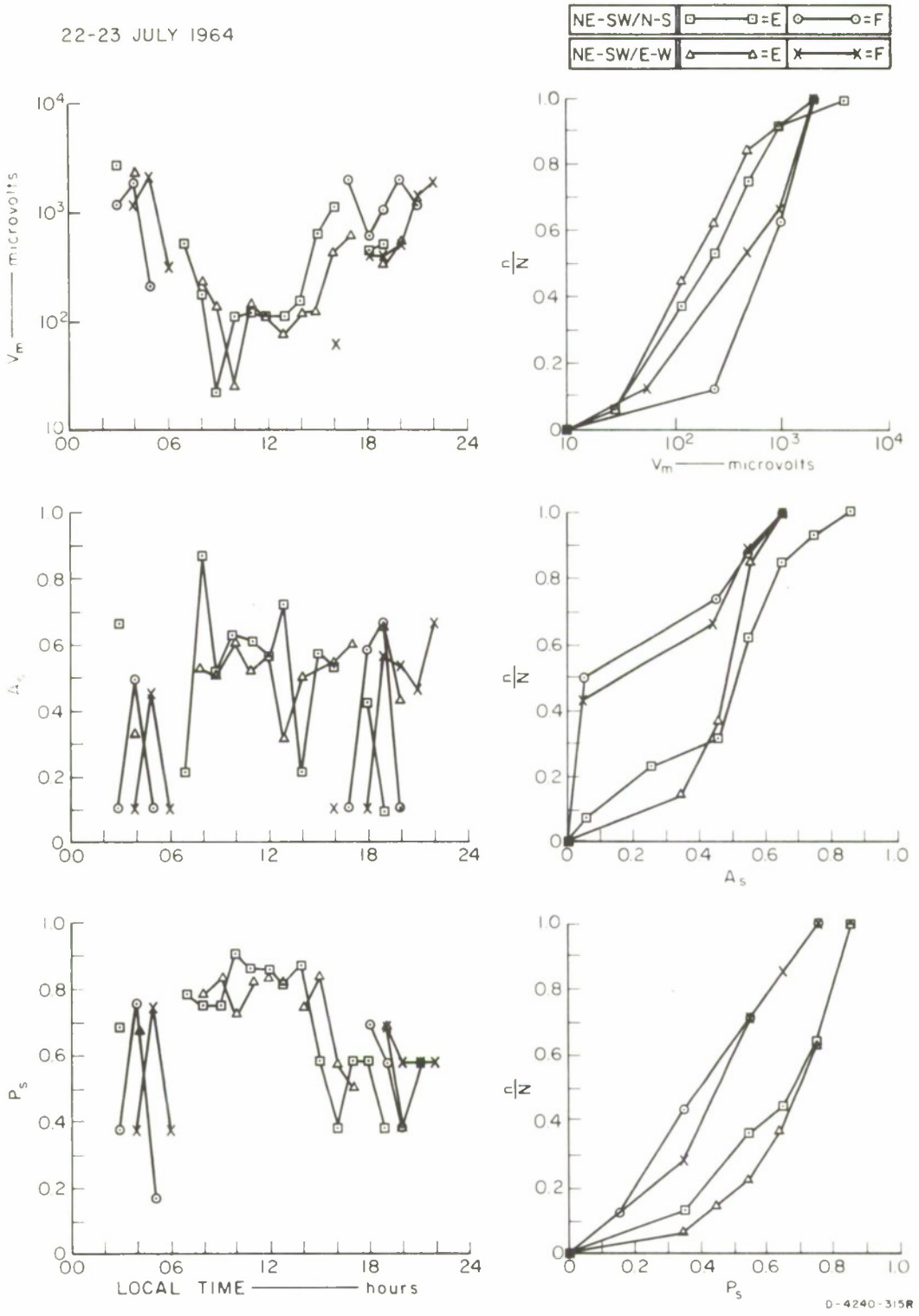

FIG. 90 3.4-MHz PULSE DATA, SATTAHIP/CHOLBURI CIRCUIT: NE-SW TRANSMITTING, 30 km

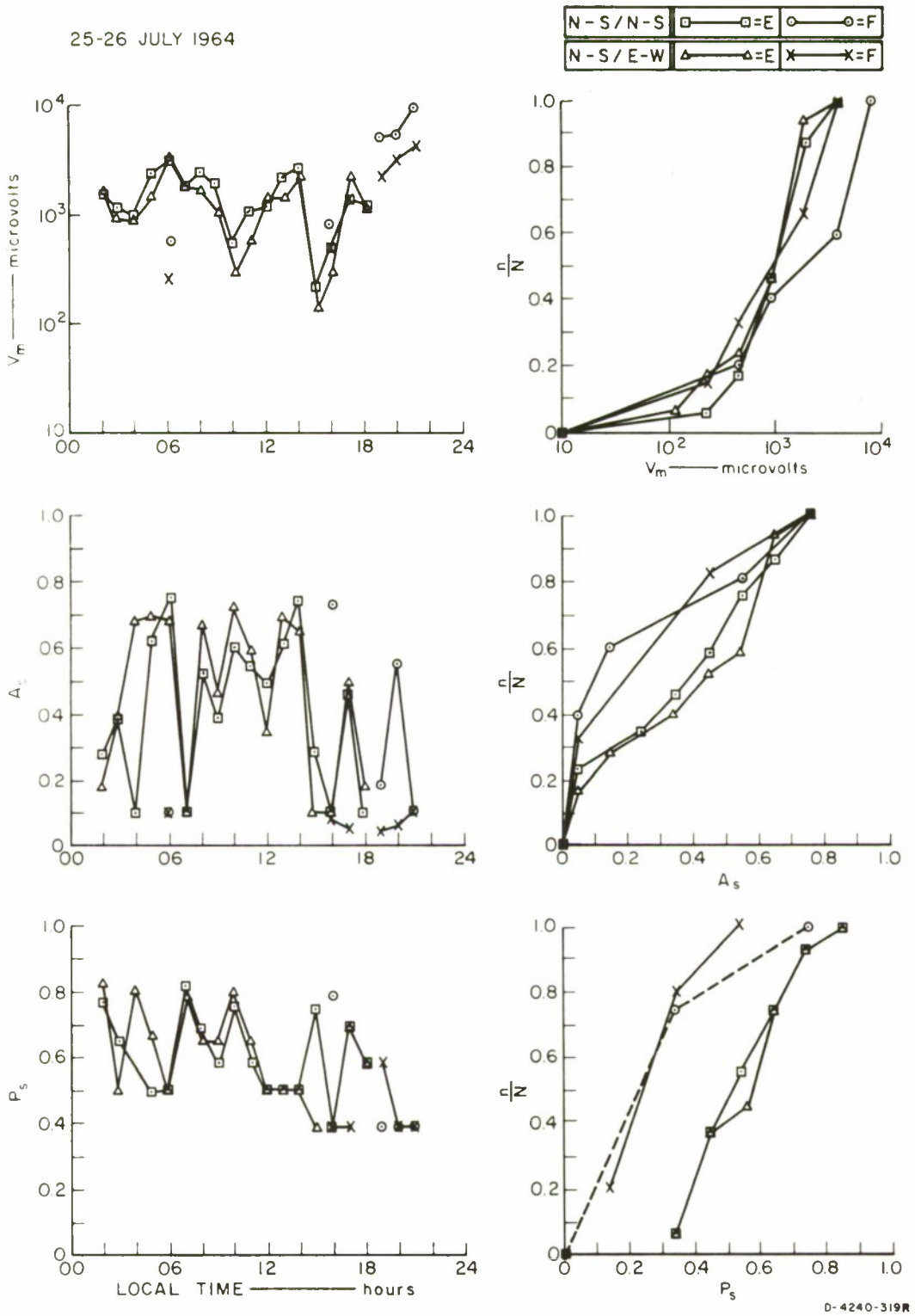

FIG. 91 3.4-MHz PULSE DATA, SATTAHIP/CHOLBURI CIRCUIT: N-S TRANSMITTING, 40 km

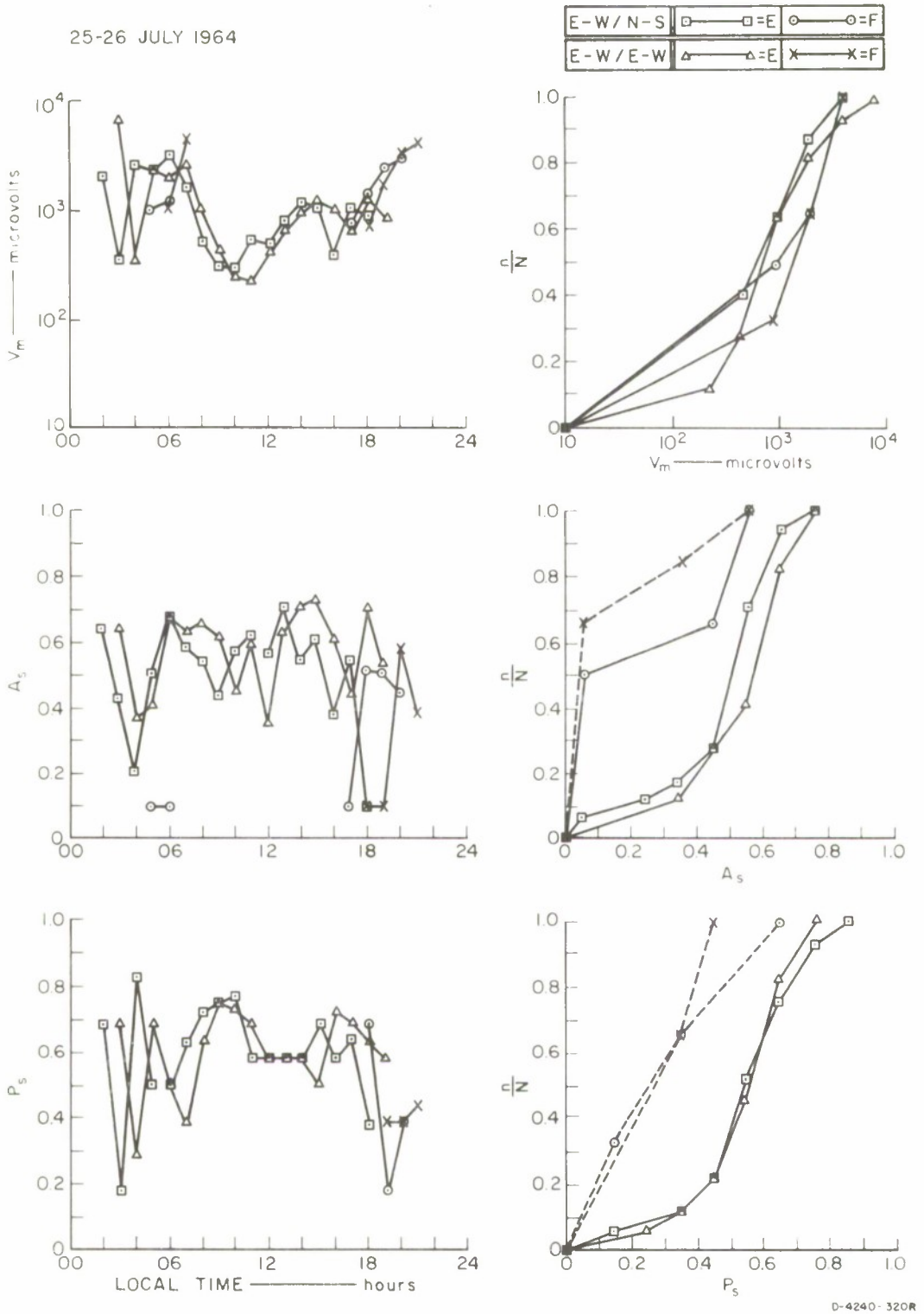

FIG. 92 3.4-MHz PULSE DATA, SATTAHIP/CHOLBURI CIRCUIT: E-W TRANSMITTING, 40 km

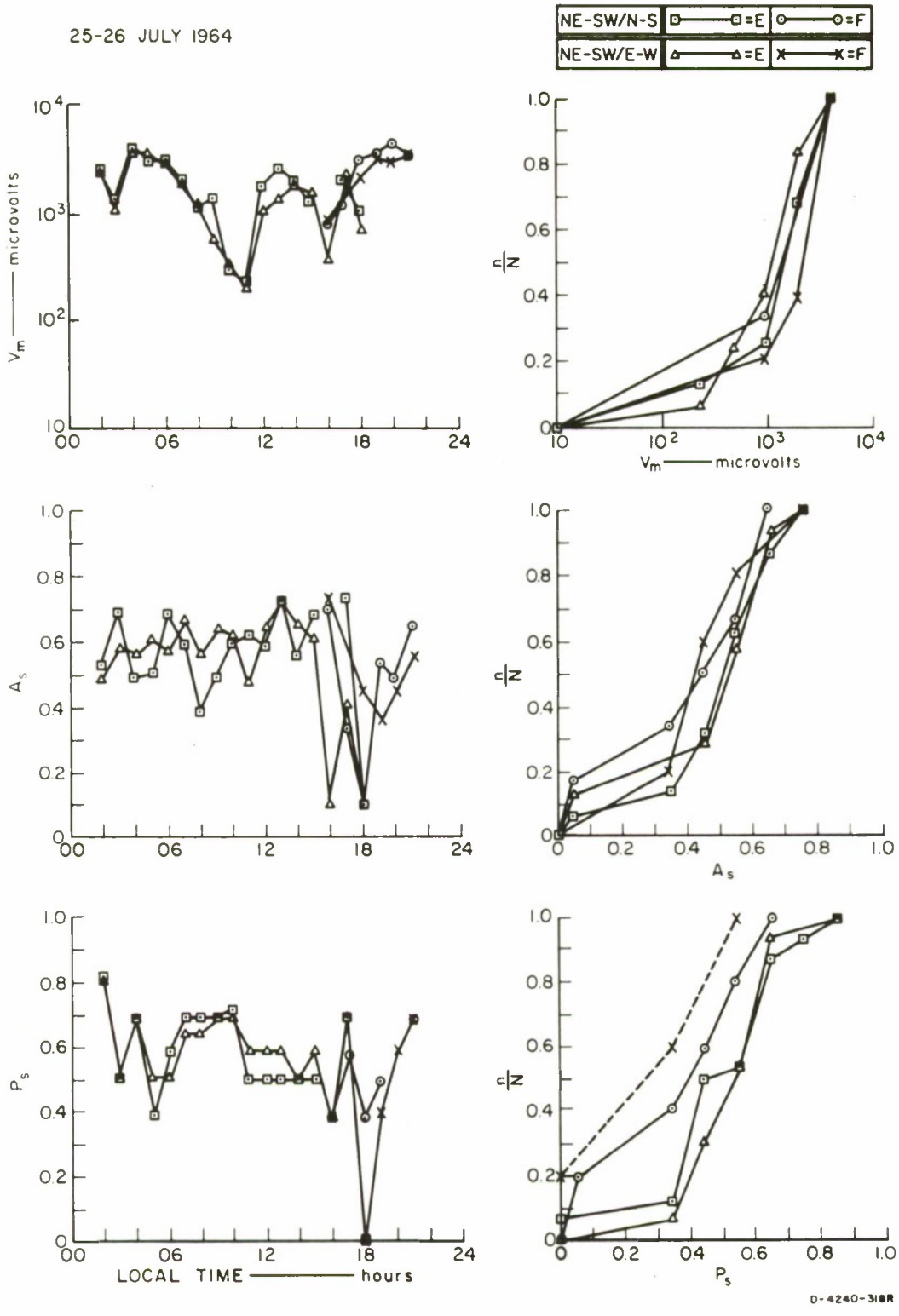

FIG. 93 3.4-MHz PULSE DATA, SATTAHIP/CHOLBURI CIRCUIT: NE-SW TRANSMITTING, 40 km

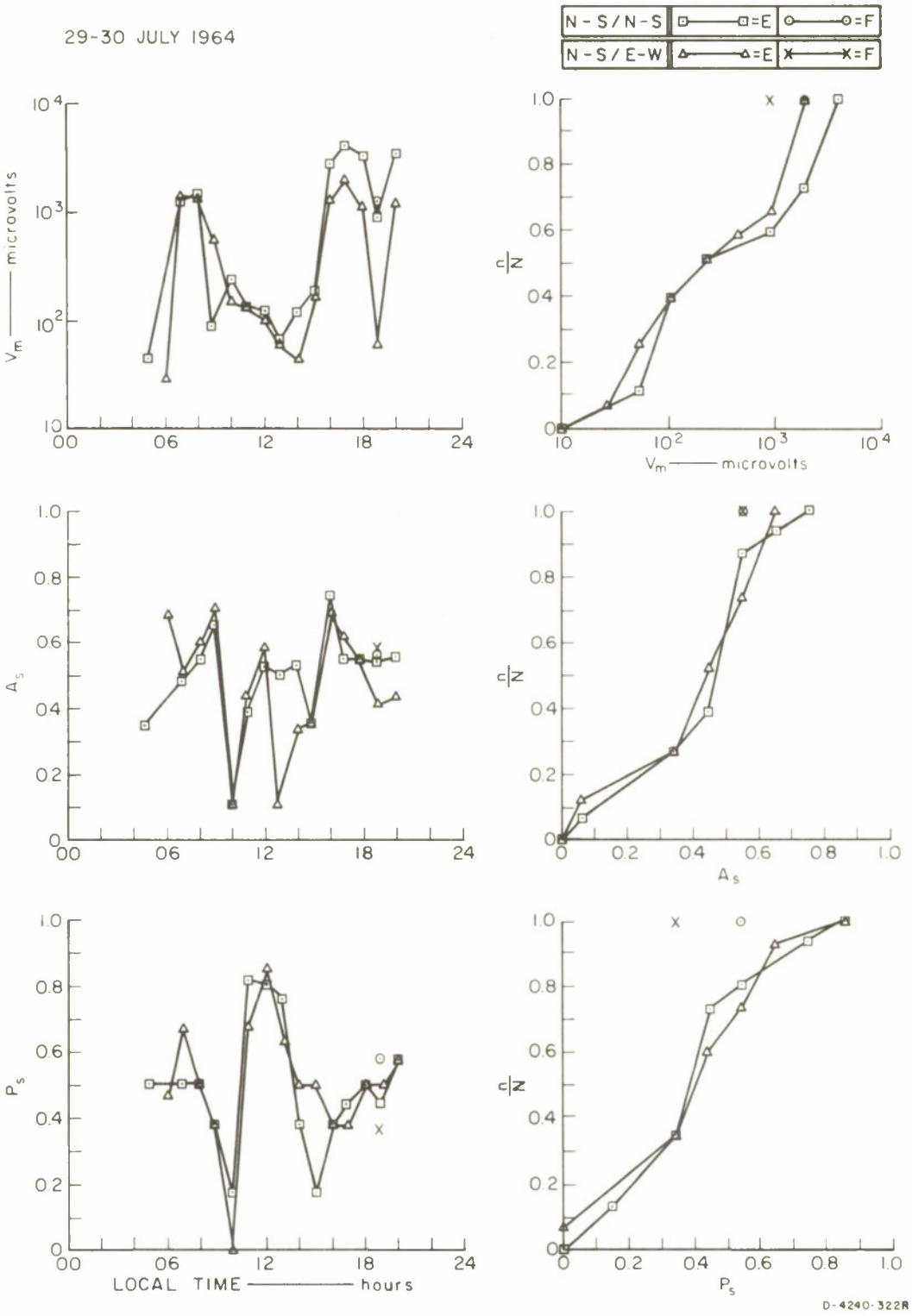

FIG. 94 3.4-MHz PULSE DATA, SATTAHIP/CHOLBURI CIRCUIT: N-S TRANSMITTING, 49 km

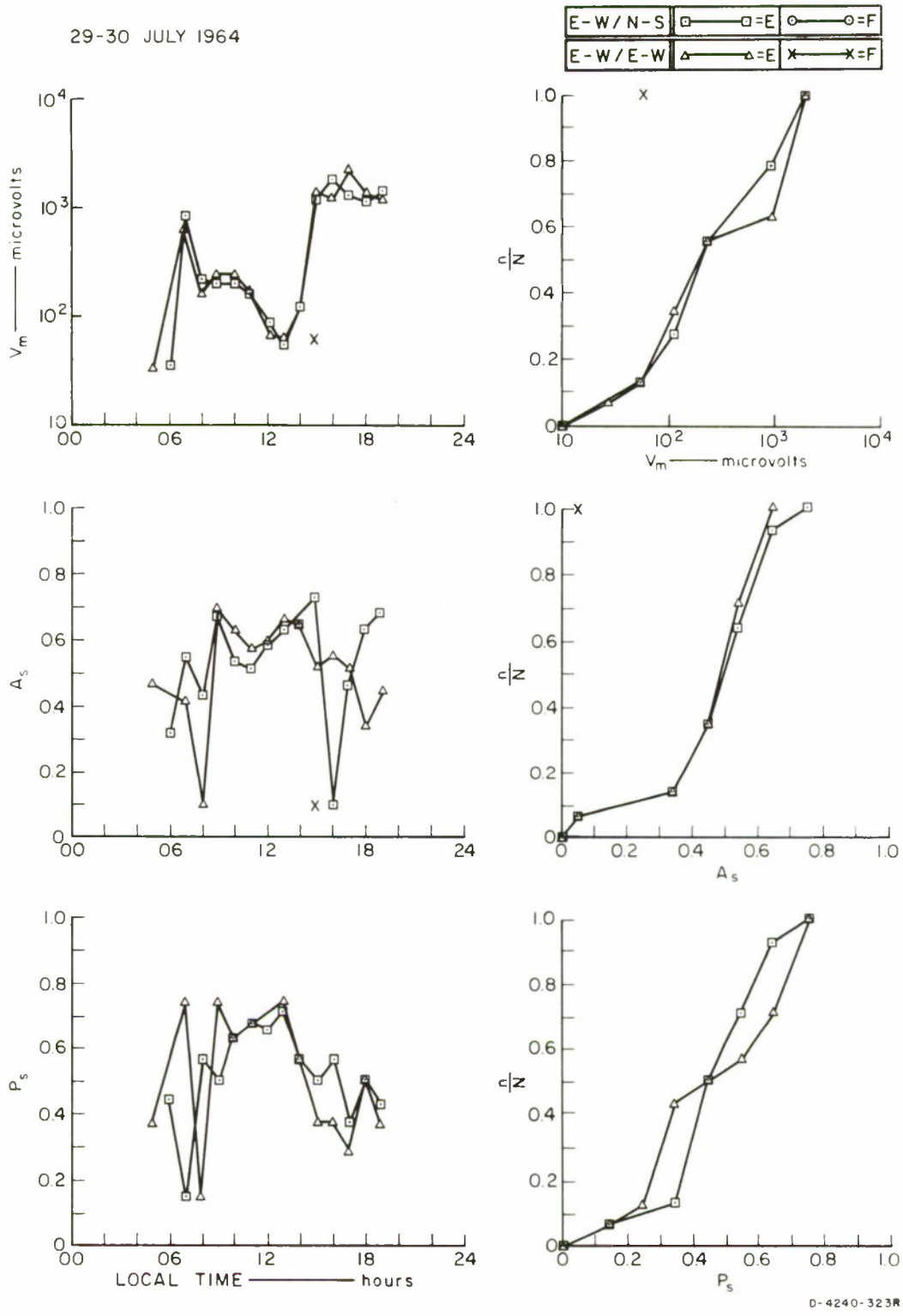

FIG. 95 3.4-MHz PULSE DATA, SATTAHIP/CHOLBURI CIRCUIT: E-W TRANSMITTING, 49 km

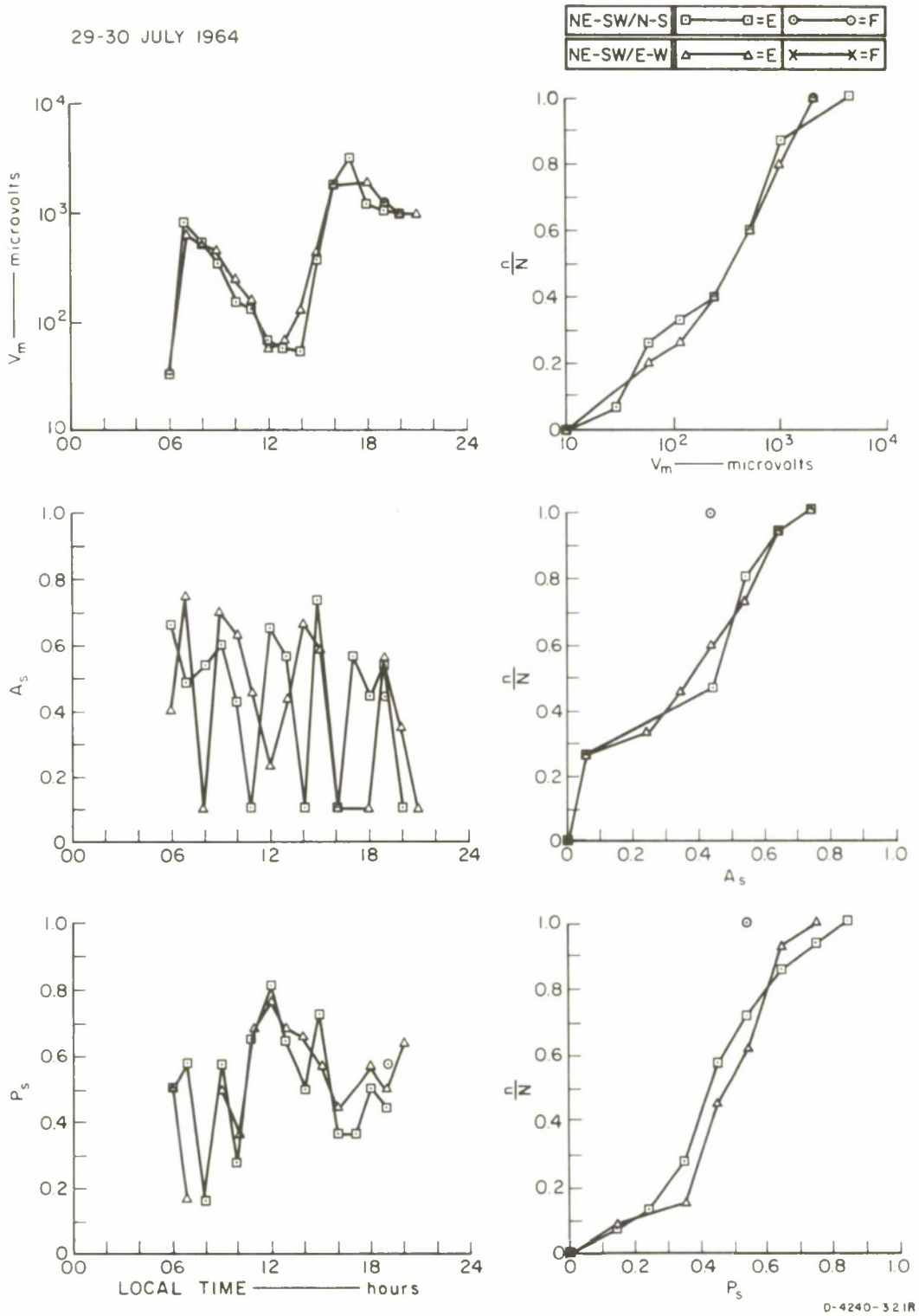

FIG. 96 3.4-MHz PULSE DATA, SATTAHIP/CHOLBURI CIRCUIT: NE-SW TRANSMITTING, 49 km

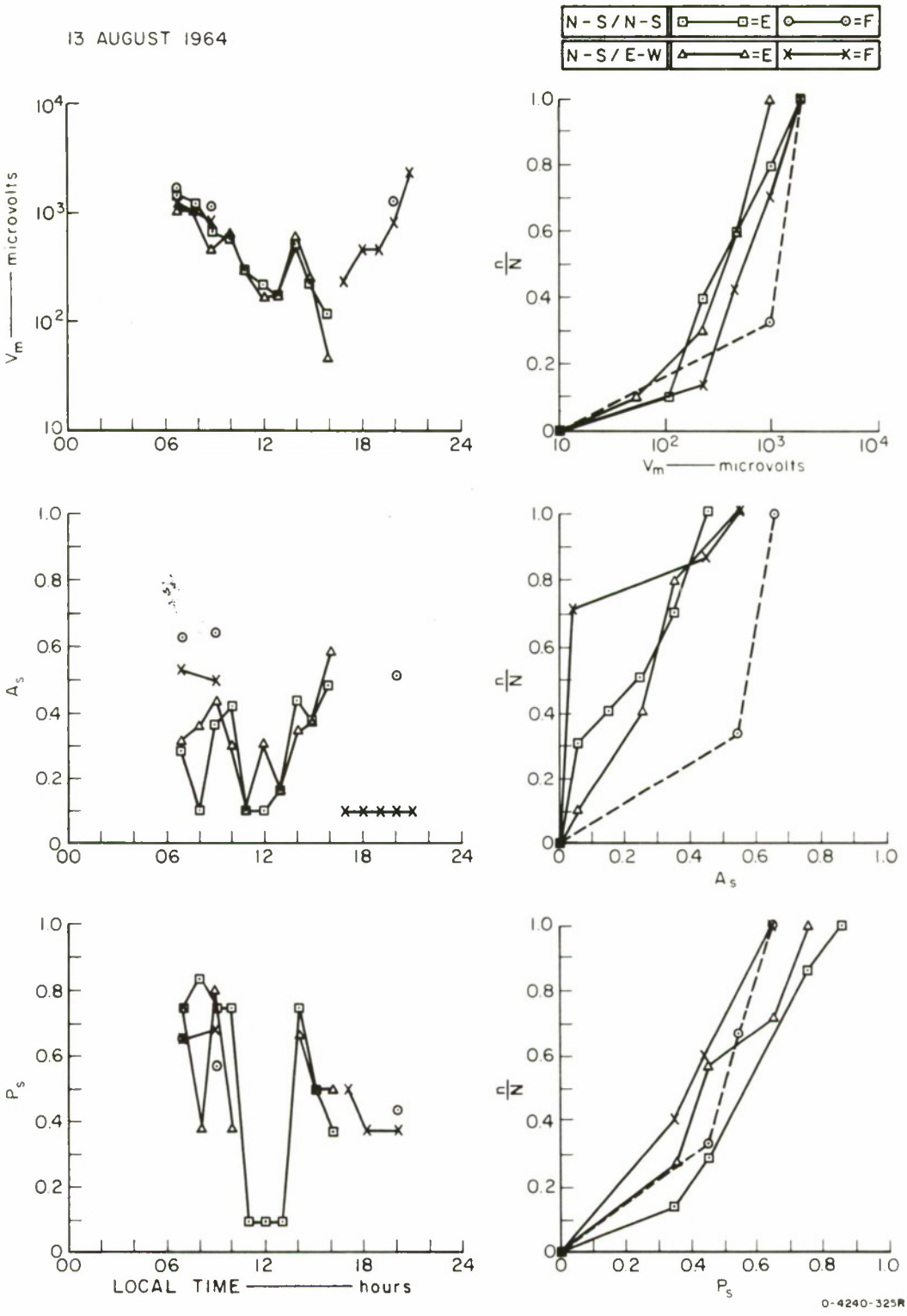

FIG. 97 3.4-MHz PULSE DATA, SATTAHIP/CHOLBURI CIRCUIT: N-S TRANSMITTING, 59 km

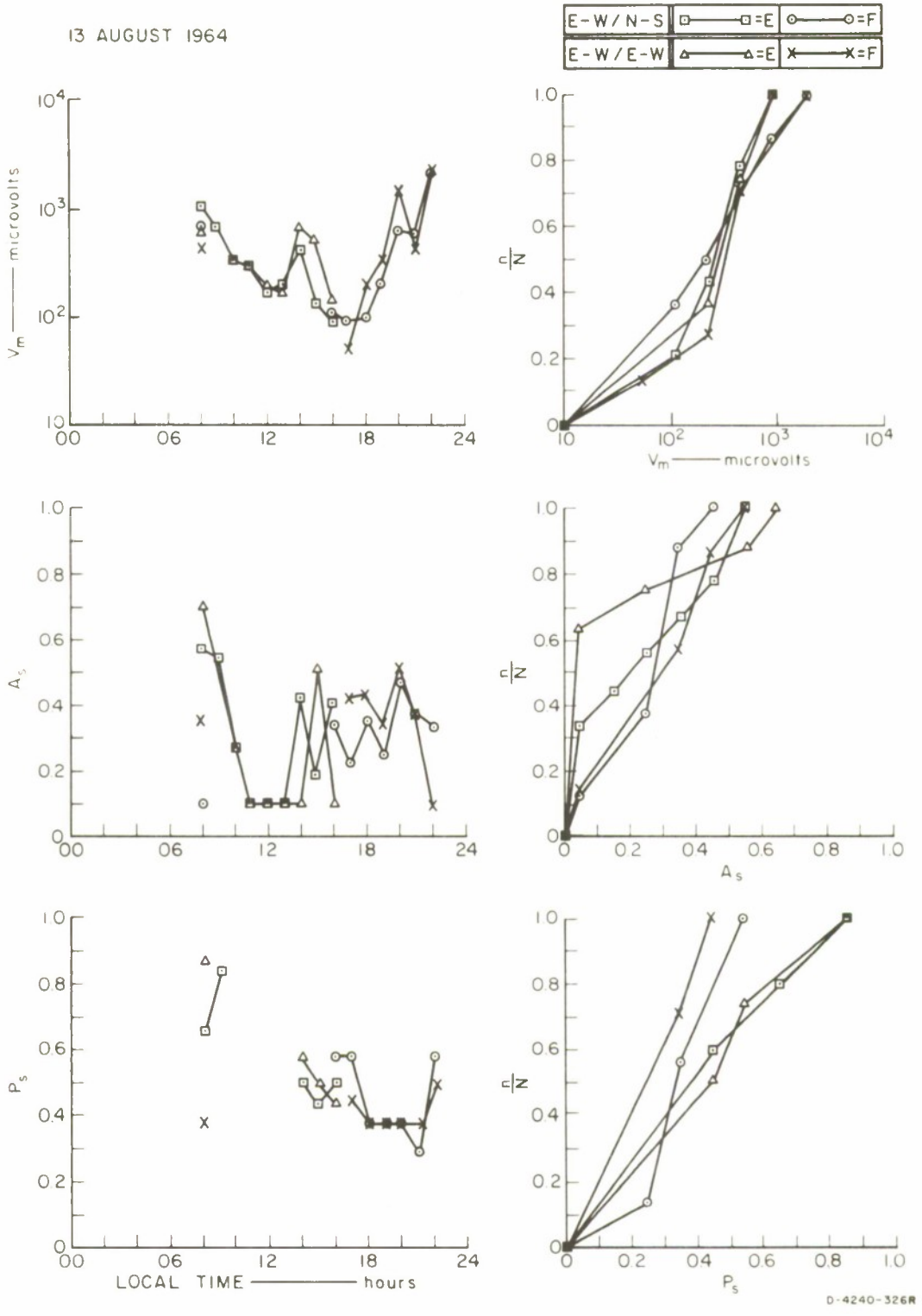

FIG. 98 3.4-MHz PULSE DATA, SATTAHIP/CHOLBURI CIRCUIT:
E-W TRANSMITTING, 59 km

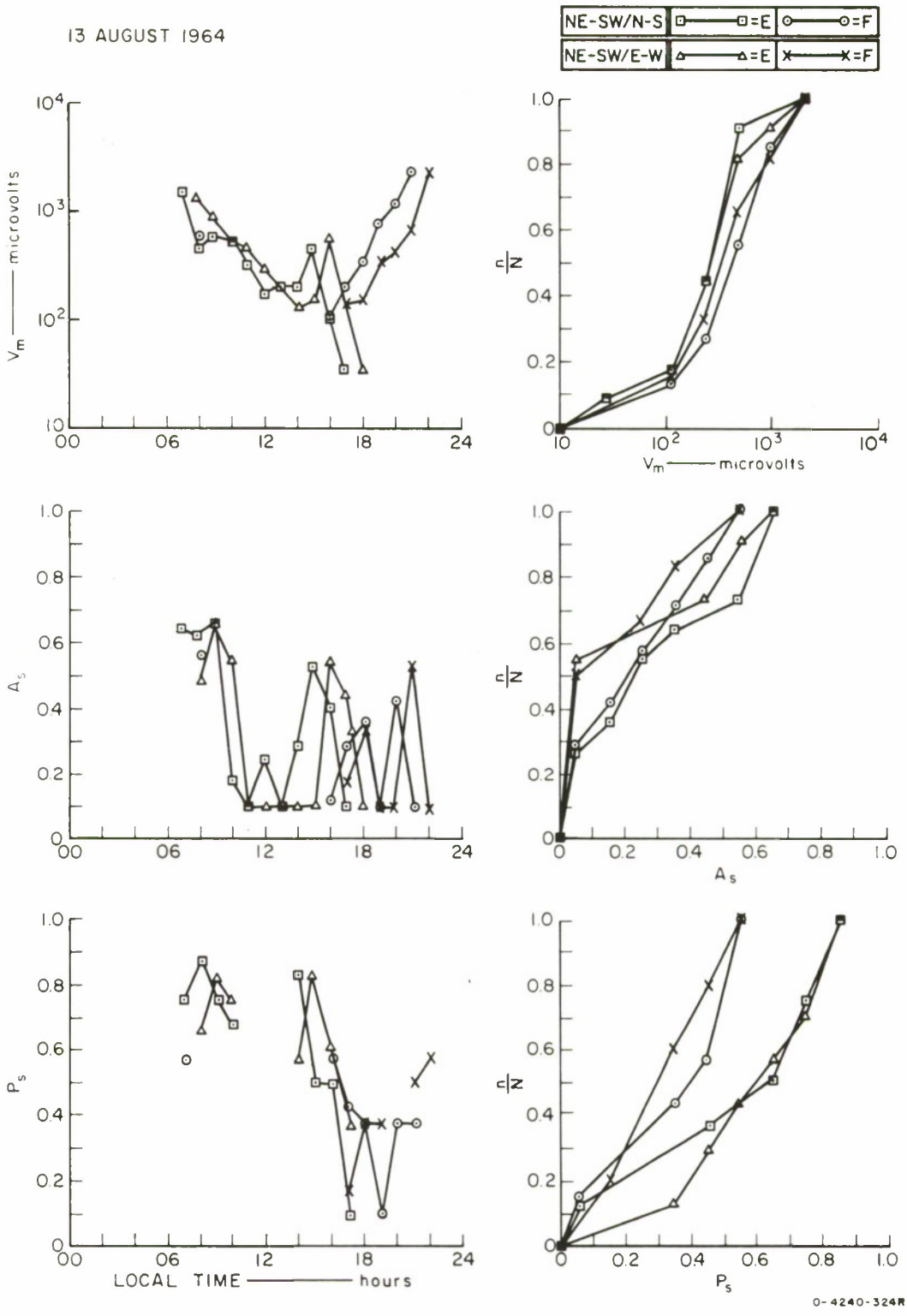

FIG. 99 3.4-MHz PULSE DATA, SATTAHIP/CHOLBURI CIRCUIT: NE-SW TRANSMITTING, 59 km

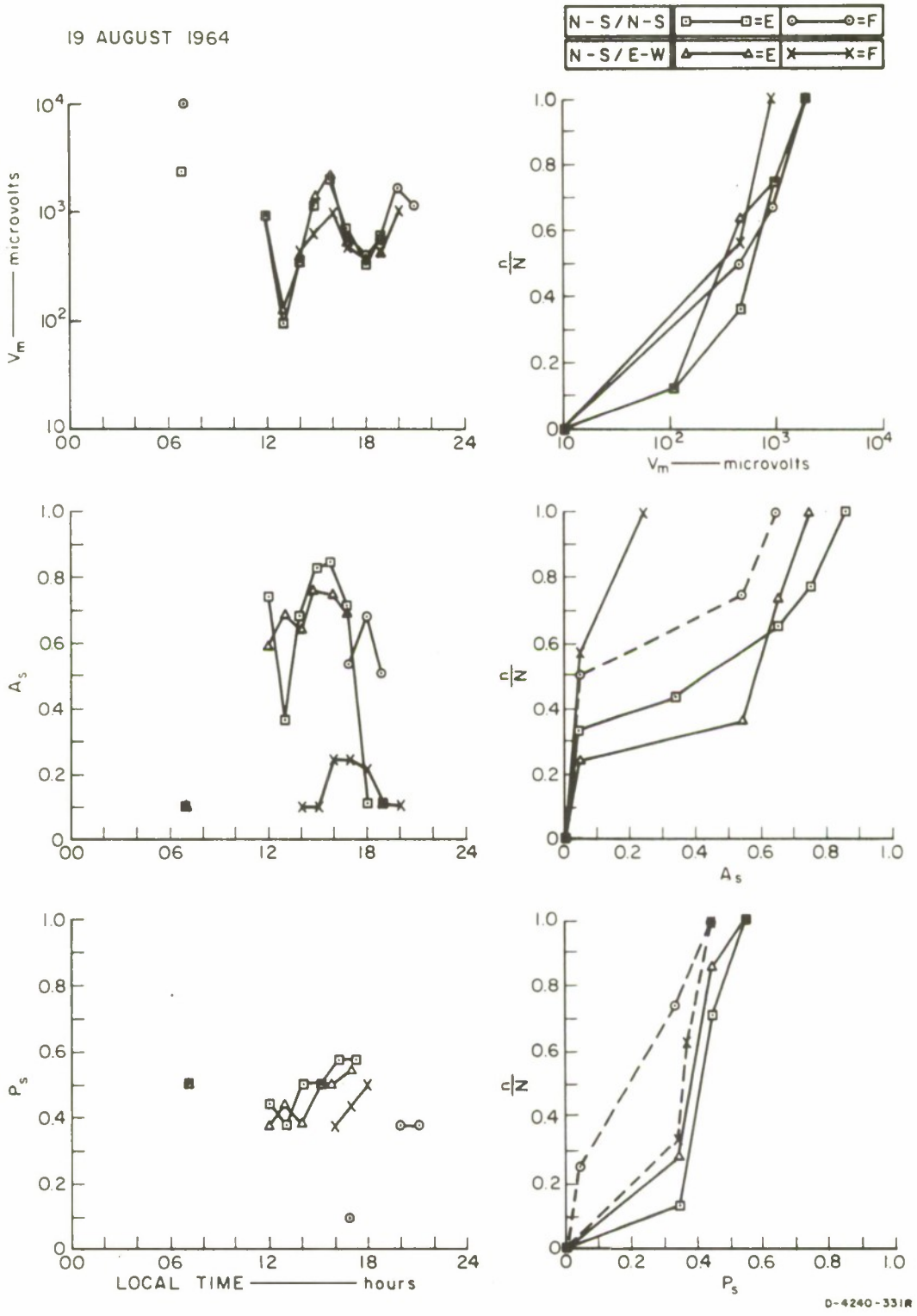

FIG. 100 3.4-MHz PULSE DATA, SATTAHIP/CHOLBURI CIRCUIT: N-S TRANSMITTING, 83 km

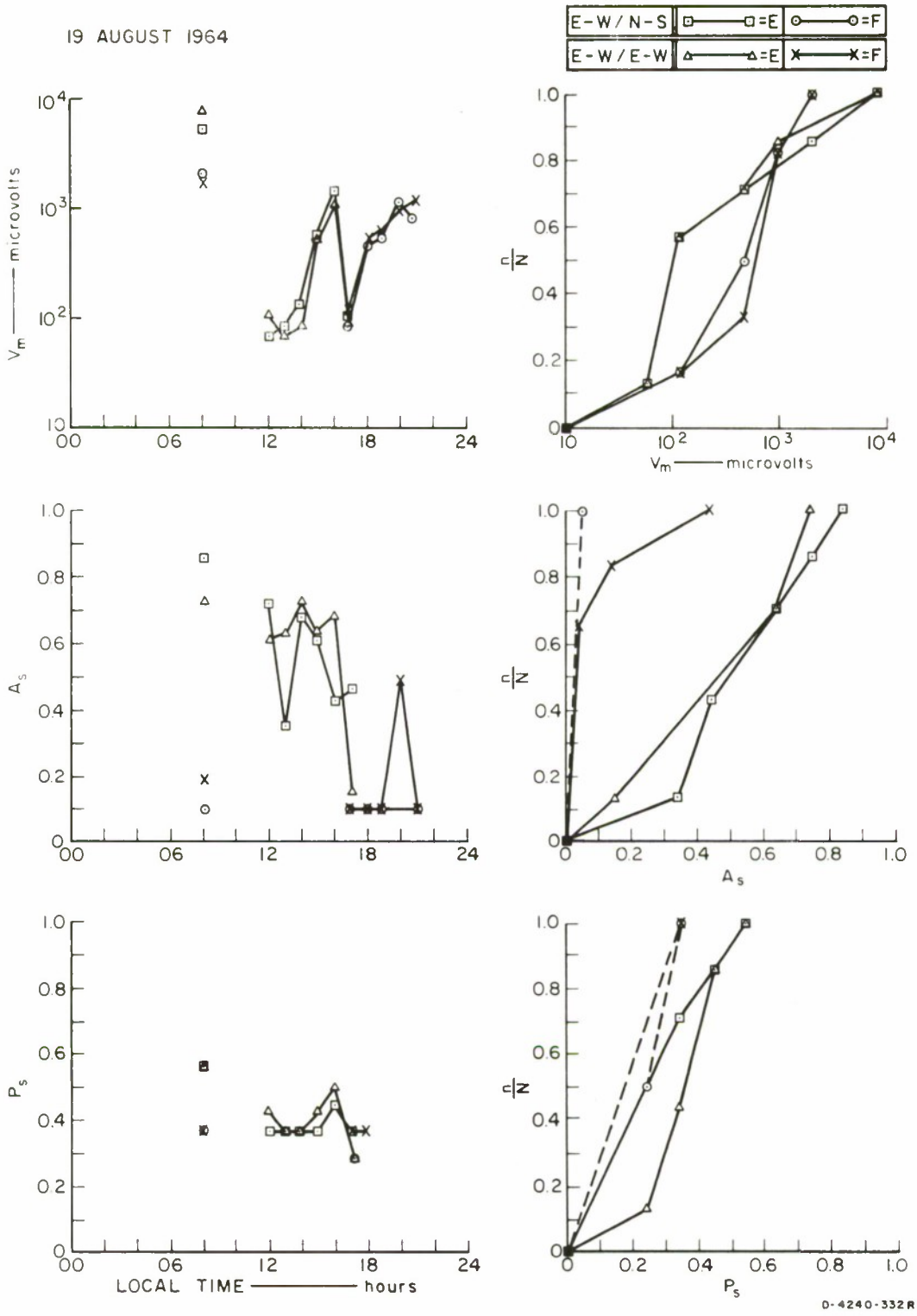

FIG. 101 3.4-MHz PULSE DATA, SATTAHIP/CHOLBURI CIRCUIT: E-W TRANSMITTING, 83 km

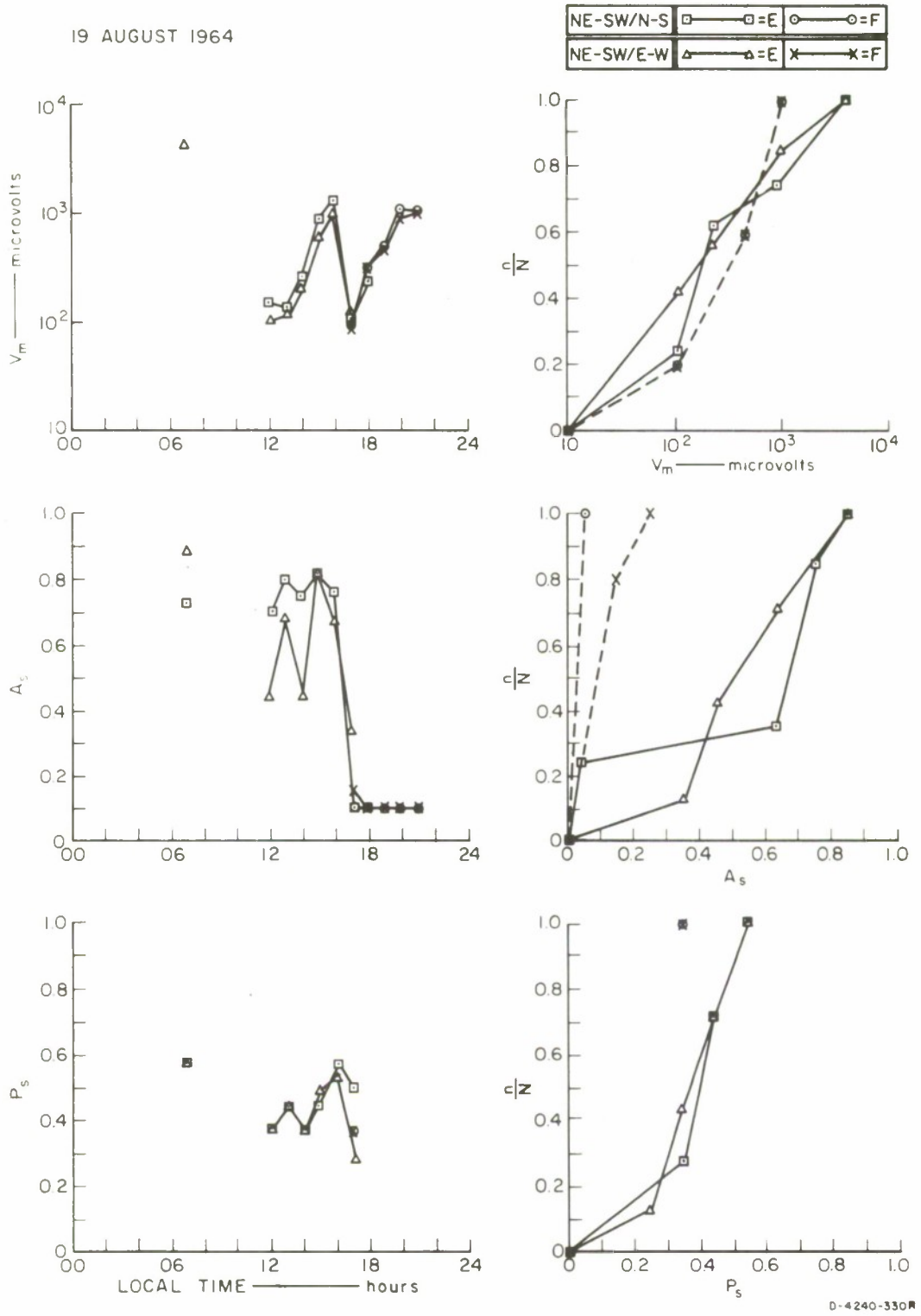

FIG. 102 3.4-MHz PULSE DATA, SATTAHIP/CHOLBURI CIRCUIT: NE-SW TRANSMITTING, 83 km

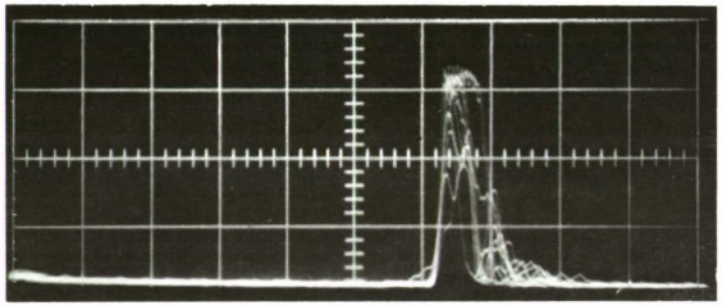

$A_s = 0.3$

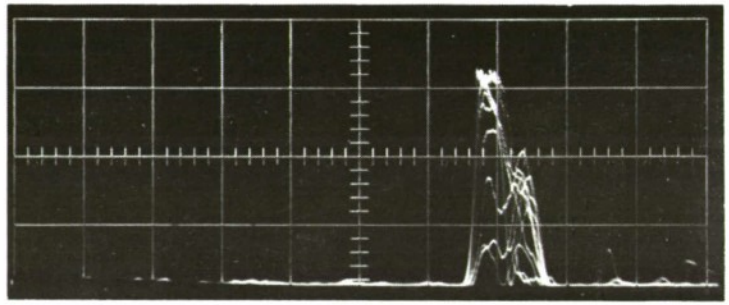

$A_s = 0.6$

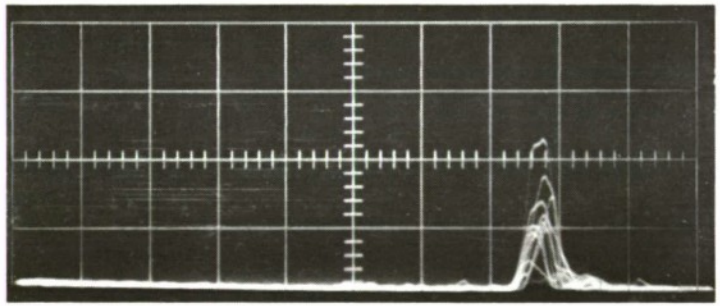

$A_s = 0.4$

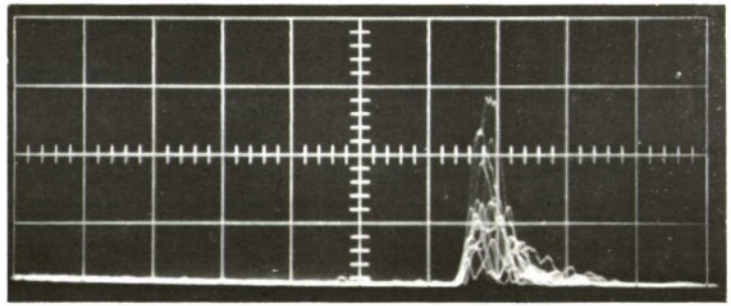

$A_s = 0.7$

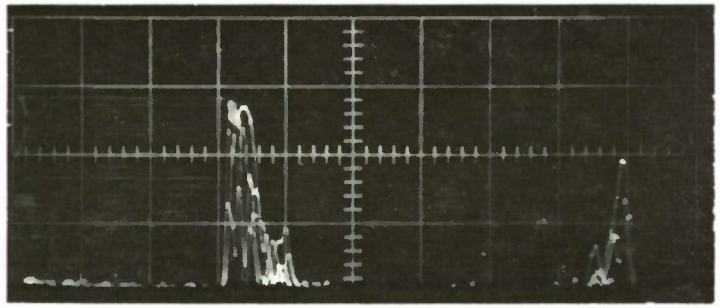

$A_s = 0.5$

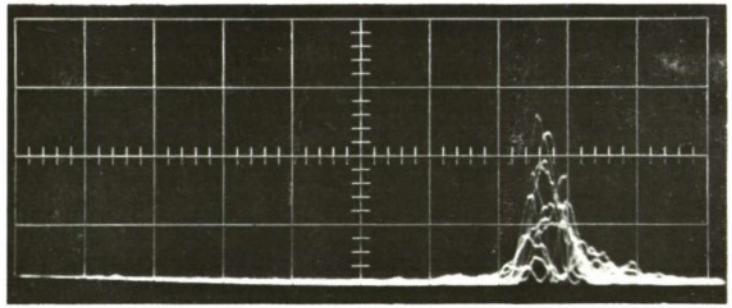

$A_s = 0.9$

D-4240-1234

FIG. 103 AMPLITUDE STABILITY VALUES, A_s, OF PULSES

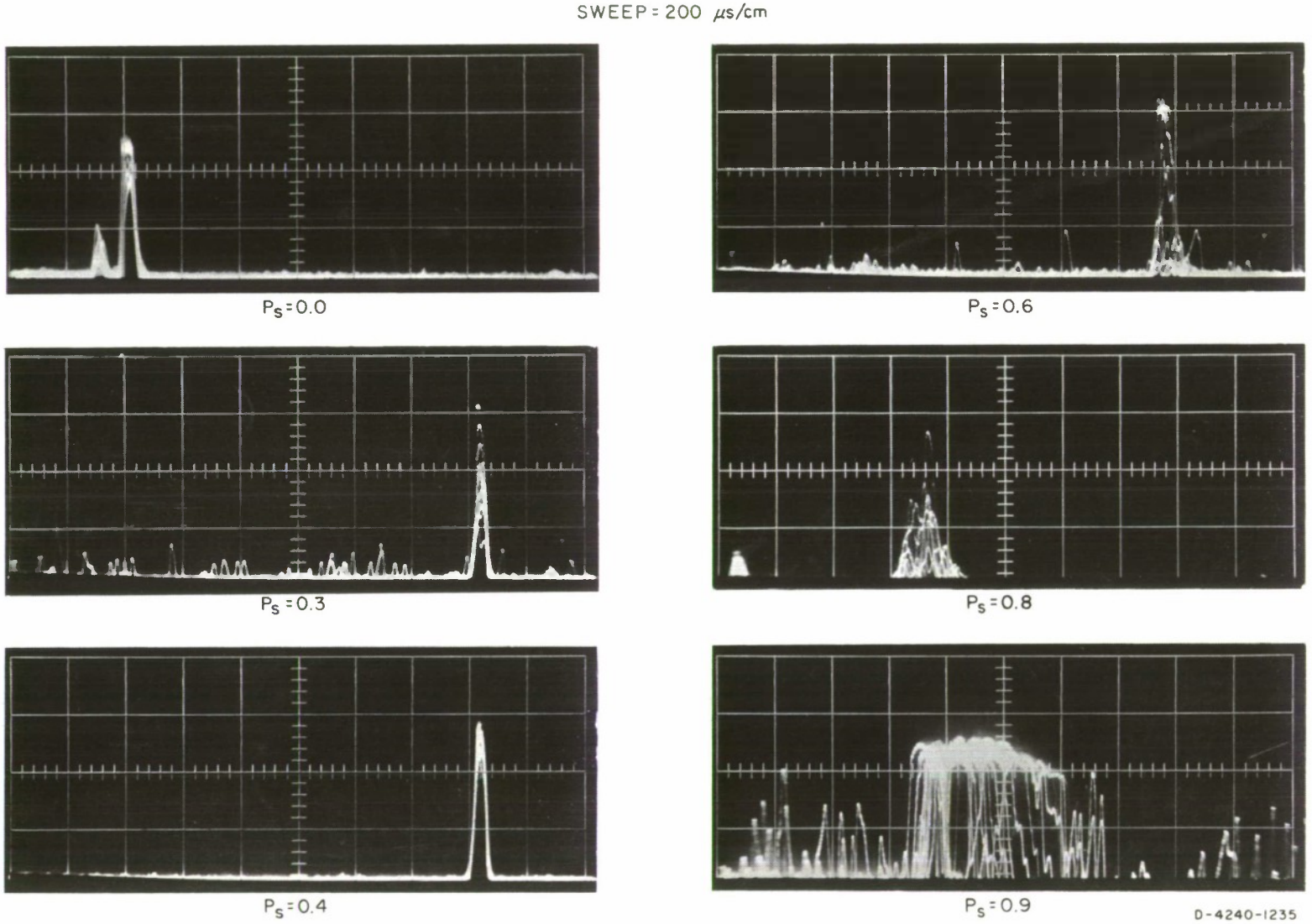

FIG. 104 PHASE STABILITY VALUES, P_s, OF PULSES

(4) Cumulative distribution n/N plots were obtained for the above V_m, A_s and P_s plots as the right-hand plots of Figs. 79 through 102. A dashed line indicates that the plot was derived from less than six data points ($N < 6$).

N is the total number of points plotted for the same transmitting/receiving antenna combination.

The axes of abscissa (V_m, A_s, P_s) are divided into ten classes, and n is the number of points in a class and other lower classes; that is, n/N is monotonic. All points are plotted at the mid-value of a class. A point plotted at $A_s = 0.35$, $n/N = 0.2$ means that 20 percent of the total points fall below $A_s = 0.4$.

a. Diurnal Variation of Pulse Amplitudes

An attempt to investigate the diurnal variation of pulse amplitudes and also to compare it with that of CW results was made by superimposing the V_m curves for all distances. The results are shown in Fig. 105 for the N-S/N-S and E-W/E-W transmitting/receiving antenna combinations and in Fig. 106 for the NE-SW/N-S and NE-SW/E-W transmitting/receiving antenna combinations. Figure 105 indicates that the N-S/N-S was the better antenna combination, thus confirming the CW results and the magneto-ionic theory, which indicate the superiority of the ordinary wave to the extraordinary wave. Comparing Fig. 105 with Fig. 106, one sees that the NE-SW is almost as good a transmitting antenna as the N-S antenna and the NE-SW/E-W is as good as the E-W/E-W; hence, there exists the possibility of improvement by a diversity reception with the NE-SW as a transmitting antenna. In general, the curves in Figs. 105 and 106 of the 3.4-MHz pulse test agree well with Figs. 45 and 48 of the 3-MHz CW test: the pre-dawn minimum, the peak after sunrise, the midday low, the second peak at sunset, and the diurnal variation of 30-40 dB.

It should be noted here that the propagation was supported mainly by the sporadic-E layer, and the exchange of energy between the ordinary and the extraordinary waves was observed to be greatest at the time of change between Es and F layers.

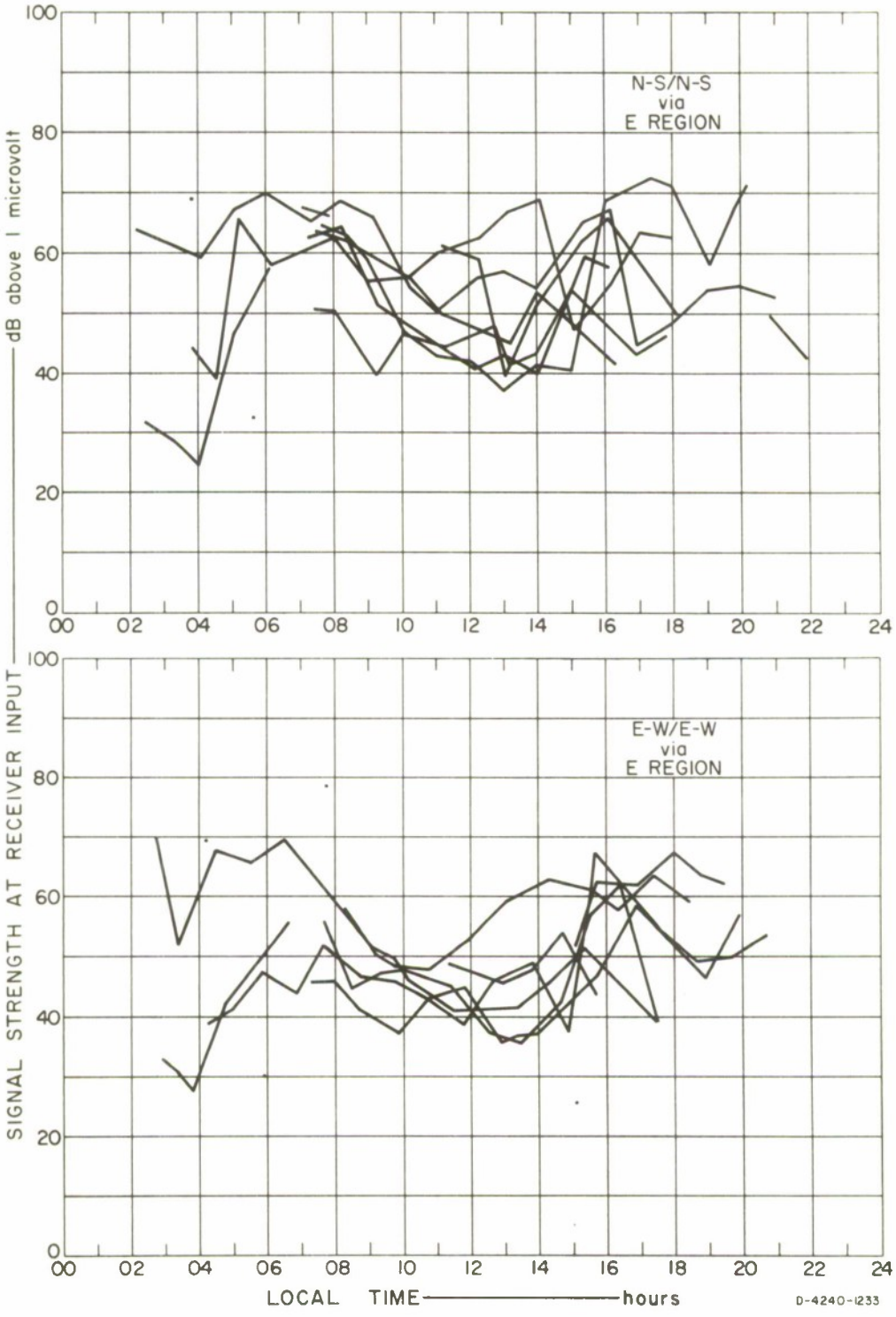

FIG. 105 DIURNAL VARIATION OF V_m: SATTAHIP, N-S AND E-W TRANSMITTING AT 3.4-MHz

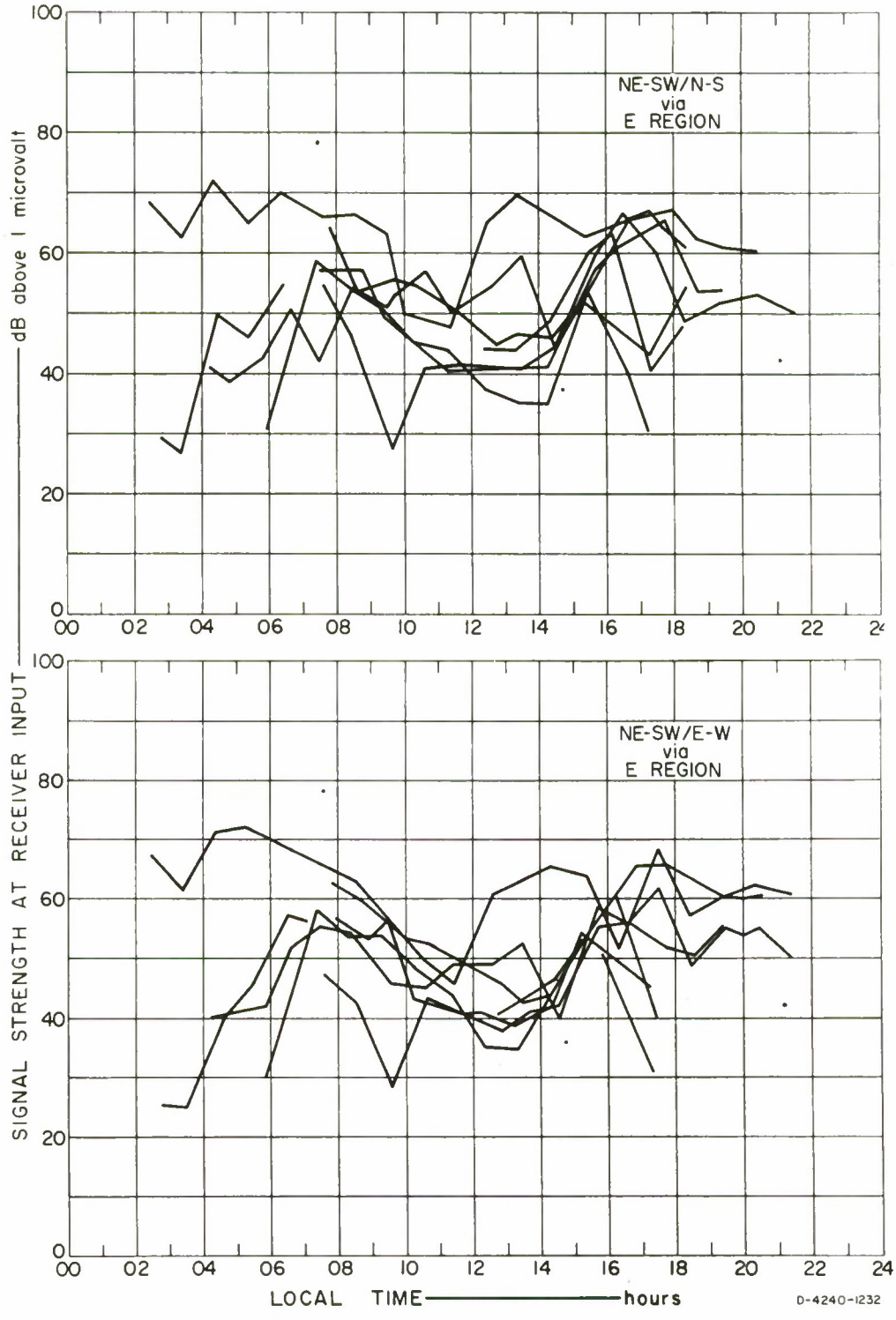

FIG. 106 DIRUNAL VARIATION OF V_m: SATTAHIP, NE-SW TRANSMITTING AT 3.4 MHz

b. Mean Pulse Amplitude versus Distance: QT Range

The mean pulse amplitude is here defined as the V_m value corresponding to n/N = 0.5. Mean pulse amplitudes, as read from Figs. 79 through 102, were plotted against ground distances between the transmitting and receiving sites. The results are shown in Fig. 107 for the N-S/N-S, N-S/E-W, E-W/E-W and the NE-SW/N-S, NE-SW/E-W transmitting/receiving antenna combinations. The overall results of these plots indicate that the N-S/N-S combination was the best and that there would be an advantage in diversity reception, not with the NE-SW, but with the N-S as a transmitting antenna and the N-S and E-W as receiving antennas. This indicates that the effect of polarization tilt, as described in Sec. II-C-4, is not significant at this small magnetic inclination (8^o-9^oN).

As previously mentioned, the idea of moving a receiving station away from the transmitting site in stages was to look for the presence of a quasi-transverse (QT) condition. The theoretical QT range obtained from Table II or Fig. 15 for the 3-MHz propagation over the Bangkok area in the N-S direction via the E region is 37-67 km. This theoretical value is supported experimentally by the fact that the mean pulse amplitude rose abruptly at 30 km, reached the peak at 40 km, and fell back to level around 60 km as shown in Fig. 107. The ordinary wave showed its superiority over the extraordinary practically throughout the whole range under study, as would be expected even in the QT-QL range [refer to discussion immediately following Eq. (40)].

c. Stability of Received Pulses

Mean A_s and mean P_s values corresponding to n/N = 0.5 were read from the right-hand plots of Figs. 79 through 102 and were plotted against ground distances. The results are shown in Fig. 108 for the N-S/N-S and E-W/E-W antenna combinations and in Fig. 109 for the NE-SW/N-S and NE-SW/E-W combinations. The mean slopes of the n/N versus A_s and the n/N versus P_s curves of Figs. 79 through 102 were also plotted in Figs. 108 and 109 in order to assist the evaluation of the stability of received pulses. (Any two curves may have the same mean value at n/N = 0.5, but may have different slopes. A higher degree slope indicates the tendency of the wave to be more stable.)

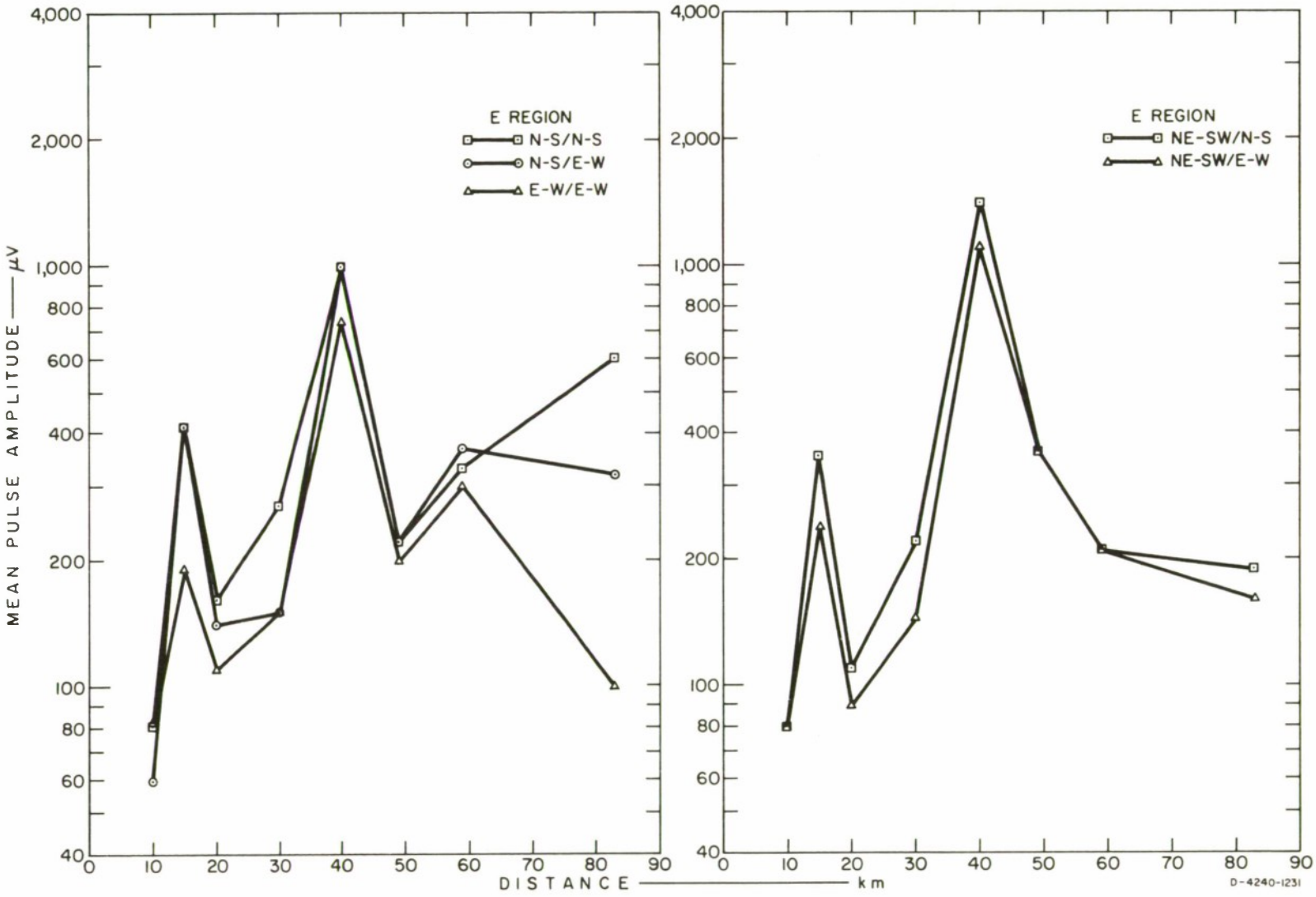

FIG. 107 MEAN PULSE AMPLITUDE AS A FUNCTION OF DISTANCE: SATTAHIP/CHOLBURI, 3.4 MHz

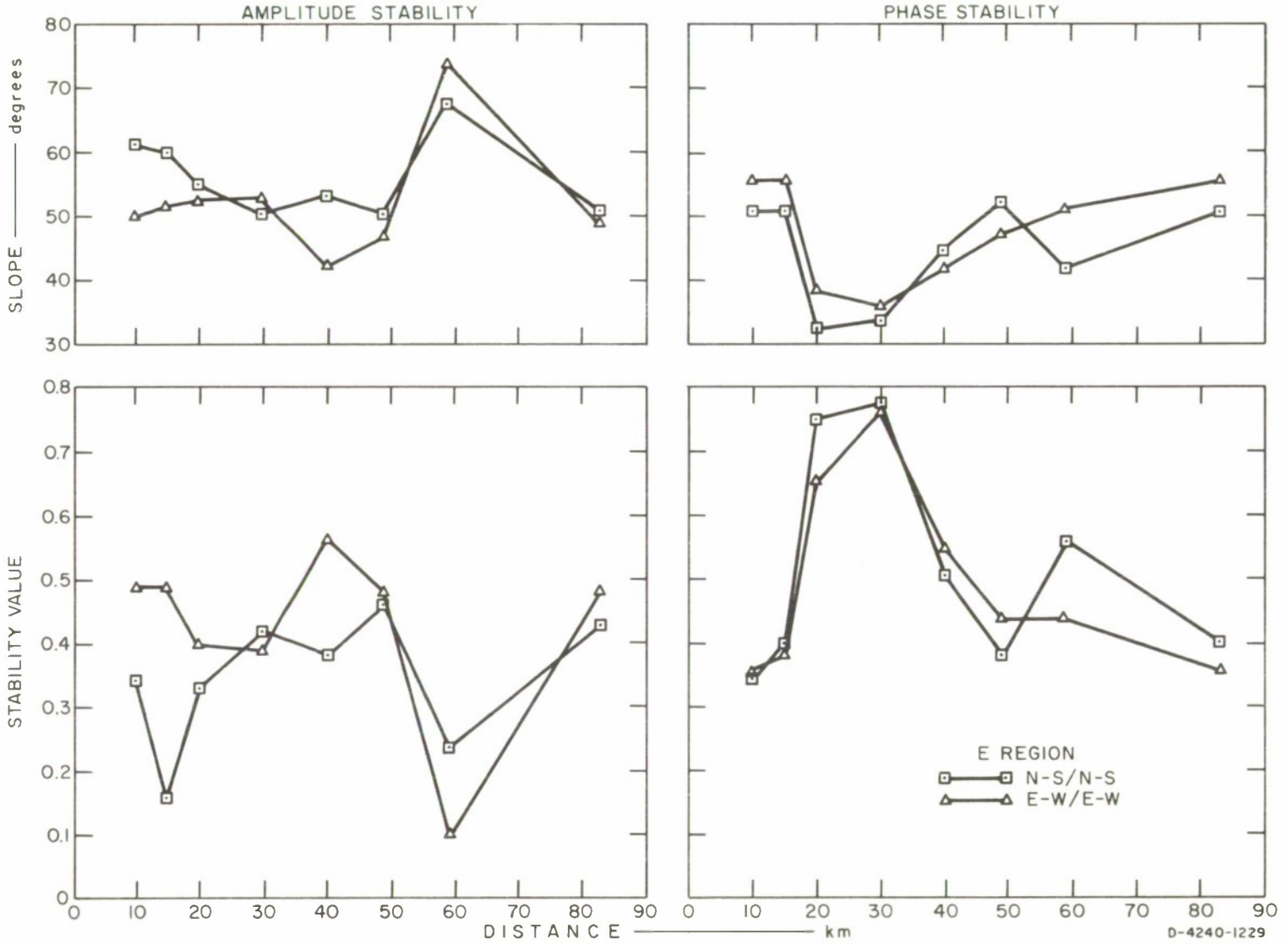

FIG. 108 PULSE STABILITY AS A FUNCTION OF DISTANCE: SATTAHIP, N-S AND E-W TRANSMITTING AT 3.4 MHz

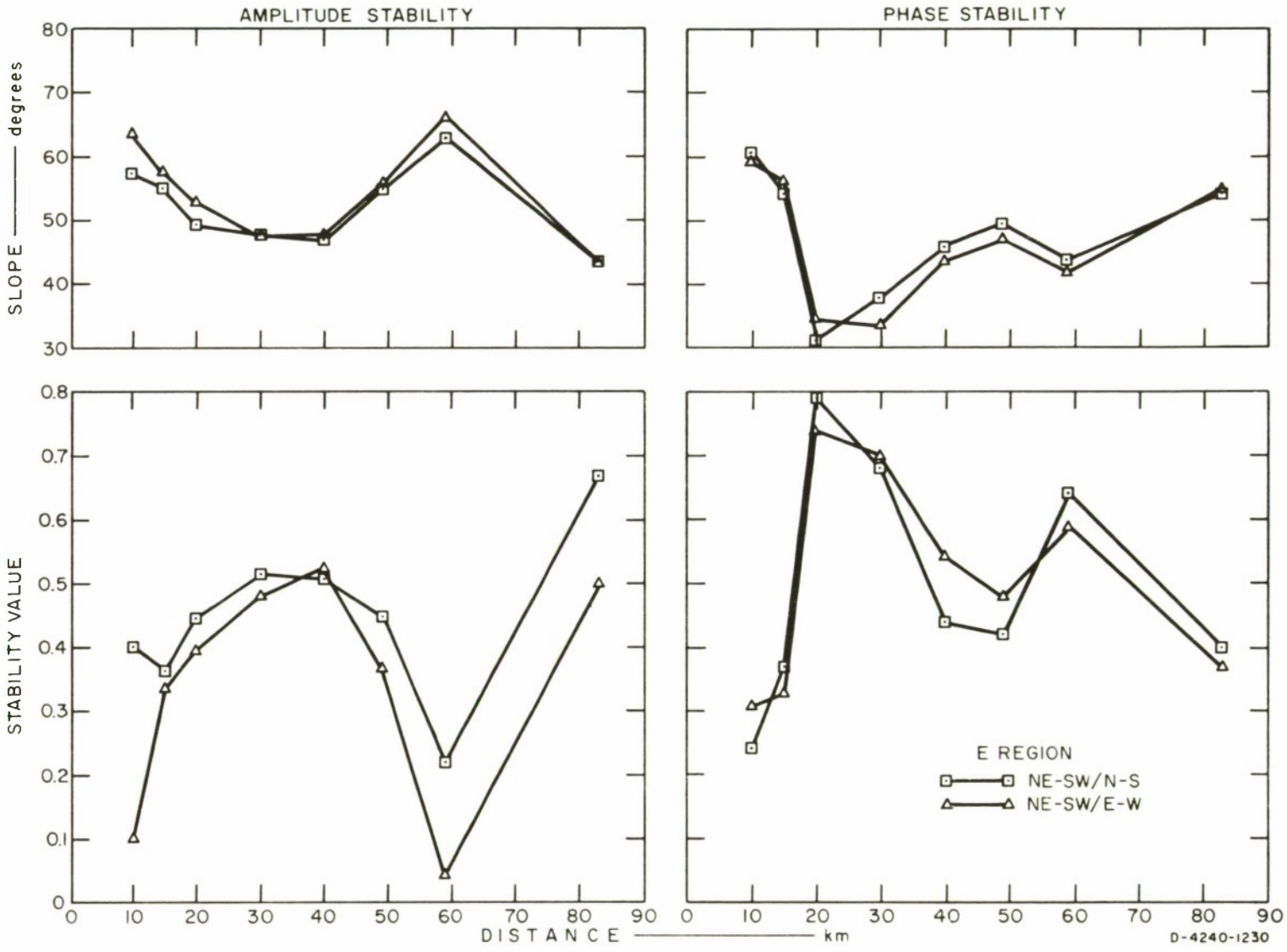

FIG. 109 PULSE STABILITY AS A FUNCTION OF DISTANCE: SATTAHIP, NE-SW TRANSMITTING AT 3.4 MHz

The extraordinary wave tended to be more stable in amplitude than the ordinary, and hence less prone to fading, as also evidenced in Fig. 56 of the CW results. The pulse stretching of both the ordinary and the extraordinary waves was not sufficiently large to be attributed to a ground backscatter. The pulse stretching of the extraordinary wave, however, tended to be greater than that of the ordinary. The possible improvement with a diversity reception was therefore indicated, although not so clearly as suggested by the V_m study above. There seemed to be no clear-cut diurnal variation in the wave stability, suggesting that fading is likely to be more or to be less at any time of the day. The 3-MHz CW results (Figs. 56 and 58) showed that the waves faded more often and more rapidly during period 2200-0600 than during the rest of the day. Together with the close study of the 3-MHz noise curve in Fig. 62 and the curves in Figs. 79 through 102, the author has been led to believe that:

(1) The mechanism of a severe fading, which is rapid and frequent, is due to the fairly low signal-to-noise ratio (the order of a few dB) and to the presence of multiple mode and/or multiple path propagation.

(2) The slow fading during the day is due mainly to the instability within the mode of propagation itself; in the present study, this would be because of the turbulence of the Es layer.

d. Confirmation by Test in Reversed Direction

The 3.4-MHz pulse test was performed in the reversed (Cholburi/Sattahip) direction; data from the reversed test were reduced and plotted in the same manner as for the Sattahip/Cholburi circuit. Diurnal variations of the signal strength and stability, together with the cumulative distribution n/N plots, are shown in Figs. 110 through 121. Mean pulse amplitudes, as read from n/N = 0.5, were plotted for the N-S/N-S, E-W/E-W, NE-SW/N-S and NE-SW/E-W antenna combinations as shown in Fig. 122, superimposed with the corresponding curves from Fig. 107. Amplitudes of the two sets, one for the S-to-N and the other for the N-to-S path, cannot be directly compared, since the measurements were not taken simultaneously (as were the radio-teletype measurements described in Secs. IV-B and IV-C-2).

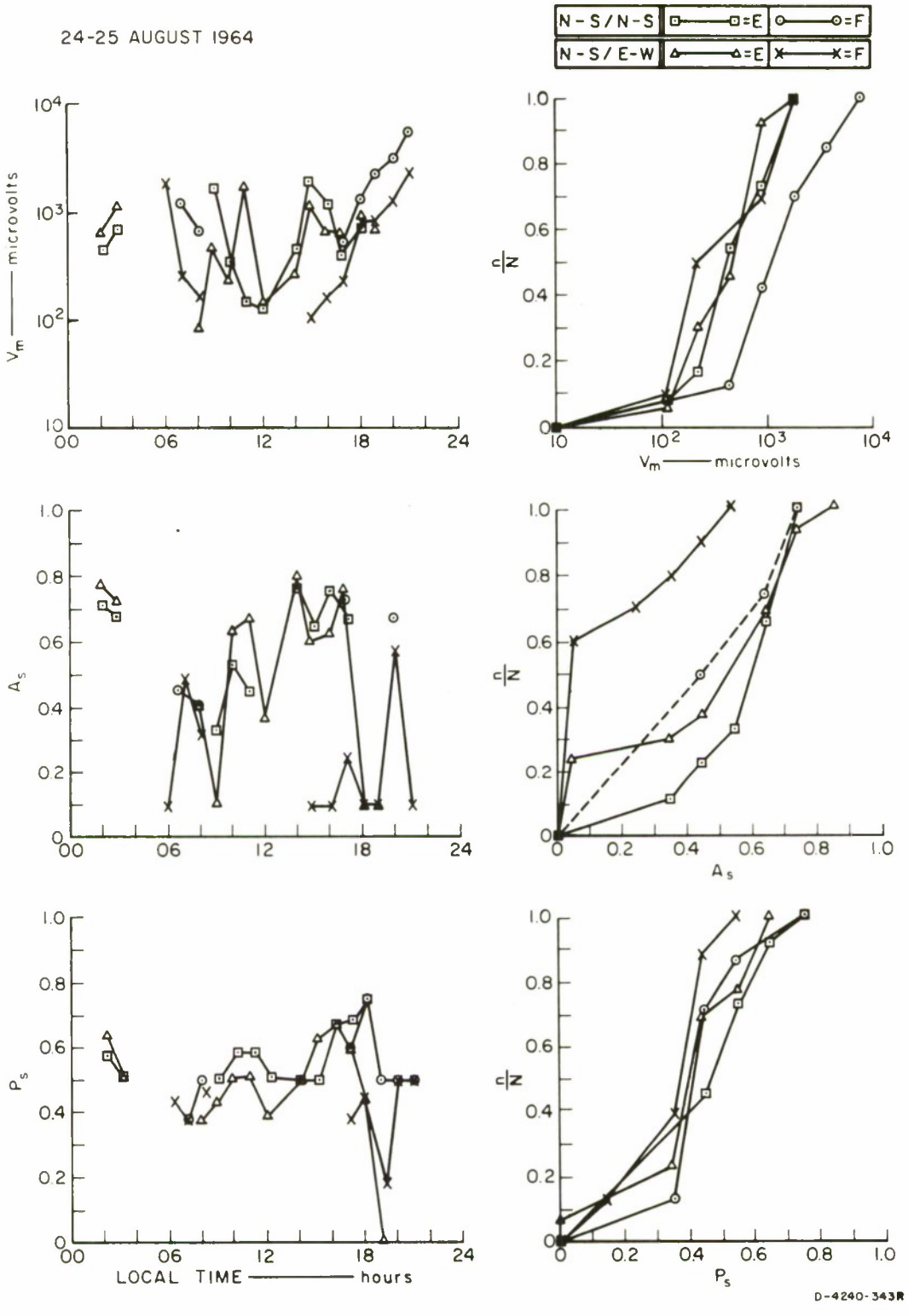

FIG. 110 3.4-MHz PULSE DATA, CHOLBURI/SATTAHIP CIRCUIT:
N-S TRANSMITTING, 24 km

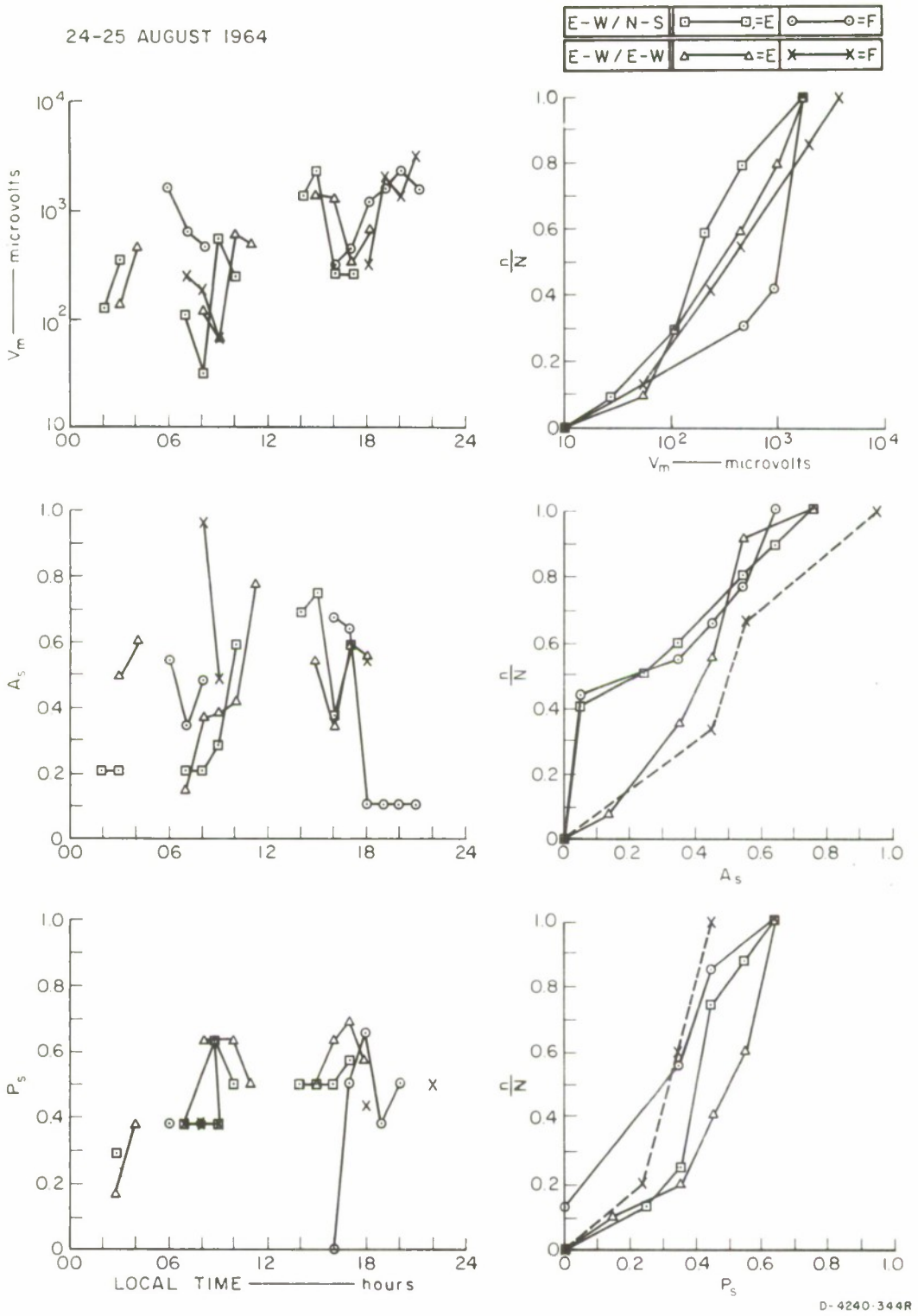

FIG. 111 3.4-MHz PULSE DATA, CHOLBURI/SATTAHIP CIRCUIT: E-W TRANSMITTING, 24 km

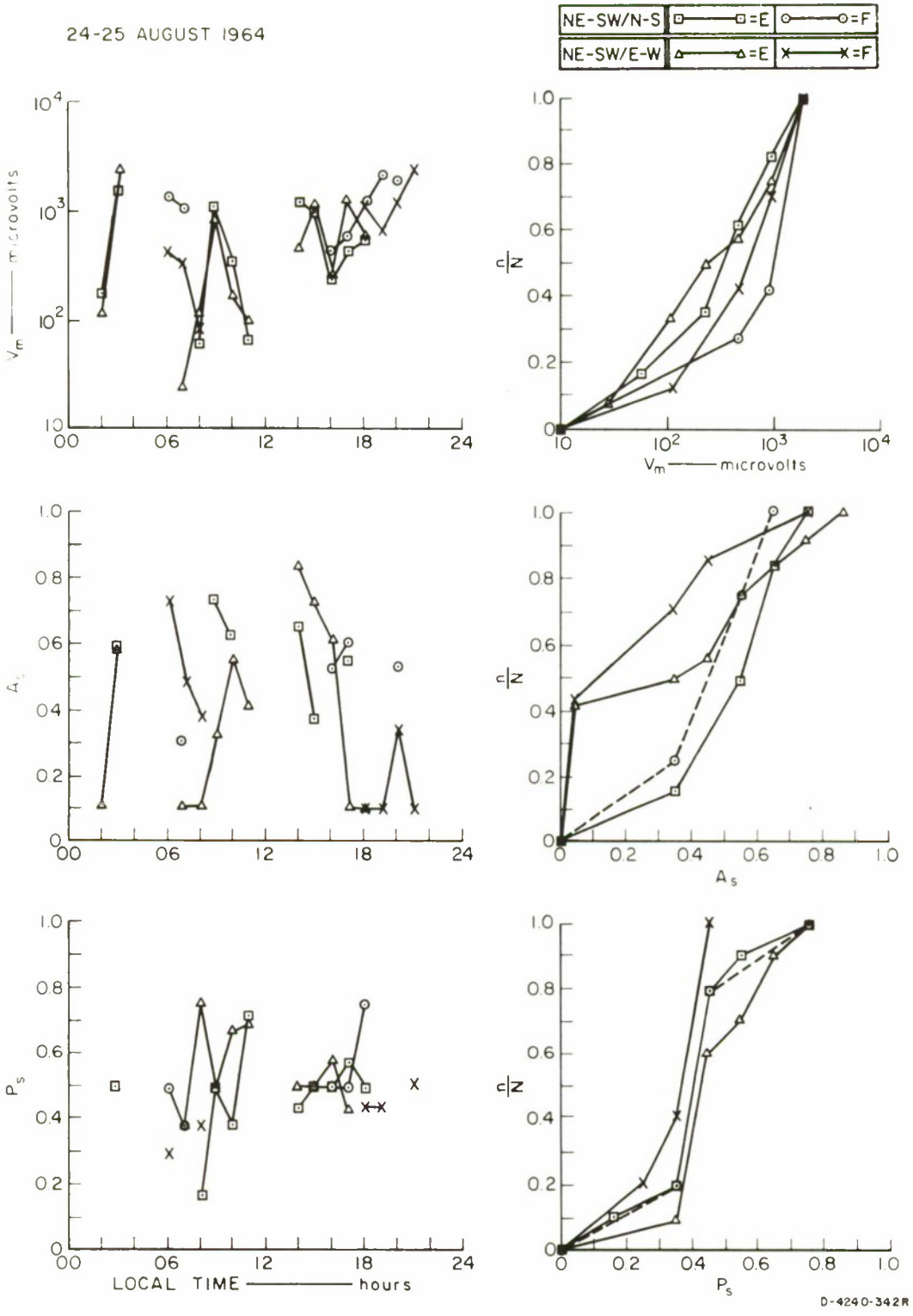

FIG. 112 3.4-MHz PULSE DATA, CHOLBURI/SATTAHIP CIRCUIT: NE-SW TRANSMITTING, 24 km

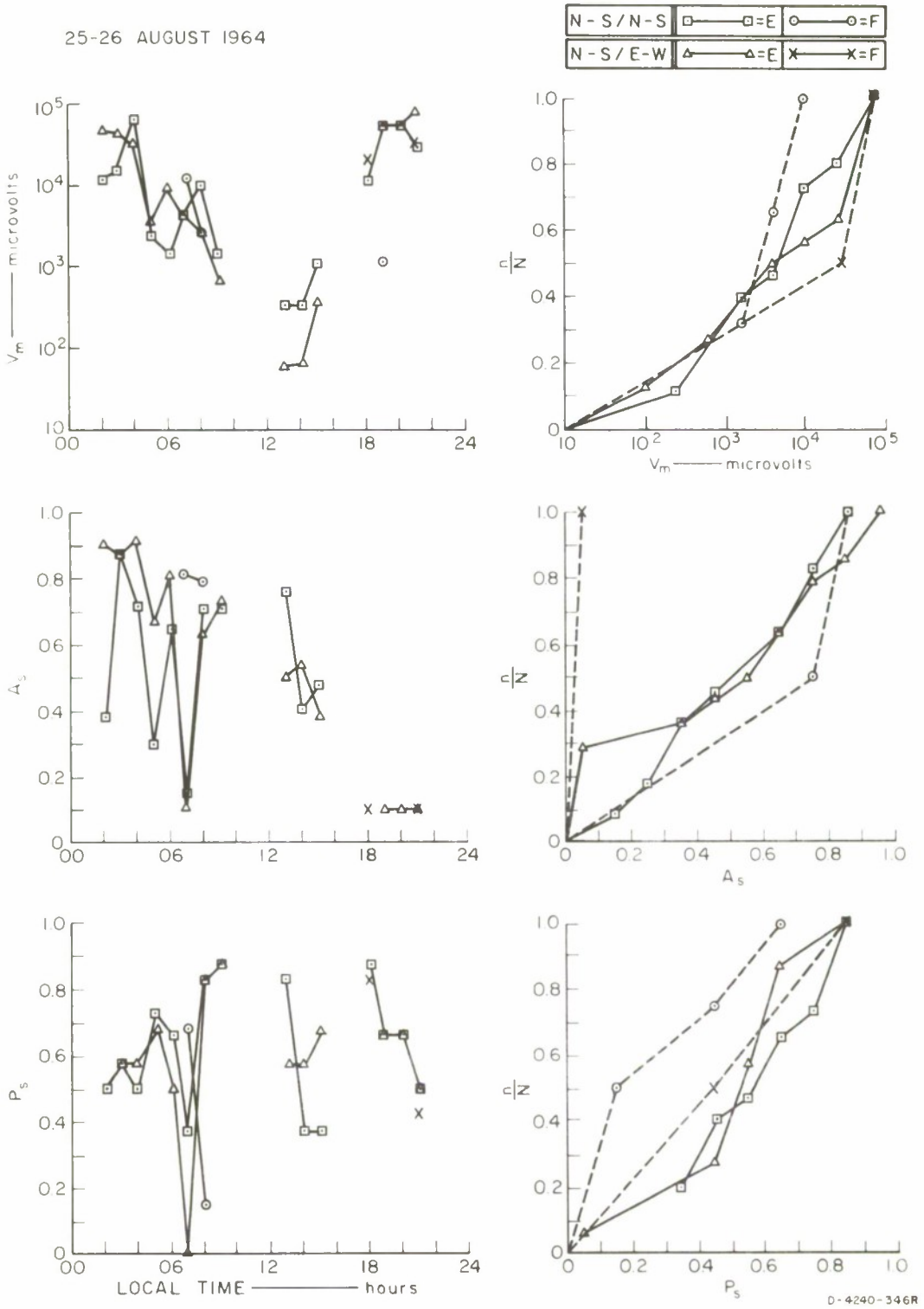

FIG. 113 3.4-MHz PULSE DATA, CHOLBURI/SATTAHIP CIRCUIT: N-S TRANSMITTING, 43 km

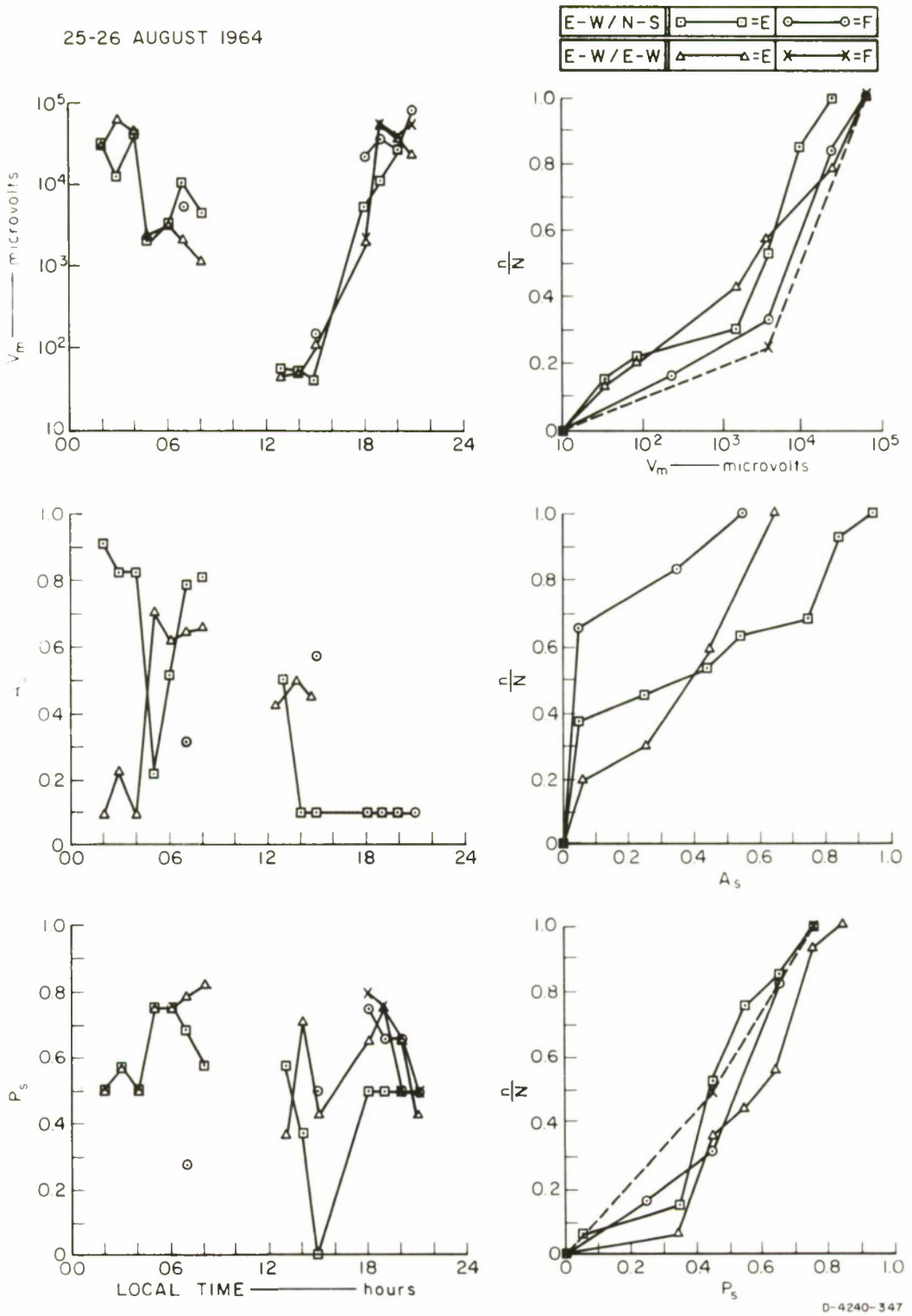

FIG. 114 3.4-MHz PULSE DATA, CHOLBURI/SATTAHIP CIRCUIT:
E-W TRANSMITTING, 43 km

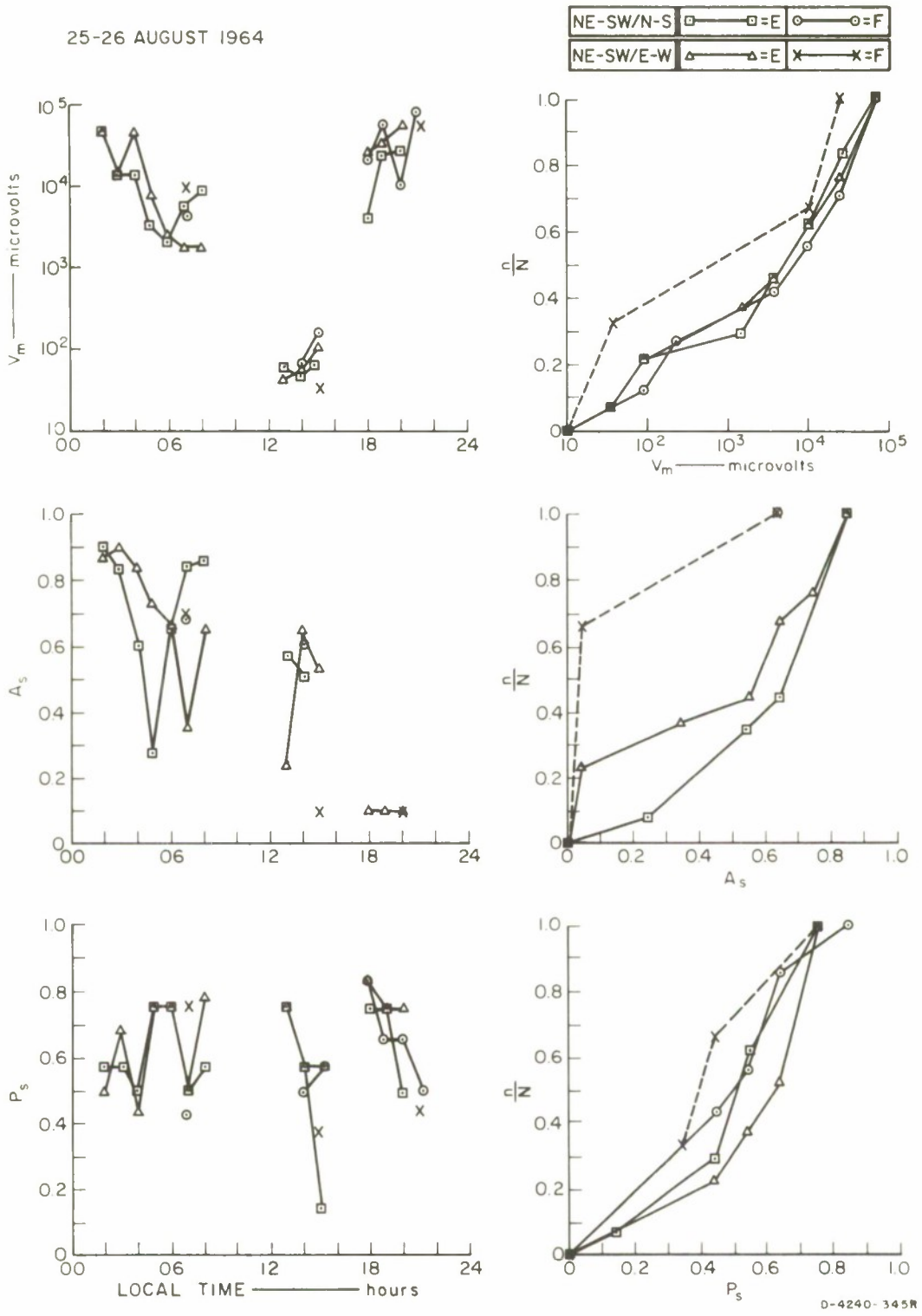

FIG. 115 3.4-MHz PULSE DATA, CHOLBURI/SATTAHIP CIRCUIT: NE-SW TRANSMITTING, 43 km

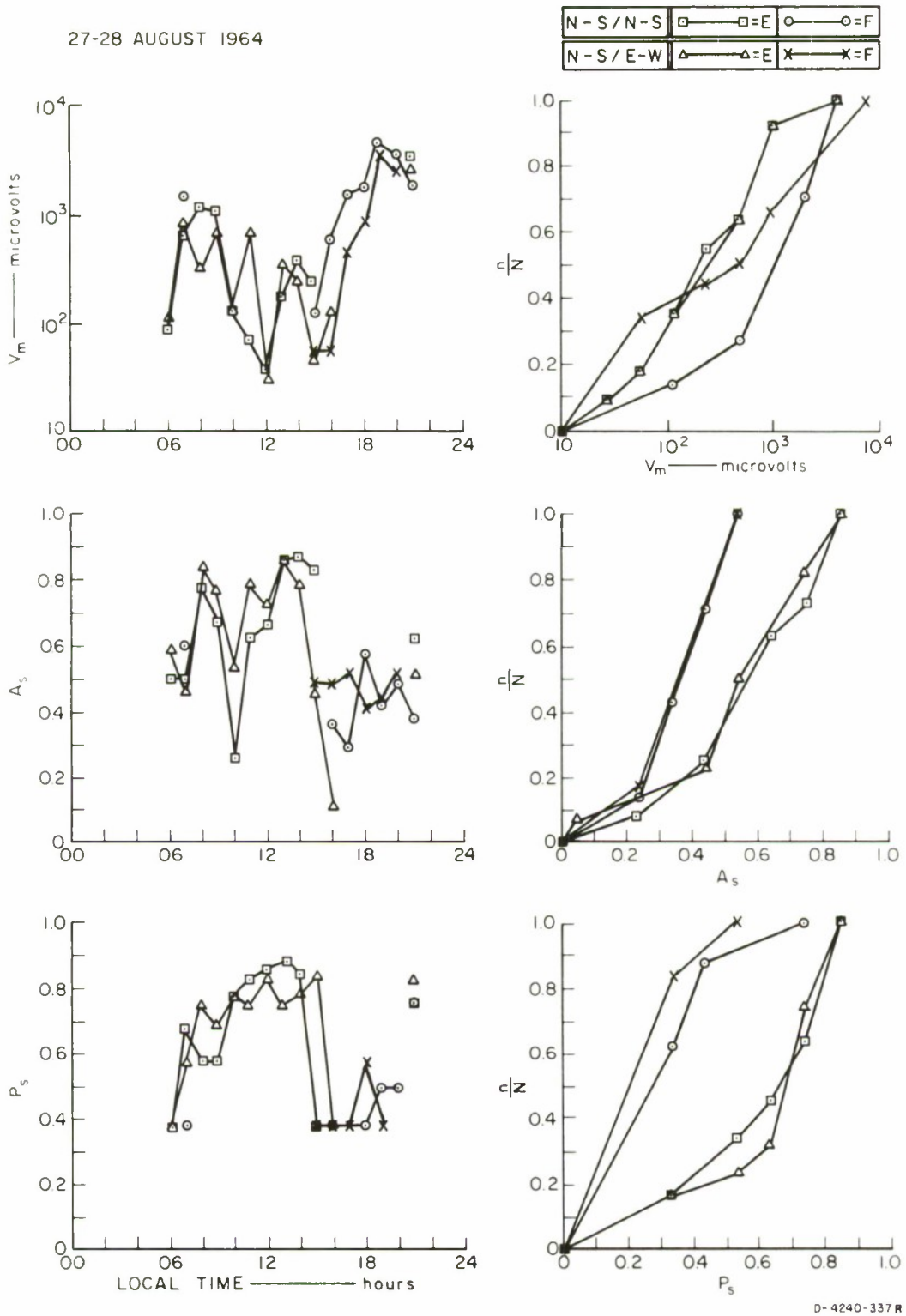

FIG. 116 3.4-MHz PULSE DATA, CHOLBURI/SATTAHIP CIRCUIT: N-S TRANSMITTING, 63 km

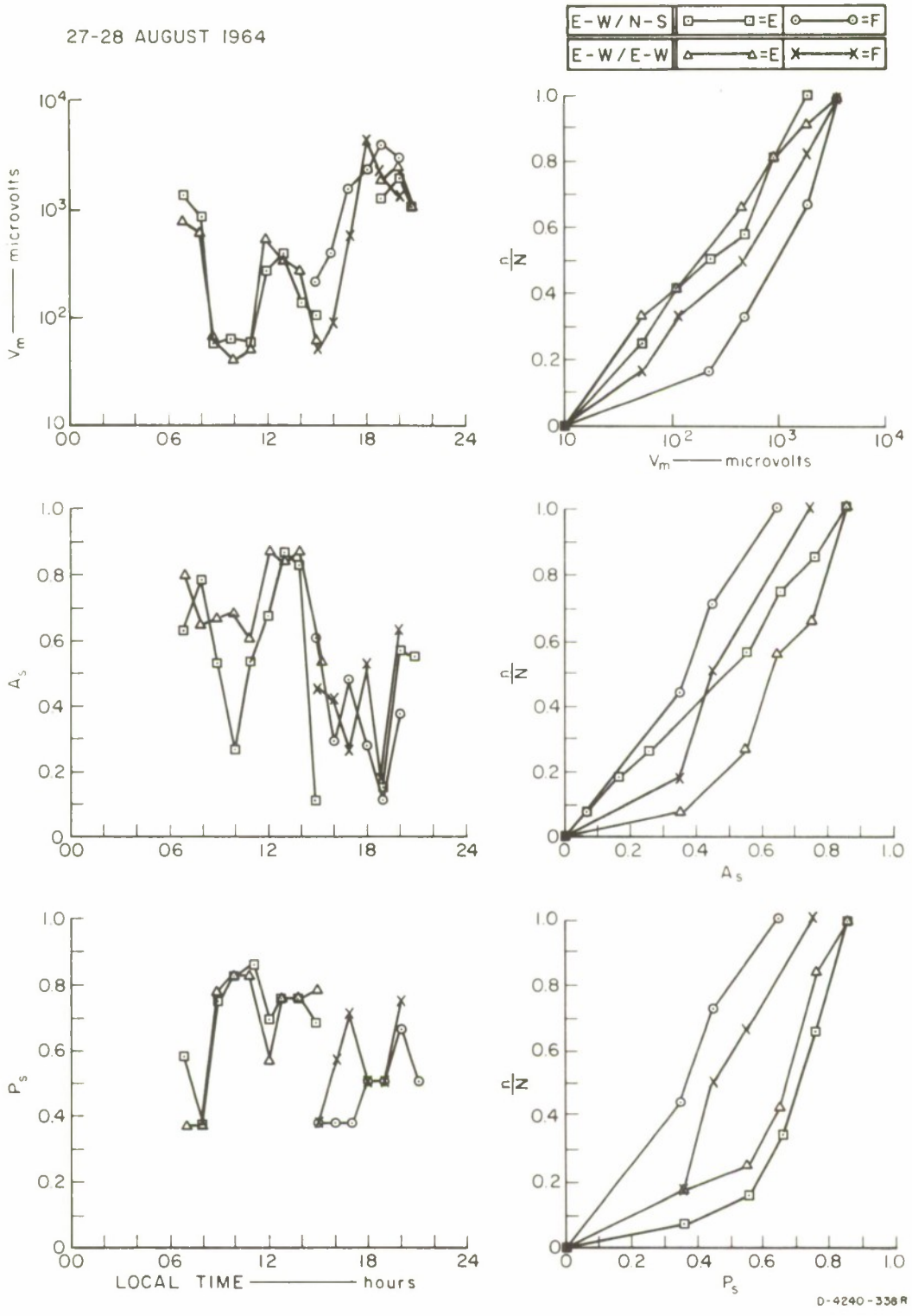

FIG. 117 3.4-MHz PULSE DATA, CHOLBURI/SATTAHIP CIRCUIT: E-W TRANSMITTING, 63 km

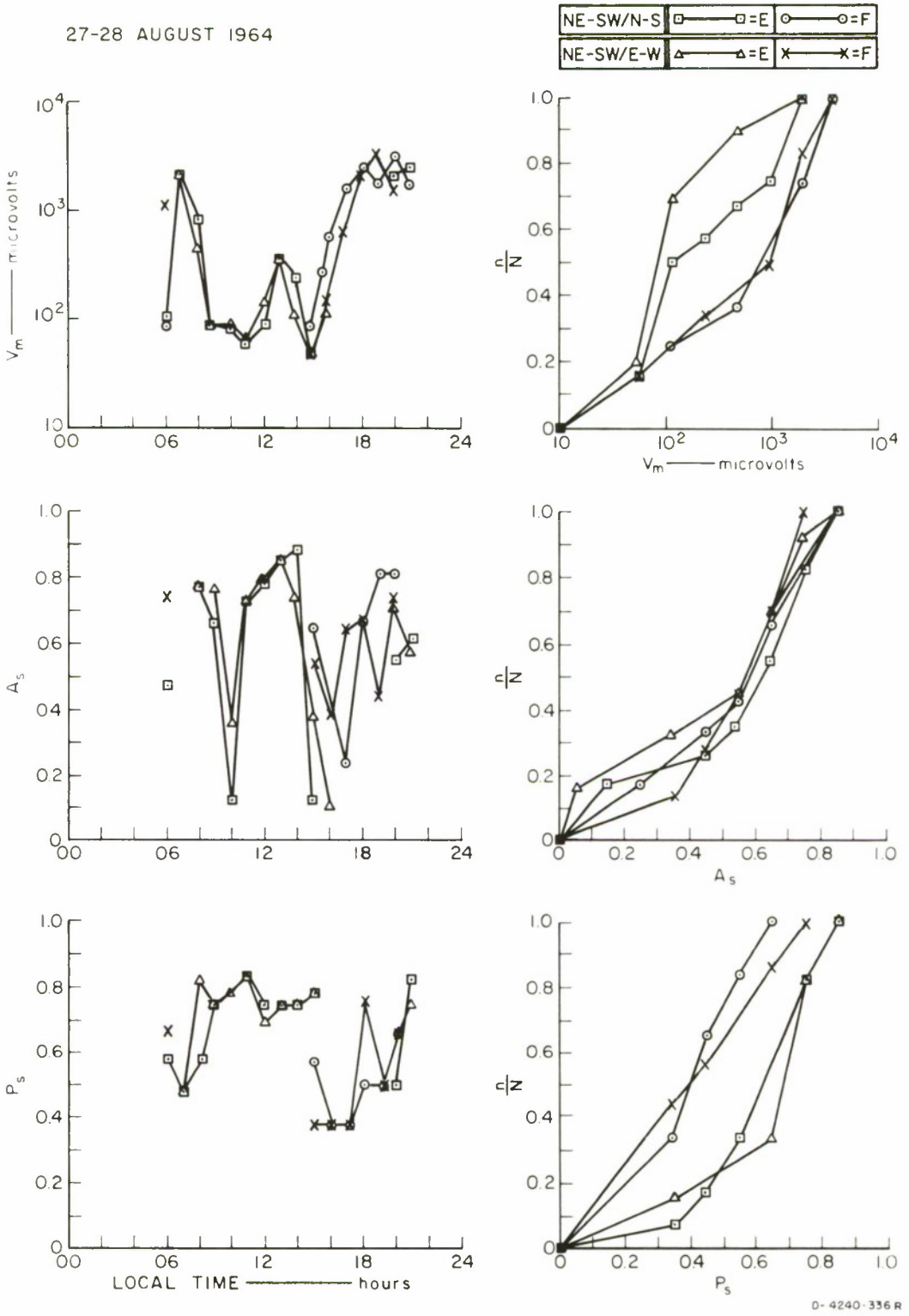

FIG. 118 3.4-MHz PULSE DATA, CHOLBURI/SATTAHIP CIRCUIT: NE–SW TRANSMITTING, 63 km

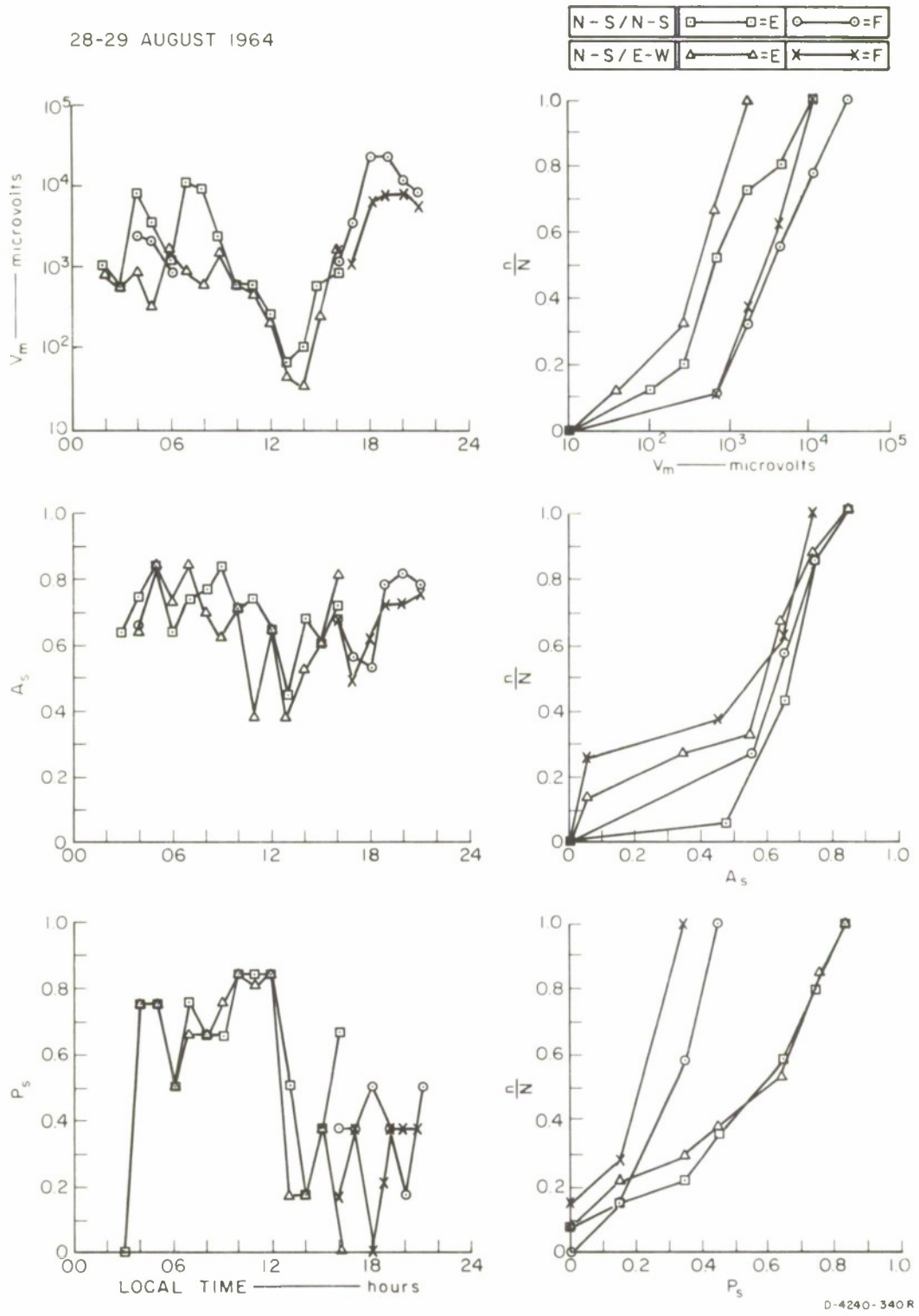

FIG. 119 3.4-MHz PULSE DATA, CHOLBURI/SATTAHIP CIRCUIT: N-S TRANSMITTING, 83 km

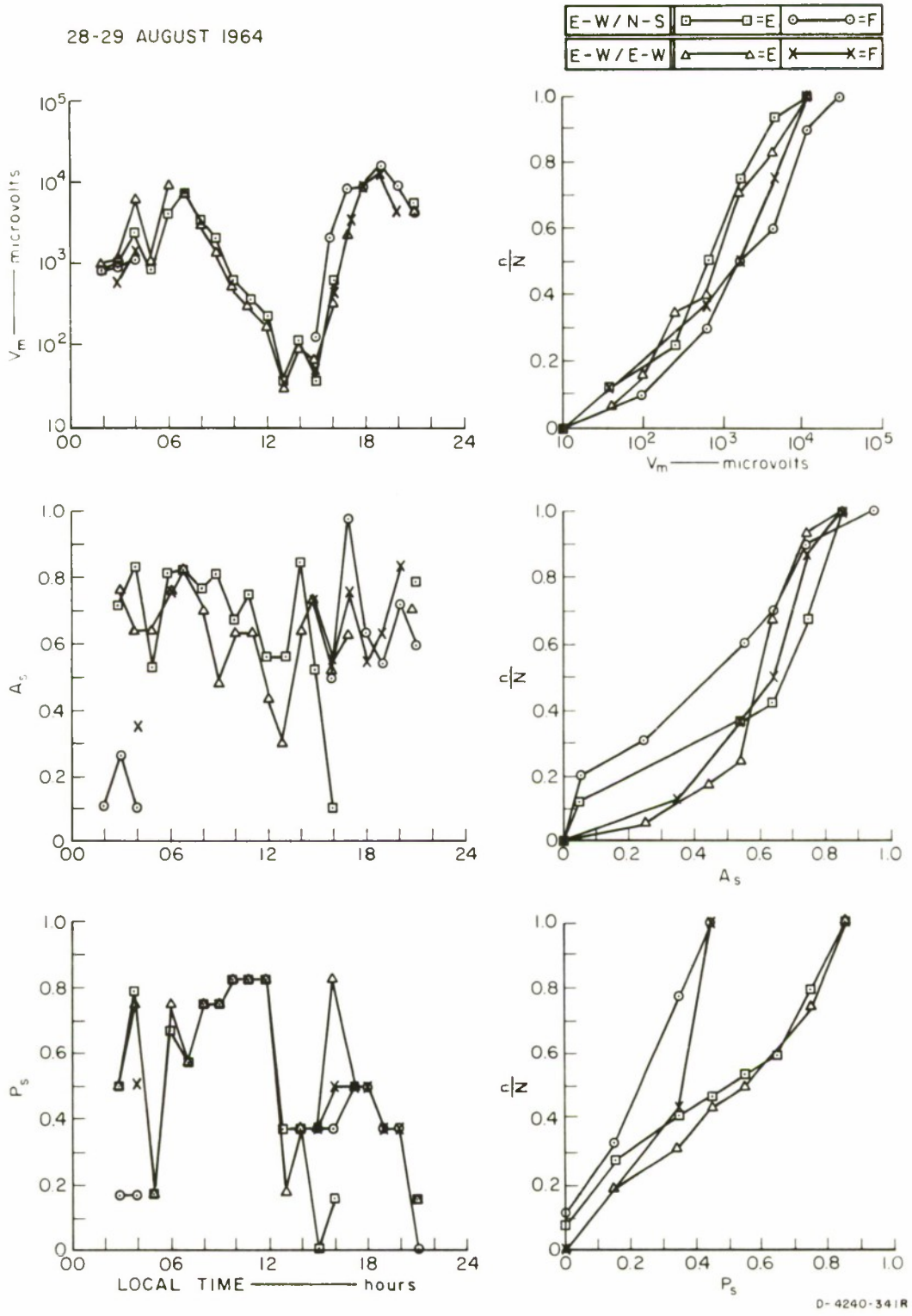

FIG. 120 3.4-MHz PULSE DATA, CHOLBURI/SATTAHIP CIRCUIT: E-W TRANSMITTING, 83 km

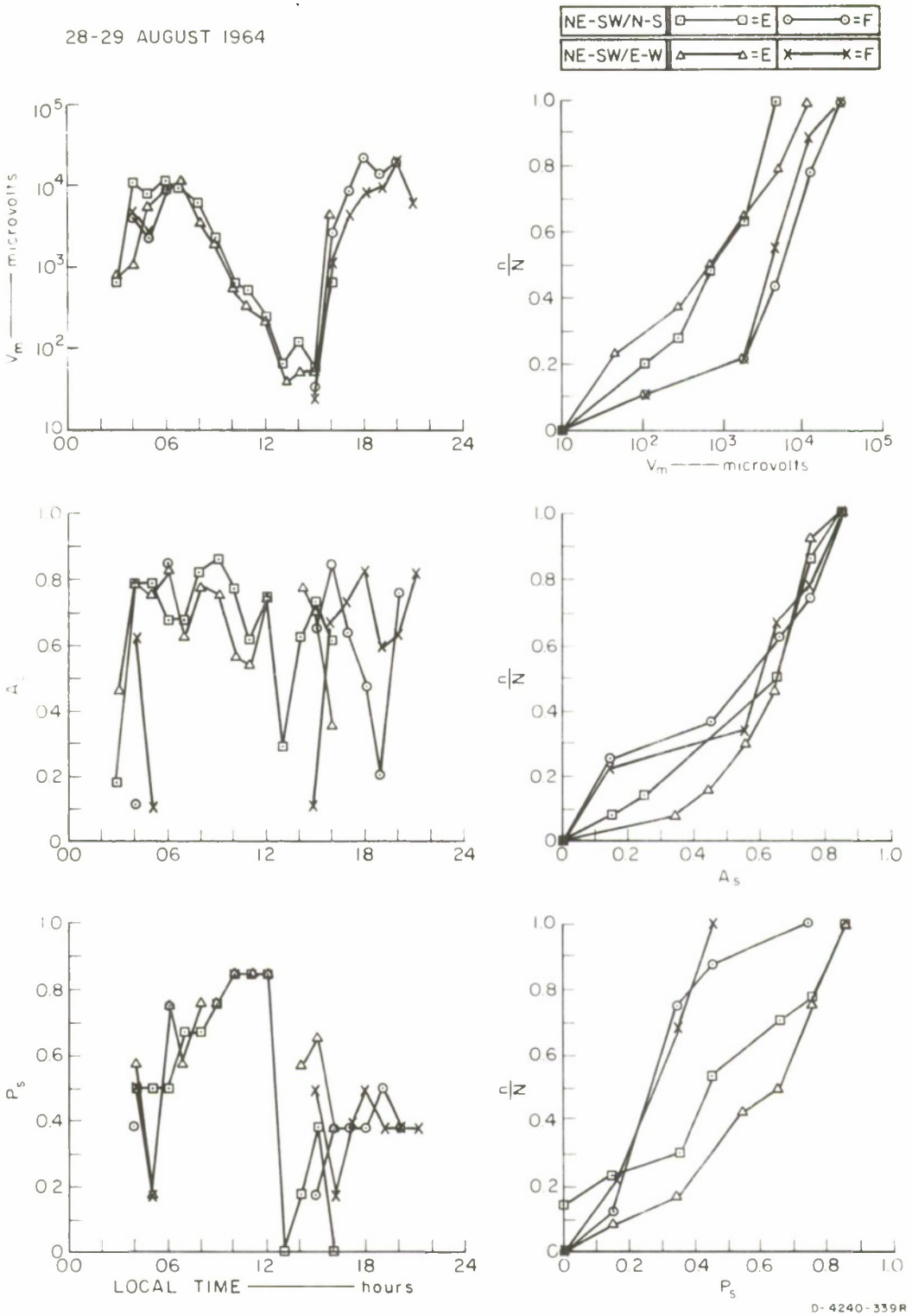

FIG. 121 3.4-MHz PULSE DATA, CHOLBURI/SATTAHIP CIRCUIT: NE-SW TRANSMITTING, 83 km

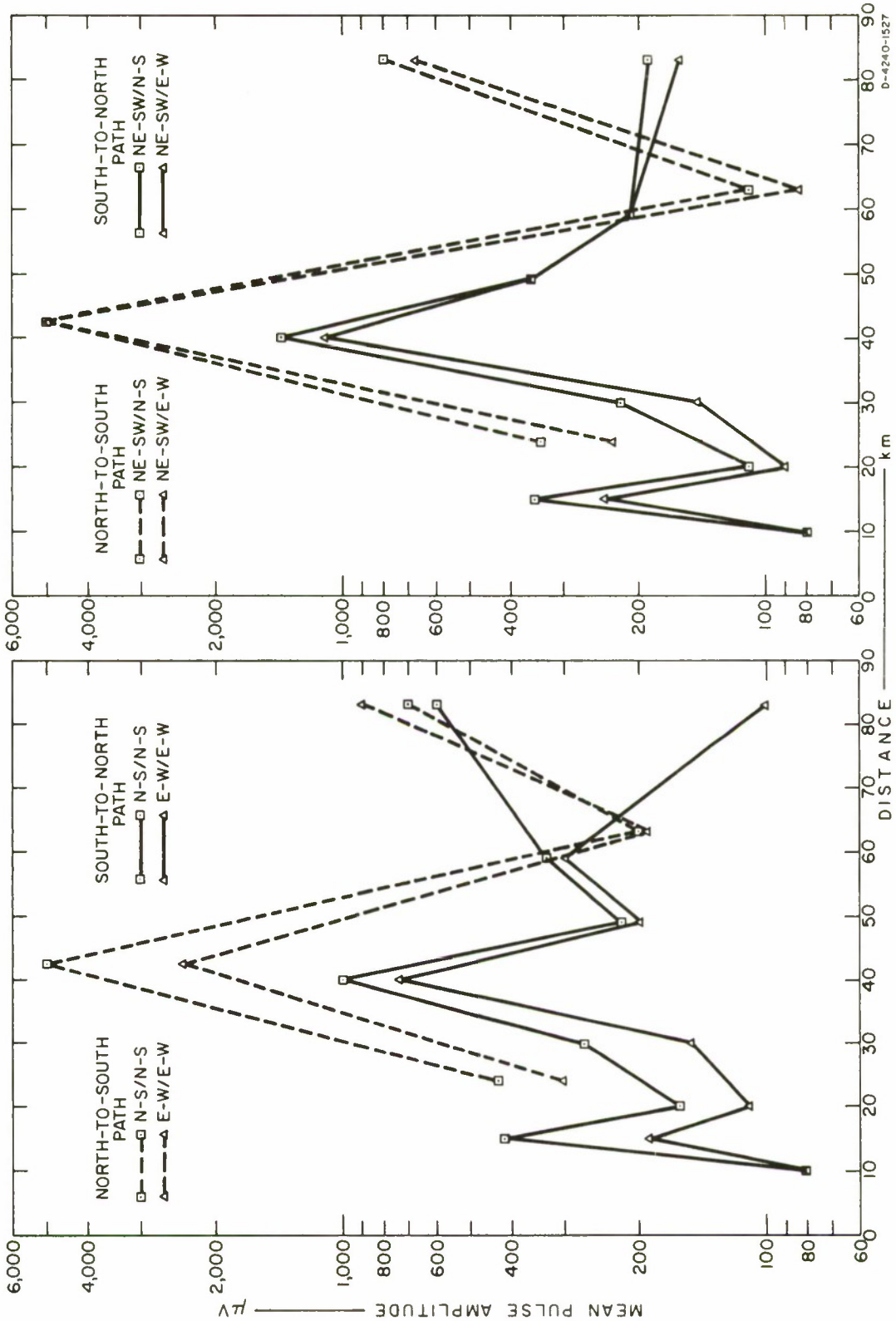

FIG. 122 MEAN PULSE AMPLITUDE AS A FUNCTION OF DISTANCE: CHOLBURI/SATTAHIP, 3.4 MHz

The behavior on the whole supports the findings in the S-to-N test: the diurnal variation, the QT region, the stability of the mode of propagation, the superiority of the ordinary wave and the possibility of improving the HF short-range propagation by an orientation diversity system. The ionospheric f plots are given in Fig. 123 separately for reference purposes for the Sattahip/Cholburi and for the Kao Pongrang/Krabinburi test periods. The 3.4 MHz was well below the foF2 during the daytime and part of the nighttime. The pulse stretching of the S-to-N propagation (Figs. 79 through 102), as well as the pulse stretching of the N-to-S propagation (Figs. 110 through 121), were relatively high during the day and low during the night, thus seemingly excluding the suggestion of the ground backscatter mechanism responsible for the 3-MHz nighttime propagation (cf. Sec. III-C-1-a).

2. Kao Pongrang/Krabinburi 3.4-MHz Pulse Test

It was found during preliminary tests and the actual tests carried out from 7 July 1964 through 20 August 1964 that tests at 3.4 MHz produced the greatest amount of information. A survey of the pulse test so conducted indicated that further study on the QT range was warranted, in a different direction of propagation, as was study of the possibility of an orientation diversity system. The Kao Pongrang/Krabinburi path was chosen for this study, since it runs approximately in a S 60^{o} E direction and the NE-SW antenna, which transmits both the ordinary and the extraordinary waves equally well and would give practically no preference to the N-S or the E-W receiving antenna as far as the broadside beaming is concerned (see the pattern effects in Fig. 19). Data reduction was carried out in the same manner previously made for the 3.4-MHz pulse test over the Sattahip/Cholburi circuit. Diurnal variations of the average pulse amplitude and of the pulse stability together with the cumulative distribution n/N plots were obtained and are shown in Figs. 124 through 138. Measurements were carried out "around-the-clock." The overall picture is that the test over this circuit supported the Sattahip/Cholburi test in most respects.

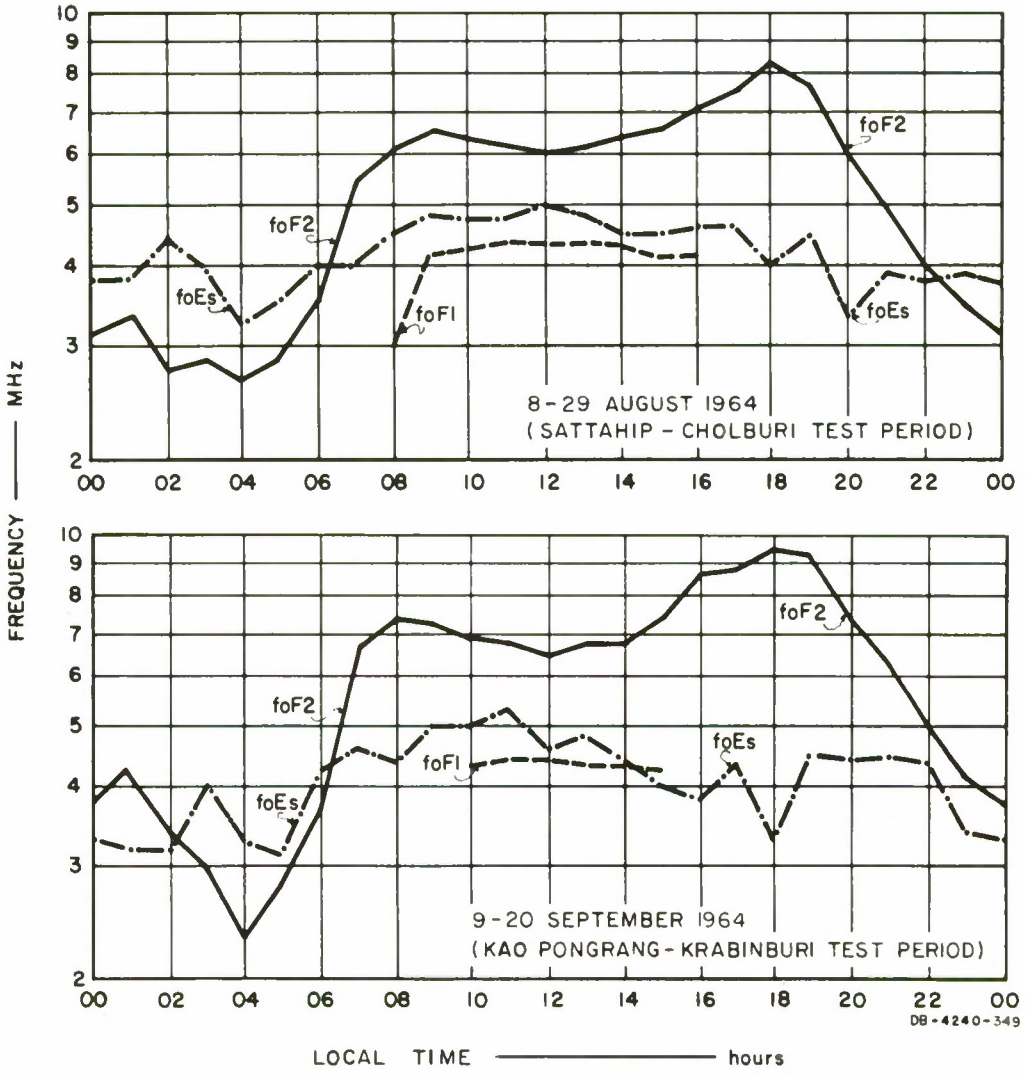

FIG. 123 f PLOT OF IONOSPHERIC VERTICAL SOUNDING OVER BANGKOK: PULSE TEST PERIODS

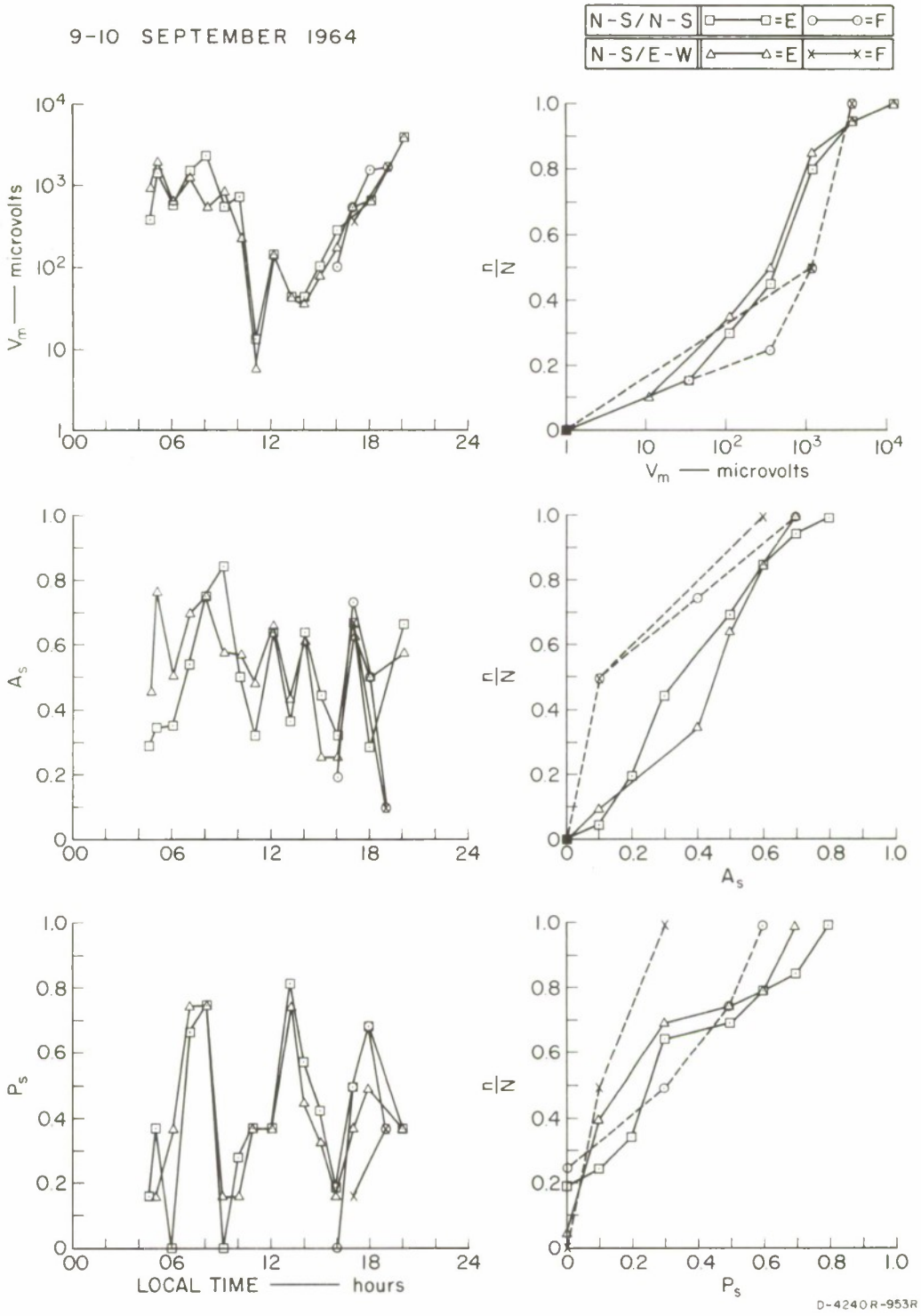

FIG. 124 3.4-MHz PULSE DATA, KAO PONGRANG/KRABINBURI CIRCUIT: N-S TRANSMITTING, 26 km

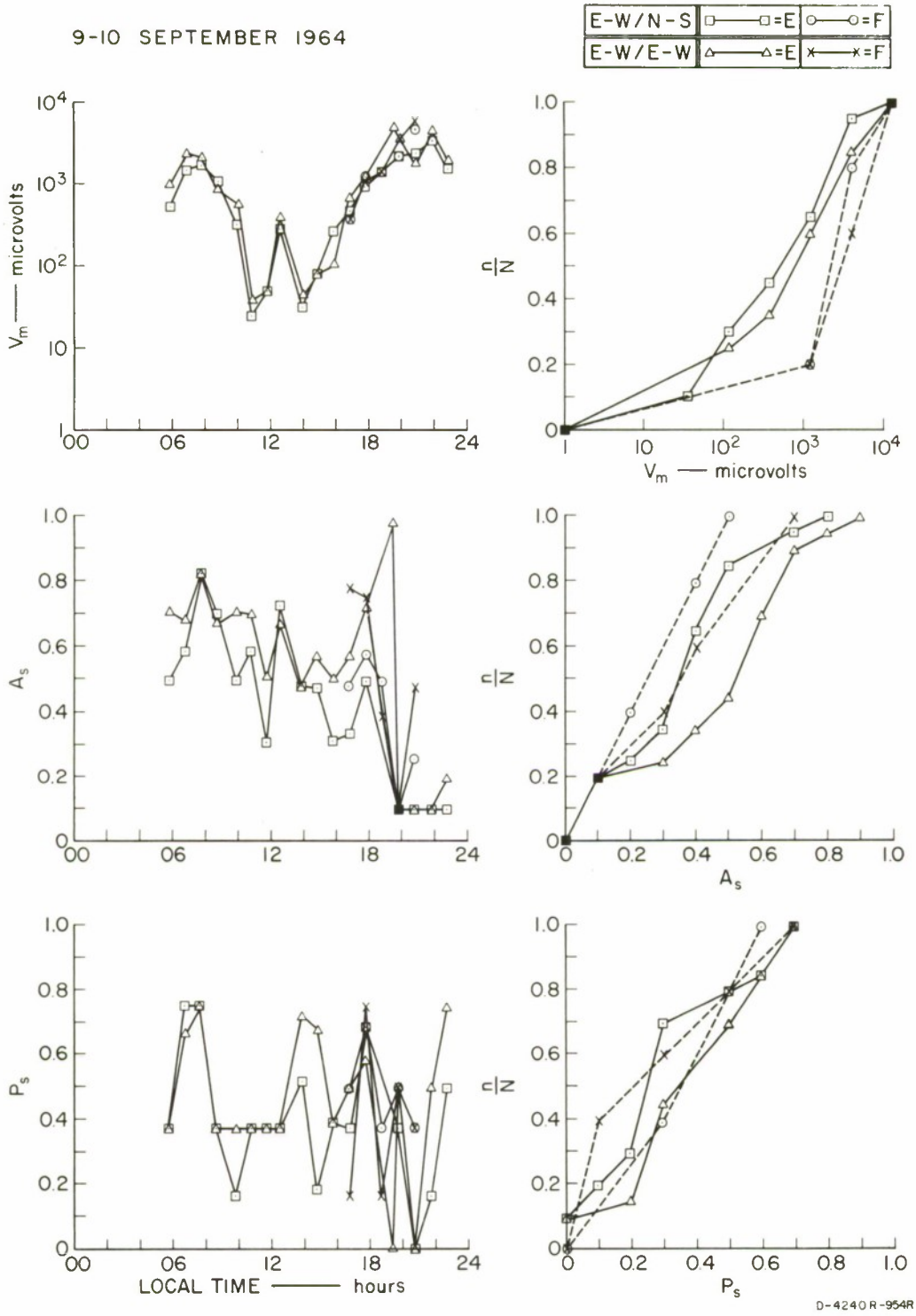

FIG. 125 3.4-MHz PULSE DATA, KAO PONGRANG/KRABINBURI CIRCUIT: E-W TRANSMITTING, 26 km

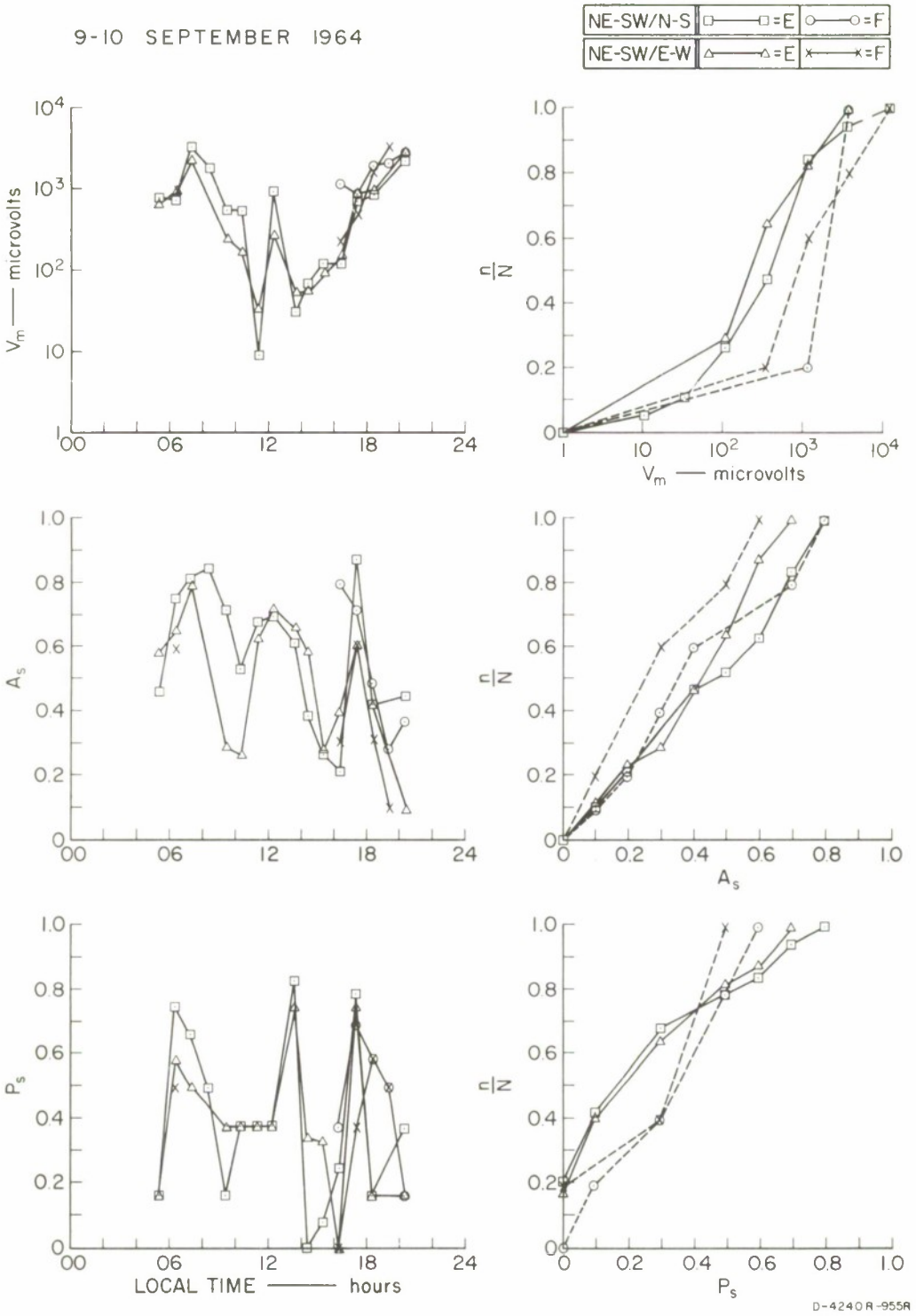

FIG. 126 3.4-MHz PULSE DATA, KAO PONGRANG/KRABINBU'RI CIRCUIT: NE-SW TRANSMITTING, 26 km

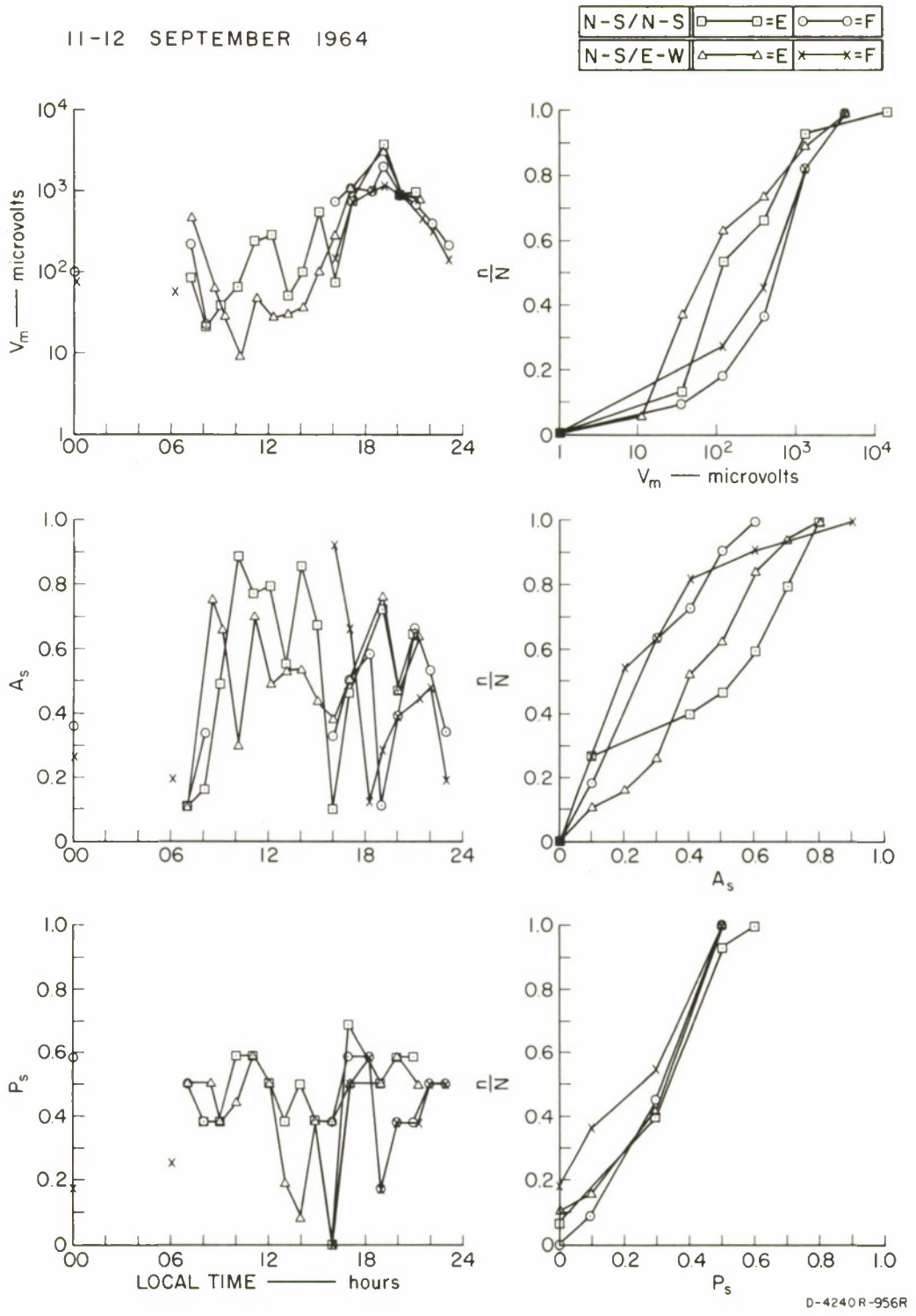

FIG. 127 3.4-MHz PULSE DATA, KAO PONGRANG/KRABINBURI CIRCUIT: N-S TRANSMITTING, 45 km

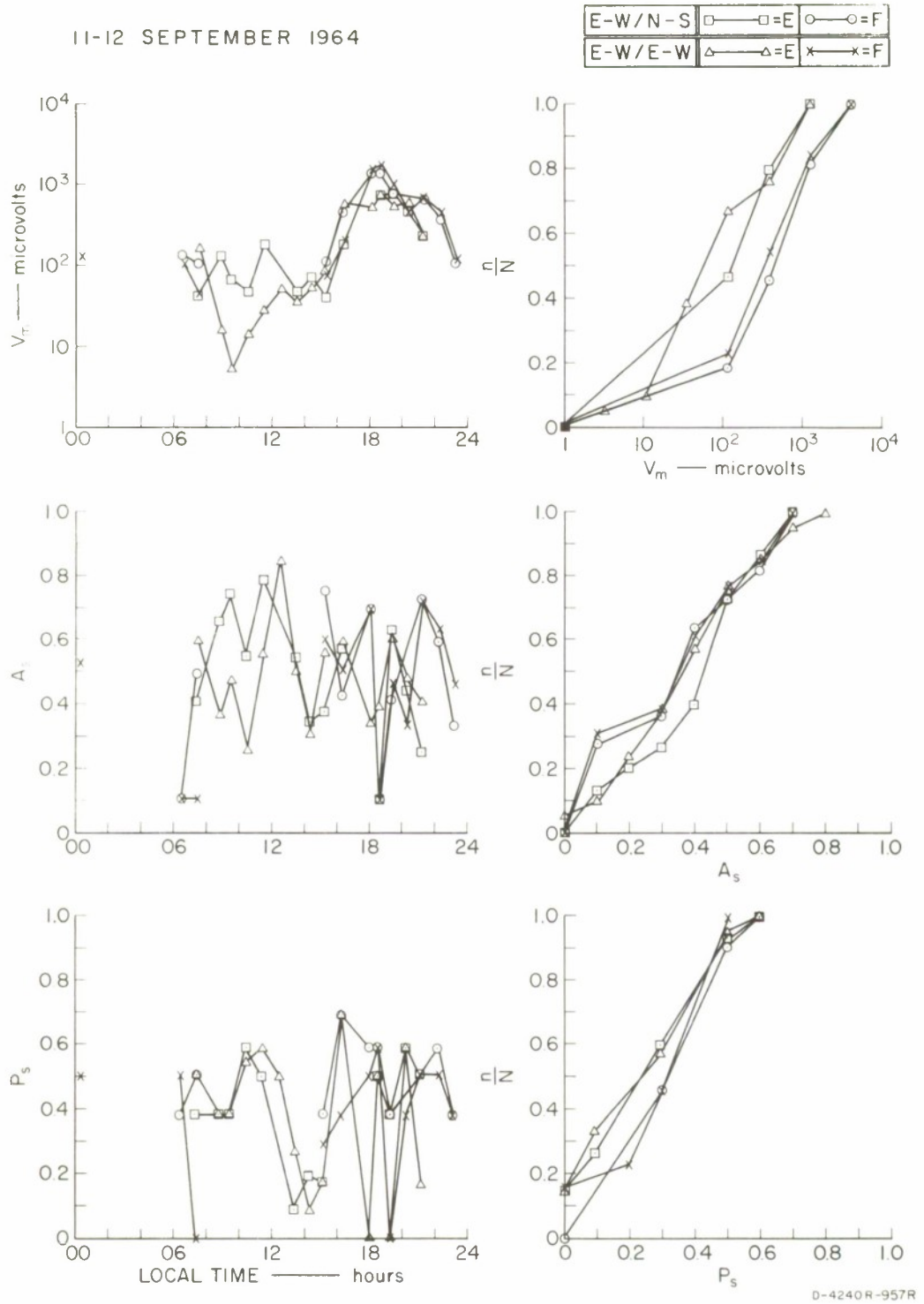

FIG. 128 3.4-MHz PULSE DATA, KAO PONGRANG/KRABINBURI CIRCUIT: E-W TRANSMITTING, 45 km

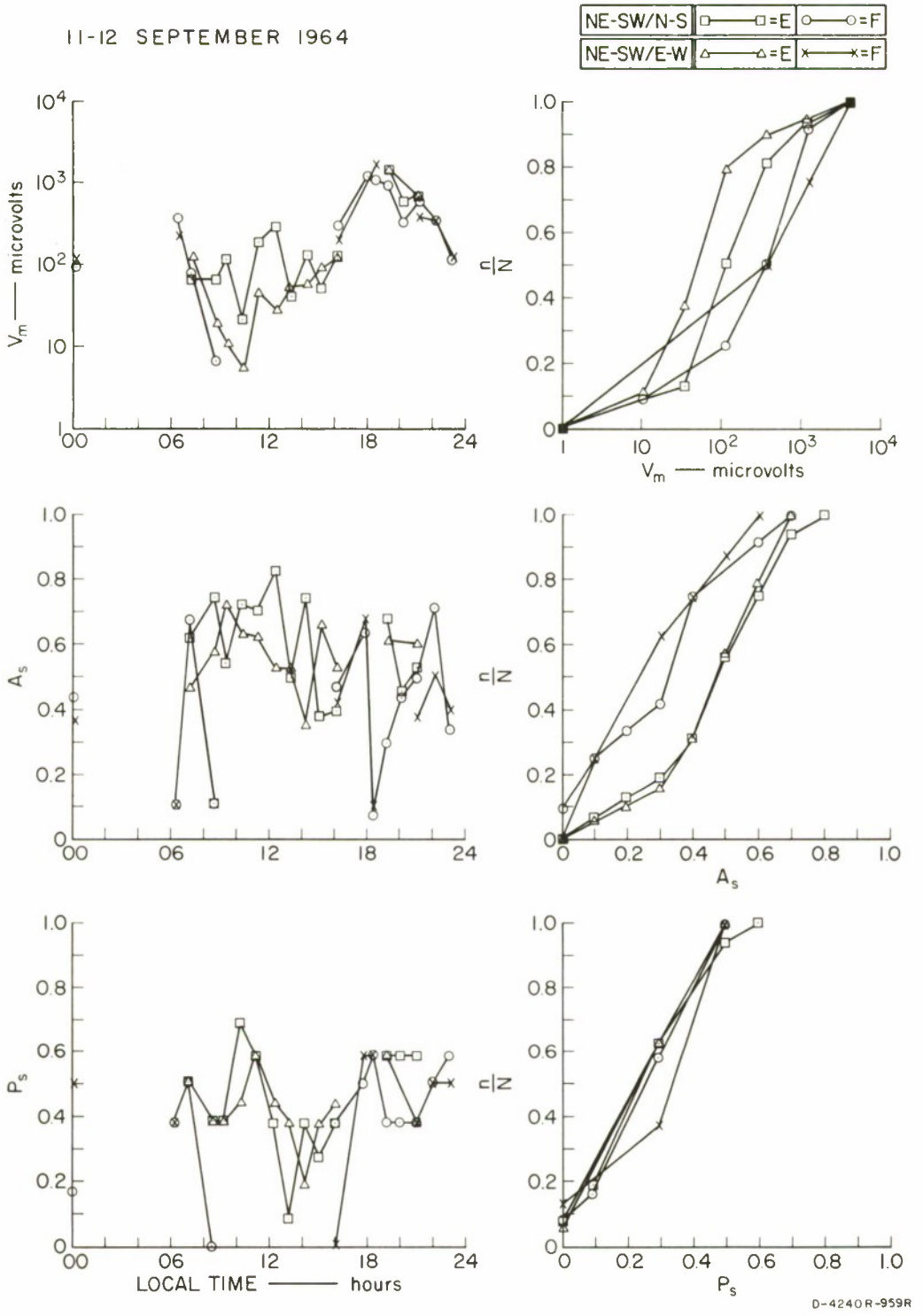

FIG. 129 3.4-MHz PULSE DATA, KAO PONGRANG/KRABINBURI CIRCUIT: NE-SW TRANSMITTING, 45 km

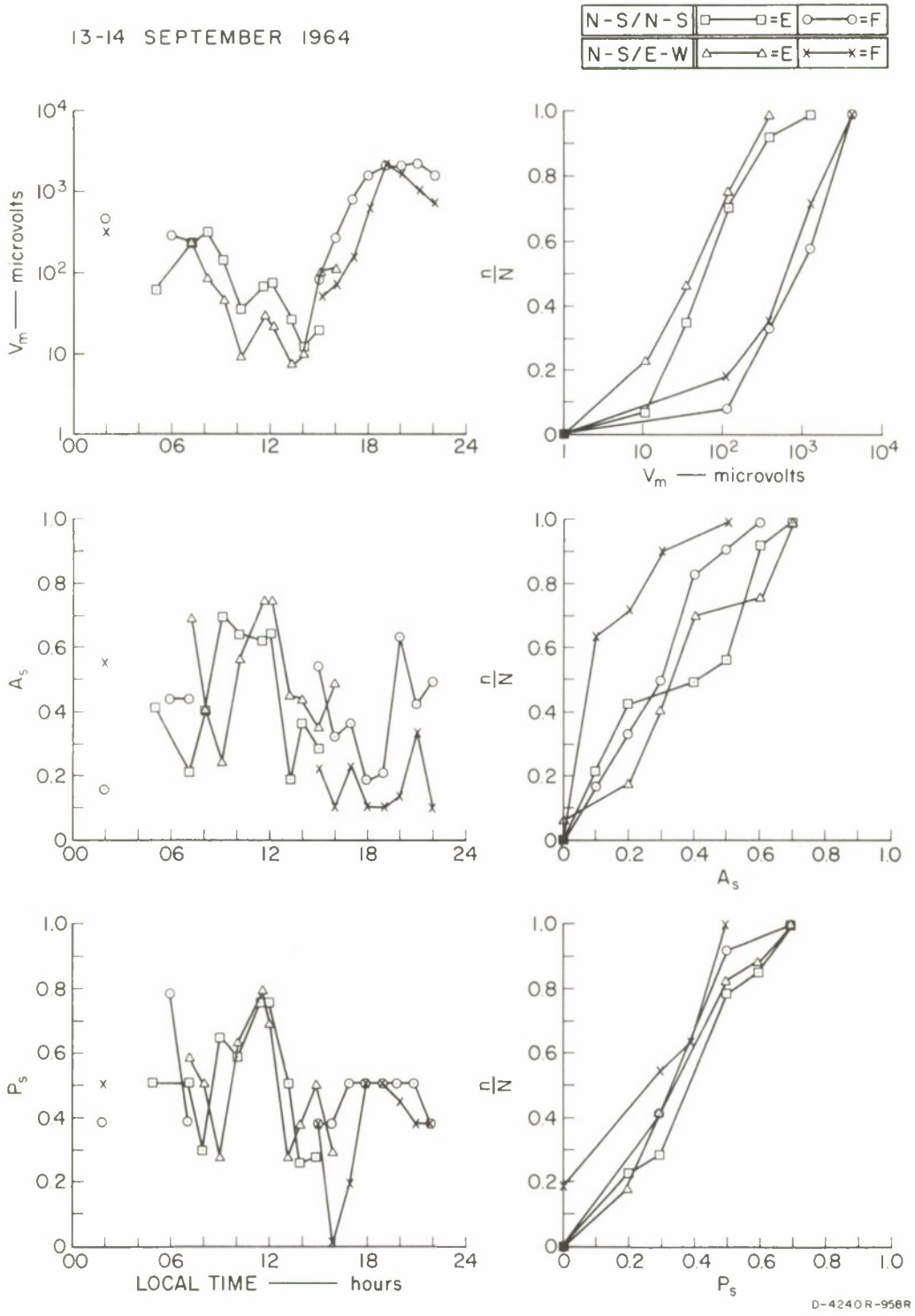

FIG. 130 3.4-MHz PULSE DATA, KAO PONGRANG/KRABINBURI CIRCUIT: N-S TRANSMITTING, 59 km

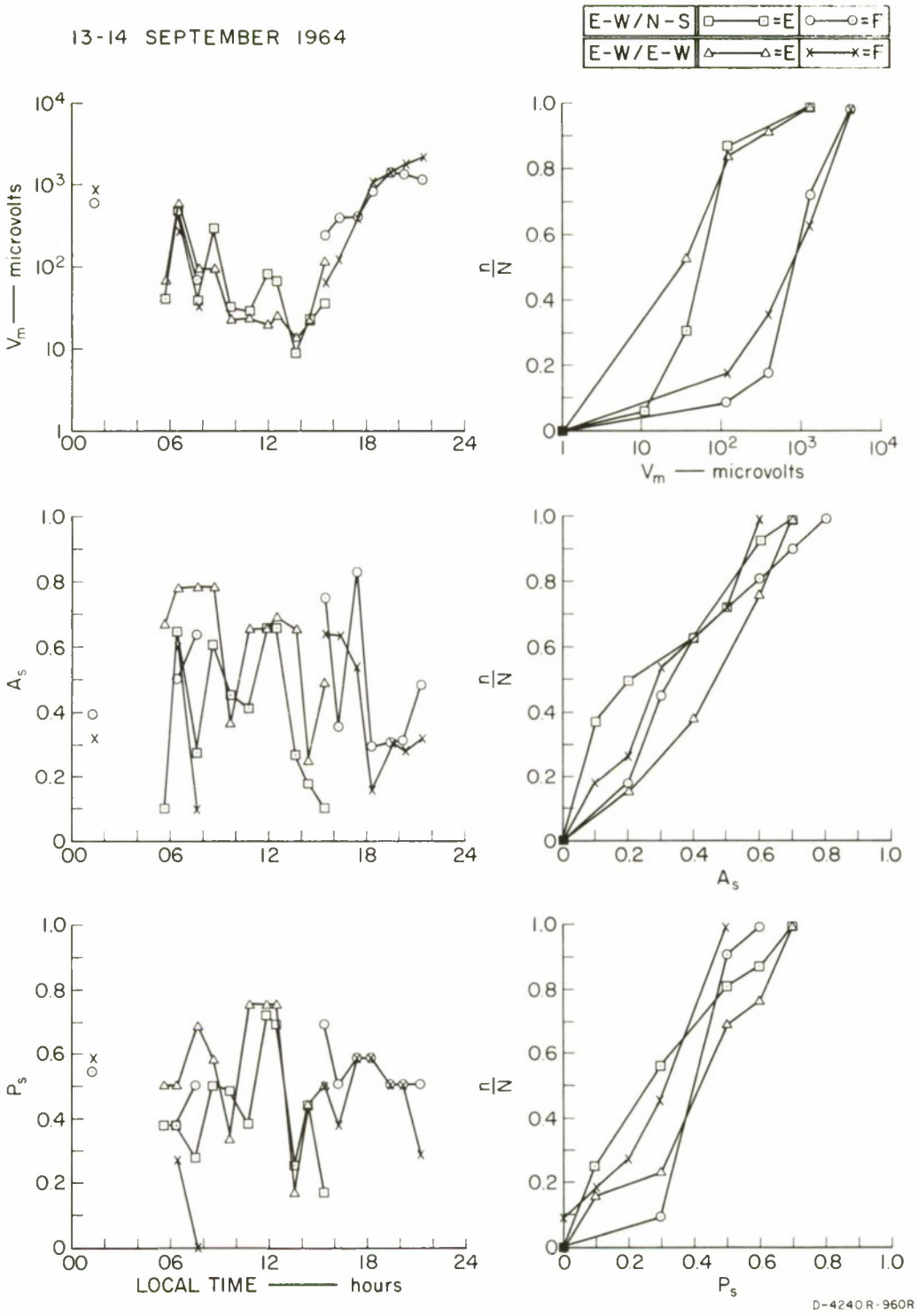

FIG. 131 3.4-MHz PULSE DATA, KAO PONGRANG/KRABINBURI CIRCUIT: E-W TRANSMITTING, 59 km

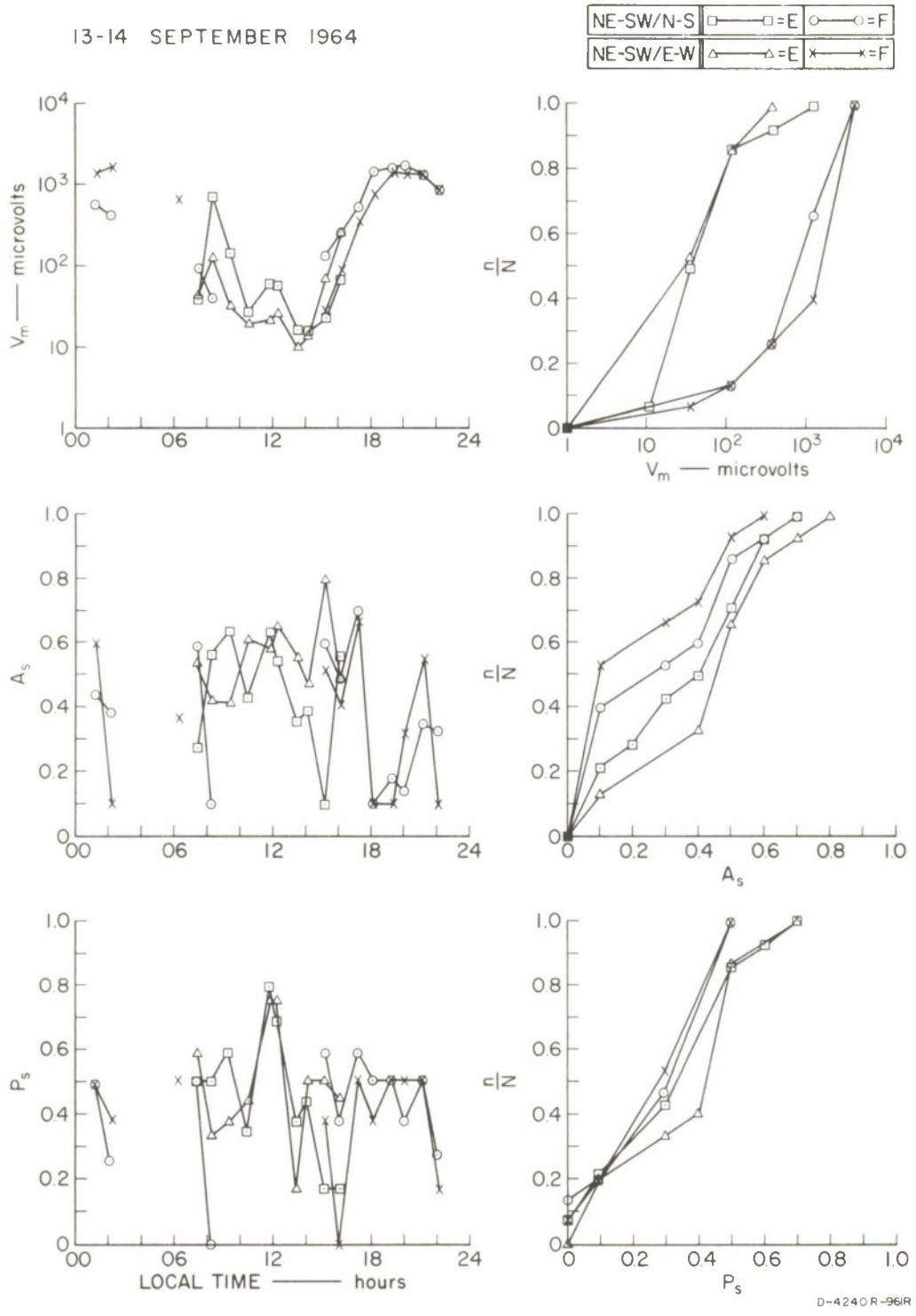

FIG. 132 3.4-MHz PULSE DATA, KAO PONGRANG/KRABINBURI CIRCUIT: NE-SW TRANSMITTING, 59 km

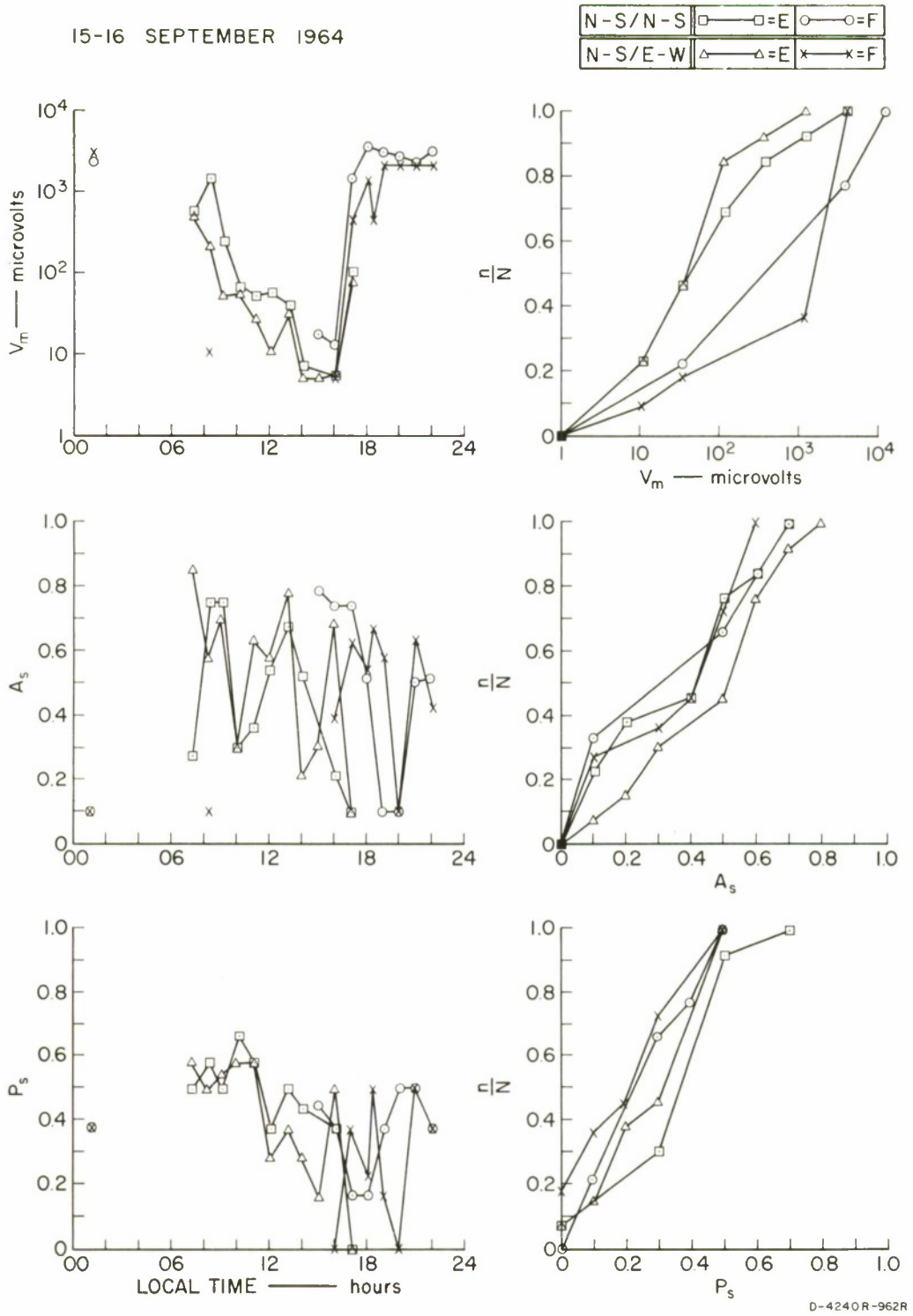

FIG. 133 3.4-MHz PULSE DATA, KAO PONGRANG/KRABINBURI CIRCUIT: N-S TRANSMITTING, 76 km

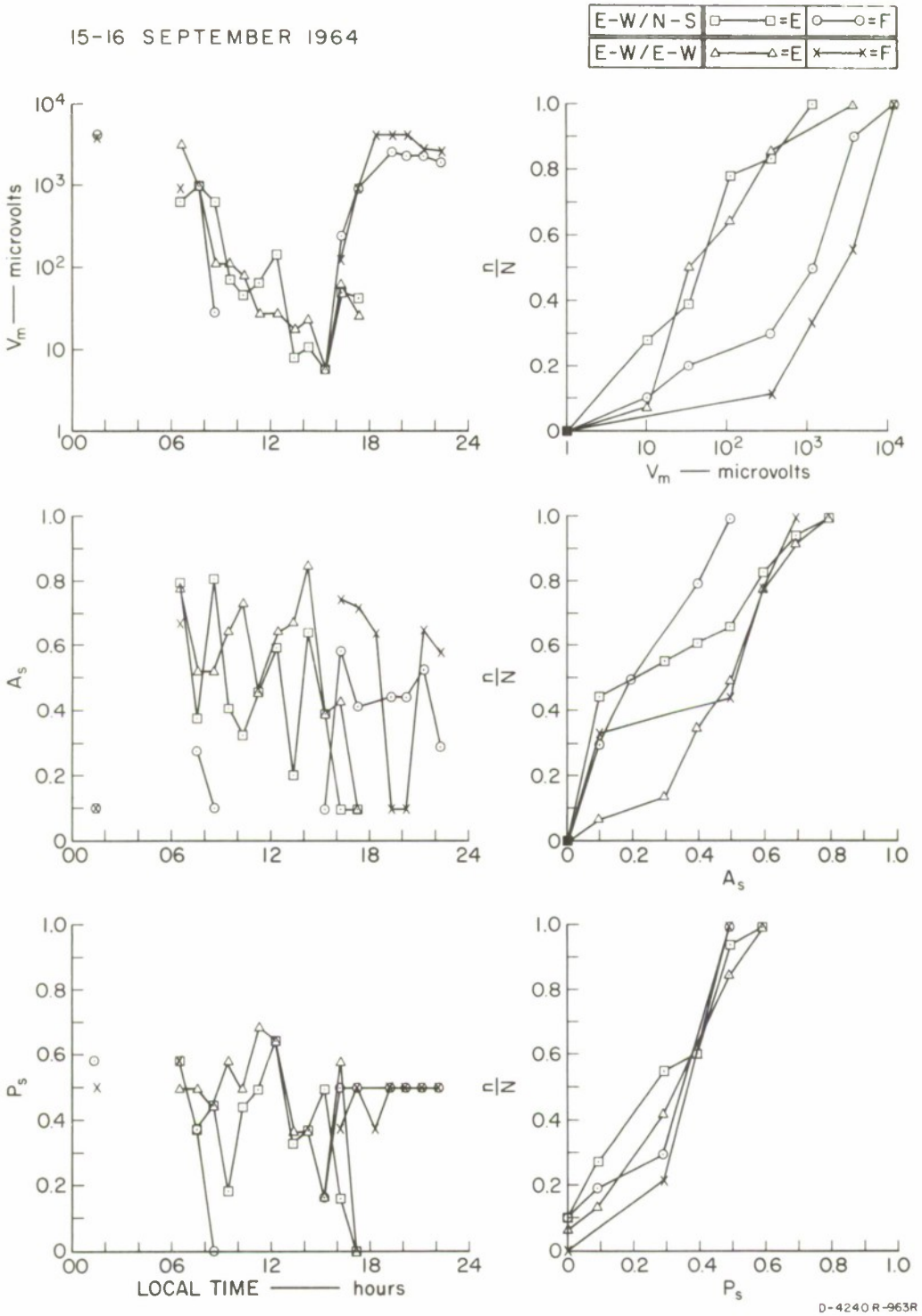

FIG. 134 3.4-MHz PULSE DATA, KAO PONGRANG/KRABINBURI CIRCUIT: E-W TRANSMITTING, 76 km

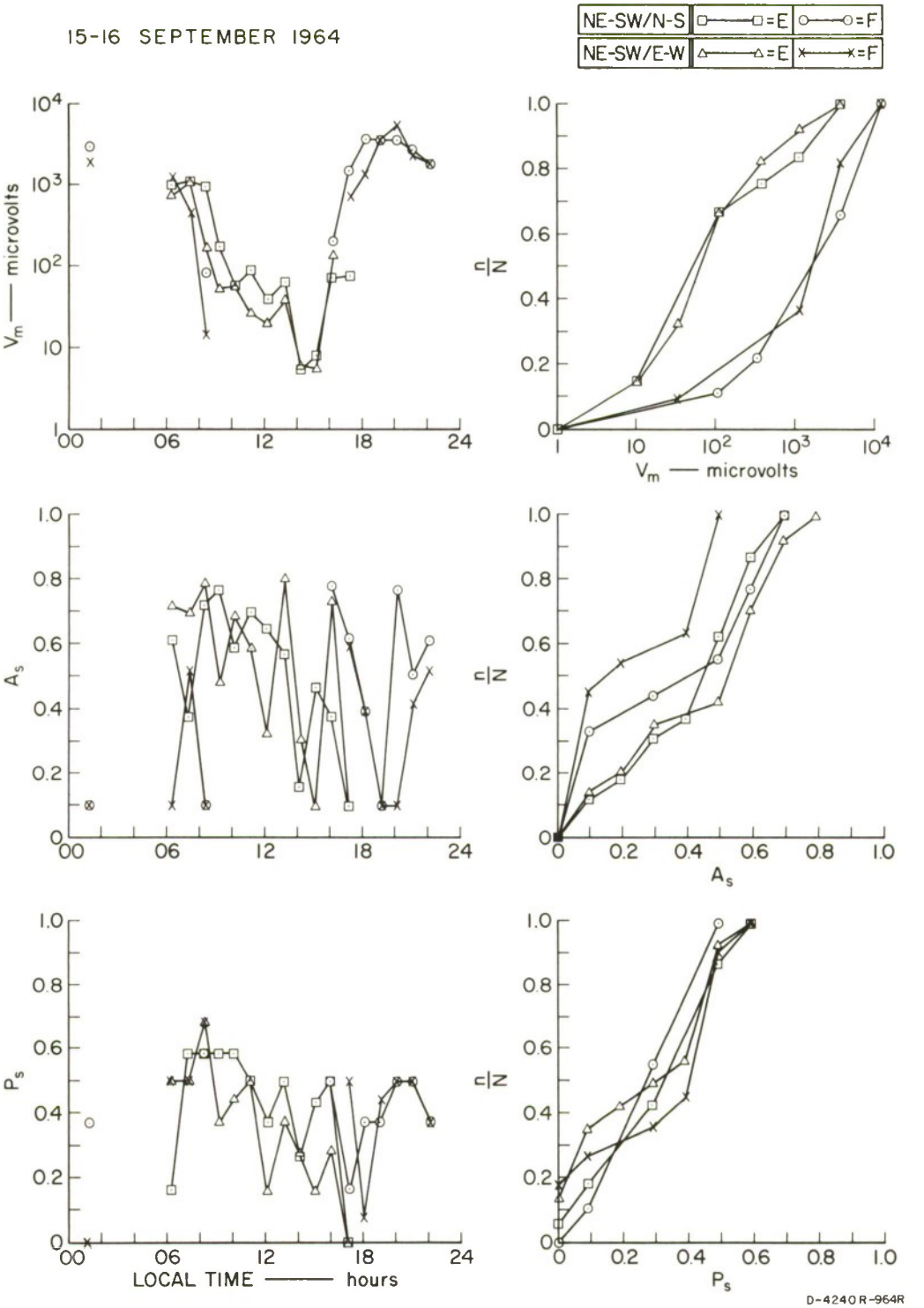

FIG. 135 3.4-MHz PULSE DATA, KAO PONGRANG/KRABINBURI CIRCUIT: NE-SW TRANSMITTING, 76 km

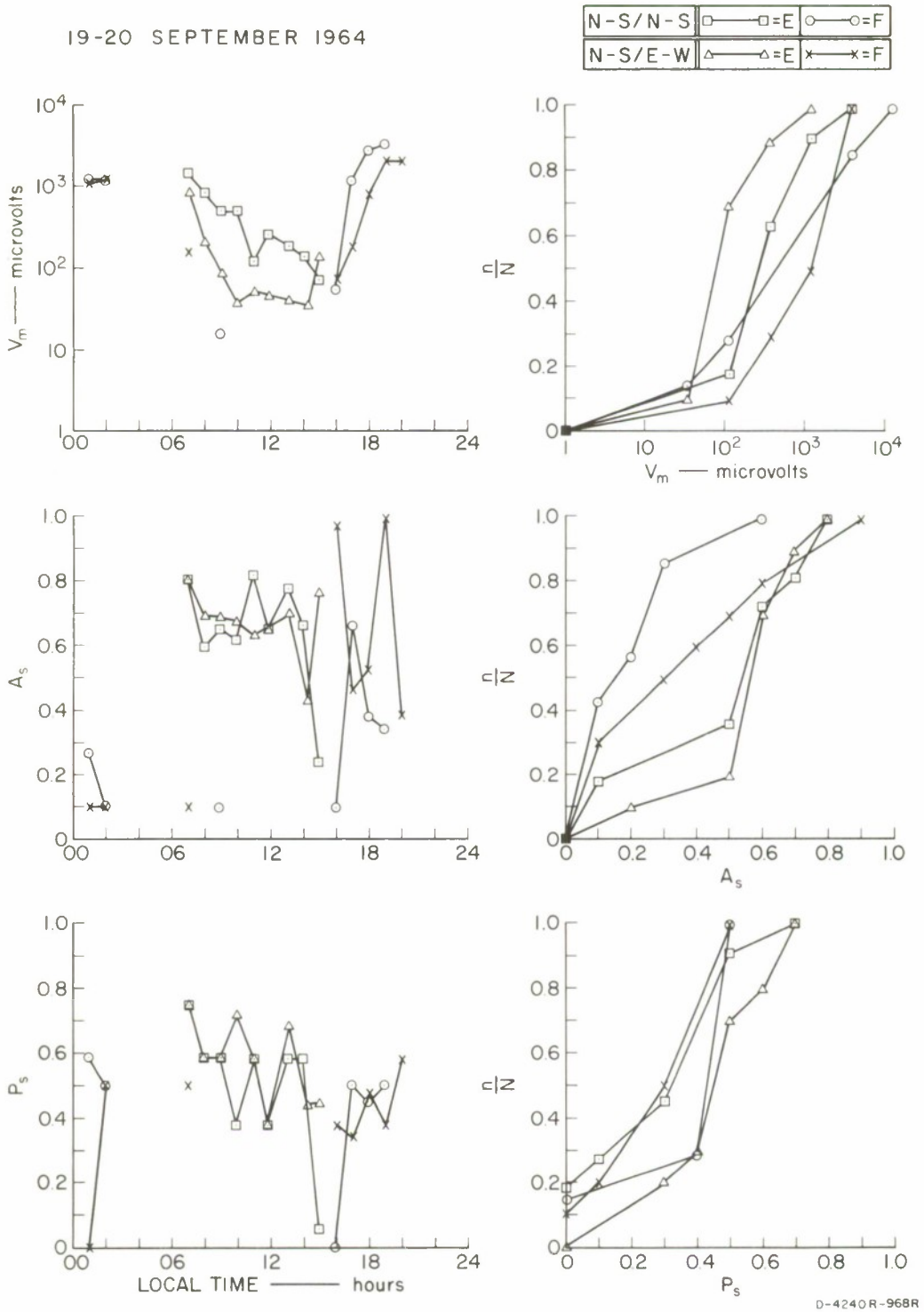

FIG. 136 3.4-MHz PULSE DATA, KAO PONGRANG/KRABINBURI CIRCUIT: N-S TRANSMITTING, 109 km

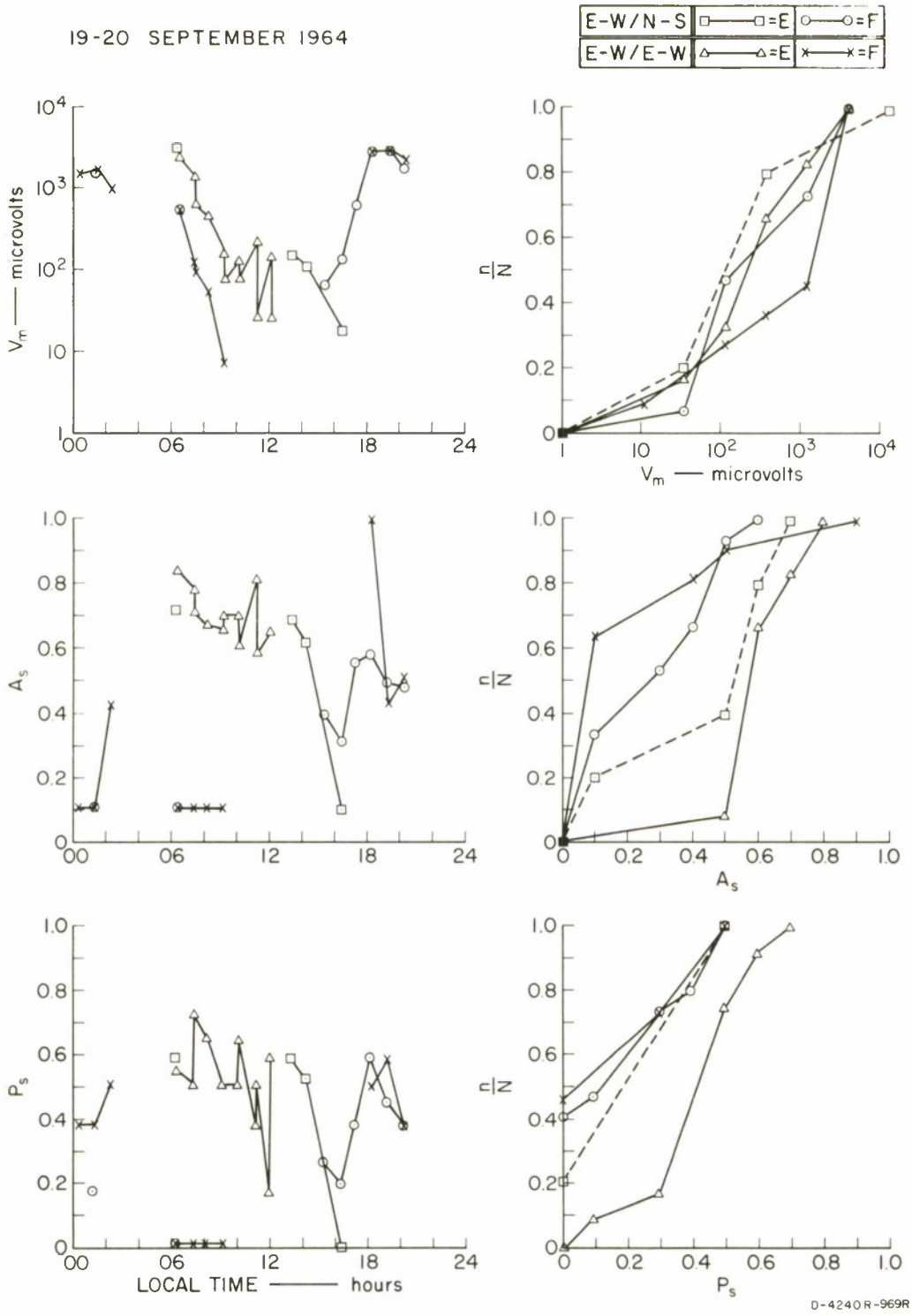

FIG. 137 3.4-MHz PULSE DATA, KAO PONGRANG/KRABINBURI CIRCUIT: E-W TRANSMITTING, 109 km

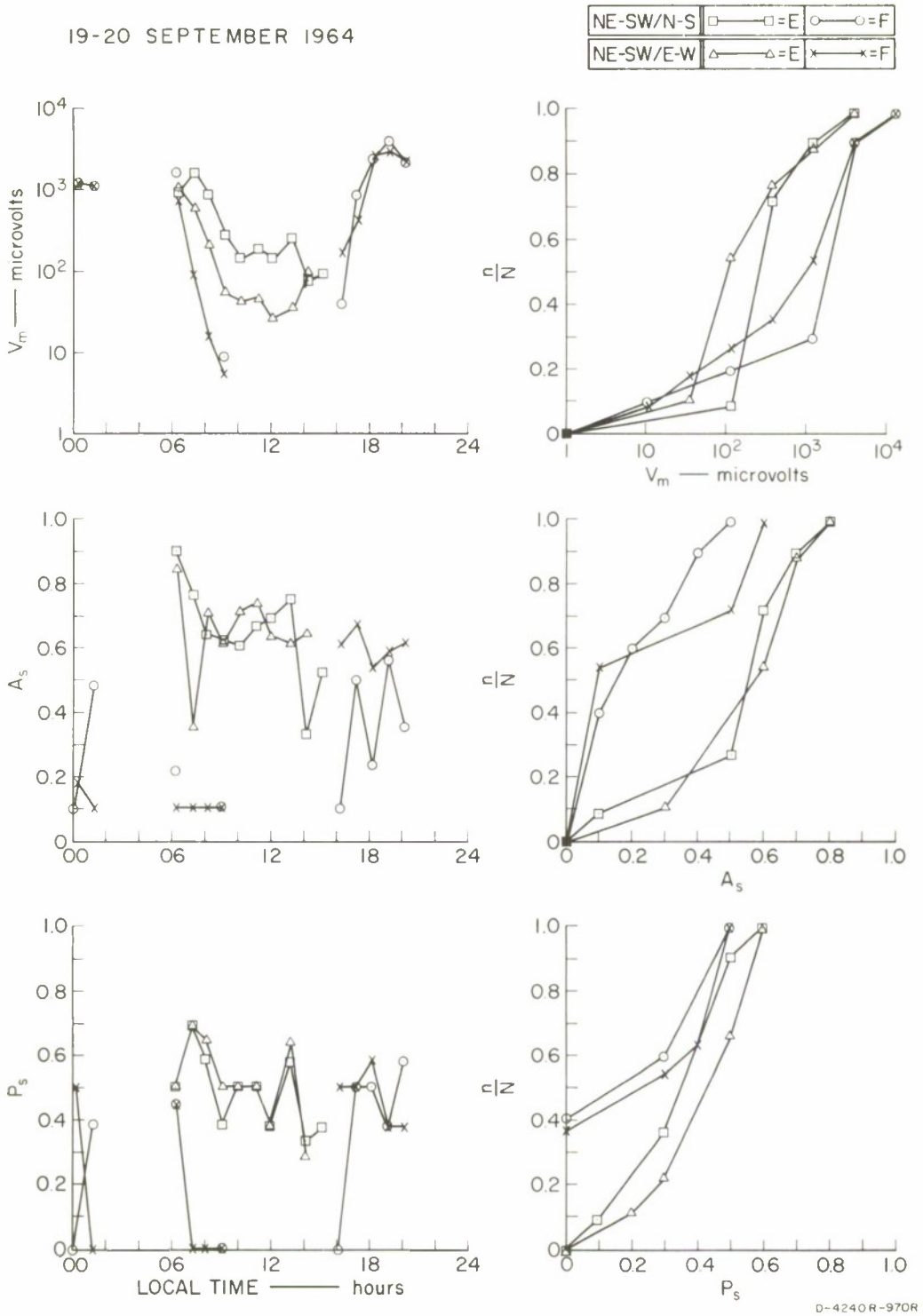

FIG. 138 3.4-MHz PULSE DATA, KAO PONGRANG/KRABINBURI CIRCUIT: NE-SW TRANSMITTING, 109 km

a. Diurnal Variation of Pulse Amplitudes

The V_m curves of all distances as shown in Figs. 124 through 138 were superimposed. Figure 139 shows the N-S/N-S and E-W/E-W antenna combinations; Fig. 140 shows the NE-SW/N-S and NE-SW/E-W combinations. The agreement of Fig. 140 with Figs. 45 and 48 of the 3-MHz CW test was very close; the second peak observed at sunset in the CW test can be seen to be supported by the F layer. This clearly shows the advantage of the pulse test over the CW test: the ability to identify modes. The F layer was seen to support the wave propagation from 1600 until about 0200. The sporadic-E layer supported propagation from 0600 till 2100.

b. Mean Pulse Amplitude versus Distance: QT Range

Mean pulse amplitudes corresponding to n/N = 0.5 in Figs. 124 through 138 were plotted against ground distances between the transmitting and receiving sites. The results are shown in Fig. 141 for the N-S/N-S, N-S/E-W, E-W/E-W and the NE-SW/N-S, NE-SW/E-W transmitting/receiving antenna combinations, and for the sporadic-E layer supporting the propagation as well as for the F layer. With Es layer supporting, the ordinary wave performed better than the extraordinary wave throughout the range under study. The signal strength of both waves decreased with an increasing distance, as expected, but was observed to rise rather steeply from the distance upward of 80 km to a high value at 110 km, which was unfortunately as far as the test team could go without undue hazard in logistic support. The rise in signal amplitudes indicated that the propagation via the E region satisfied the QT condition and the theoretical QT range of a 3-MHz wave over this path via the E region may be obtained from Table II or Fig. 15 as 70-135 km. The theoretical QT range of a 3-MHz wave over this same path but via the F layer (as obtained from Table II or Fig. 16) is 120-235 km; hence, the wave propagation via the F layer should not satisfy the QT condition. This statement is confirmed by the test results, which showed random fluctuation of signal strength and even the superiority of the extraordinary wave over the ordinary wave at some distances. The results strongly indicate the advisability of using orientation diversity reception with the N-S antenna transmitting,

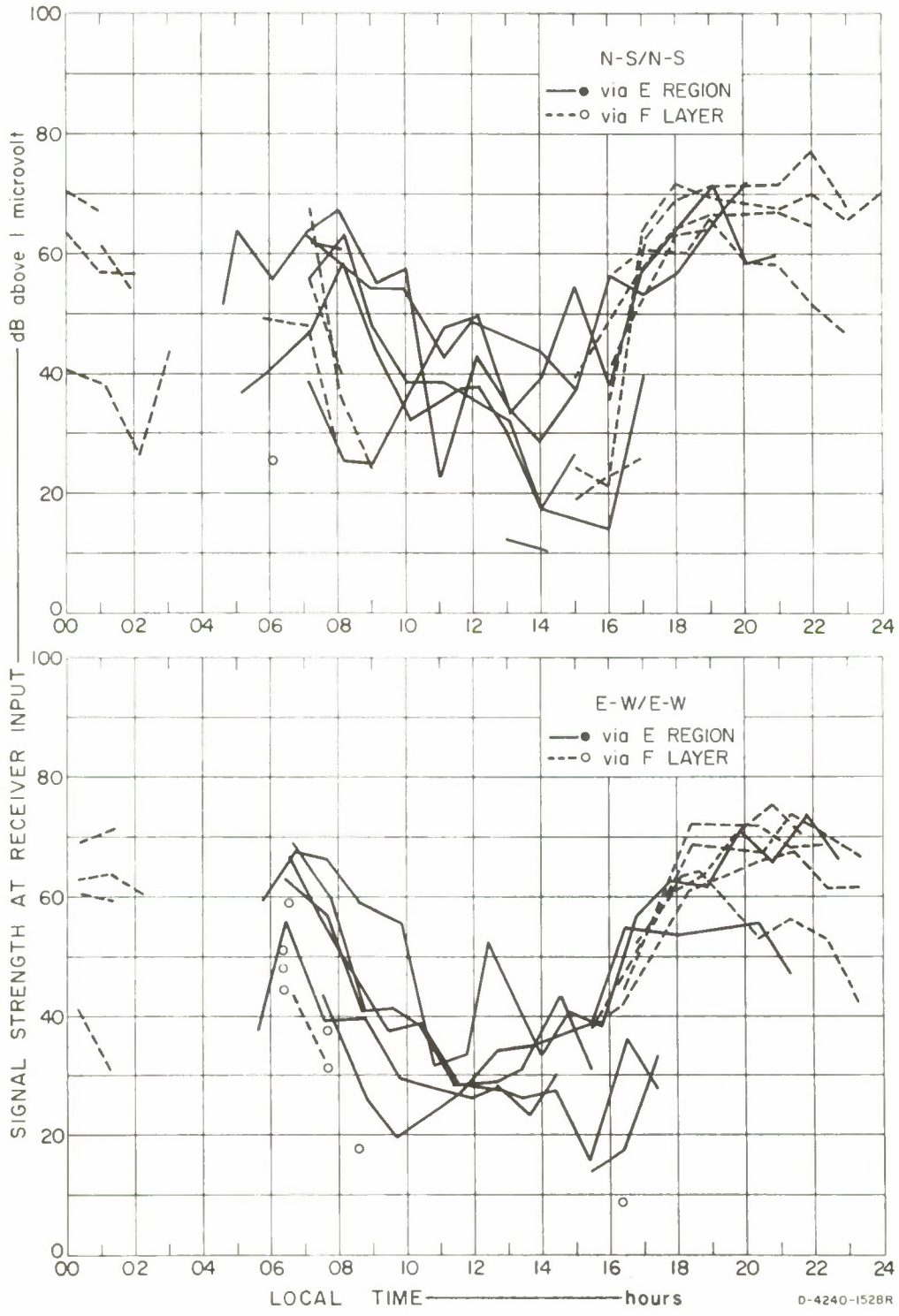

FIG. 139 DIRUNAL VARIATION OF V_m: KAO PONGRANG, N-S AND E-W TRANSMITTING AT 3.4 MHz

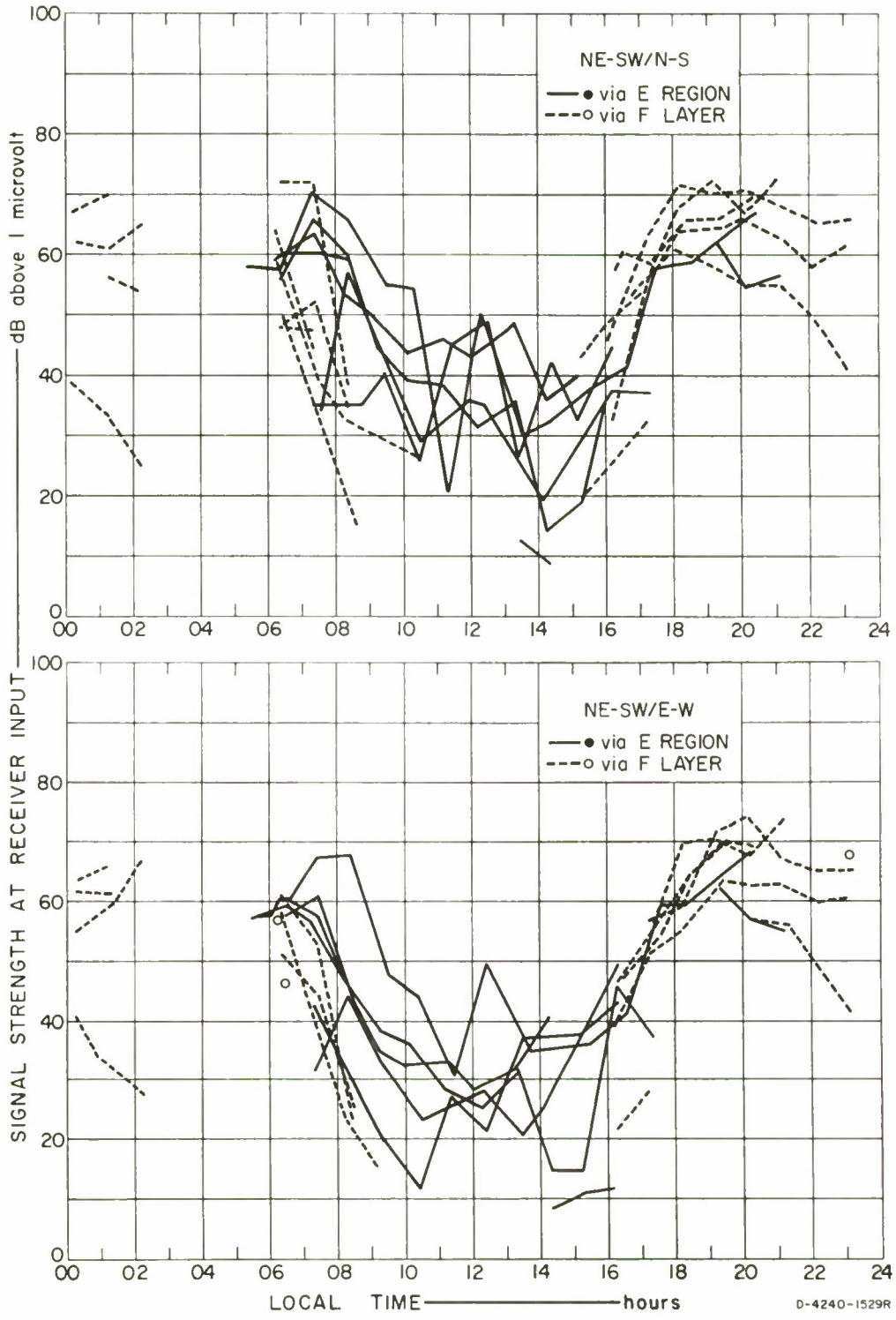

FIG. 140 DIURNAL VARIATION OF V_m: KAO PONGRANG, NE–SW TRANSMITTING AT 3.4 MHz

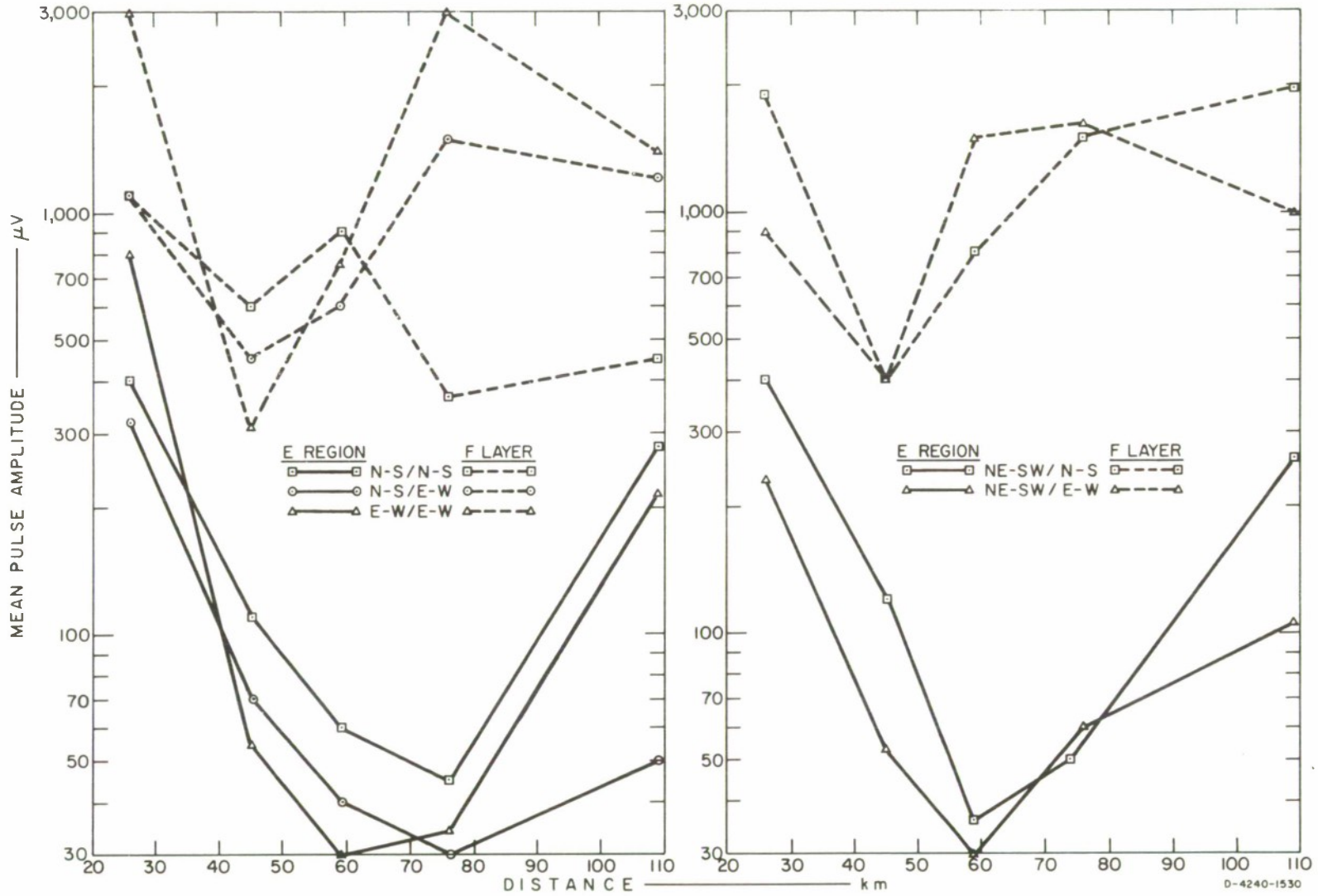

FIG. 141 MEAN PULSE AMPLITUDE AS A FUNCTION OF DISTANCE: KAO PRONGRANG/KRABINBURI, 3.4 MHz

if the major traffic is to be during the day, and with the NE-SW antenna transmitting at night. The magnetic inclination over the test region is 11^{0}-12^{0}N.

c. Stability of Received Pulses

Figures 142 and 143 were obtained in a similar manner as Figs. 108 and 109 and indicate the stability study of pulse amplitudes and pulse widths for the N-S and E-W antennas transmitting and for the NE-SW antenna transmitting, respectively. Since the propagation was supported by the E region during the day and by the F layer during the night, the curves for both of these layers were combined in Figs. 142 and 143, which show that the waves supported by the F layer were more amplitude stable than those supported by the Es layer. This was not as one would normally expect; however, one is to be reminded that the way the amplitude stability value versus local time was plotted, while giving a good indication of diurnal variations as well as the cumulative distribution of the A_s values, cannot give a direct comparison of actual stabilities since [by the definition of A_s in Eq. (48)] there is no indication that pulse amplitudes would mostly be near the V_{max}, V_{min}, or the average V_m value, and no indication of how rapidly the pulse amplitude would fluctuate. Observations made during the actual viewing of pulse reception must supplement plots of the A_s as a function of local time: they yielded the result that the stability of the waves was practically the same whether they were supported by the Es or the F layer. On the whole, therefore, a turbulent Es layer and a comparatively calm F layer with little or no spread F were indicated during the pulse-test period. This statement is supported by the study of phase stability of the pulses, which showed roughly the equal amount of pulse stretching in the Es-layer supported and the F-layer supported waves.

3. Sattahip/Cholburi 1.7-MHz Pulse Test

Pulse measurements at 1.7 MHz were carried out only in the Sattahip/Cholburi (S-to-N) direction, mostly during the time period of 0200-1000, except for some few days when measurements were made between 0200 and 2200.

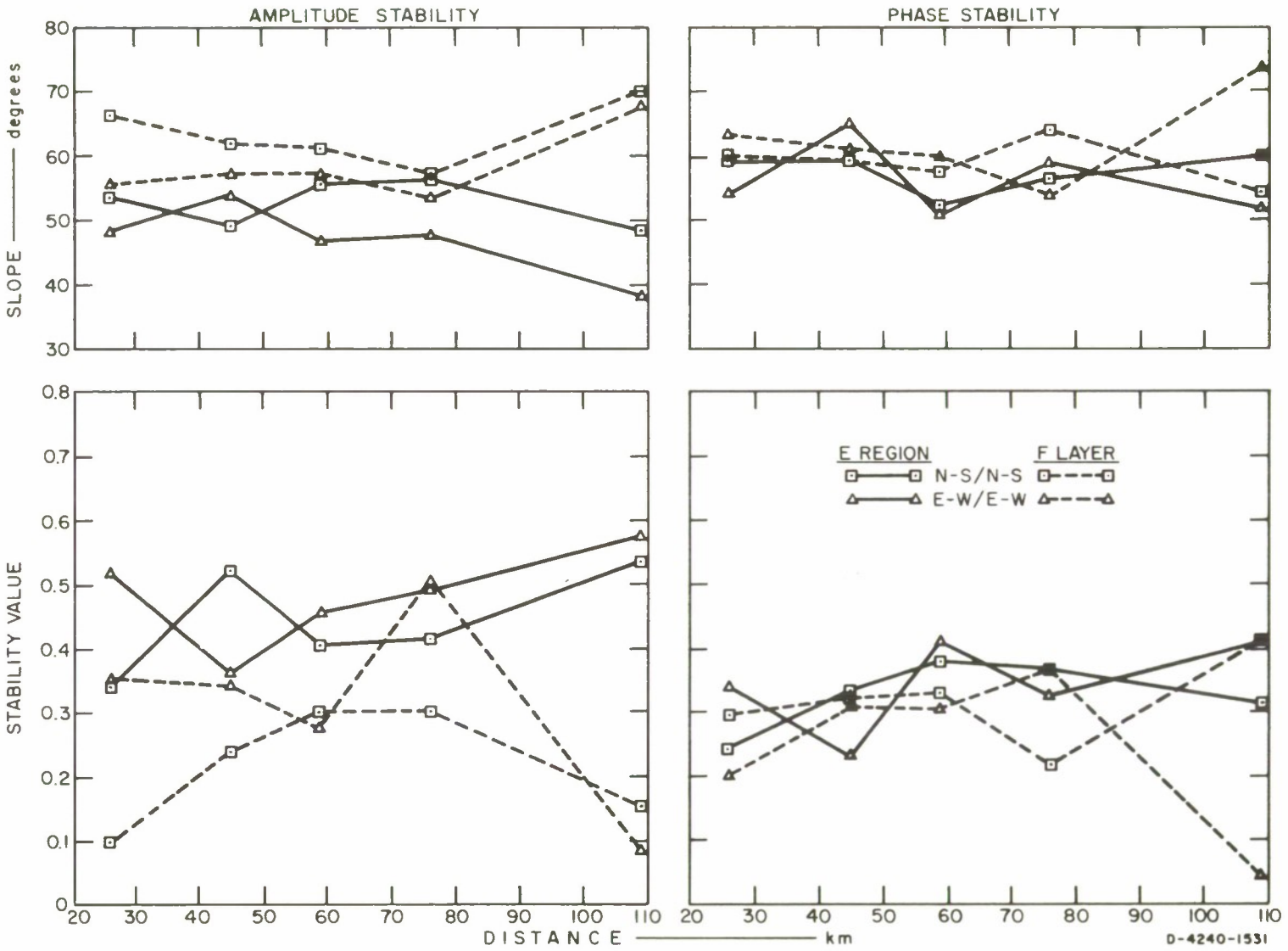

FIG. 142 PULSE STABILITY AS A FUNCTION OF DISTANCE: KAO PONGRANG, N-S AND E-W TRANSMITTING AT 3.4 MHz

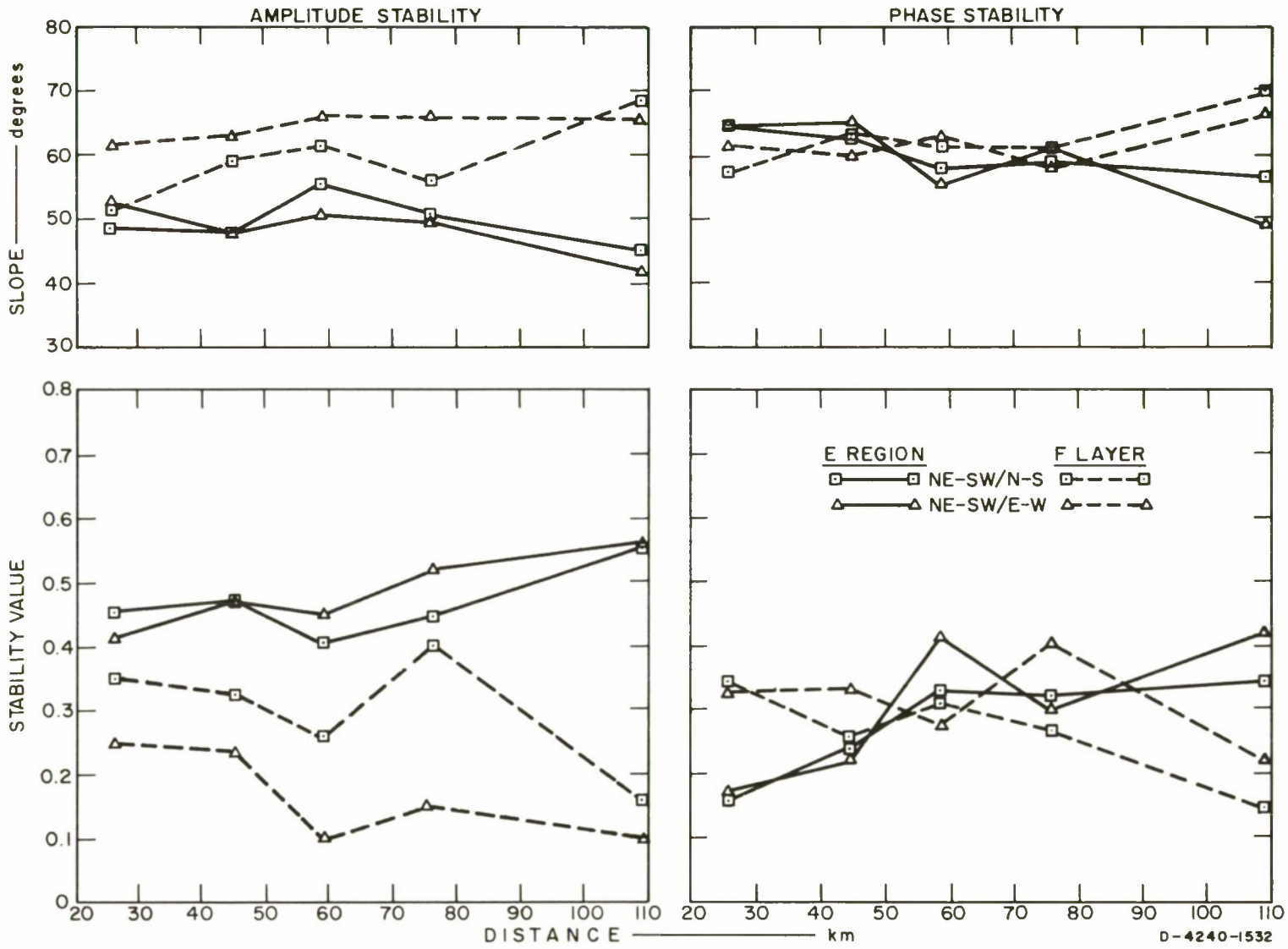

FIG. 143 PULSE STABILITY AS A FUNCTION OF DISTANCE: KAO PONGRANG, NE-SW TRANSMITTING AT 3.4 MHz

Average pulse amplitudes obtained at all distances were plotted against time as shown in Fig. 144 for the N-S/N-S and E-W/E-W antenna combinations and as shown in Fig. 145 for the NE-SW/N-S and NE-SW/E-W combinations. Figure 144 clearly indicates the superiority of the ordinary wave over the extraordinary and, together with Fig. 145, indicates that no advantage might be gained by the use of orientation diversity at 1.7 MHz; these results firmly support the CW test results described in Sec. III-C-1 and III-C-5. Additional supporting features were the same trend of diurnal variations: a difference of about 40 dB between the nighttime high field strength and the daytime low field strength (see Figs. 45 and 46). The pulse test also indicated the existence of multimode propagation, i.e., multiple reflections at the Es layer at sunrise and sunset, and the existence of multipath, i.e., simultaneous propagations via the Es and the F layers at night as well as during the post-sunset period; this accounts for the greater frequency of fading of the 1.7-MHz CW propagation at sunrise and during the post-sunset period (see Fig. 56 and Sec. III-C-3-a).

The quality of reception was found to be comparable for measurements made at receiving sites of 20 km and further (up to 83 km, the maximum range of the test circuit) away from the transmitting site; the reception was very poor at 10 km, becoming improved at 15 km. The N-S/N-S antenna combination also proved to be the best of all other combinations, thus confirming the theoretical QT range of 20-86 km as obtained in Table II or Fig. 13 for the 1.7-MHz propagation via the E region.

4. Sattahip/Cholburi 5.1-MHz Pulse Test

The 5.1-MHz wave was investigated mostly between 0630 and 2100 in order to compare its daytime performance with that of the 3.4-MHz wave. Diurnal variations of average pulse amplitudes obtained at all distances are shown superimposed in Fig. 146 for the N-S/N-S and E-W/E-W antenna combinations and in Fig. 147 for the NE-SW/N-S and NE-SW/E-W combinations. The theoretical QT range (as obtained for the 5-MHz propagation from Table II or Figs. 17 and 18) is 72-107 km via the F1 layer and 104-156 km via the F2 layer. The 5.1-MHz pulse transmission was supported during the test

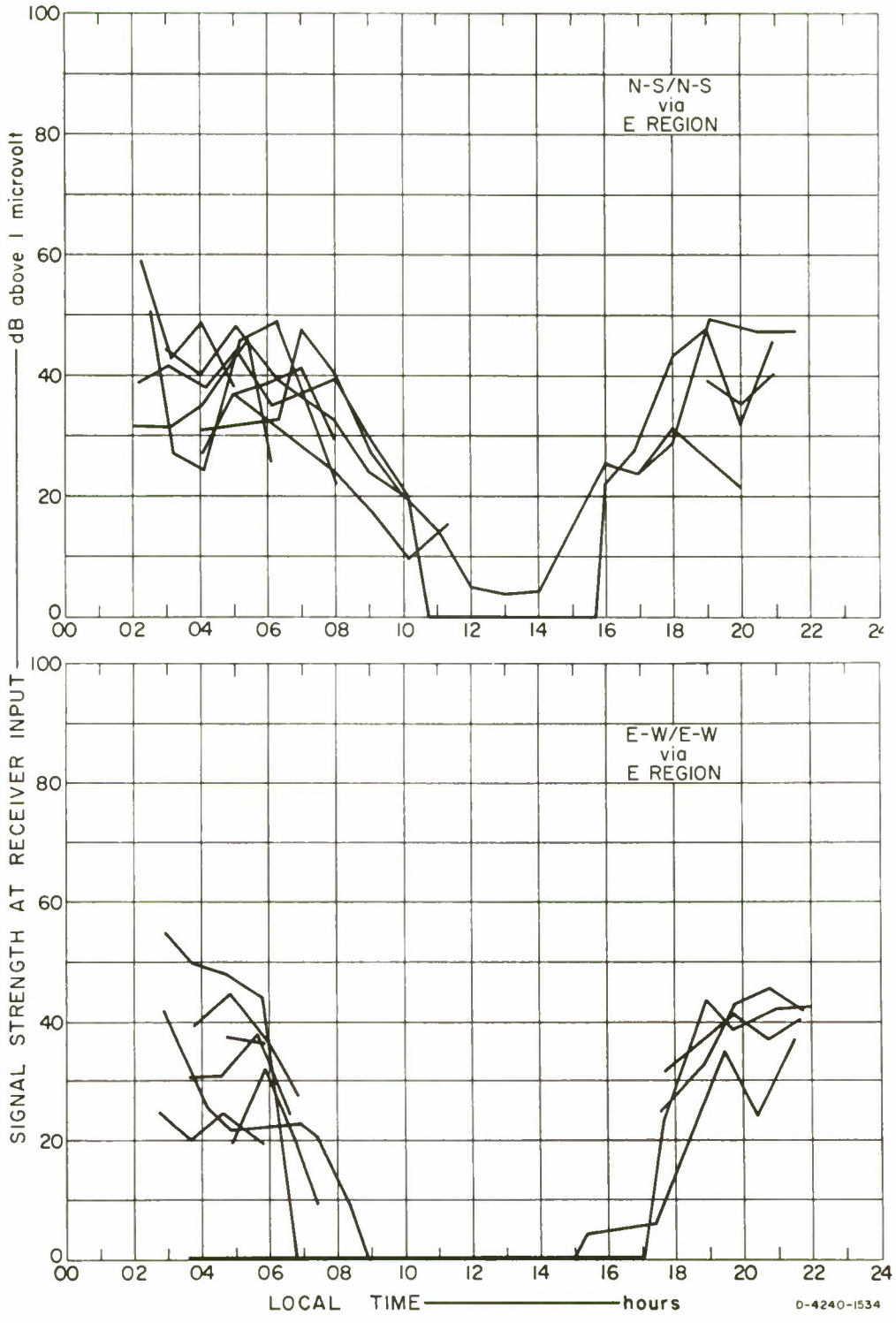

FIG. 144 DIRUNAL VARIATION OF V_m: SATTAHIP, N-S AND E-W TRANSMITTING AT 1.7 MHz

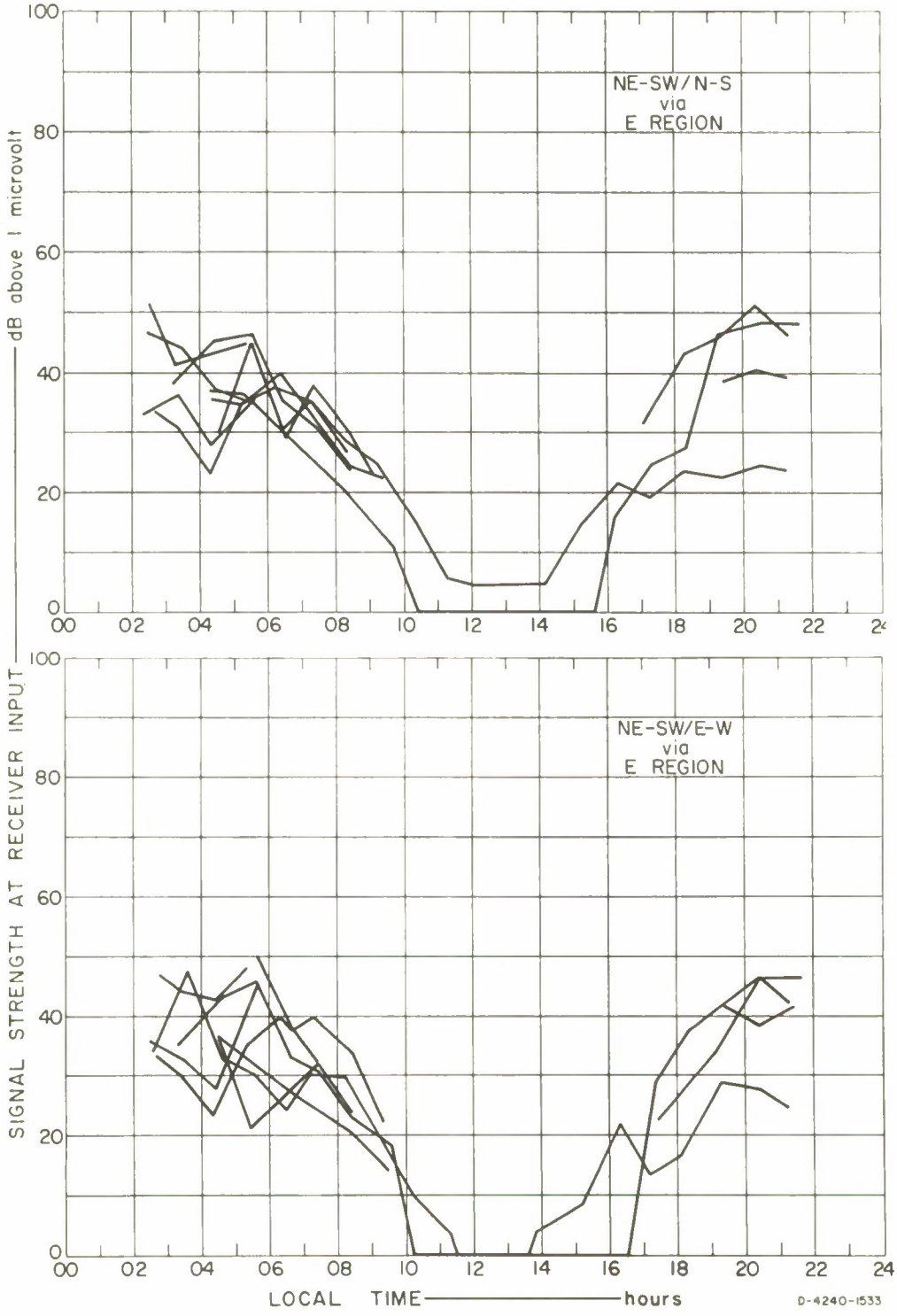

FIG. 145 DIURNAL VARIATION OF V_m: SATTAHIP, NE-SW TRANSMITTING AT 1.7 MHz

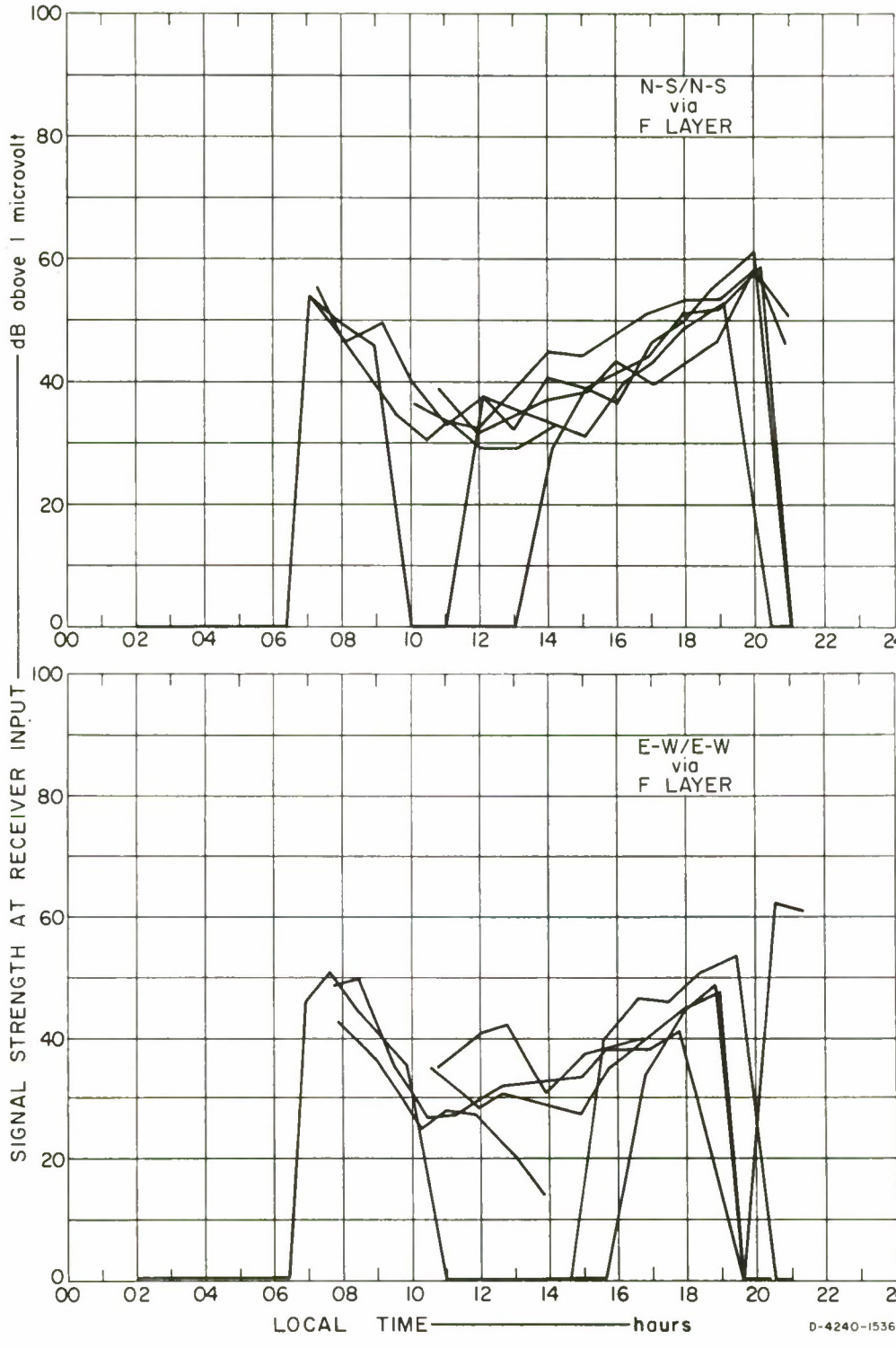

FIG. 146 DIRUNAL VARIATION OF V_m: SATTAHIP, N-S AND E-W TRANSMITTING AT 5.1 MHz

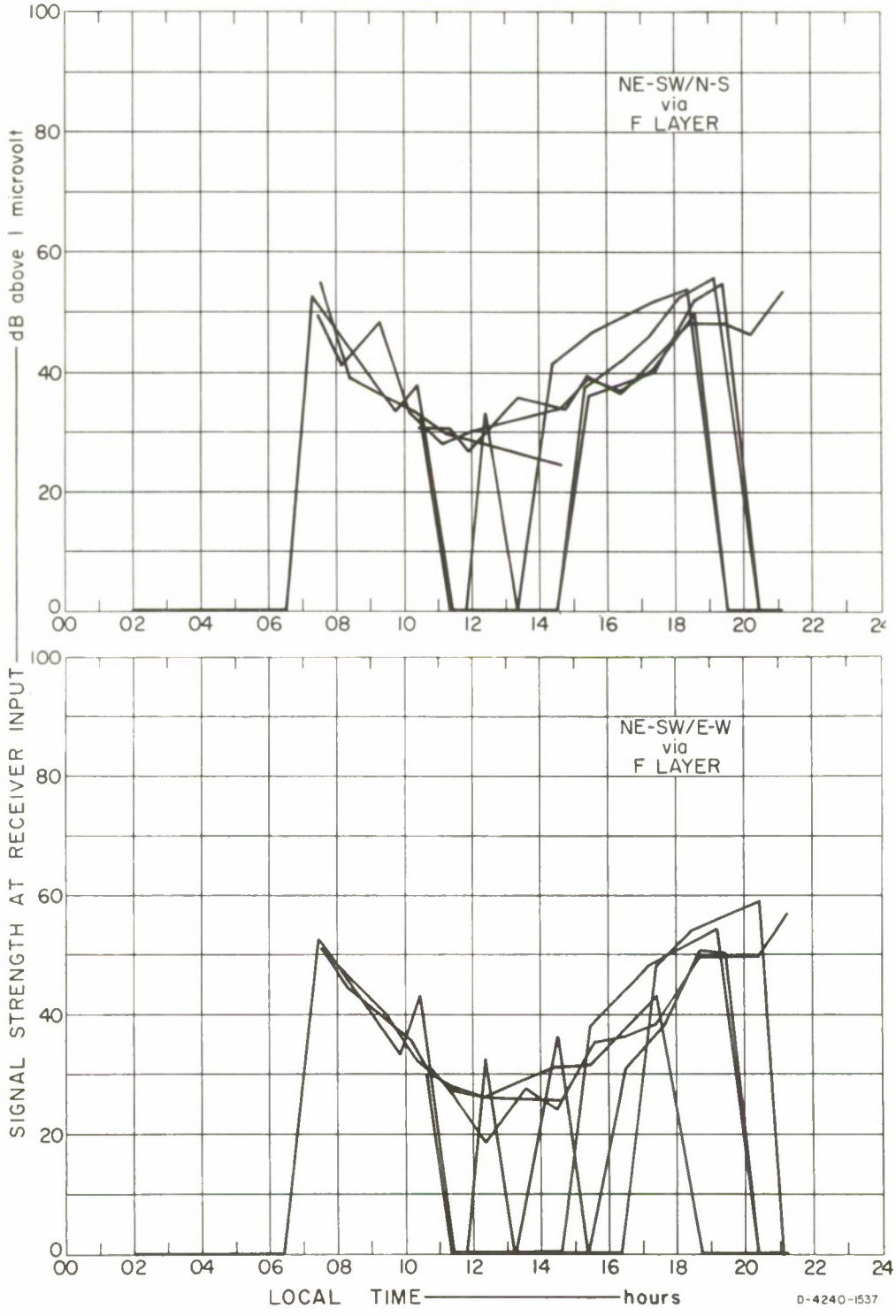

FIG. 147 DIURNAL VARIATION OF V_m: SATTAHIP, NE–SW TRANSMITTING AT 5.1 MHz

period mainly by the F2 layer; hence the test circuit was not yet in the QT range, as evidenced by the absence of distinct performance at any particular distances. The N-S/N-S combination was clearly the best antenna combination; demonstrating the superiority of the ordinary wave over the extraordinary wave, even for the S-to-N path as well as for the range outside the QT condition but not yet within the QL, as predicted by the magneto-ionic theory. The general trend of diurnal variations of the pulse transmission agrees with that of the CW results as shown in Figs. 45 and 50. Although the curves in Figs. 146 and 147 show no reception between 0200 and 0630, the author observed on three days during the measurements the presence of pulses in the noise; the pulses were identifiable by their stationary behavior in comparison with the random nature of noise pulses, as well as by their intermittent rise, disappearance, or shift in time of arrival. The 5.1-MHz frequency was known to exceed the foEs and foF2 frequencies (see the f plot of Fig. 163 for the Sattahip/Cholburi test period); the intermittent behaviors of "steady" pulses in the noise thus suggest the presence of ground backscatter, ionospheric scatter, or both.

Diurnal variations of the pulse stability at all distances are shown in Fig. 148 for the N-S/N-S antenna combination, which, when compared with the corresponding curves of the 3.4-MHz transmission in Figs. 79 through 102, indicates that the 5.1-MHz wave was more stable in both amplitude and (especially) phase than the 3.4-MHz wave. This finding possibly explains the daytime fading of the 5-MHz CW wave to levels lower than the 3-MHz wave, as observed in Sec. III-C-3-a (Figs. 56 and 57). Since the last paragraph of Sec. III-C-1-e states that 3 MHz was shown (by CW test results and the results of voice communication via the Collins KWM-2A) to be a better overall frequency during the day than 5 MHz, the finding of comparatively very little pulse stretching of 5.1-MHz propagation is significant in that a higher degree of reliability would be assured when using this frequency instead of 3.4 MHz for communication circuits on which the importance of phase stability of pulse transmission is emphasized. The preliminary survey of results of the HF Communication MRDC Special Project[22] indicated that the radio-teletype

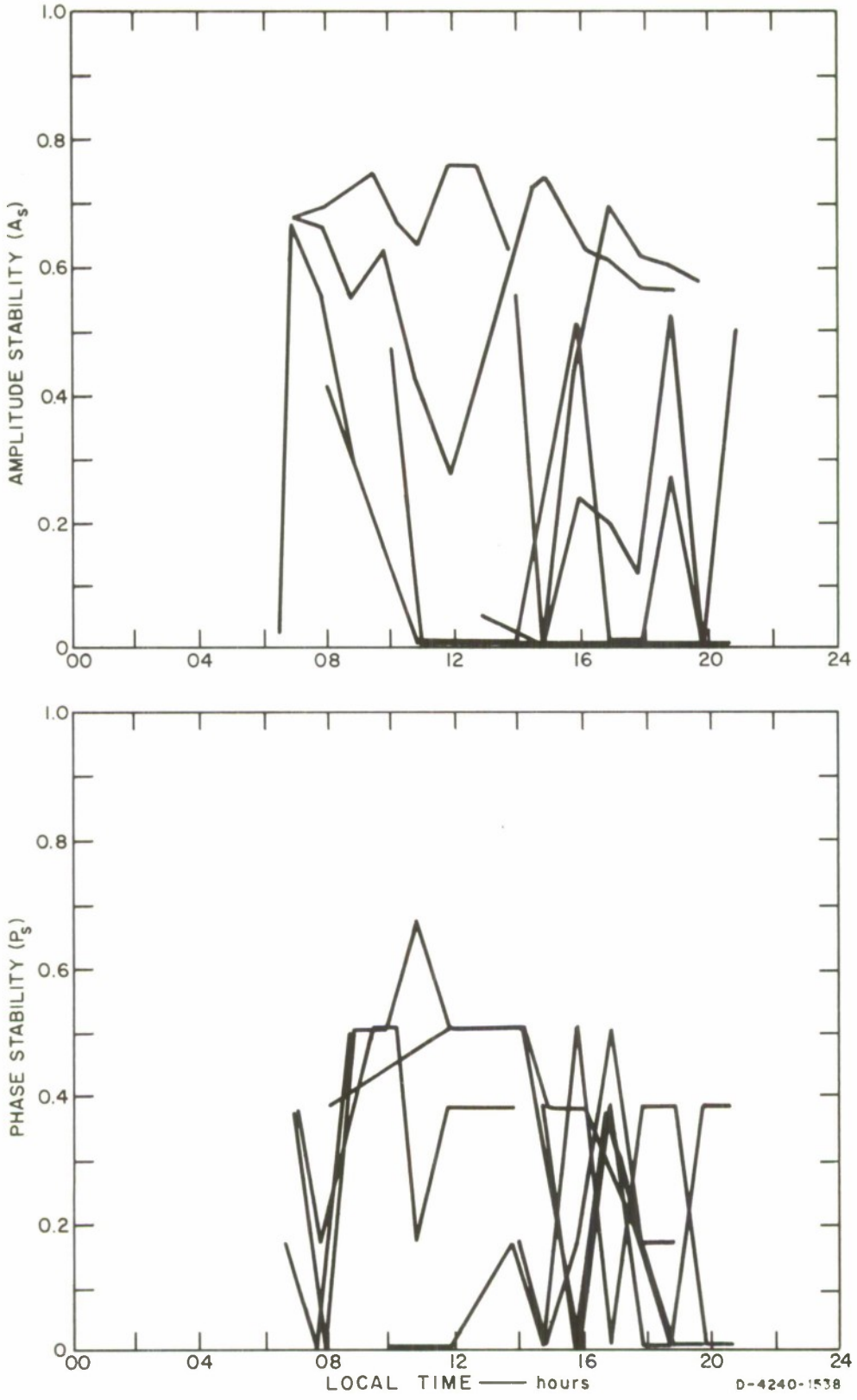

FIG. 148 DIURNAL VARIATION OF PULSE STABILITY, 5.1-MHz ORDINARY WAVE VIA F LAYER

transmission between Bangkok and Chantaburi (see Fig. 26) at 5.885 MHz produced less error than the transmission at 3.567 MHz during most of the daytime and part of the nighttime, the foF2 frequencies then being comparable to ones occurring during the period of the present pulse measurements.

V RADIO-TELETYPE MEASUREMENTS

A. PURPOSE

A preliminary study of CW and pulse data indicated that, although one pure characteristic wave was more suitable than the other for ionospheric propagation during a particular time of the day, communication might be further improved by the use of orientation-diversity reception system. One such system uses crossed horizontal dipoles--one dipole oriented parallel to and the other orthogonal to the geomagnetic meridian--and will be referred to as crossed-orientation diversity. Another system, which will be referred to as hybrid space-polarization diversity, combines the advantages of "polarization" diversity employing N-S and E-W horizontal dipoles with the advantages of space diversity where the two dipoles are spaced a certain distance apart. This distance, normally approximately two wavelengths, might be reduced by orientation of spaced antennas for diversity.

An investigation using radio-teletype equipment was designed to test the truth of the above statements and to obtain an indication of the best form of orientation-diversity system.

B. TEST PROCEDURE

Brief measurements at 3.4 MHz were carried out over the Bangkok/Ayudhaya circuit with AN/GRC-26A radio-teletype sets[23] as shown in Fig. 149, to investigate and compare the performance of the hybrid space-polarization diversity reception and that of the reception of one characteristic wave, the ordinary. Tests were conducted in both directions with little difference in time when possible, so that the S-to-N and the N-to-S transmissions might be directly compared.

Various types of orientation diversity reception were investigated and compared with the usual space diversity reception of radio-teletype

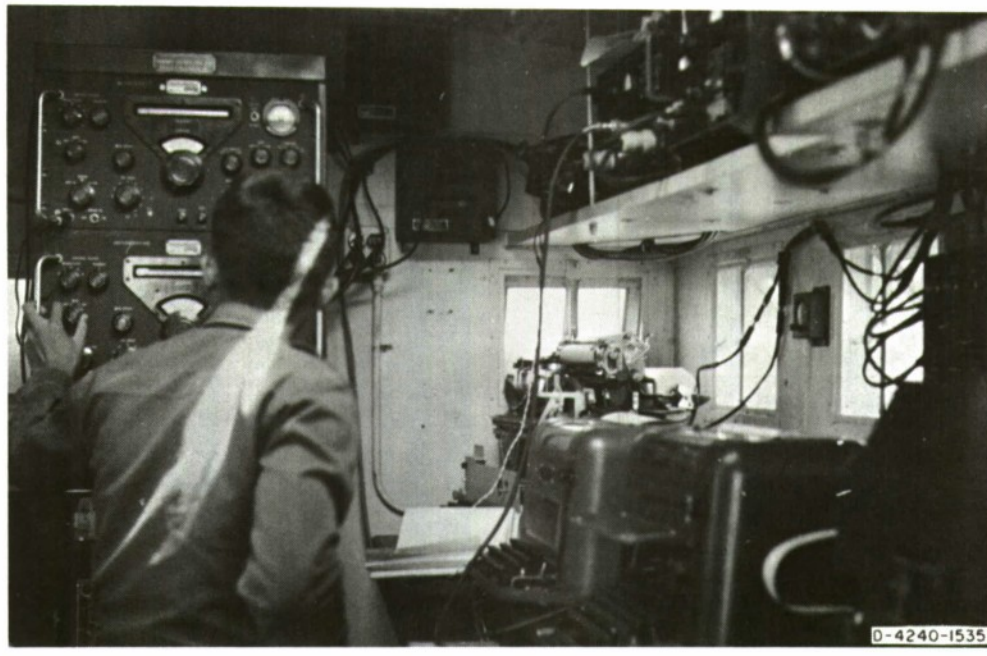

FIG. 149 PHOTOGRAPH OF AN/GRC-26A RADIO-TELETYPE EQUIPMENT

by measurements over the NW-SE Bangkok/Cholburi circuit of approximately 65 km ground distance, the same distance as that of the Bangkok/Ayudhaya circuit (see Fig. 26). The spacing for the spaced antennas was 600 ft, as recommended in U.S. Army Technical Manual TM 11-5820-202-10;[23] at 3.4 MHz, this corresponds to two wavelengths. The spacing for the hybrid antennas was 450 ft (approximately 1.5 wavelengths). Antenna systems employed are illustrated in Fig. 150. The Bangkok/Cholburi test circuit was chosen because the NE-SW antenna, beside being the recommended antenna for the space-diversity system, launches the ordinary wave as well as the extraordinary and thus is suitable for the investigation of orientation-diversity schemes utilizing both of these waves.

C. RESULTS AND DISCUSSION

1. General

Radio-teletype messages afford an efficient and ready means of assessing communication performance. A five-unit teletype code character consists of a combination of space/mark impulses, as illustrated in Fig. 151.[24] The five 20-ms space/mark information bits of a character

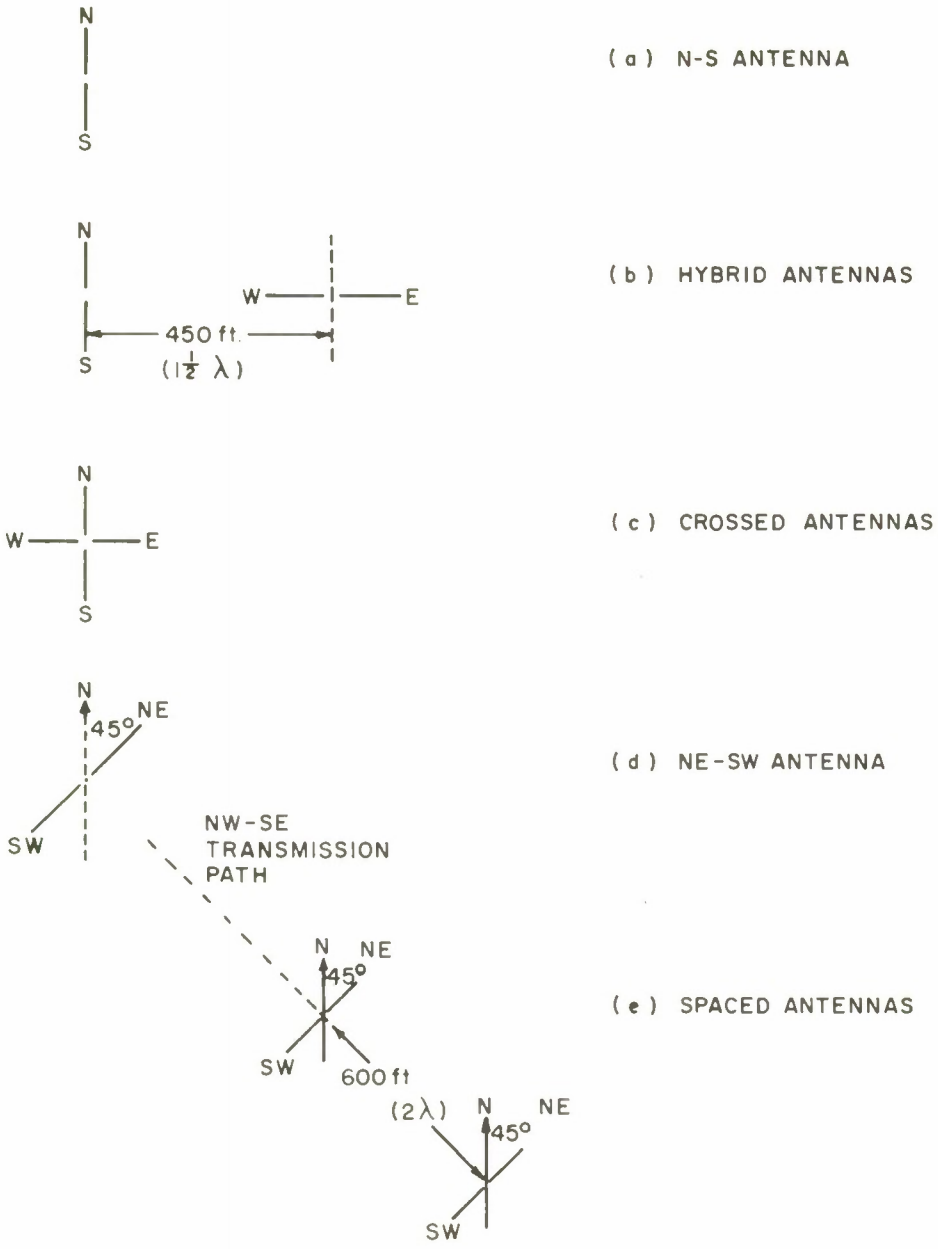

ANTENNA SYSTEMS FOR:

(a) ORDINARY-WAVE RECEPTION OR TRANSMISSION
(b) HYBRID SPACE-POLARIZATION DIVERSITY RECEPTION
(c) CROSSED-ORIENTATION DIVERSITY RECEPTION
(d) ORDINARY- AND EXTRAORDINARY-WAVE TRANSMISSION
(NOTE: MAGNETIC DECLINATION OVER THE TEST AREA ≅ 10° W)
(e) SPACE DIVERSITY RECEPTION FOR THE BANGKOK-TO-CHOLBURI PATH (N135°S)

D-4240-475

FIG. 150 ANTENNA SYSTEMS

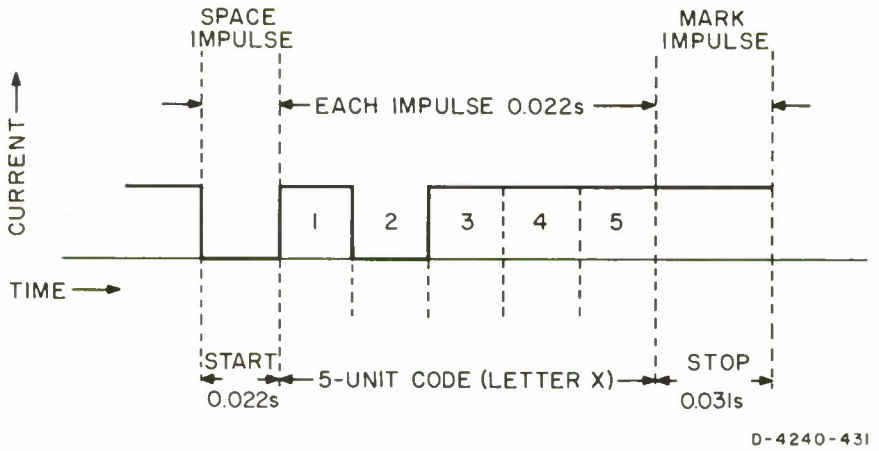

FIG. 151 FIVE-UNIT SPACE/MARK CODE OF ONE CHARACTER (Letter X)

are preceded by a 20-ms space start and followed by a 30-ms mark stop. The normal sending rate is 60 five-character words per minute. Thus, a large amount of information--say 2100 space/mark bits--may be obtained in 1 min of transmission, and a deep fade or interference as brief as 1/45 s may bring about an error in any one character. By counting the number of errors made in the space/mark pulses of each character, a percentage copy of radio-teletype messages may be obtained and averaged over a period of several brief transmissions of around 200-400 characters per transmission. The brief and fast transmission and reception with radio-teletype equipment makes possible measurements in quantity and in quick succession for any two test locations.

2. The Ordinary-Mode Single Channel versus Hybrid Space-Polarization Diversity (Bangkok/Ayudhaya)

It can be seen from the results of the test on the ordinary mode versus hybrid space-polarization diversity, as shown in the top portion of Fig. 152, that the S-to-N propagation definitely performed better than the N-to-S propagation. This is supported by the fact that, for the 3.4-MHz E-mode propagation, the angle θ at entry into the ionosphere is approximately 86° for the S-to-N path, which is almost within the QT condition (allowing $\pm 3^{\circ}$ off 90°), while for the N-to-S path it is 64° and is out of the QT condition at entry. For the F1 mode of propagation

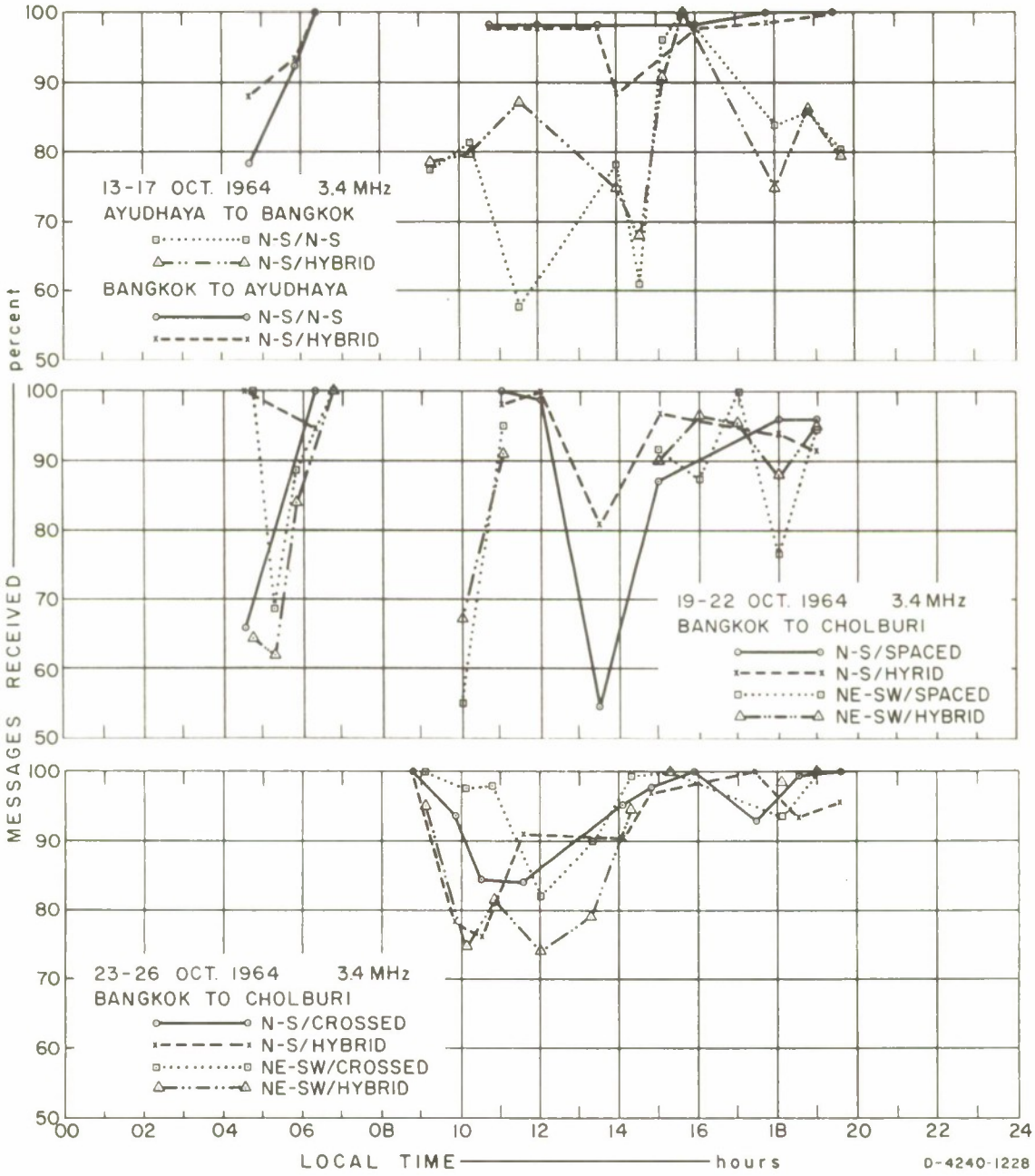

FIG. 152 COMPARISON OF TELETYPE DIVERSITY SYSTEMS

at 3.4 MHz, the angle θ at entry for the S-to-N path is 93^{0} and is just within the QT condition, while the entry angle for the N-to-S path of 71^{0} is out of the required QT condition. For a particular direction over this Bangkok-Ayudhaya path, the results as obtained graphically do not indicate a strong preference for either the N-S/N-S or the N-S hybrid transmitting/receiving antenna combinations. Although a preference for the N-S/hybrid combination is indicated at times, for example during the pre-dawn period, the N-S/N-S combination (and hence the ordinary wave) gave slightly better overall performance. This latter statement is further supported by close observations on the actual performance of the radio-teletype sets by experienced operators and the author. One may thus say that the transmitting/receiving antenna combinations performed equally well at 3.4 MHz and the hybrid spacing of 1.5 wavelengths, and that--for simplicity and lower cost--the N-S/N-S combination would be the choice. It is believed, however, that the N-S/hybrid combination with the appropriate spacing should perform better than the N-S/N-S during periods of difficult contact.

3. Space Diversity versus Hybrid Space-Polarization Diversity (Bangkok/Cholburi)

Results as shown in the middle part of Fig. 152 compare the space diversity and hybrid space-polarization diversity reception systems. Although these four curves are essentially the same, there is an indication of the N-S/spaced combination (i.e., space diversity with the N-S antenna transmitting) having been poorer than the NE-SW/spaced combination (i.e., space diversity with the NE-SW antenna transmitting). This would be expected, since the NE-SW antenna would be the appropriate transmitting antenna for the space diversity system for reception in the NW-SE direction. One may observe from these curves that there is no preference for either the space diversity system using the appropriate NE-SW/spaced antenna combination or the hybrid space-polarization diversity system using the N-S/hybrid or the NE-SW/hybrid combination. One would be led to expect the hybrid space-polarization diversity system to perform better than the space diversity, since in the hybrid case there are two factors that may improve performance: the spacing between the two

receiving antennas and the difference in the polarization of the waves reaching the two antenna inputs. It should be noted, however, that the antenna spacing in the hybrid diversity case was only 1.5 wavelengths, while the spacing in the space diversity case was 2 wavelengths. If the hybrid antennas had also been spaced 2 wavelengths apart, the results might have been as expected. Further discussion and also a suggestion on this subject will be taken up in the next section. The equal performance of the hybrid and space diversity systems under these conditions is encouraging, however, since the greater ease in antenna layout and construction for the hybrid diversity system may be readily visualized.

4. Crossed-Orientation Diversity versus Hybrid Space-Polarization Diversity (Bangkok/Cholburi)

The investigation of orientation diversity (crossed dipoles) versus hybrid space-polarization diversity as carried out in this dipole-orientation project should be regarded as the pilot test for a future antenna project on diversity systems involving design and evaluation. The crossed-orientation diversity is, in fact, the hybrid space-polarization diversity with zero spacing between the centers of N-S and E-W antennas. The results, as shown in the lower portion of Fig. 152, indicate with a fair degree of certainty that the NE-SW/crossed transmitting/receiving antenna combination is superior to the hybrid arrangement of N-S and E-W antennas for receiving with either the N-S or the NE-SW antenna transmitting. Judging by the arrangement of diversity antennas alone, one would have expected the hybrid antennas to perform better than the crossed antennas; but the results obtained were quite on the contrary. These surprising results, if supported by a larger sample size with additional investigation on effects of varying the antenna spacing, will be of great value, because of the economy of the area required for orthogonally crossed dipoles and the ease with which they can be erected. The possibility of achieving this tactical requirement alone warrants a thorough investigation of an optimum diversity system for HF short-range communication. There was an indication also that the NE-SW/crossed arrangement performs slightly better than the N-S/crossed combination, supporting the inference that the extraordinary wave may help should the ordinary wave temporarily fail.

5. Relative Performance of Various Transmitting/Receiving Antenna Combinations

The foregoing investigations with radio-teletype equipment were designed with the expectation that the hybrid space-polarization diversity system of reception would prove superior to other systems of not more than two horizontal dipoles for reception. As it turned out, the hybrid diversity system as used was somewhat outperformed by the simpler arrangement of two orthogonally crossed dipoles (the crossed-orientation system), and it could not be said to have performed better than the simplest N-S/N-S system utilizing only one wave mode--the ordinary wave--for both transmission and reception. Although the hybrid diversity system with the proper spacing between hybrid antennas may turn out to perform better than the crossed-orientation diversity system, its use would be discouraged by two major factors: the requirements for a large space and for the necessary knowledge of the suitable antenna spacing for as little correlation of the antenna outputs as possible.

Although the samples measured are not sufficiently large for the obtained results to be regarded as conclusive, the analysis of these results strongly indicates that, for short-range sky-wave communication in geomagnetic equatorial region, the orientation diversity system of reception involving N-S and E-W horizontal dipoles is superior to the space diversity system, which is recommended in the U.S. Army Technical Manuals[23] with no mention of restriction on range or area of application.

VI CONCLUSIONS AND RECOMMENDATIONS

This present work of dipole orientation with a view to optimizing the orientation of a linearly polarized antenna for short-range communication via the ionosphere near the geomagnetic equator may be regarded as a significant step towards the improvement of HF communication in the area, e.g., a forest, where a gain of 6 dB or so makes a difference. It is significant in a sense that, within a specified condition, an unorthodox method is evolved with advantage over the existing method widely practiced all over the world. For a short-range skywave communication up to about 100 km in the geomagnetic equatorial region and for a difficult "skip" zone under certain conditions, the normal main-beam-to-main-beam propagation with linearly polarized antennas physically orthogonal to the line joining their phase centers has been proved by this present work to be inferior to the unorthodox type of propagation utilizing one of the characteristic wave modes--such as the ordinary wave--with both transmitting and receiving antennas physically oriented in the N-S direction, notwithstanding the actual direction of propagation between the two communication sites.

The CW measurements gave us the confidence in the ordinary wave mode during most hours of the day; the most significant result was the superiority of the N-S/N-S transmitting/receiving antenna combination, i.e., the ordinary wave, by about 13 dB (1.7 MHz), 6 dB (3 MHz), and 7 dB (5 MHz) over the E-W/E-W arrangement that would methodically be selected for the S-to-N Bangkok-to-Ayudhaya path (refer to Secs. III-C-1-b, d, and e). The CW test also told us to change, if required, to the extraordinary wave mode, which became superior during a part of the nighttime when the ordinary wave suffered a greater overall absorption over the whole path: 4 dB (1.7 MHz 0330-0600), 3 dB (3 MHz 2000-0600), and 2 dB (5 MHz 1830-2230). The contrasting features of the two wave modes with regard to the fading characteristics and the noise picked up by the receiving antenna indicated that the use of an orientation

diversity system of reception, with receiving antennas in the N-S and in the E-W directions, might be advantageous.

The pulse measurements, on the whole, supported the CW test results and gave additional information on the ionospheric region or layer that actively supported the propagation at a particular frequency and in a particular time of the day, on the presence or absence of multipaths and/or multimode propagation, and on the stability of various wave modes determined by different transmitting/receiving antenna combinations. The sporadic-E layer was seen to support a sky-wave propagation during the day and, in many cases, well into the night. The F layer took over from the sporadic-E layer during part of the night when the wave frequency was above the foEs but still somewhat below the foF2 frequency, thus explaining the rise in amplitude after sunset evidenced in the CW test. The stability study of various wave modes, together with the presence of multipaths, did not explain the severe fading during the pre-dawn period as shown in the CW test results. The severe fading was hence attributed mainly to interference by noise, which rose and became comparable to the signal amplitude that was diminishing when the signal frequency was becoming comparable to (or even rising beyond) the foF2 frequency. Information on noise should thus be included in the task of a frequency assignment. The pulse test confirmed the superiority of the ordinary wave mode and indicated that the orientation diversity system of reception did not perform significantly better than the simplest arrangement of N-S/N-S transmitting/receiving antenna combination, except during part of the nighttime and when the transmitting and receiving sites were outside the QT range. The existence of the QT range, predicted in a theoretical study, was proved by the pulse test.

The radio-teletype measurements briefly carried out in this orientation work clearly backed up the idea of utilizing pure characteristic waves for HF short-range sky-wave communication. The single channel using the N-S/N-S antenna combination (i.e., the ordinary wave mode) was seen to be better than the diversity system of dual receiving channels most of the time, except the pre-dawn period when it was better to transmit with a N-S antenna and to receive with N-S and E-W antennas

in the orientation diversity system. The test indicated that a somewhat better performance might be obtained with the orientation diversity system instead of the usual space diversity system of reception. The study also included the hybrid space-polarization diversity system, wherein the N-S and E-W receiving antennas were separated a certain distance apart. Although there was no clear indication of the hybrid space-polarization system performing better than the purely polarization system with crossed dipoles (i.e., the orientation diversity), as one would have expected, the author strongly suggests that the hybrid space-polarization system should be investigated in greater detail and with more variable parameters: the transmitting/receiving antenna combinations, the distance between the two receiving antennas in diversity, the frequency, and the distance. The measurements should be carried out in parallel with the C-2 sounder and the radio-teletype circuit in actual operation, and the results should be evaluated in accompaniment with appropriate noise data. Some of these features have been included in the MRDC Special Project, the report on which is presently in preparation.[22]

It should be emphasized that, owing to the radiation-pattern effects shown in Fig. 19, the use of N-S dipoles for both transmitting and receiving with no regard to the direction of propagation (instead of the usual arrangement of placing the transmitting and receiving antennas broadside to each other) would generally involve a loss of field strength less than 3 dB over the distance of 100 km. This is true in the case of a sky-wave propagation via the ionosphere under no influence of the earth's magnetic field. With the effect of the magnetic field over the geomagnetic equatorial region, it has been shown that such usage of N-S dipoles for both transmitting and receiving--and hence the utilization of the pure characteristic ordinary wavemode--would involve a relative gain over the orthodox antenna arrangement of 6-18 dB, depending on ionospheric conditions at the time of propagation.

The following are recommendations in the handling of HF short-range (up to 100 km or so) sky-wave communication in the region around the geomagnetic equator, thus applicable to most parts of Thailand:

1. Horizontal half-wave dipole antennas are preferable to vertical quarter-wave whip antennas in all environments, especially in the dense forest: other linearly polarized antennas, whether singly or in arrays, may be used in place of dipoles. Although VHF equipment is typically used rather than HF communication over a very short range in the open, it should be pointed out that if HF skywave will work over a 100 km path, it will also work over shorter paths.

2. Horizontal dipoles for both transmitting and receiving should be oriented in the magnetic N-S direction, notwithstanding the actual direction of transmission for paths shorter than 100 km. This N-S/N-S transmitting/receiving antenna combination greatly simplifies the layout of antennas for a system of communication involving more than two stations. For paths greater than 100 km use the classical broadside dipole alignment.

3. The frequency of propagation should be selected as near as possible to the 80 percent value of the predicted foF2 frequency averages over the block time period of interest. The use of foEs frequencies should also be considered, especially when they exceed the foF2, e.g., during a predawn period.

4. Should the quality of reception become poor because the signal strength is dropping low into the background noise, either or both of the two procedures should be tried, whichever is more convenient:

   (a) Shift the operating frequency to the next one allocated, preferably to the lower frequency first and to the higher one if necessary and improved.

   (b) Try E-W dipoles (the single-channel system is assumed) if this alternative is available.

5. If facilities for diversity reception are provided in the system, the cross N-S and E-W antennas [see Fig. 150(c)] should be used for receiving and the N-S antenna for transmitting; if in difficulty, one, part, or all of the four procedures should be tried, whichever is more convenient:

   (a) Change to single-channel operation with the N-S/N-S transmitting/receiving antenna combination.

   (b) Change the N-S transmitting antenna into the NE-SW type.

   (c) Change the operating frequency to the next one allocated.

   (d) Change the crossed antennas for reception into the hybrid type [see Fig. 150(b)] with a separation distance of 2 wavelengths or more.

REFERENCES

1. J. W. Herbstreit and W. Q. Crichlow, "Measurement of Factors Affecting Jungle Radio Communication," Report ORB-2-3, Operational Research Branch, Office of the Chief Signal Officer, Washington, D.C. (10 November 1943).

2. DSIR, Wellington, New Zealand, "Radio Propagation Through New Guinea Rain Forest," Report No. 8, Operational Research Section, Landforces Headquarters, Melbourne, Australia (1944).

3. "Electrical Communication Systems Engineering," U.S. Army Technical Manual TM 11-486-6; Art 14-12, "Horizontal Half-Wave Dipole Antenna," Paragraph d. (U.S. Government Printing Office, Washington, D.C., changed 23 August 1956).

4. A. J. Aikens, R. S. Tucker, and A. G. Chapman, "HF Sky-Wave Transmission over Short or Moderate Distances Using Half-Wave Horizontal or Sloping Antennas," Final Report, NDRC Project C-79, Part III, National Defense Research Committee, p. 15 (15 July 1944).

5. W. R. Piggot, "The Calculation of the Median Sky Wave Field Strength in Tropical Regions," DSIR Radio Research Special Report 23 (Her Majesty's Stationery Office, London, 1959).

6. G. H. Hagn, "Orientation of Linearly Polarized HF Antennas for Short-Path Communication via the Ionosphere near the Geomagnetic Equator," Research Memorandum 5, Contract DA 36-039 AMC-00040(E), SRI Project 4240, Stanford Research Institute, Menlo Park, California (August 1963).

7. Hagn, op. cit., Revised Edition (June 1964).

8. E. V. Appleton, "Wireless Studies of the Ionosphere," J. Inst. Elec. Engrs. (London), Vol. 71, p. 642 (1932).

9. J. D. Whitehead, "The Quasi-Transverse (Q.T.) Approximation to Appleton's Magneto-Ionic Equation," J. Atmos. Terrest. Phys., Vol. 2, pp. 361-362 (1952).

10. F. H. Hibberd, "Q.L. and Q.T. Approximation to the Magneto-Ionic Equations and Their Validity," J. Atmos. Terrest. Phys., Vol. 24, pp. 843-851 (1962).

11. J. A. Ratcliffe, The Magneto-Ionic Theory and Its Applications to the Ionosphere, pp. 75-76 (Cambridge University Press, Cambridge, England, 1959).

12. K. G. Budden, Radio Waves in the Ionosphere, p. 40 and pp. 70-72 (Cambridge University Press, Cambridge, England, 1961).

13. G. H. Hagn, "Absorption of Ionospherically Propagated HF Radio Waves under Conditions Where the Quasi-Transverse (QT) Approximation is Valid," Special Technical Report 9, Contract DA 36-039 AMC-00040(E), SRI Project 4240, Stanford Research Institute, Menlo Park, California (September 1964).

14. Ratcliffe, op. cit., pp. 65-69.

15. Piggot, op. cit., p. 31

16. Budden, op. cit., pp. 225-270.

17. Ratcliffe, op. cit., pp. 76-78.

18. NBS, "Ionospheric Radio Propagation," Circular 462, National Bureau of Standards, pp. 24-26 (25 June 1948).

19. H. F. Bush, "Project Yo-Yo Field Experiments," Report on ARPA Order No. 299-62 and Contract Nonr-2507(00), ACF Electronics Division, ACF Industries, Hyattsville, Maryland, p. 6-4 (13 September 1962), FOR OFFICIAL USE ONLY.

20. Vichai T. Nimit, "Ionospheric Data: Bangkok, Thailand," Ionospheric Data Report - January 1964, Contract DA 36-039 AMC-00040(E), Order No. 5384-PM-63-91, Thai-U.S. Military Research and Development Center, Supreme Command Headquarters, Bangkok, Thailand.

21. J. W. Wright and T. N. Gautier, "Note on a Test of the Equivalence Theorem for Sporadic E Propagation," J. Res. NBS, Part D, Radio Propagation, Vol. 64D, No. 4, pp. 347-348 (July-August 1960).

22. P. Nacaskul, Lt. Cdr., R.T.N., "HF Communication MRDC Special Project: Bangkok-Chantaburi," in preparation.

23. "Operator's Manual Radio Sets AN/GRC-26A AN/GRC-26B and AN/GRC-26C," U.S. Army Technical Manual TM 11-5820-202-10, p. 24 (U.S. Government Printing Office, Washington, D.C., January 1959).

24. "Teletypewriter Set AN/GGC, Teletypewriter Reperforator Transmitters TT-76/GGC and TT-76A/GGC," U.S. Army Technical Manual TM 11-2225, p. 102, (U.S. Government Printing Office, Washington, D.C., April 1957).

PROJECT PERSONNEL

PROJECT LEADER: Lt. Cdr. Paibul Nacaskul, R.T.N.

CW AND PULSE TEAM

MRDC-THAILAND: Lt. Cdr. Paibul Nacaskul, R.T.N.

M. Sgt. Sathorn Meeudon, R.T.A.F.

First C.P.O. Manit Downkhanon, R.T.N.

Second C.P.O. Chalerm Keosang, R.T.N.

SRI BANGKOK: John W. Chapman

Frank Phillips

Kenneth L. Taylor

Robert D. Daniel

RADIO-TELETYPE TEAM

ROYAL THAI ARMY FIRST SIGNAL BATTALION:

Lt. Sak Suyananda

Third M. Sgt. Sawat Prabthong

Cpl. Chaggris Kaewtae

Cpl. Charoon Suksamran

Cpl. Tuthin Haadsai

Cpl. Pirom Maniratana

DISTRIBUTION LIST

Organization	No. of Copies
Commanding General U.S. Army Electronics Command Fort Monmouth, New Jersey 07703 Attn: AMSEL-RD-DO ARPA Coordinator	1
Commanding General U.S. Army Electronics Command Fort Monmouth, New Jersey 07703 Attn: AMSEL-NL-R-4 R. N. Herring	24
Marine Corps Liaison Officer U.S. Army Electronics Command Fort Monmouth, New Jersey 07703 Attn: AMSEL-RD-LNR	1
Commanding General U.S. Army Electronics Command Fort Monmouth, New Jersey 07703 Attn: AMSEL-10-T	1
Commanding General U.S. Army Electronics Command Fort Monmouth, New Jersey 07703 Attn: AMSEL-RD-GFA Mr. John Chappell	1
Commanding General U.S. Army Electronics Command Fort Monmouth, New Jersey 07703 Attn: AMSEL-NL-D-5	1
Commanding General U.S. Army Electronics Command Fort Monmouth, New Jersey 07703 Attn: AMSEL-HL-CT-R	1
Commanding General U.S. Army Materiel Command Washington, D.C. 20315 Attn: AMCRD-SR	1
Director Advanced Research Projects Agency Remote Area Conflict Washington, D.C. 20301 Attn: Lt. Col. T. W. Doeppner	2
Chief of Research and Development Department of the Army Washington, D.C. 20315 Attn: Lt. Col. N. F. J. Allen	1
Office of the Chief Communications-Electronics Department of the Army Washington, D.C. 20315 Attn: Electronics Systems Directorate	1
Director U.S. Naval Research Laboratory Washington, D.C. 20390 Attn: Code 2027	1
Chief of Naval Research Naval Research Laboratory Washington, D.C. 20390 Attn: Code 4321 Mr. Irwin Schiff	1

Organization	No. of Copies
Chief of Research and Development Headquarters, Department of the Army Washington, D.C. 20301 Attn: Chief Environmental Sciences Division	1
Defense Intelligence Agency Washington, D.C. 20301 Attn: Special Warfare Office	1
Headquarters U.S. Marine Corps Washington, D.C. 20390 Attn: Code A04C Mr. R. J. Sgro	1
Director Advanced Research Projects Agency The Pentagon Washington, D.C. 20301 Attn: TIO	2
Advanced Research Projects Agency R&D Field Unit APO San Francisco, California 96346	1
OSD/ARPA - USAEL APO San Francisco, California 96346 Attn: Lt. Col. A. P. Sidon	7D
Commanding General U.S. Army Security Agency Arlington Hall Station Arlington, Virginia 22212 Attn: IARD-R-E	1
Commanding General, USASA Arlington Hall Station Arlington, Virginia 22212 Attn: DCSR&D	3
Institute for Defense Analyses 400 Army-Navy Drive Arlington, Virginia 22202 Attn: Classified Library	1
Defense Documentation Center Cameron Station Alexandria, Virginia 22314	5D
Headquarters L. G. Hanscom Field Bedford, Massachusetts 01730 Attn: ESWE Captain Ruta	1
U.S. Army Liaison Office MIT Lincoln Laboratory, Room A-21D Lexington, Massachusetts 02173 Attn: A. D. Bedrosian	1
Director OSD/ARPA RDFO (ME) APO New York, New York 09694	1
Rome Air Development Center Griffiss Air Force Base, New York 13441 Attn: EMASA Mr. Vincent Coyne	1

DISTRIBUTION LIST (Continued)

Organization	No. of Copies
Rome Air Development Center Griffiss Air Force Base, New York 13440 Attn: EMD Mr. Fred Diamond	1
Rome Air Development Center (EMTLD) Griffiss Air Force Base, New York 13440 Attn: Documents Library	1
Director National Security Agency Fort George G. Meade, Maryland 20755 Attn: TDL	1
Commanding Officer U.S. Army Limited War Laboratory Aberdeen Proving Ground, Maryland 21005 Attn: CROLWL-6A	1
Commanding Officer U.S. Army War Limited Laboratory Aberdeen Proving Ground, Maryland 21005 Attn: CRO-AM-6	1
Wilson Nuttall Raimond Engineers, Incorporated Chesterton, Maryland 21620 Attn: Library	1
Tropical Science Center Aptdo. 2959 San Jose, Costa Rica Attn: Dr. L. R. Holdridge	1
Commanding Officer U.S. Army Combat Development Command Fort Bragg, North Carolina 28307 Attn: C. T. Swaringen	1
President U.S. Army Airborne Board and Special Warfare Board Fort Bragg, North Carolina 28307	1
Commandant Special Warfare School Fort Bragg, North Carolina 28307	1
Commanding General Special Warfare Center Fort Bragg, North Carolina 28307	1
Commanding General U.S. Army Missile Command Redstone Arsenal, Alabama 35809 Attn: AMSMI-RNM	1
Director Air University Library Maxwell Air Force Base, Alabama 36112 Attn: AUL3T-66-453	1
Director Waterways Experiment Station P.O. Box 631 Vicksburg, Mississippi 39180 Attn: Mr. A. Rula	1
Remote Area Conflict Information Center (RACIC) Battelle Memorial institute 505 King Avenue Columbus, Ohio 43201	1

Organization	No. of Copies
Commander Aeronautical Systems Division Wright-Patterson Air Force Base, Ohio 45433 Attn: ASJT (Mr. Ricker)	1
Department of Geography University of Denver Denver, Colorado 80202 Attn: Dr. Thomas M. Griffiths Project Duty	1
Commanding General U.S. Army Electronic Proving Ground Fort Huachuca, Arizona 85613 Attn: STEEP-ET	1
California Institute of Technology Jet Propulsion Laboratory 4800 Oak Grove Drive Pasadena, California 93105 Attn: STA-Library R. E. Walker, Supervisor	1
General Research Corporation P.O. Box 3587 Santa Barbara, California 93105	1
Booz-Allen Applied Research, Inc. 135 South LaSalle Street Chicago, Illinois 60603	1
Booz-Allen Applied Research, Inc. 4733 Bethesda Avenue Bethesda, Maryland 20014 Attn: Library	1
Booz-Allen Applied Research, Inc. OSO/ARPA RDC-T APO San Francisco, California 96346	1
Atlantic Research Corporation Jansky and Bailey Division Shirley Highway at Edsall Road Alexandria, Virginia 22314	1
OSD/ARPA - USAEL APO San Francisco, California 96346 Attn: Lt. Col. A. P. Sidon	1
U.S. Program/Project Manager The Mallard Project Fort Monmouth, New Jersey 07703 Attn: AMCPM-MLD-TM	1
Defense Communications Planning Group Building 56, U.S. Naval Observatory Washington, D.C. 20305 Attn: Code 700 Mr. Z. J. Stevens	1
Director Communications and Electronics Office of the Joint Chiefs of Staff Washington, D.C. 20301	1
Director Military Research and Development Center Supreme Command Headquarters Bangkok, Thailand Attn: Captain Prapat Chandaket, R.T.N.	10

UNCLASSIFIED

Security Classification

DOCUMENT CONTROL DATA - R & D

(Security classification of title, body of abstract and indexing annotation must be entered when the overall report is classified)

1. ORIGINATING ACTIVITY *(Corporate author)*
Stanford Research Institute
Menlo Park, California 94025

2a. REPORT SECURITY CLASSIFICATION
UNCLASSIFIED

2b. GROUP
N/A

3. REPORT TITLE
ORIENTATION MEASUREMENTS IN THAILAND WITH HF DIPOLE ANTENNAS FOR TACTICAL COMMUNICATION

4. DESCRIPTIVE NOTES *(Type of report and inclusive dates)*
Special Technical Report 31

5. AUTHOR(S) *(First name, middle initial, last name)*
Paibul Nacaskul, Lt. Cdr., R.T.N.

6. REPORT DATE
June 1967

7a. TOTAL NO. OF PAGES
248

7b. NO. OF REFS
24

8a. CONTRACT OR GRANT NO.
DA 36-039 AMC-00040(E)

b. PROJECT NO.
Order No. 5384-PM-63-91

c.
ARPA Order No. 371

d.

9a. ORIGINATOR'S REPORT NUMBER(S)
Special Technical Report 31
SRI Project 4240

9b. OTHER REPORT NO(S) *(Any other numbers that may be assigned this report)*

10. DISTRIBUTION STATEMENT
Distribution of this document is unlimited.

11. SUPPLEMENTARY NOTES

12. SPONSORING MILITARY ACTIVITY
Advanced Research Projects Agency
Washington, D.C.

13. ABSTRACT

The magneto-ionic theory is described with a view to optimizing the orientation of a linearly polarized antenna such as a half-wave dipole for short-range communication via the ionosphere near the geomagnetic equator. The practical application, together with its limitations, is also considered. Continuous-wave measurements, performed with the goal of determining a suitable wave mode of propagation and hence the desired orientation of horizontal dipoles, demonstrate the superiority of the ordinary wave (north-south dipoles) for overall performance over a major part of the day when communication traffic is normally active. The coupling between the ordinary and the extraordinary modes is studied and the stability within a particular mode of propagation is discussed, together with its susceptibility to atmospheric noise. Pulse measurements confirm the results of the CW measurements and give additional information on the amplitude and phase stability of received waves, and on ionospheric layers supporting these waves. The overall results of the CW and pulse tests suggest that, although the optimum orientation of horizontal dipoles for both transmission and reception is parallel to the earth's magnetic field, communication performance may be further improved by orientation diversity reception. The use of an additional horizontal dipole aligned orthogonally to the north-south dipole permits utilization of the extraordinary mode whenever the ordinary wave fades or becomes inferior. Orientation diversity and its properties have been investigated by radio-teletype measurements, which afford a ready means for assessing the performance of various antenna systems for transmission and reception. Initial investigations indicate that system performance of the diversity-combining teletype can be significantly improved by use of orientation diversity. The overall results of this study produce a simplified method of planning antenna configurations for tactical HF communication in Thailand.

DD FORM 1 NOV 65 1473 (PAGE 1)

S/N 0101-807-6801

UNCLASSIFIED

Security Classification

14 KEY WORDS	LINK A		LINK B		LINK C	
	ROLE	WT	ROLE	WT	ROLE	WT
Antenna orientation						
Communication						
High frequency (HF)						
Propagation modes						
Magneto-ionic theory						
Dipoles						
Ordinary wave						
Extraordinary wave						
Ionosphere						
Orientation diversity						
Thailand						
SEACORE						